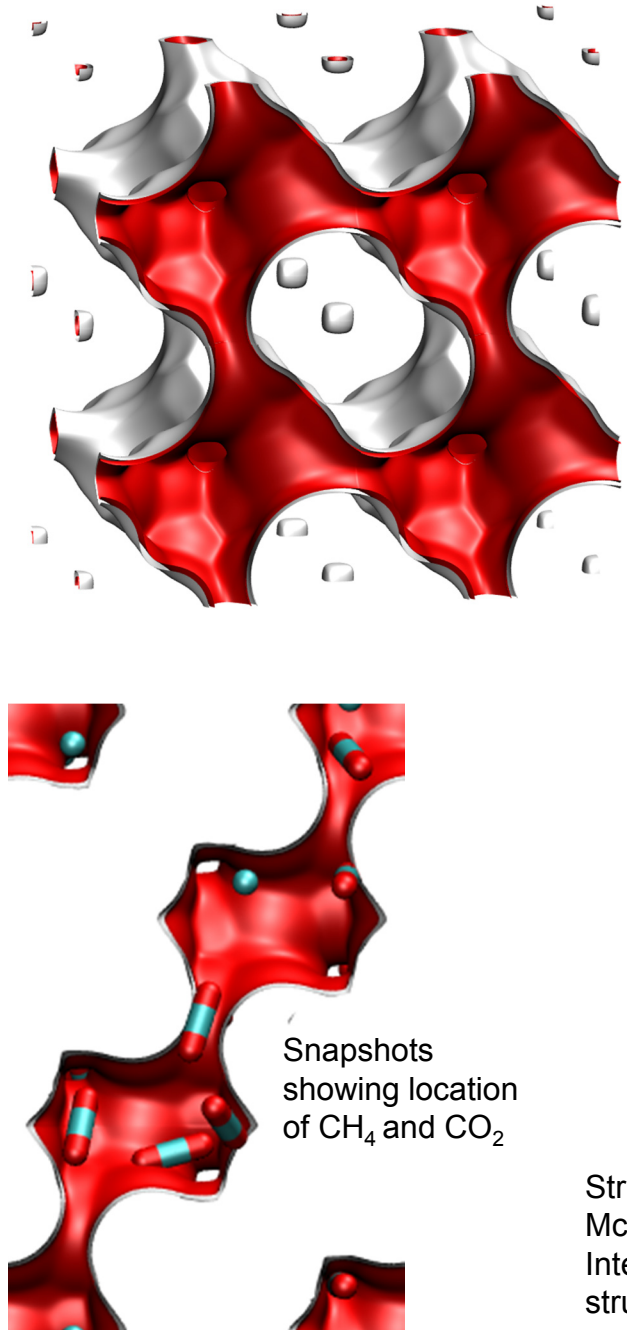
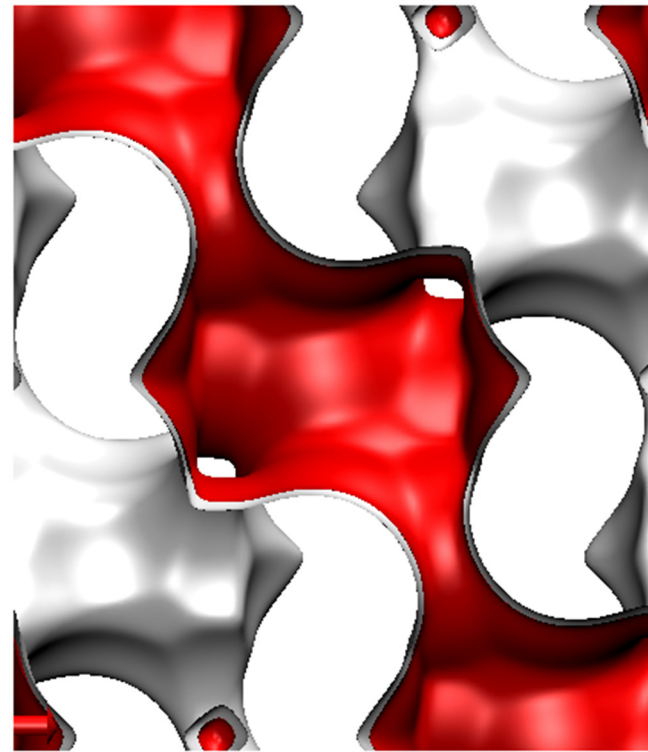
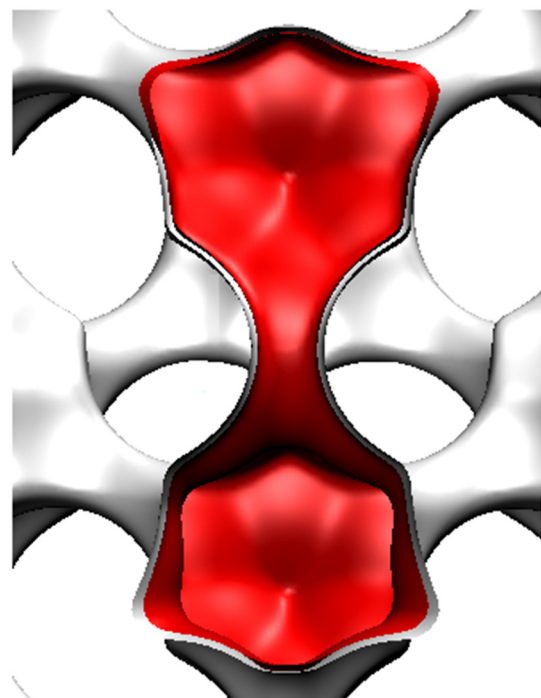


Cage-type structures with narrow windows

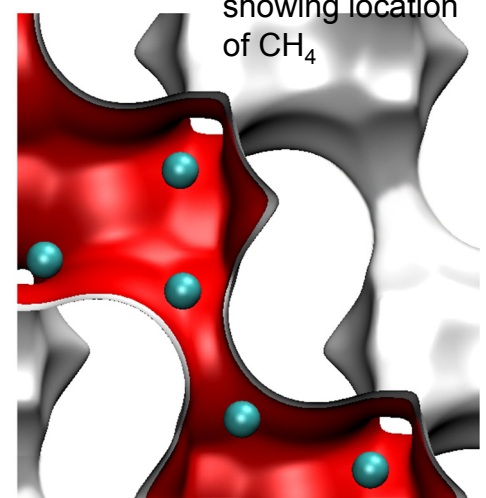
CHA landscape



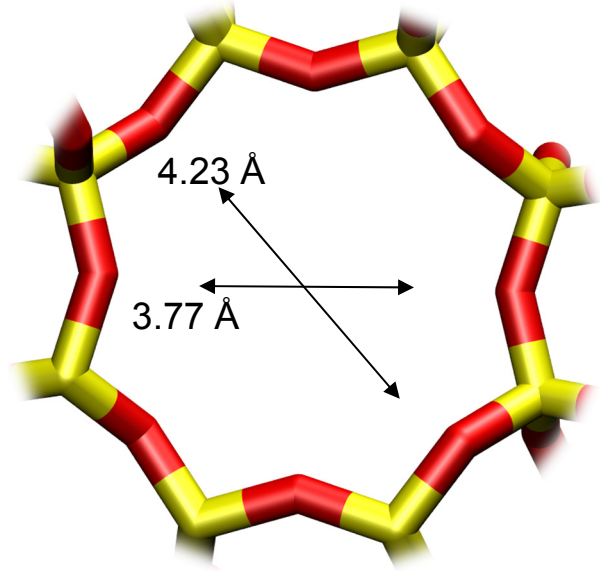
There are 6 cages per unit cell. The volume of one CHA cage is 316.4 \AA^3 , slightly larger than that of a single cage of DDR (278 \AA^3), but significantly lower than FAU (786 \AA^3).



Structural information from: C. Baerlocher, L.B. McCusker, Database of Zeolite Structures, International Zeolite Association, <http://www.iza-structure.org/databases/>



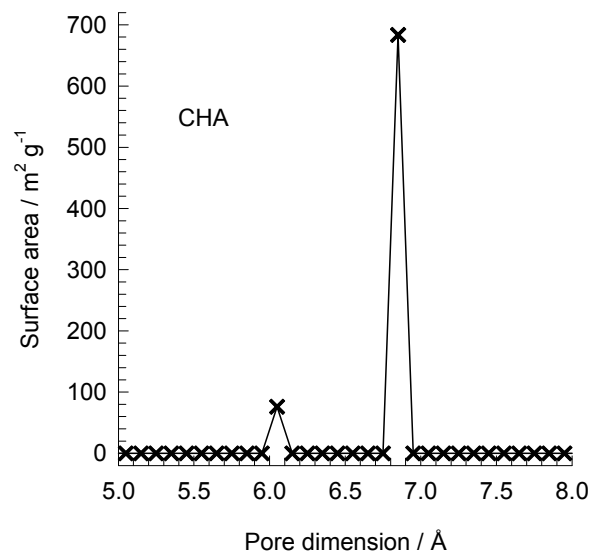
CHA window and pore dimensions



CHA

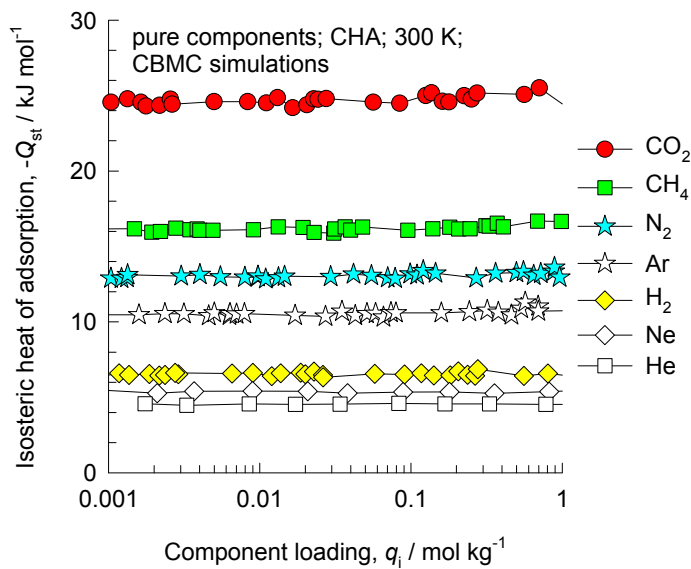
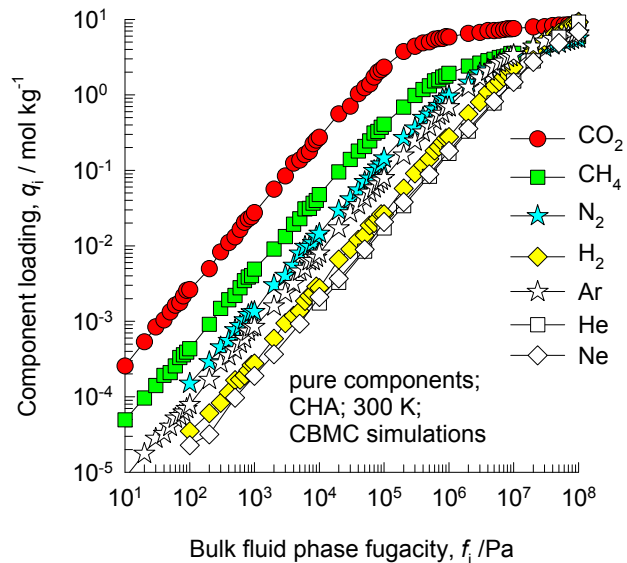
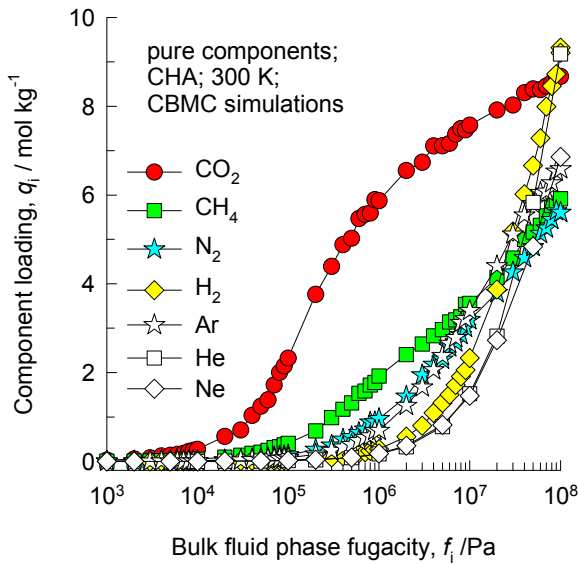
The window dimensions calculated using the van der Waals diameter of framework atoms = 2.7 Å are indicated above by the arrows.

This plot of surface area versus pore dimension is determined using a combination of the DeLaunay triangulation method for pore dimension determination, and the procedure of Dürren for determination of the surface area.

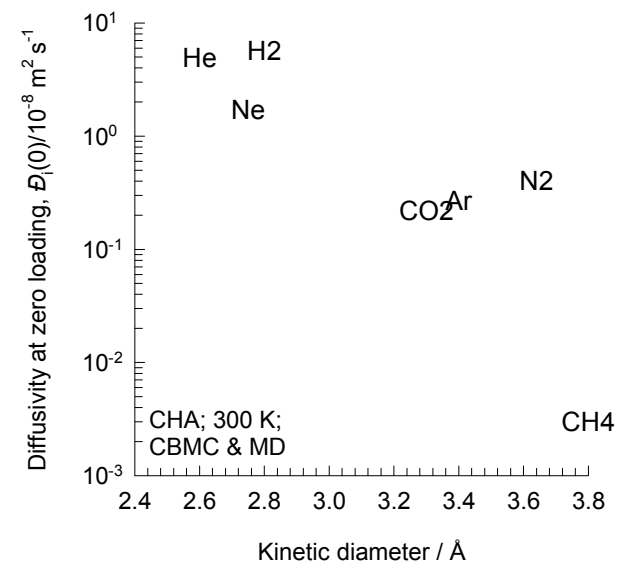
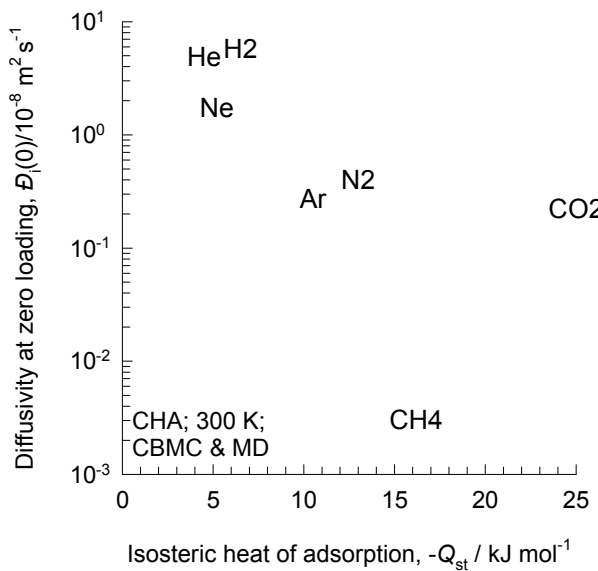
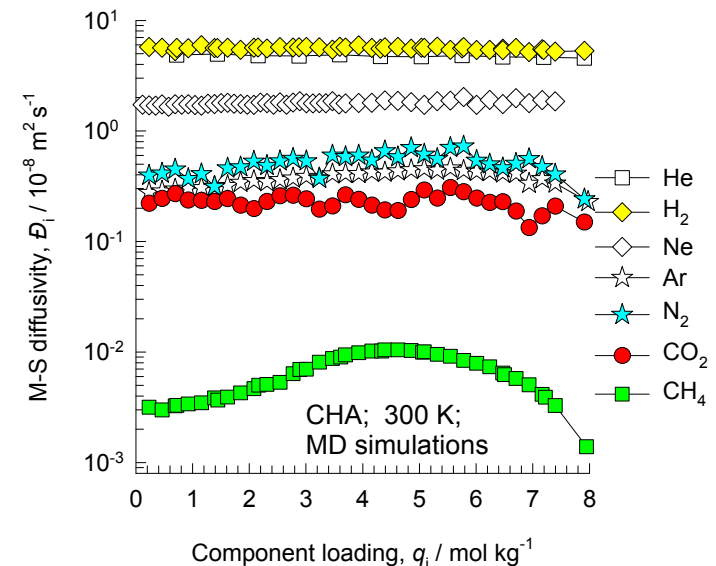
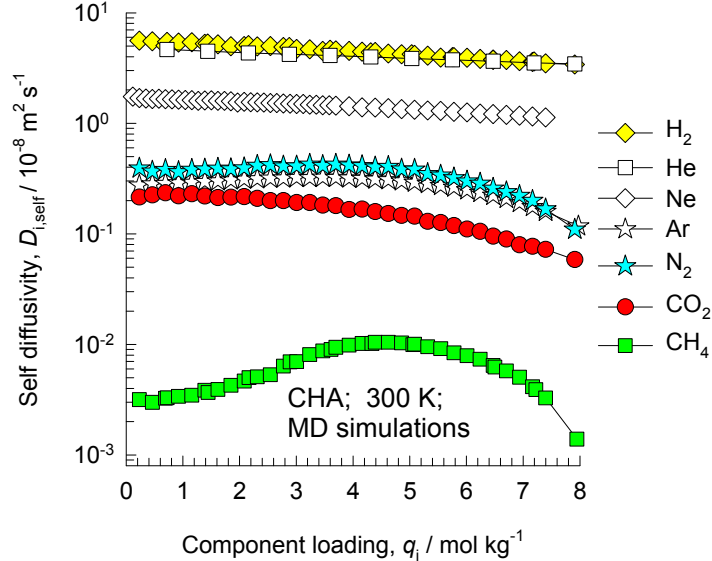


| CHA | |
|--|----------|
| $a / \text{\AA}$ | 15.075 |
| $b / \text{\AA}$ | 23.907 |
| $c / \text{\AA}$ | 13.803 |
| Cell volume / \AA^3 | 4974.574 |
| conversion factor for [molec/uc] to [mol per kg Framework] | 0.2312 |
| conversion factor for [molec/uc] to [kmol/m³] | 0.8747 |
| $\rho / \text{kg/m}^3$ | 1444.1 |
| MW unit cell [g/mol(framework)] | 4326.106 |
| ϕ , fractional pore volume | 0.382 |
| open space / $\text{\AA}^3/\text{uc}$ | 1898.4 |
| Pore volume / cm^3/g | 0.264 |
| Surface area / m^2/g | 758.0 |
| DeLaunay diameter / \AA | 3.77 |

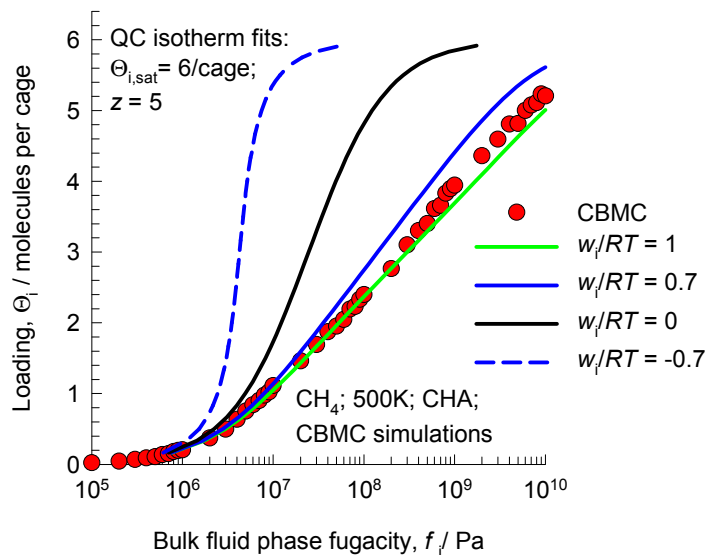
CHA CBMC simulations of isotherms, and isosteric heats of adsorption



CHA MD simulations of unary self-, and M-S diffusivities



CHA Modeling the loading dependence of CH₄ diffusivity



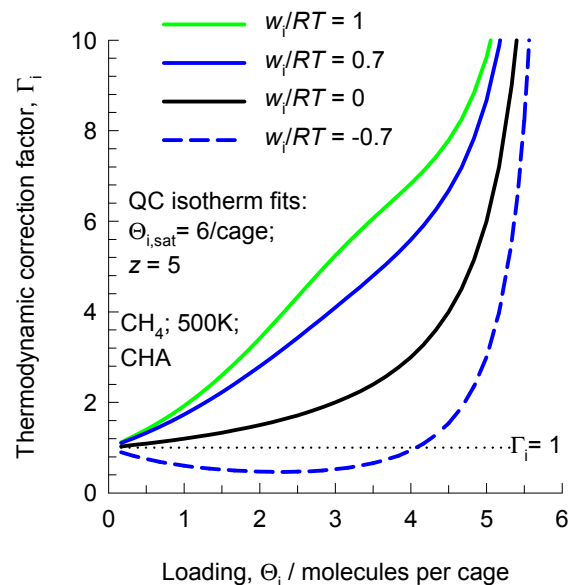
Quasi - Chemical isotherm

$$b_i f_i = \frac{\theta_i}{(1-\theta_i)} \left(\frac{2(1-\theta_i)}{\varsigma_i + 1 - 2\theta_i} \right)^z$$

$$\theta_i = c_i / c_{i,sat} = q_i / q_{i,sat} = \Theta_i / \Theta_{i,sat}$$

$$\varsigma_i = \sqrt{1 - 4\theta_i(1-\theta_i)(1 - \exp(-w_i/RT))}$$

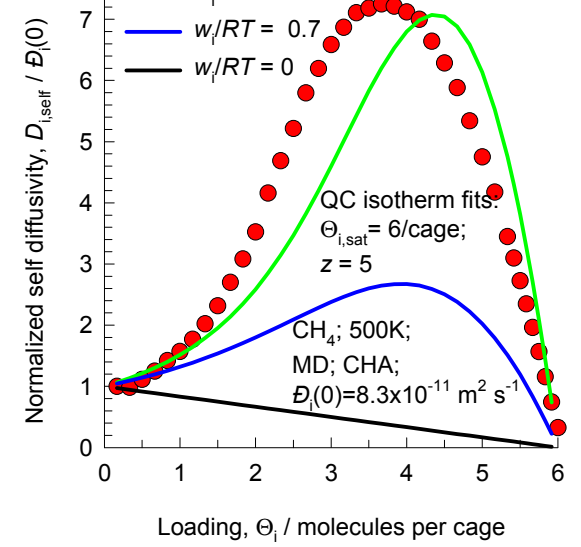
$$\Gamma_i = \frac{1}{(1-\theta_i)} \left(1 + \frac{z}{2} \frac{(1-\varsigma_i)}{\varsigma_i} \right)$$



Krishna, Paschek and Baur (2004) model

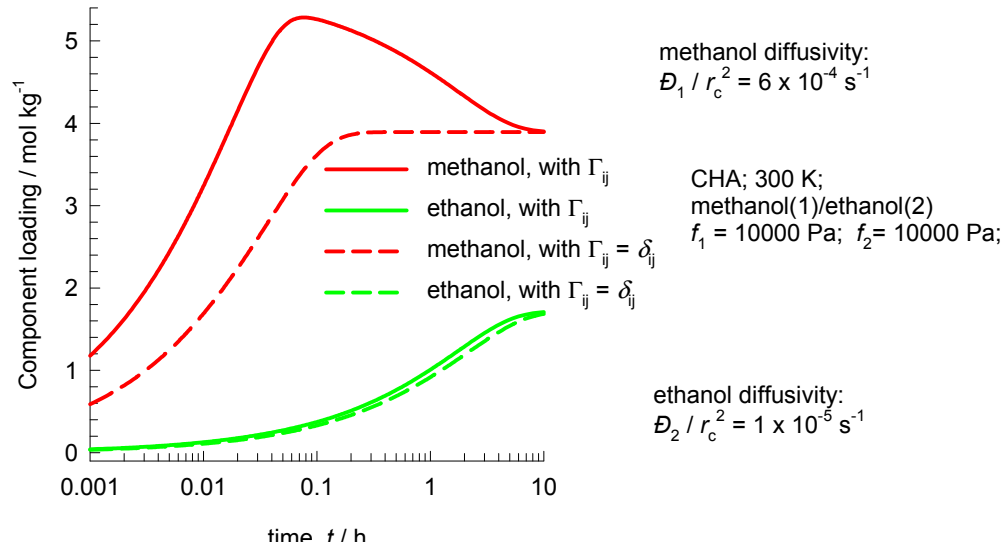
$$D_i = D_i(0) \left(\frac{1+\varsigma_i}{2(1-\theta_i)} \right)^{-z} \left(1 + \frac{(\varsigma_i - 1 + 2\theta_i) \exp(w_i/RT)}{2(1-\theta_i)} \right)^{z-1}$$

$$\varsigma_i = \sqrt{1 - 4\theta_i(1-\theta_i)(1 - \exp(-w_i/RT))}$$



The model used to describe the concentration dependence of D_i is described in detail in Krishna, R.; Paschek, D.; Baur, R. Modelling the occupancy dependence of diffusivities in zeolites, Microporous Mesoporous Mater. 2004, 76, 233-246.

CHA: Transient uptake of methanol – ethanol mixture



In these simulations, both the M-S diffusivities are assumed to be independent of loading. The overshoot in methanol is not, therefore, a result of the loading dependence of its M-S diffusivity.

The pure component isotherms are dual-Langmuir-Freundlich fits of CBMC simulated pure component isotherms of alcohols in CHA available in

Krishna, R.; van Baten, J. M. Entropy-based separation of linear chain molecules by exploiting differences in the saturation capacities in cage-type zeolites, Sep. Purif. Technol. 2011, 76, 325-330.

The overshoot in the methanol uptake is a direct consequence of thermodynamic coupling caused by the off-diagonal elements of

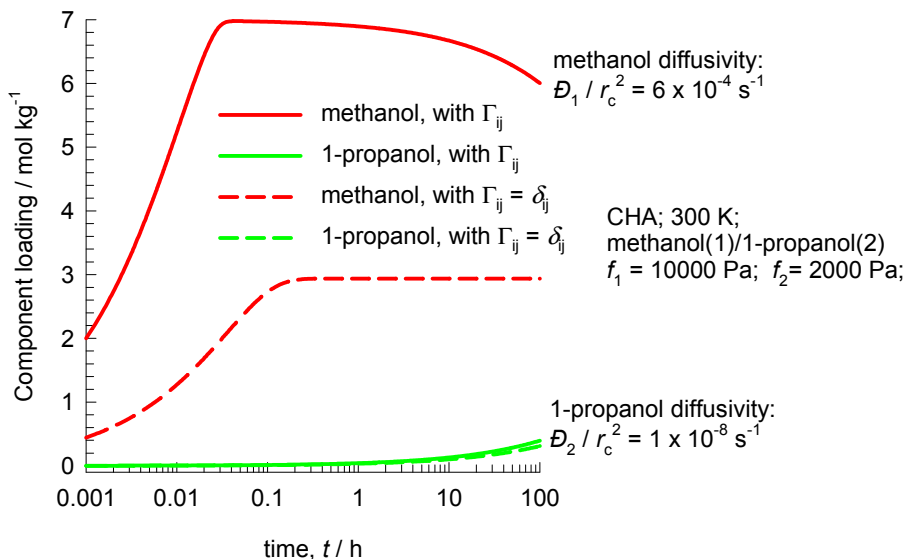
$$\begin{bmatrix} \Gamma_{11} & \Gamma_{12} \\ \Gamma_{21} & \Gamma_{22} \end{bmatrix} \quad \text{where} \quad \Gamma_{ij} = \frac{q_i}{f_i} \frac{\partial f_i}{\partial q_j}$$

If the thermodynamic coupling is ignored, i.e. we assume $\Gamma_i = \delta_{ij}$; Kronecker delta

the methanol overshoot disappears.

$$\begin{bmatrix} \Gamma_{11} & \Gamma_{12} \\ \Gamma_{21} & \Gamma_{22} \end{bmatrix} = \begin{bmatrix} 1 & 0 \\ 0 & 1 \end{bmatrix}$$

CHA: Transient uptake of methanol – 1-propanol mixture



In these simulations, both the M-S diffusivities are assumed to be independent of loading. The overshoot in methanol is not, therefore, a result of the loading dependence of its M-S diffusivity.

The pure component isotherms are dual-Langmuir-Freundlich fits of CBMC simulated pure component isotherms of alcohols in CHA available in

Krishna, R.; van Baten, J. M. Entropy-based separation of linear chain molecules by exploiting differences in the saturation capacities in cage-type zeolites, Sep. Purif. Technol. 2011, 76, 325-330.

The overshoot in the methanol uptake is a direct consequence of thermodynamic coupling caused by the off-diagonal elements of

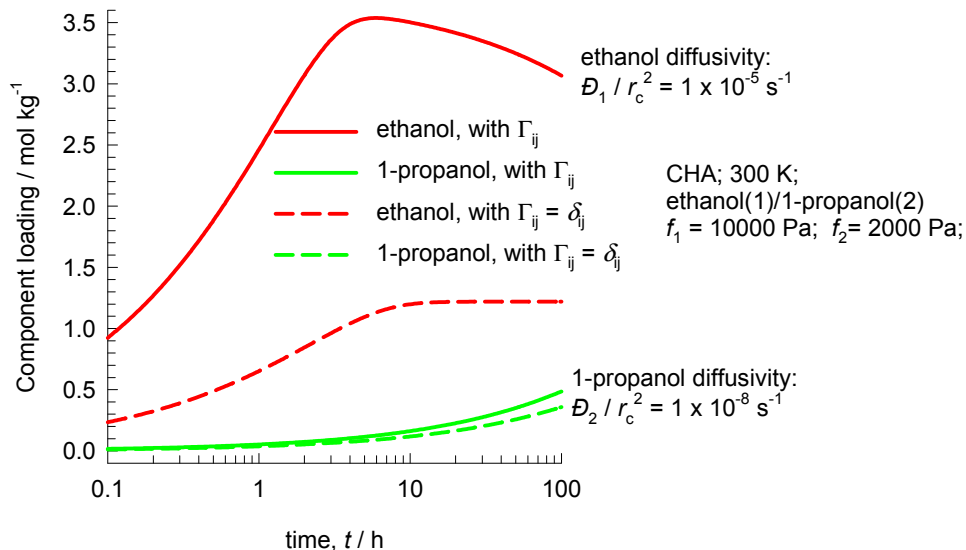
$$\begin{bmatrix} \Gamma_{11} & \Gamma_{12} \\ \Gamma_{21} & \Gamma_{21} \end{bmatrix} \quad \text{where} \quad \Gamma_{ij} = \frac{q_i}{f_i} \frac{\partial f_j}{\partial q_i}$$

If the thermodynamic coupling is ignored, i.e. we assume $\Gamma_i = \delta_{ij}$; Kronecker delta

the methanol overshoot disappears.

$$\begin{bmatrix} \Gamma_{11} & \Gamma_{12} \\ \Gamma_{21} & \Gamma_{21} \end{bmatrix} = \begin{bmatrix} 1 & 0 \\ 0 & 1 \end{bmatrix}$$

CHA: Transient uptake of ethanol – 1-propanol mixture



In these simulations, both the M-S diffusivities are assumed to be independent of loading. The overshoot in ethanol is not, therefore, a result of the loading dependence of its M-S diffusivity.

The pure component isotherms are dual-Langmuir-Freundlich fits of CBMC simulated pure component isotherms of alcohols in CHA available in

Krishna, R.; van Baten, J. M. Entropy-based separation of linear chain molecules by exploiting differences in the saturation capacities in cage-type zeolites, Sep. Purif. Technol. 2011, 76, 325-330.

The overshoot in the ethanol uptake is a direct consequence of thermodynamic coupling caused by the off-diagonal elements of

$$\begin{bmatrix} \Gamma_{11} & \Gamma_{12} \\ \Gamma_{21} & \Gamma_{21} \end{bmatrix} \quad \text{where} \quad \Gamma_{ij} = \frac{q_i}{f_i} \frac{\partial f_j}{\partial q_j}$$

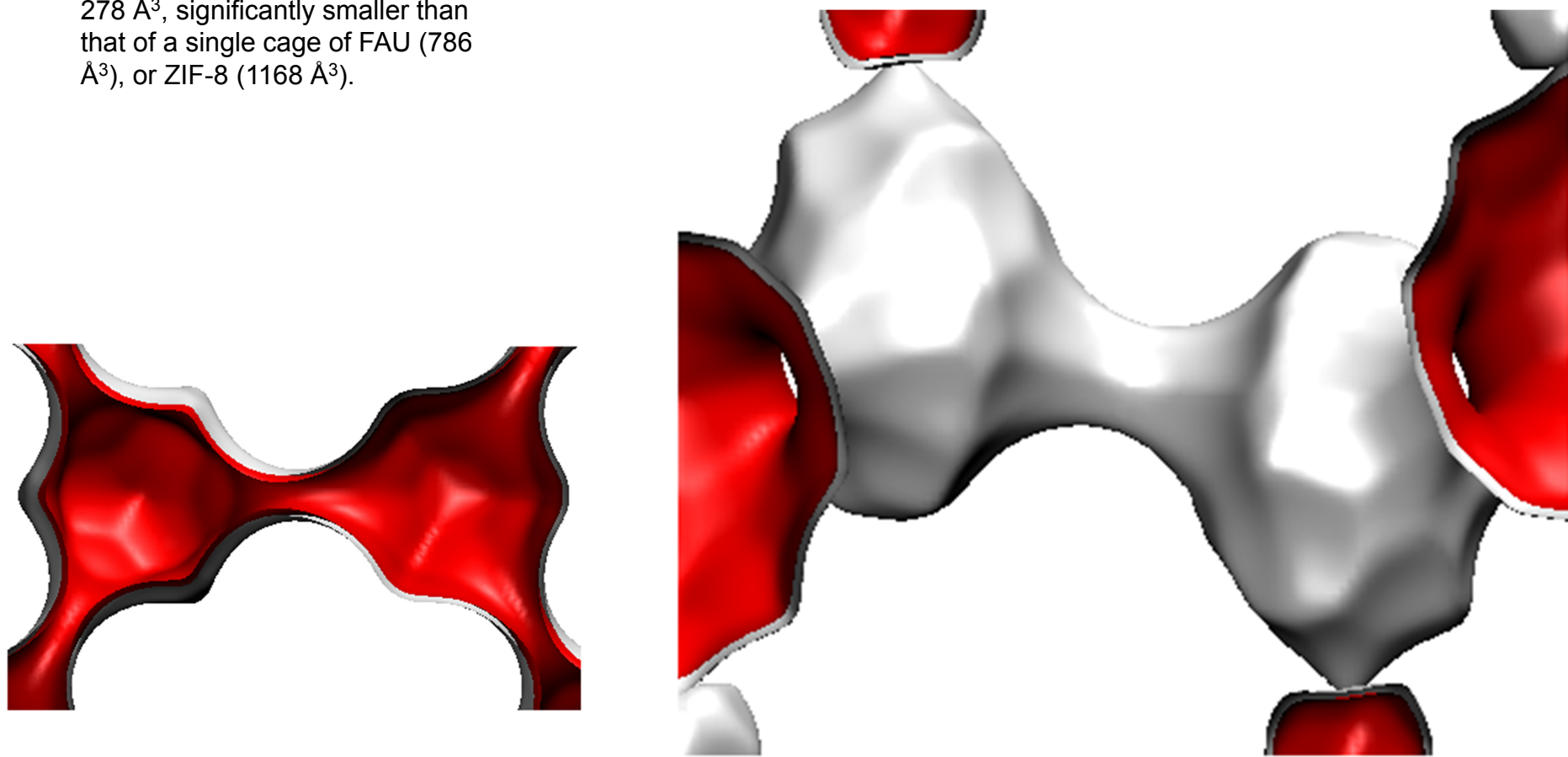
If the thermodynamic coupling is ignored, i.e. we assume $\Gamma_i = \delta_{ij}$; Kronecker delta

the ethanol overshoot disappears.

$$\begin{bmatrix} \Gamma_{11} & \Gamma_{12} \\ \Gamma_{21} & \Gamma_{21} \end{bmatrix} = \begin{bmatrix} 1 & 0 \\ 0 & 1 \end{bmatrix}$$

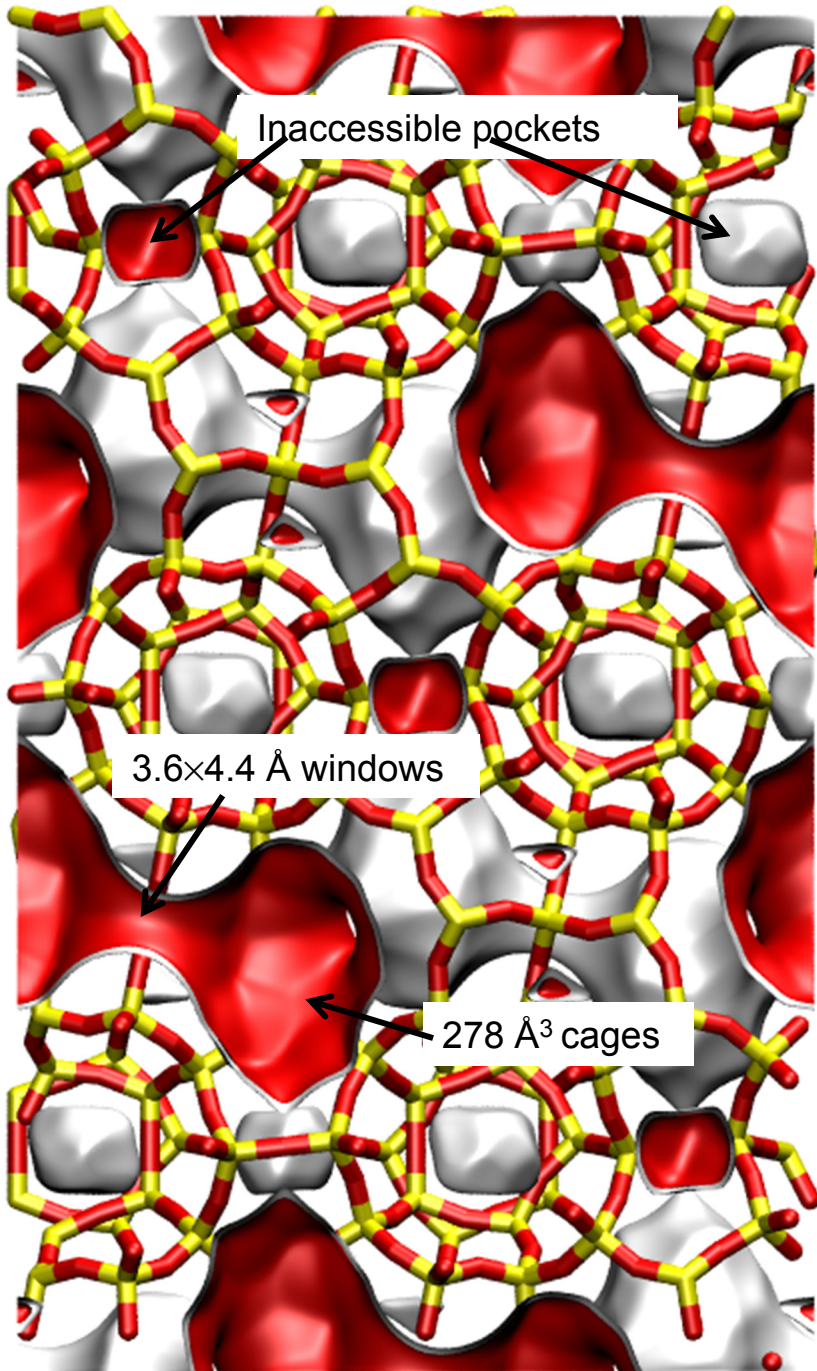
DDR landscape

There are 12 cages per unit cell. The volume of one DDR cage is 278 \AA^3 , significantly smaller than that of a single cage of FAU (786 \AA^3), or ZIF-8 (1168 \AA^3).



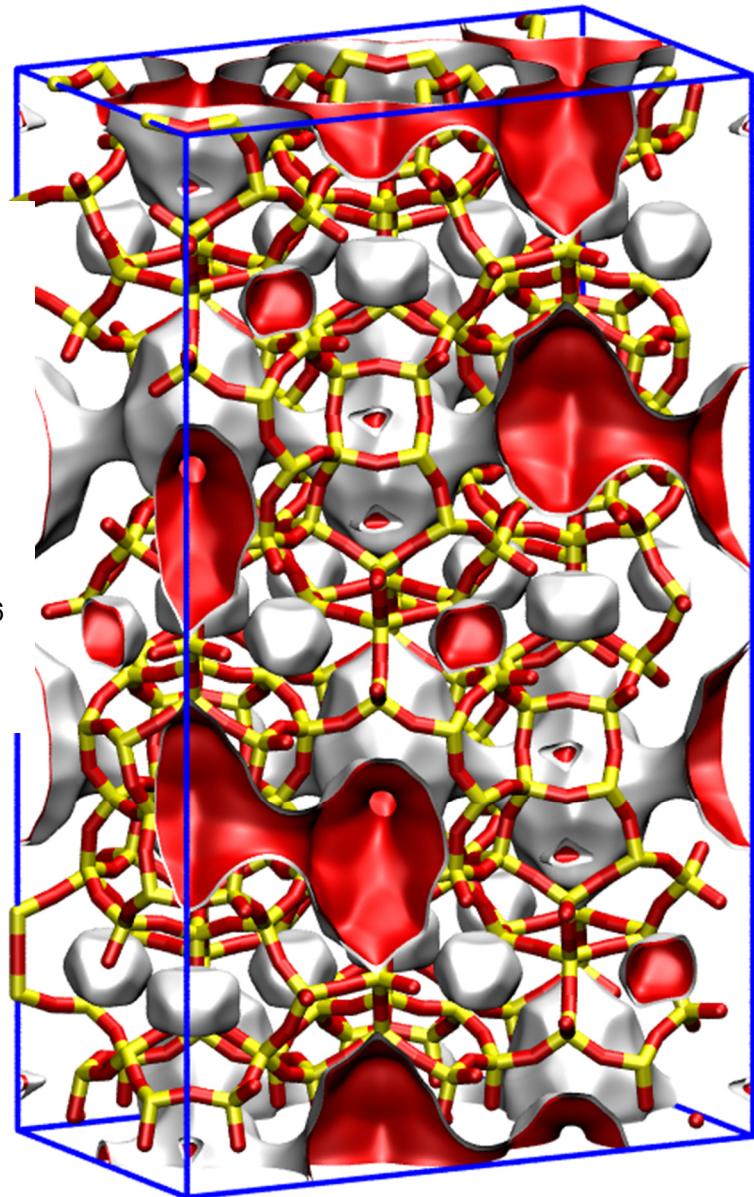
Structural information from: C. Baerlocher, L.B. McCusker, Database of Zeolite Structures, International Zeolite Association, <http://www.iza-structure.org/databases/>

To convert from molecules per unit cell to mol kg⁻¹, multiply by 0.06936.
The pore volume is 0.182 cm³/g.

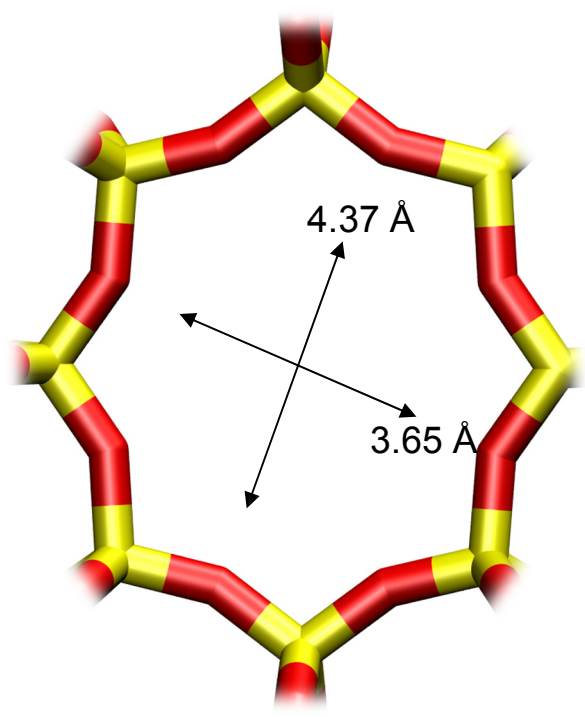


DDR landscapes without blocking

In all our simulations the inaccessible pockets of DDR were blocked. This aspect is explained in our paper
R. Krishna and J.M. van Baten, Comment on Comparative Molecular Simulation Study of CO₂/N₂ and CH₄/N₂ Separation in Zeolites and Metal-Organic Frameworks, Langmuir, 26 (2010) 2975-2978



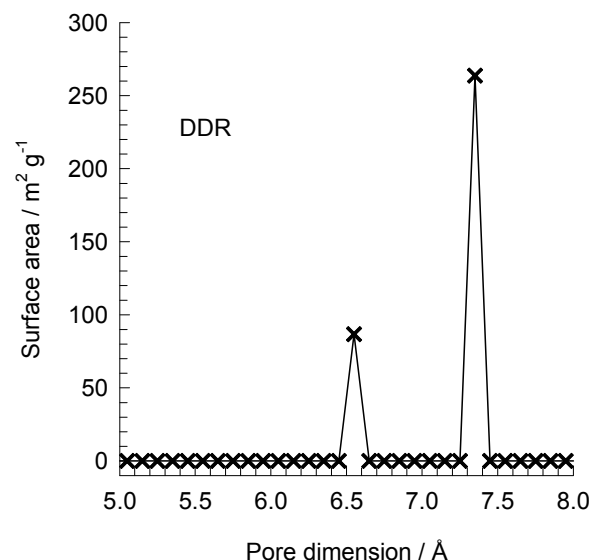
DDR window and pore dimensions



DDR

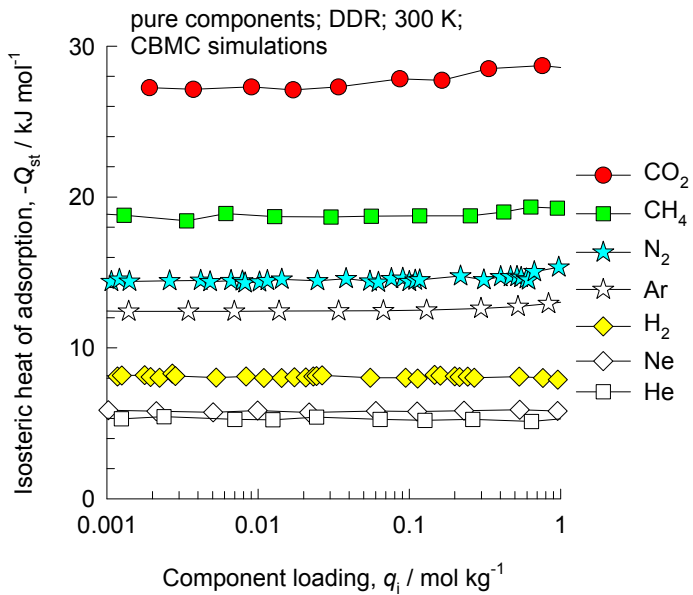
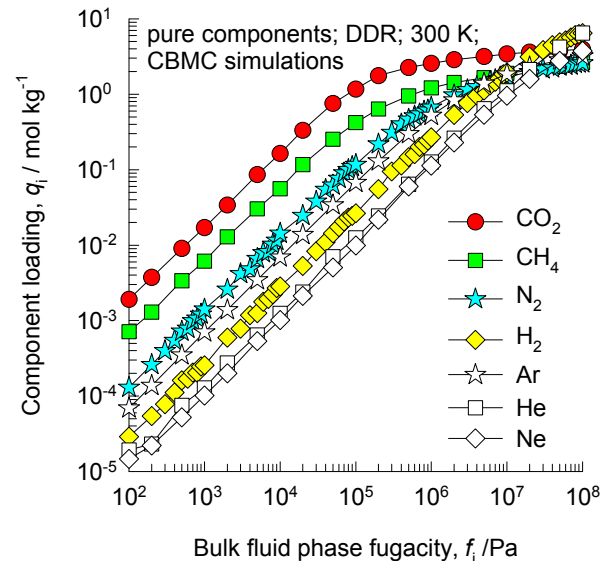
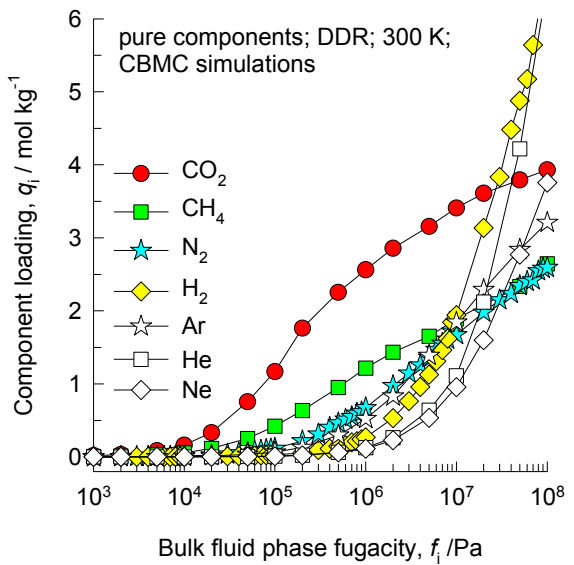
The window dimensions calculated using the van der Waals diameter of framework atoms = 2.7 Å are indicated above by the arrows.

This plot of surface area versus pore dimension is determined using a combination of the DeLaunay triangulation method for pore dimension determination, and the procedure of Düren for determination of the surface area.

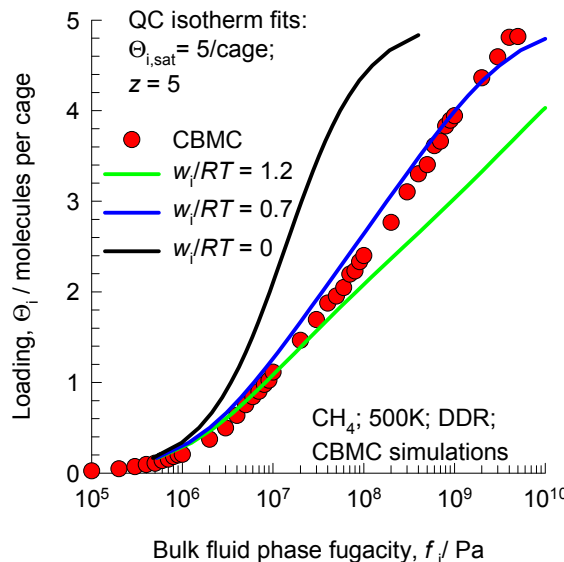


| | DDR |
|--|----------|
| a /Å | 24.006 |
| b /Å | 13.86 |
| c /Å | 40.892 |
| Cell volume / Å³ | 13605.72 |
| conversion factor for [molec/uc] to [mol per kg Framework] | 0.0693 |
| conversion factor for [molec/uc] to [kmol/m³] | 0.4981 |
| ρ [kg/m³] | 1759.991 |
| MW unit cell [g/mol(framework)] | 14420.35 |
| ϕ , fractional pore volume | 0.245 |
| open space / Å³/uc | 3333.5 |
| Pore volume / cm³/g | 0.139 |
| Surface area /m²/g | 350.0 |
| DeLaunay diameter /Å | 3.65 |

DDR CBMC simulations of isotherms, and isosteric heats of adsorption



DDR Modeling the loading dependence of CH₄ diffusivity



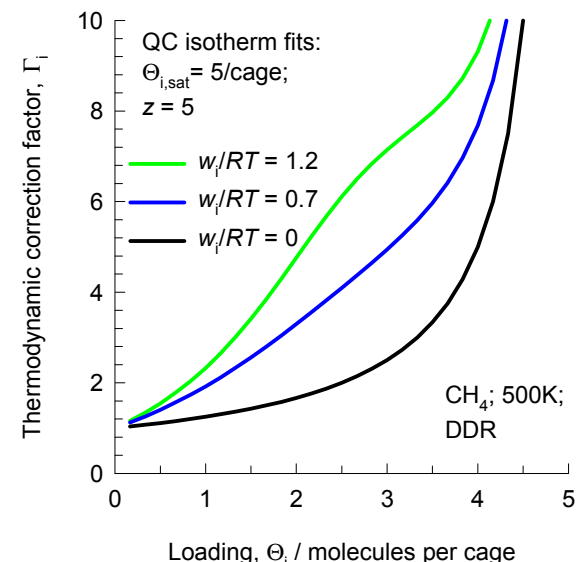
Quasi - Chemical isotherm

$$b_i f_i = \frac{\theta_i}{(1-\theta_i)} \left(\frac{2(1-\theta_i)}{\varsigma_i + 1 - 2\theta_i} \right)^z$$

$$\theta_i = c_i / c_{i,sat} = q_i / q_{i,sat} = \Theta_i / \Theta_{i,sat}$$

$$\varsigma_i = \sqrt{1 - 4\theta_i(1-\theta_i)(1 - \exp(-w_i/RT))}$$

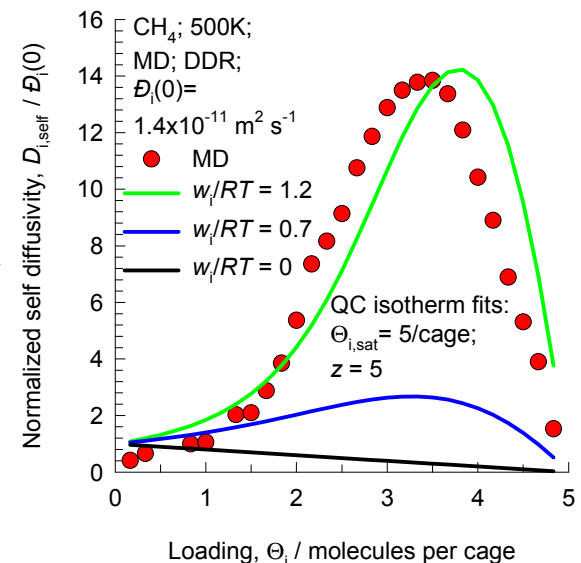
$$\Gamma_i = \frac{1}{(1-\theta_i)} \left(1 + \frac{z}{2} \frac{(1-\varsigma_i)}{\varsigma_i} \right)$$



Krishna, Paschek and Baur (2004) model

$$D_i = D_i(0) \left(\frac{1+\varsigma_i}{2(1-\theta_i)} \right)^{-z} \left(1 + \frac{(\varsigma_i - 1 + 2\theta_i) \exp(w_i/RT)}{2(1-\theta_i)} \right)^{z-1}$$

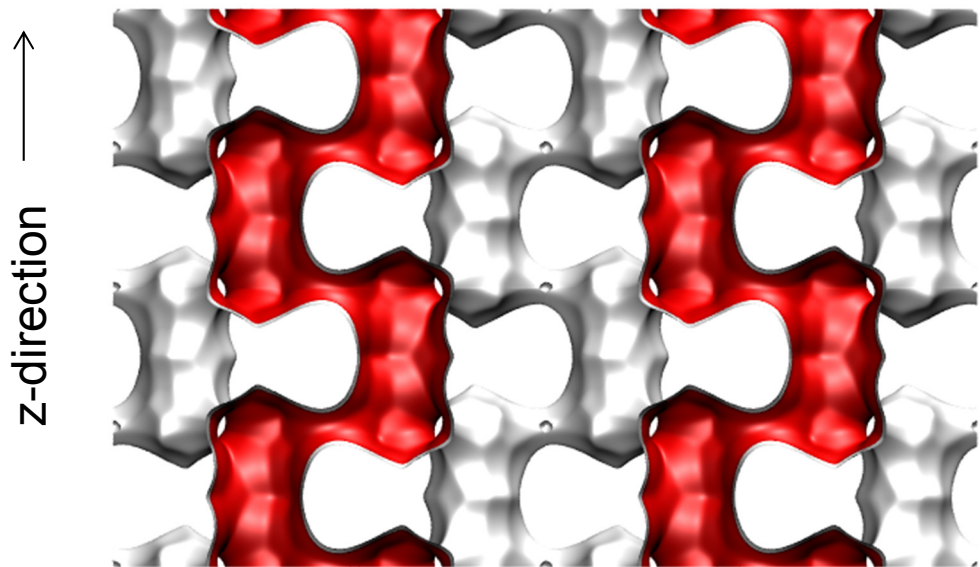
$$\varsigma_i = \sqrt{1 - 4\theta_i(1-\theta_i)(1 - \exp(-w_i/RT))}$$



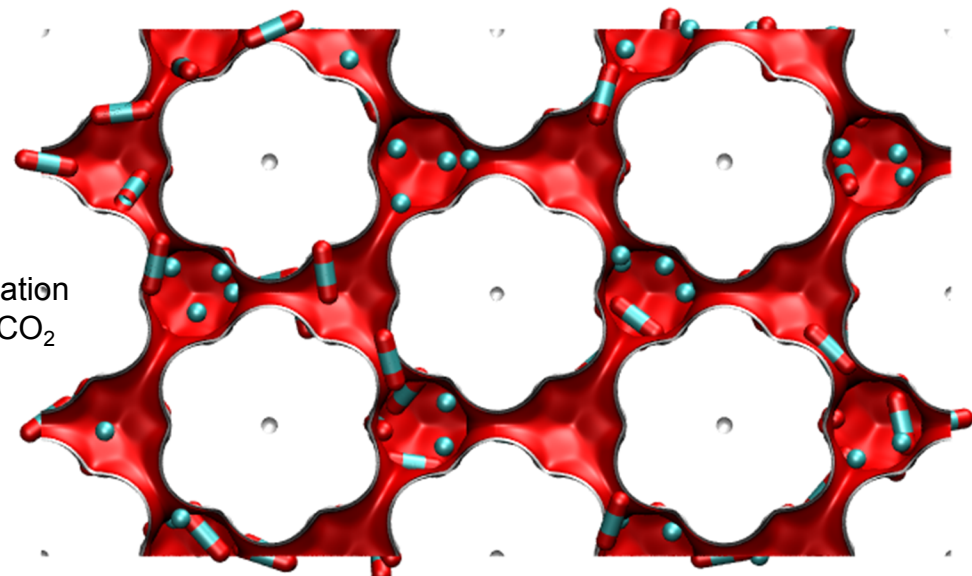
The model used to describe the concentration dependence of D_i is described in detail in
Krishna, R.; Paschek, D.; Baur, R. Modelling the occupancy dependence of diffusivities in zeolites, *Microporous Mesoporous Mater.* 2004, 76, 233-246.

ERI pore landscape

There are 4 cages per unit cell.
The volume of one ERI cage is 408.7 \AA^3 ,
significantly smaller than that of a single cage
of FAU-Si (786 \AA^3), or ZIF-8 (1168 \AA^3).



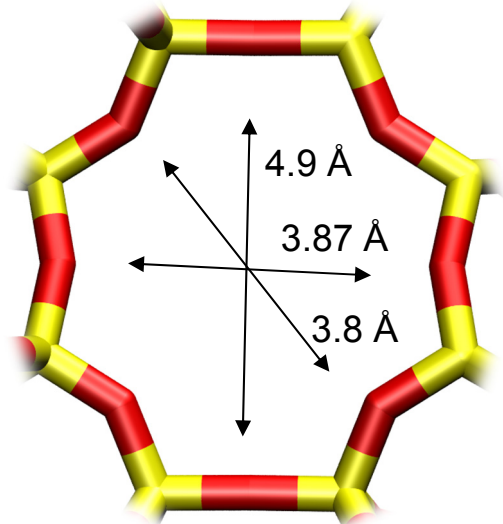
x-y projection



Snapshots
showing location
of CH₄ and CO₂

Structural information from: C. Baerlocher, L.B. McCusker, Database of Zeolite Structures, International Zeolite Association, <http://www.iza-structure.org/databases/>

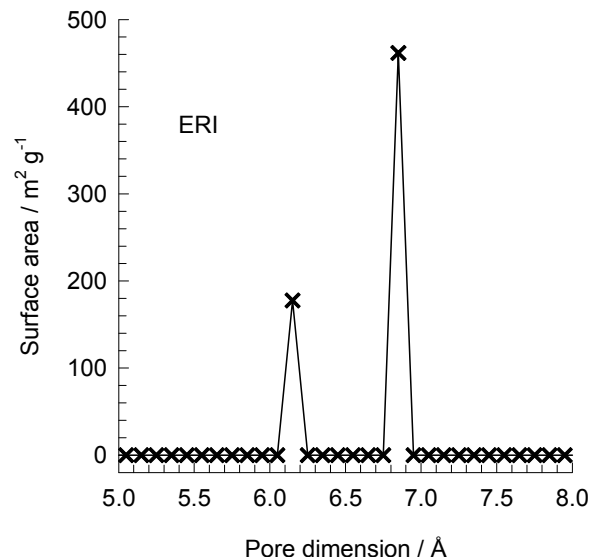
ERI window and pore dimensions



ERI

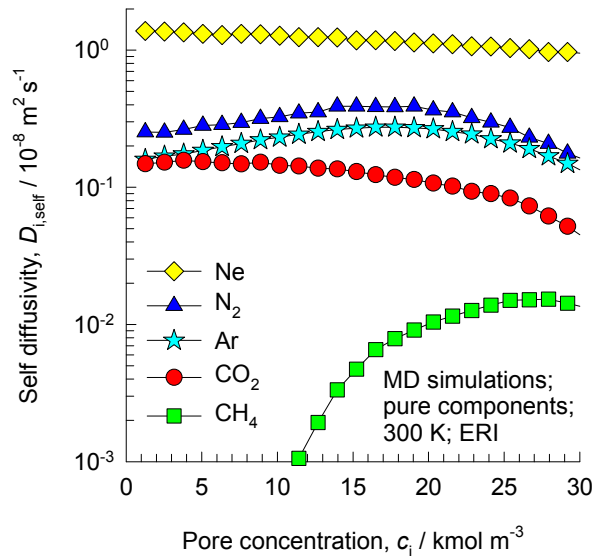
The window dimensions calculated using the van der Waals diameter of framework atoms = 2.7 Å are indicated above by the arrows.

This plot of surface area versus pore dimension is determined using a combination of the DeLaunay triangulation method for pore dimension determination, and the procedure of Düren for determination of the surface area.

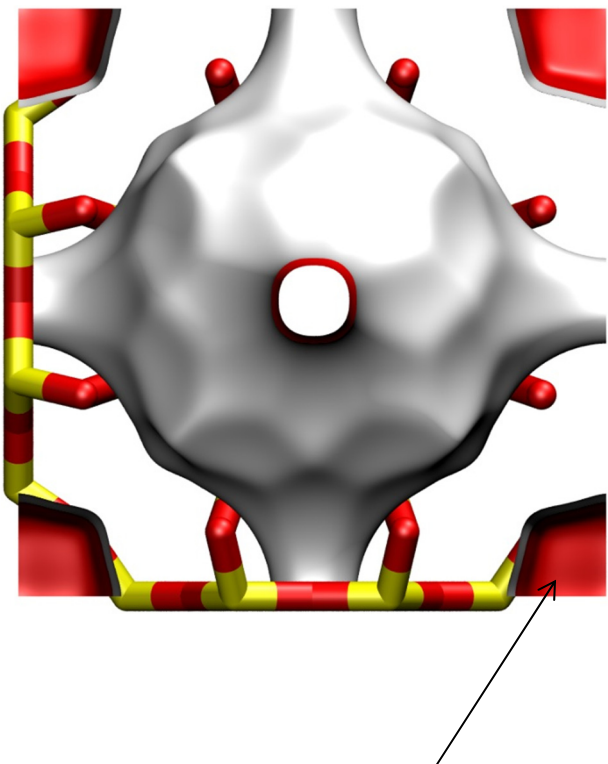


| | ERI |
|--|----------|
| a /Å | 22.953 |
| b /Å | 13.252 |
| c /Å | 14.81 |
| Cell volume / Å³ | 4504.804 |
| conversion factor for [molec/uc] to [mol per kg Framework] | 0.2312 |
| conversion factor for [molec/uc] to [kmol/m³] | 1.0156 |
| ρ [kg/m³] | 1594.693 |
| MW unit cell [g/mol(framework)] | 4326.106 |
| ϕ , fractional pore volume | 0.363 |
| open space / Å³/uc | 1635.0 |
| Pore volume / cm³/g | 0.228 |
| Surface area /m²/g | 635.0 |
| DeLaunay diameter /Å | 3.81 |

ERI MD simulations of unary self-diffusivities



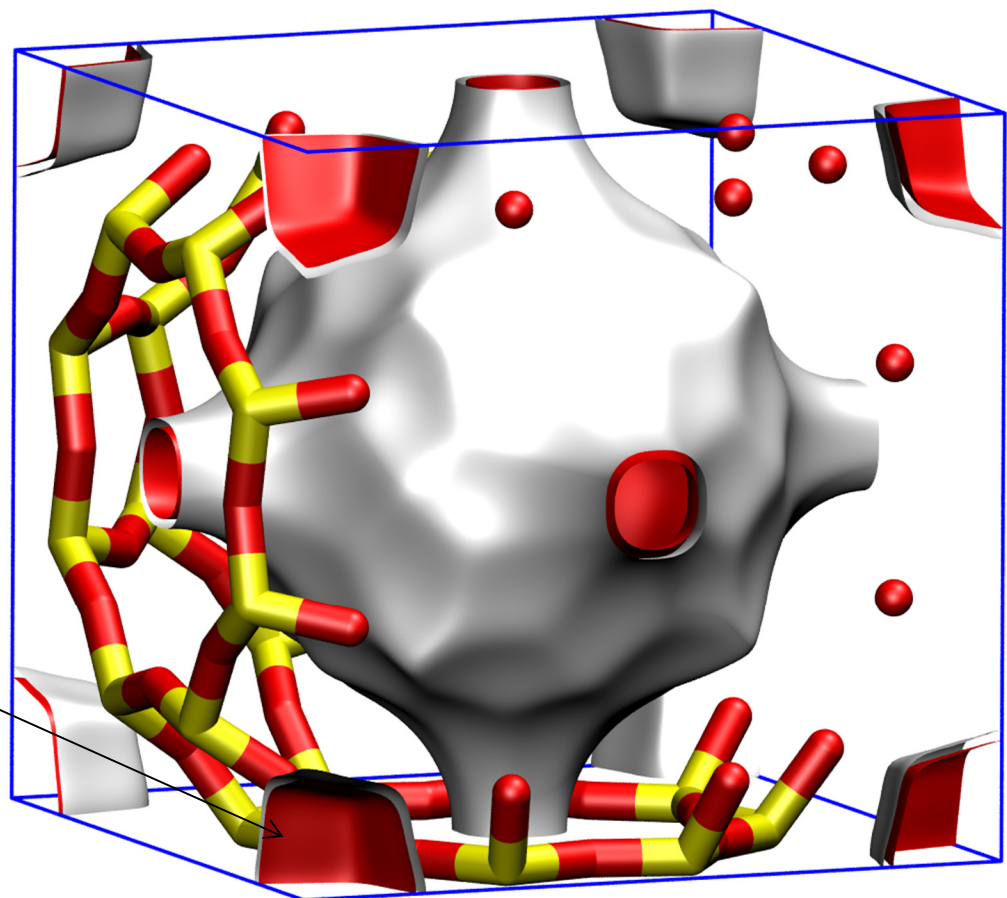
ITQ-29 pore landscape



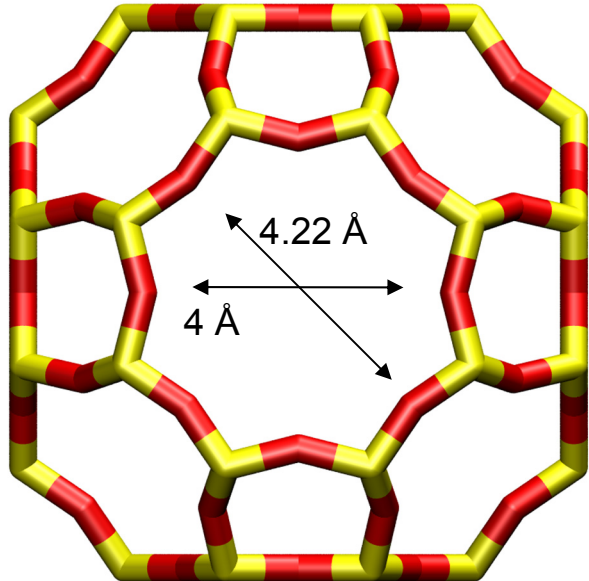
Inaccessible
sodalite cages
have been
blocked in
these
simulations

There is 1 cage per unit cell.
The volume of one ITQ-29 cage is
677.6 Å³, intermediate in size
between a single cage of ZIF-8
(1168 Å³) and of DDR (278 Å³).

The structural information for ITQ-29 is not available in the IZA atlas and is taken from Corma, Nature, 437 (2004) 287. The window size is slightly smaller than that of LTA Si.

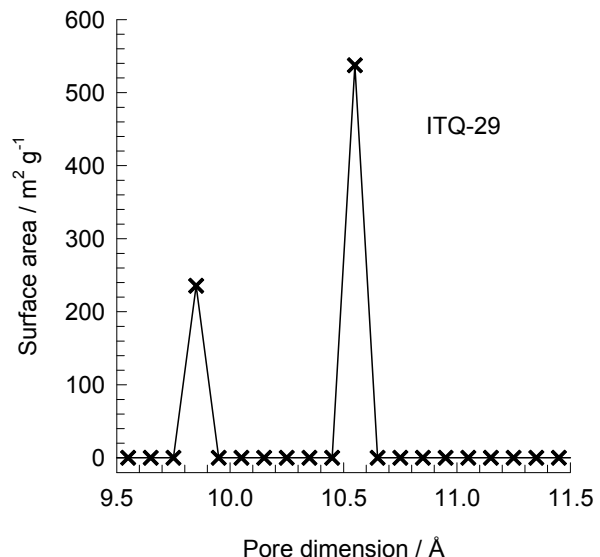


ITQ-29 window and pore dimensions



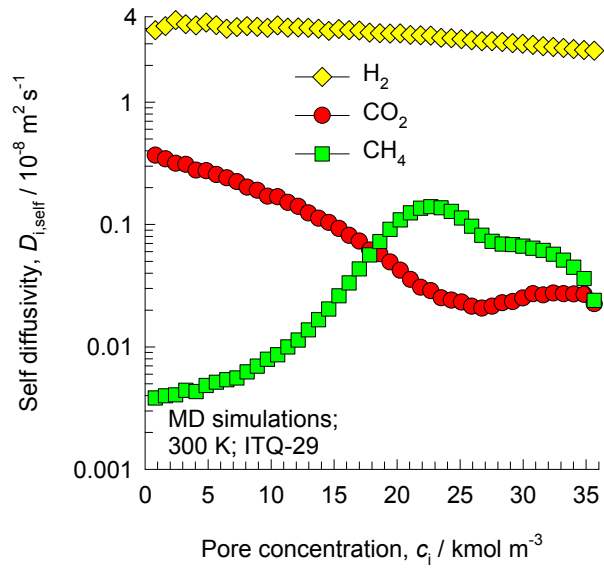
The window dimension calculated using the van der Waals diameter of framework atoms = 2.7 Å is indicated above by the arrows.

This plot of surface area versus pore dimension is determined using a combination of the DeLaunay triangulation method for pore dimension determination, and the procedure of Düren for determination of the surface area.

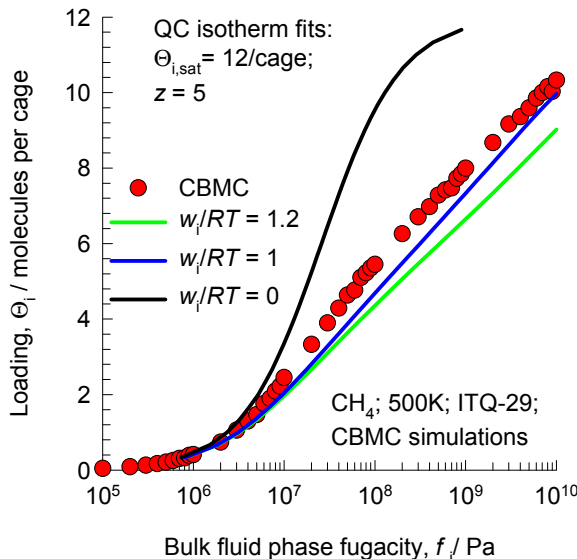


| ITQ-29 | |
|--|----------|
| a /Å | 11.867 |
| b /Å | 11.867 |
| c /Å | 11.867 |
| Cell volume / Å³ | 1671.178 |
| conversion factor for [molec/uc] to [mol per kg Framework] | 0.6935 |
| conversion factor for [molec/uc] to [kmol/m³] | 2.4508 |
| ρ [kg/m³] | 1432.877 |
| MW unit cell [g/mol(framework)] | 1442.035 |
| ϕ , fractional pore volume | 0.405 |
| open space / Å³/uc | 677.6 |
| Pore volume / cm³/g | 0.283 |
| Surface area /m²/g | 773.0 |
| DeLaunay diameter /Å | 3.98 |

ITQ-29 MD simulations of unary self- diffusivities



ITQ-29 Modeling the loading dependence of CH₄ diffusivity



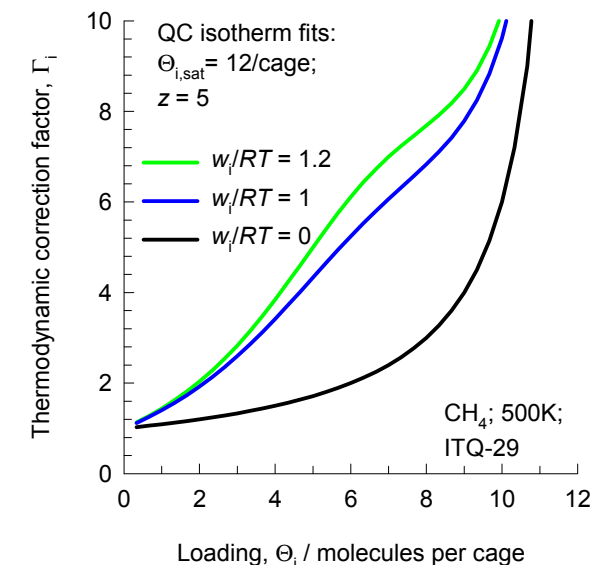
Quasi - Chemical isotherm

$$b_i f_i = \frac{\theta_i}{(1-\theta_i)} \left(\frac{2(1-\theta_i)}{\varsigma_i + 1 - 2\theta_i} \right)^z$$

$$\theta_i = c_i / c_{i,sat} = q_i / q_{i,sat} = \Theta_i / \Theta_{i,sat}$$

$$\varsigma_i = \sqrt{1 - 4\theta_i(1-\theta_i)(1 - \exp(-w_i/RT))}$$

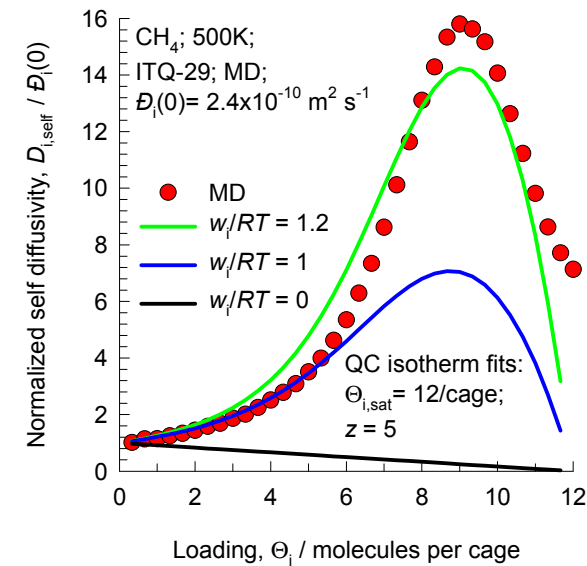
$$\Gamma_i = \frac{1}{(1-\theta_i)} \left(1 + \frac{z}{2} \frac{(1-\varsigma_i)}{\varsigma_i} \right)$$



Krishna, Paschek and Baur (2004) model

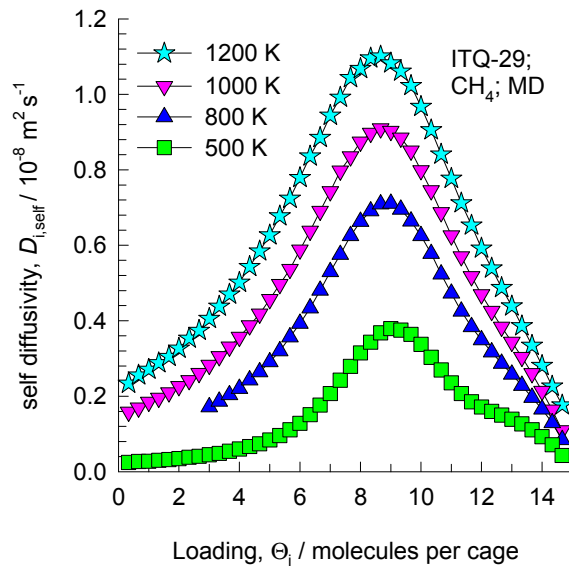
$$D_i = D_i(0) \left(\frac{1 + \varsigma_i}{2(1 - \theta_i)} \right)^{-z} \left(1 + \frac{(\varsigma_i - 1 + 2\theta_i)\exp(w_i/RT)}{2(1 - \theta_i)} \right)^{z-1}$$

$$\varsigma_i = \sqrt{1 - 4\theta_i(1-\theta_i)(1 - \exp(-w_i/RT))}$$

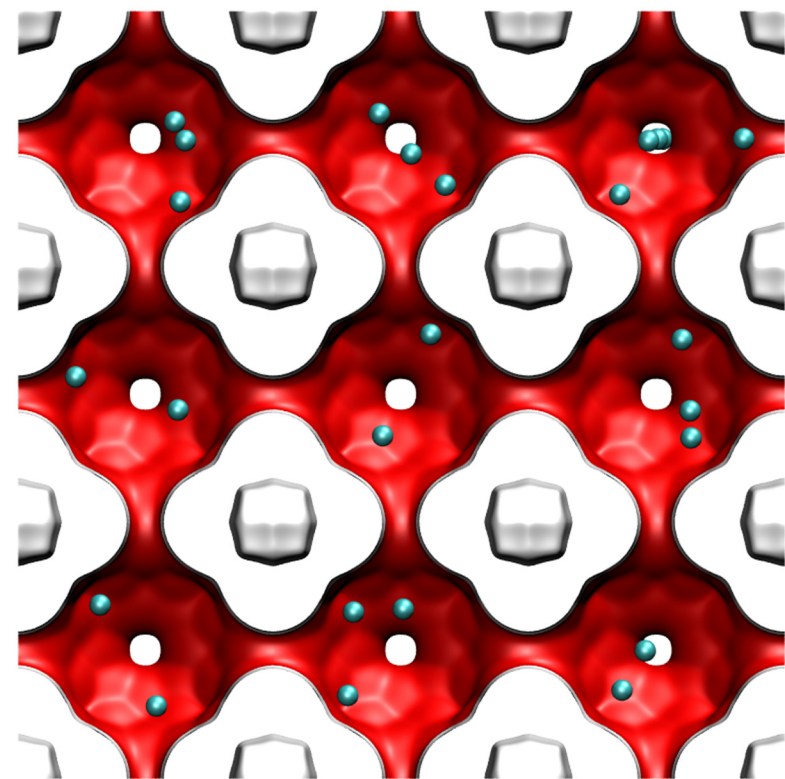
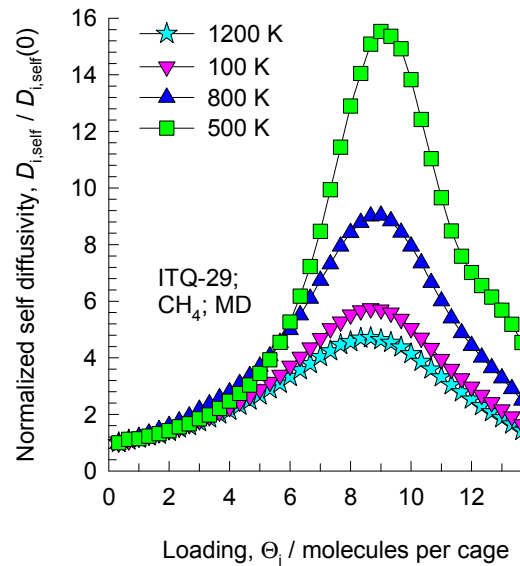


The model used to describe the concentration dependence of D_i is described in detail in
Krishna, R.; Paschek, D.; Baur, R. Modelling the occupancy dependence of diffusivities in zeolites, *Microporous Mesoporous Mater.* 2004, 76, 233-246.

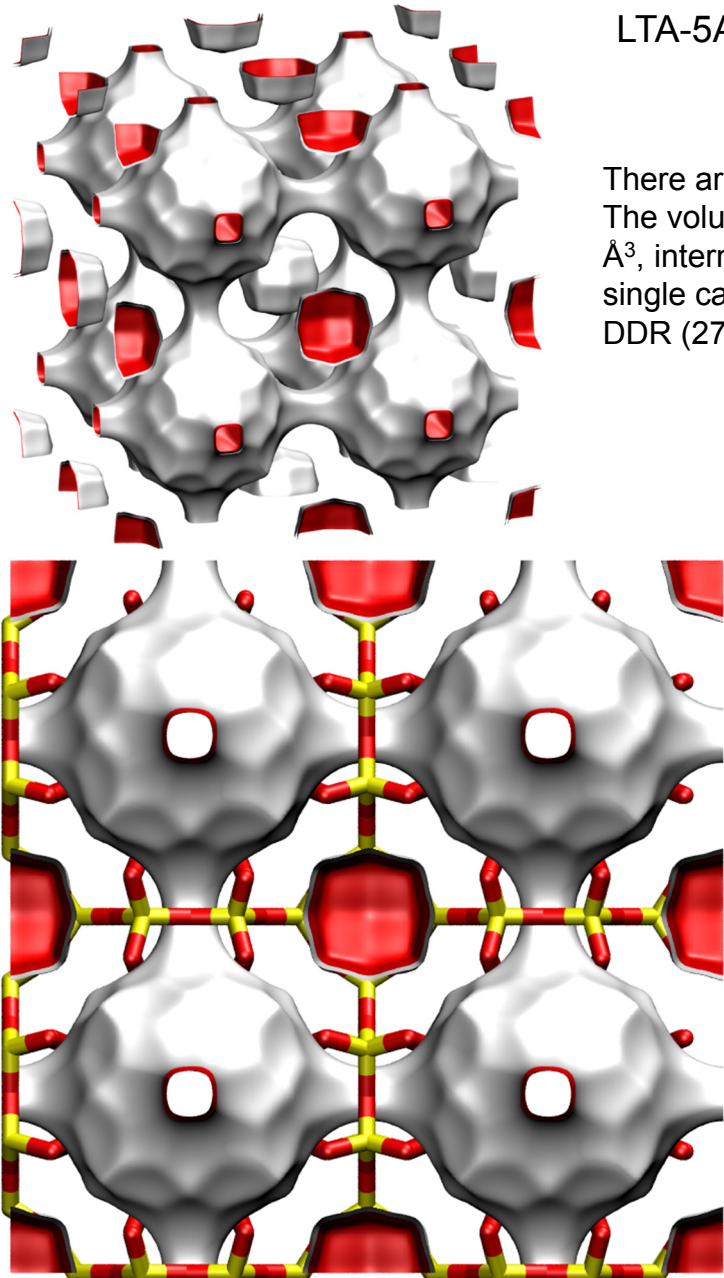
ITQ-29, diffusivity of CH₄



These data are for rigid frameworks

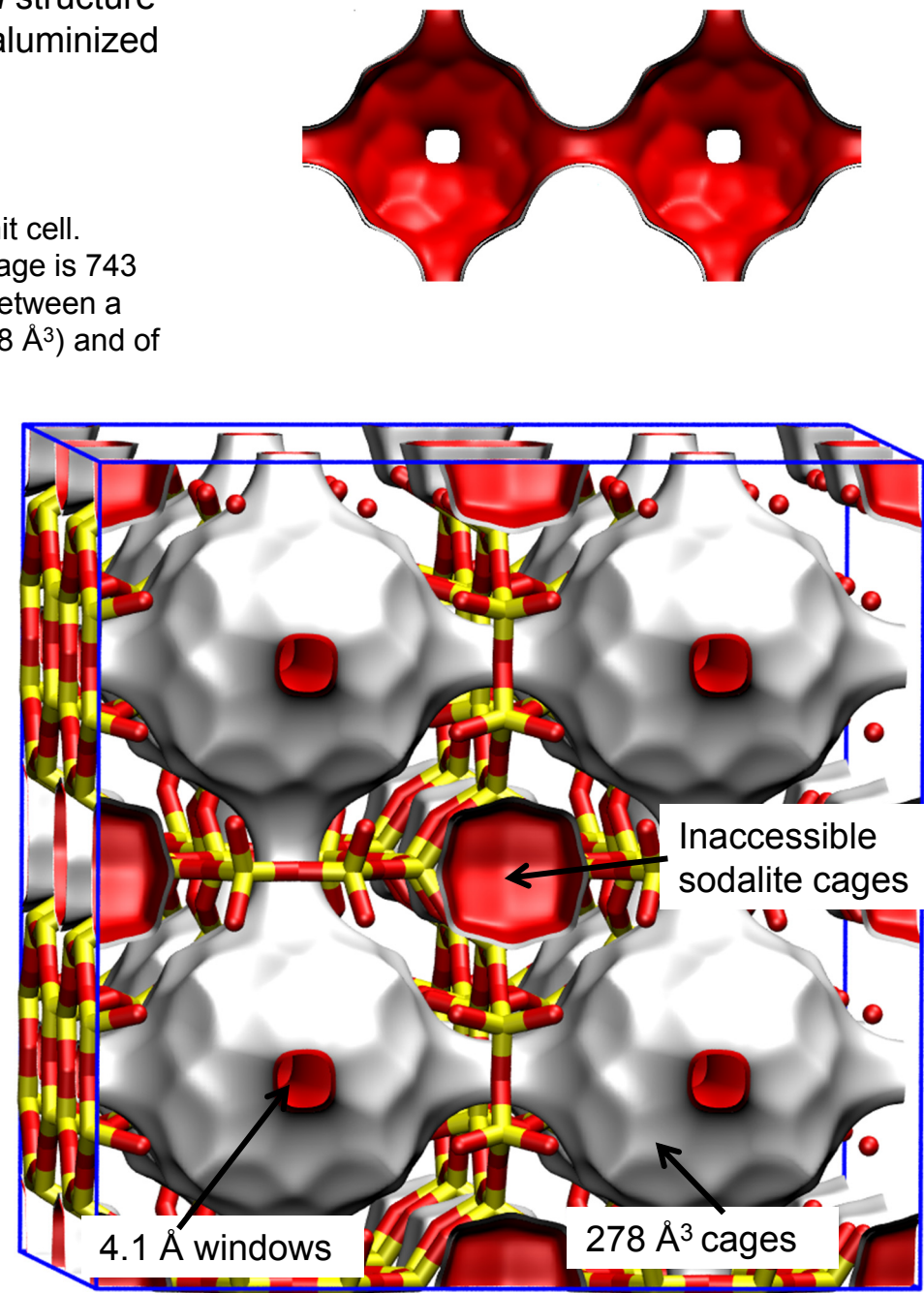


LTA-Si landscapes



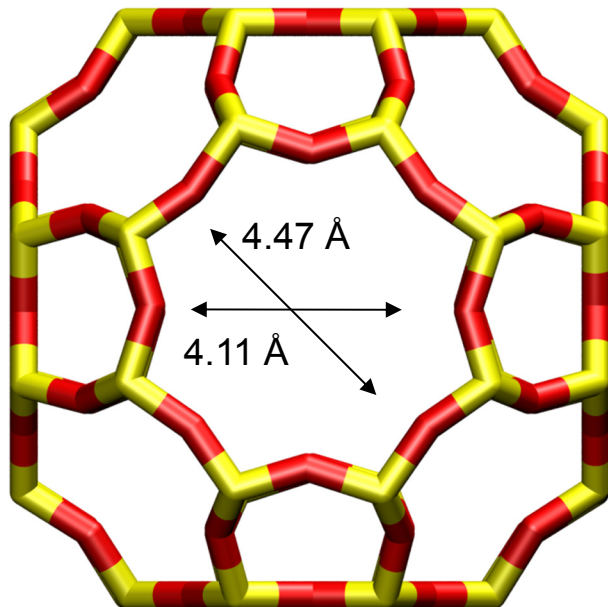
This is a *hypothetical* structure constructed from dealuminized LTA-5A structure

There are 8 cages per unit cell. The volume of one LTA cage is 743 \AA^3 , intermediate in size between a single cage of ZIF-8 (1168 \AA^3) and of DDR (278 \AA^3).



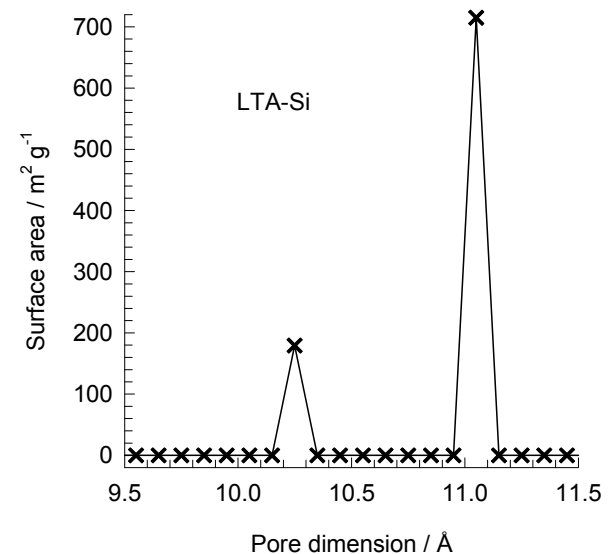
LTA-Si window and pore dimensions

8-ring
window
of LTA



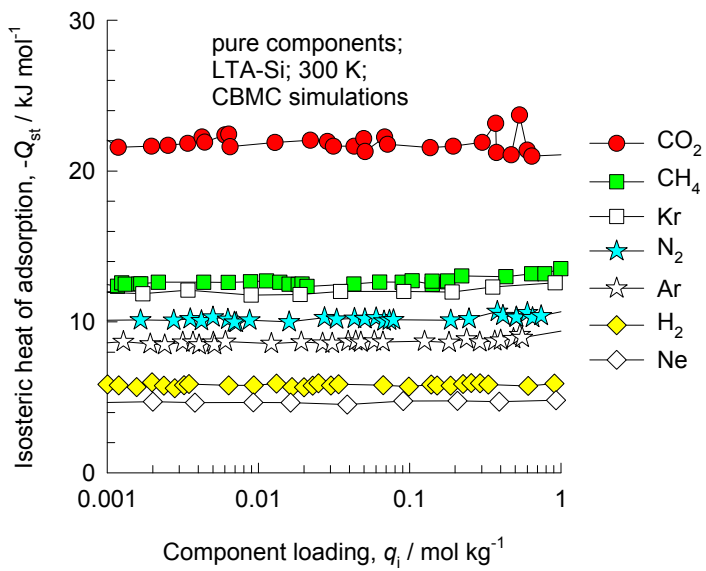
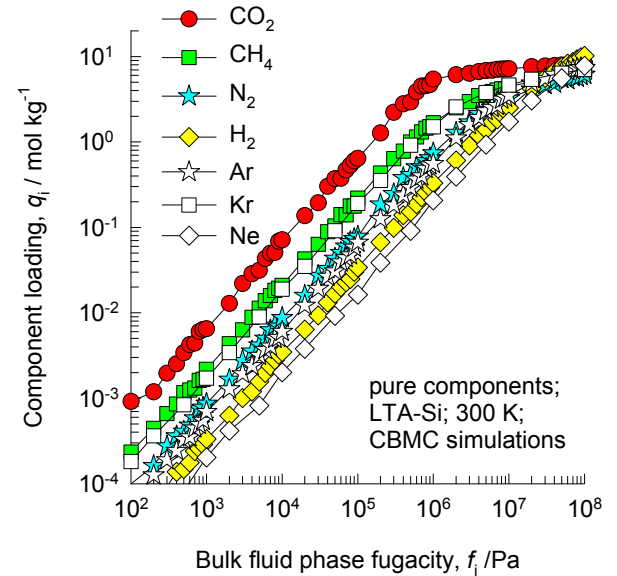
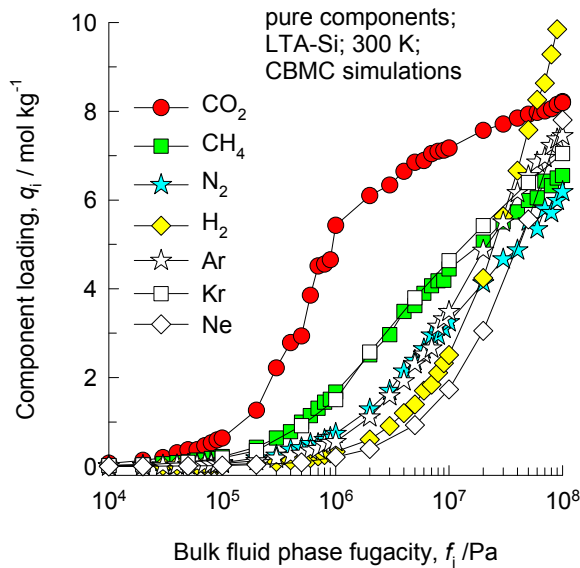
The window dimension calculated using the van der Waals diameter of framework atoms = 2.7 Å is indicated above by the arrows.

This plot of surface area versus pore dimension is determined using a combination of the DeLaunay triangulation method for pore dimension determination, and the procedure of Dürén for determination of the surface area.

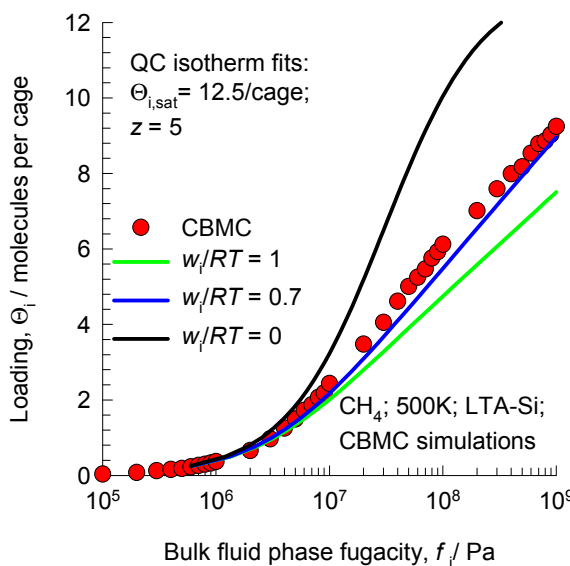


| LTA-Si | |
|--|----------|
| $a / \text{\AA}$ | 24.61 |
| $b / \text{\AA}$ | 24.61 |
| $c / \text{\AA}$ | 24.61 |
| Cell volume / \AA^3 | 14905.1 |
| conversion factor for [molec/uc] to [mol per kg Framework] | 0.0867 |
| conversion factor for [molec/uc] to [kmol/m ³] | 0.2794 |
| $\rho / [\text{kg}/\text{m}^3]$ | 1285.248 |
| MW unit cell [g/mol(framework)] | 11536.28 |
| ϕ , fractional pore volume | 0.399 |
| open space / $\text{\AA}^3/\text{uc}$ | 5944.4 |
| Pore volume / cm^3/g | 0.310 |
| Surface area / m^2/g | 896.0 |
| DeLaunay diameter / \AA | 4.10 |

LTA-Si CBMC simulations of isotherms, and isosteric heats of adsorption



LTA-Si Modeling the loading dependence of CH₄ diffusivity



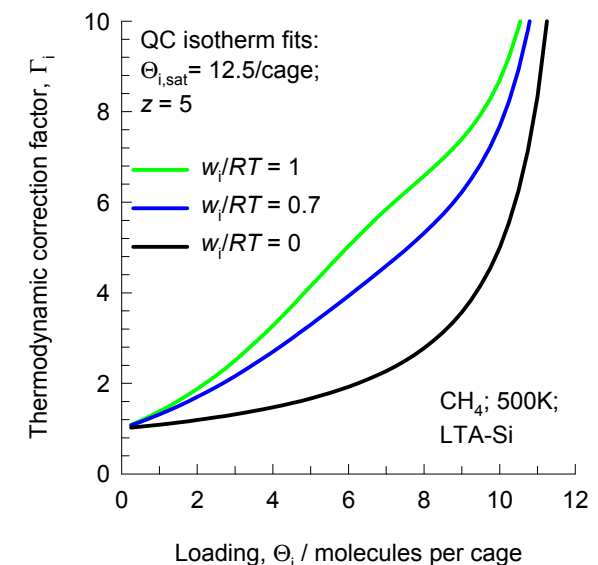
Quasi - Chemical isotherm

$$b_i f_i = \frac{\theta_i}{(1-\theta_i)} \left(\frac{2(1-\theta_i)}{\varsigma_i + 1 - 2\theta_i} \right)^z$$

$$\theta_i = c_i / c_{i,sat} = q_i / q_{i,sat} = \Theta_i / \Theta_{i,sat}$$

$$\varsigma_i = \sqrt{1 - 4\theta_i(1-\theta_i)(1 - \exp(-w_i/RT))}$$

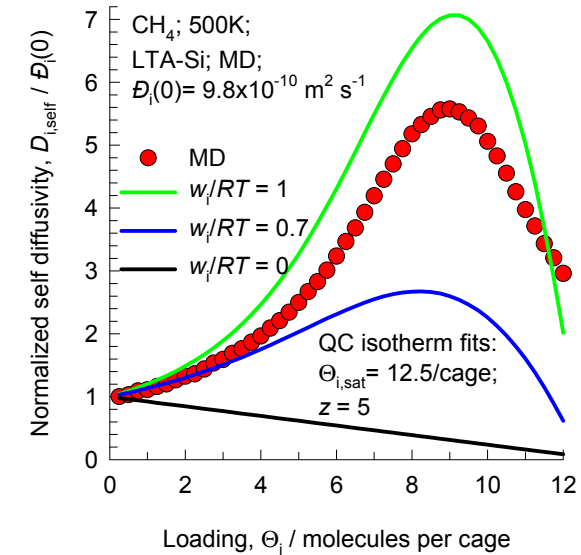
$$\Gamma_i = \frac{1}{(1-\theta_i)} \left(1 + \frac{z}{2} \frac{(1-\varsigma_i)}{\varsigma_i} \right)$$



Krishna, Paschek and Baur (2004) model

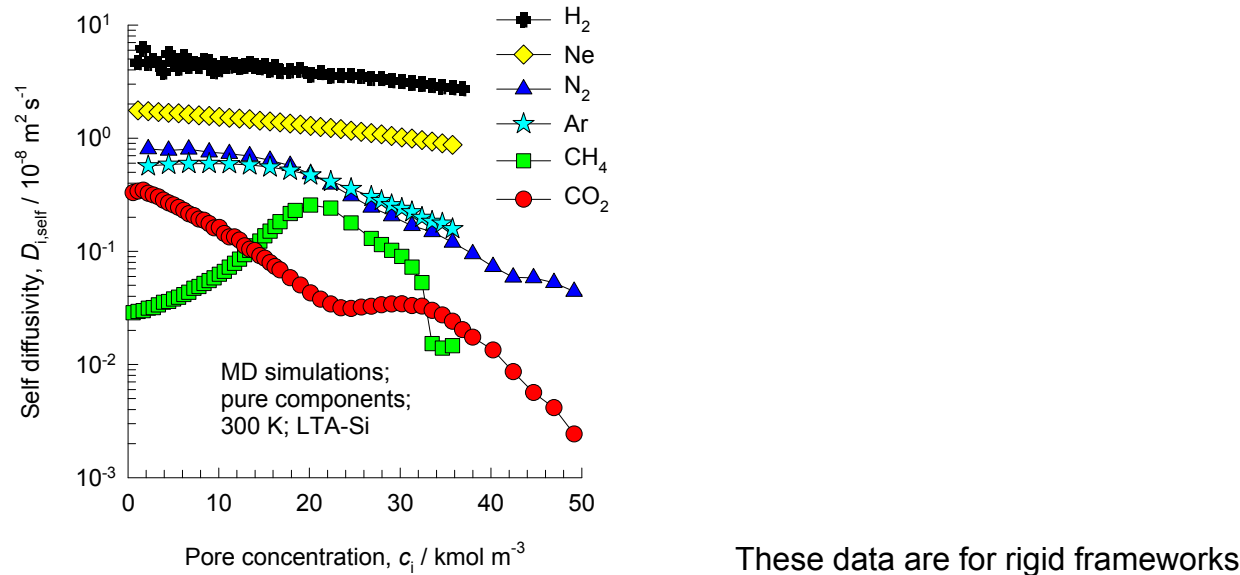
$$D_i = D_i(0) \left(\frac{1+\varsigma_i}{2(1-\theta_i)} \right)^{-z} \left(1 + \frac{(\varsigma_i - 1 + 2\theta_i) \exp(w_i/RT)}{2(1-\theta_i)} \right)^{z-1}$$

$$\varsigma_i = \sqrt{1 - 4\theta_i(1-\theta_i)(1 - \exp(-w_i/RT))}$$



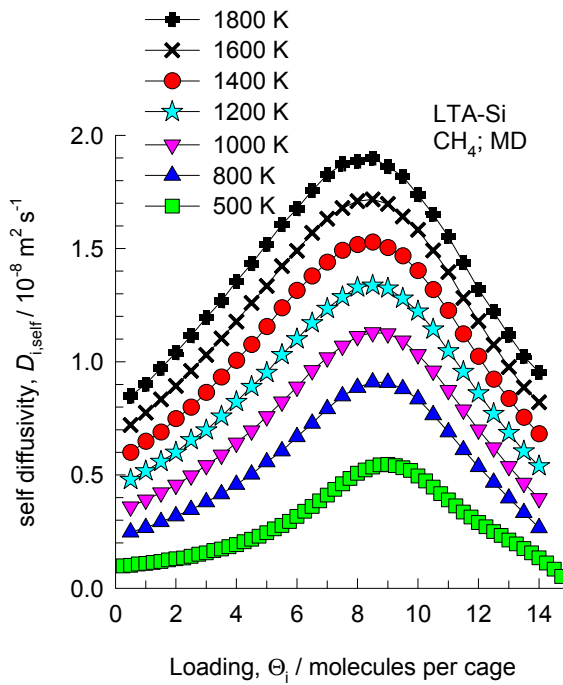
The model used to describe the concentration dependence of D_i is described in detail in Krishna, R.; Paschek, D.; Baur, R. Modelling the occupancy dependence of diffusivities in zeolites, *Microporous Mesoporous Mater.* 2004, 76, 233-246.

LTA-Si, self-diffusivities of various guest molecules

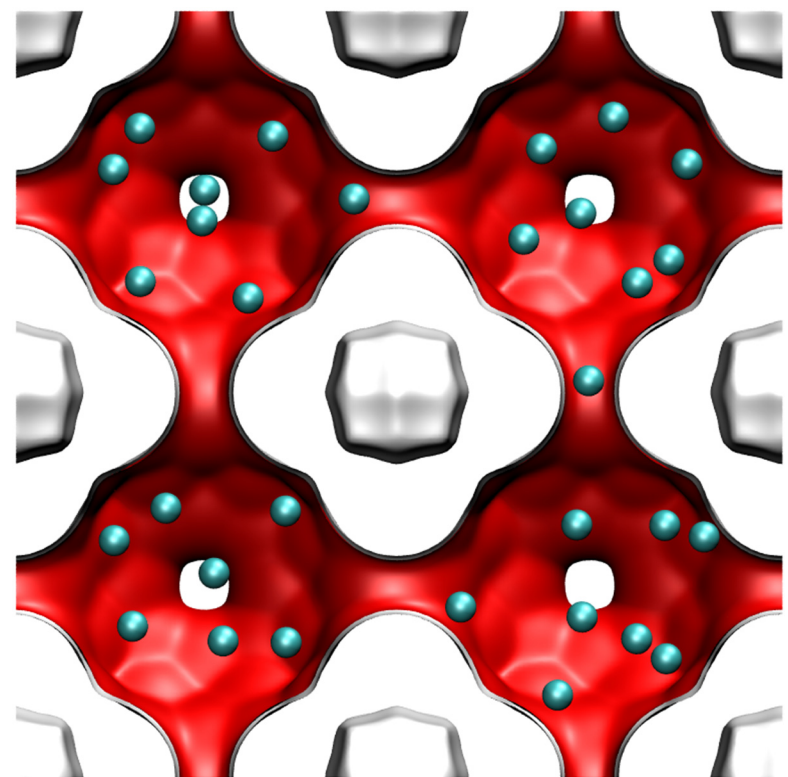
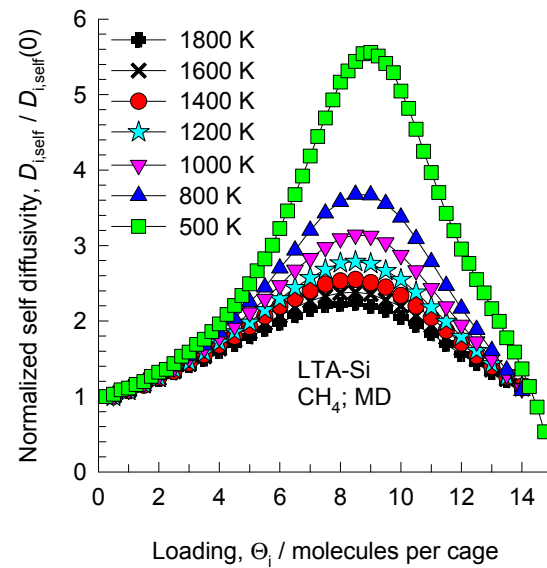


These data are for rigid frameworks

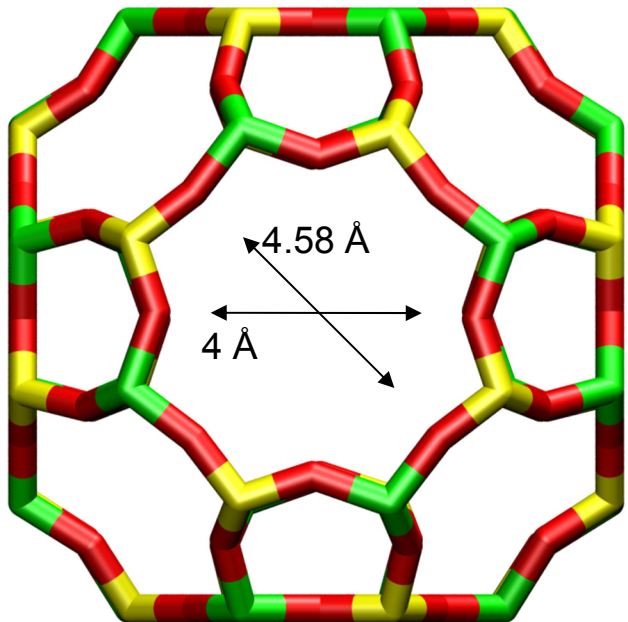
LTA-Si, self-diffusivity of CH₄



These data are for rigid frameworks



LTA-4A



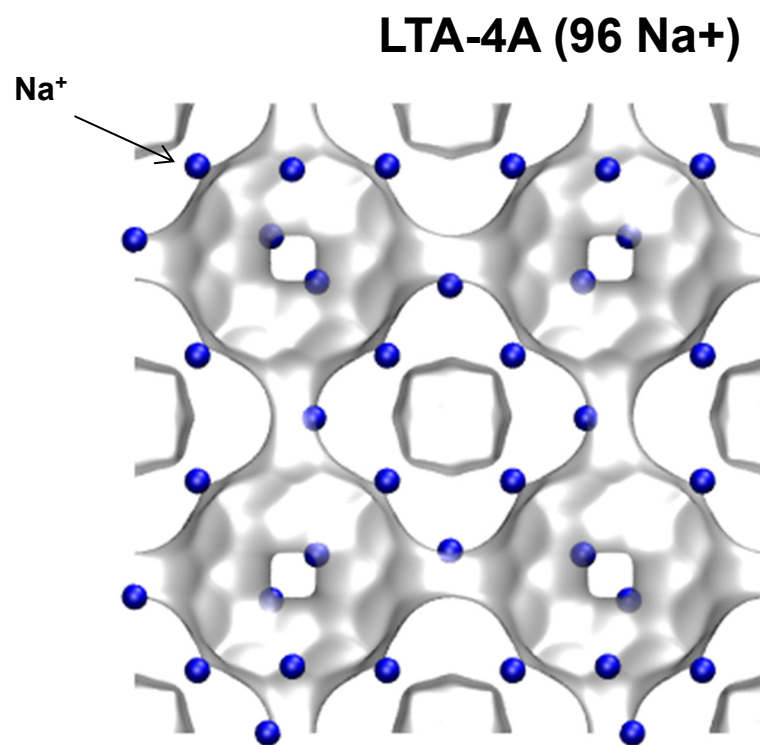
LTA-4A

The window dimension calculated using the van der Waals diameter of framework atoms = 2.7 Å is indicated above by the arrow.

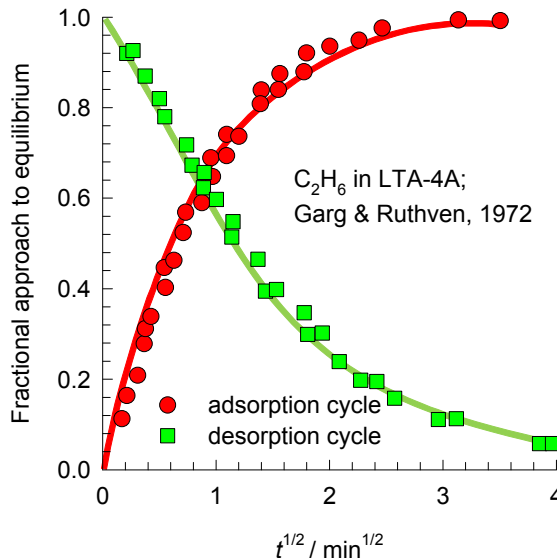
Note that the Na^+ ions partially block the windows and therefore the diffusivities in LTA-4A are significantly lower than that for LTA Si. These cannot be determined from MD.

| | LTA-4A |
|--|----------|
| $a / \text{\AA}$ | 24.555 |
| $b / \text{\AA}$ | 24.555 |
| $c / \text{\AA}$ | 24.555 |
| Cell volume / \AA^3 | 14805.39 |
| conversion factor for [molec/uc] to [mol per kg Framework] | 0.0733 |
| conversion factor for [molec/uc] to [kmol/m ³] | 0.2991 |
| $\rho [\text{kg/m}^3]$ (with cations) | 1529.55 |
| MW unit cell [g/mol(framework+cations)] | 13637.27 |
| ϕ , fractional pore volume | 0.375 |
| open space / $\text{\AA}^3/\text{uc}$ | 5552.0 |
| Pore volume / cm^3/g | 0.245 |
| Surface area / m^2/g | |
| DeLaunay diameter / \AA | 4.00 |

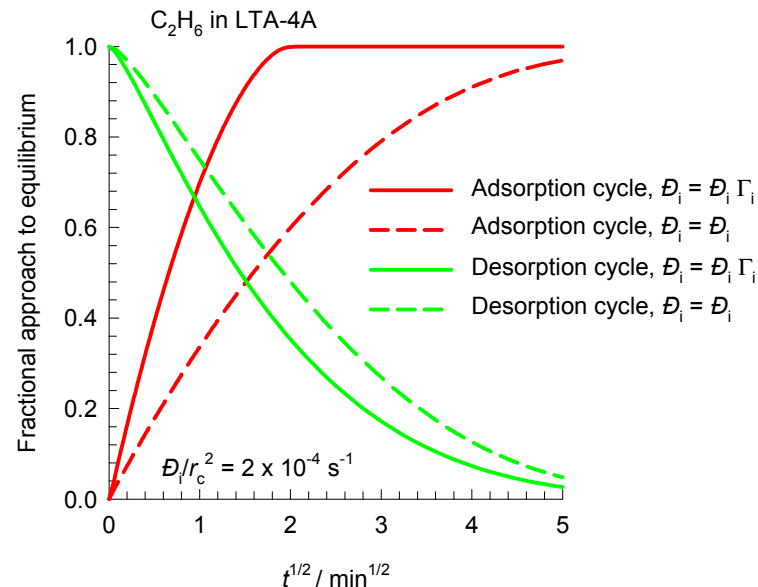
LTA-4A



LTA-4A: Transient uptake of C₂H₆



The data are re-plotted using the information contained in
Garg, D. R.; Ruthven, D. M. Effect of the concentration dependence of diffusivity on zeolitic sorption curves, Chem. Eng. Sci. 1972, 27, 417-423. .

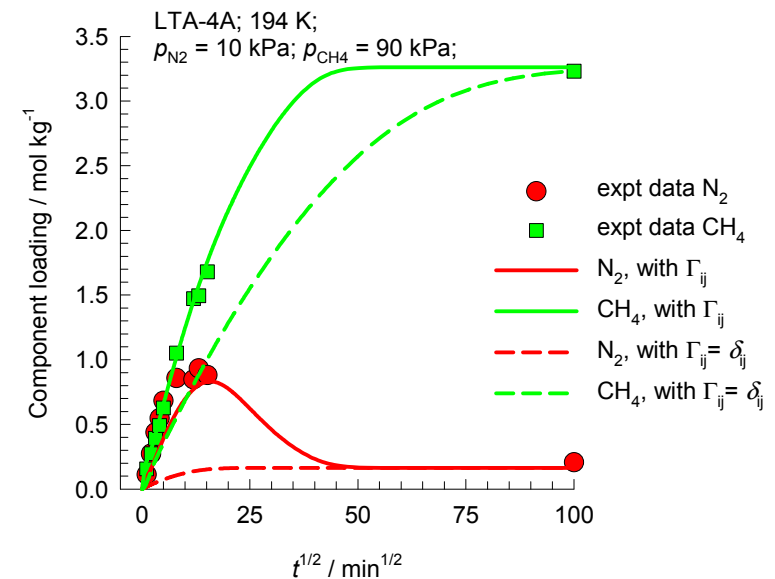
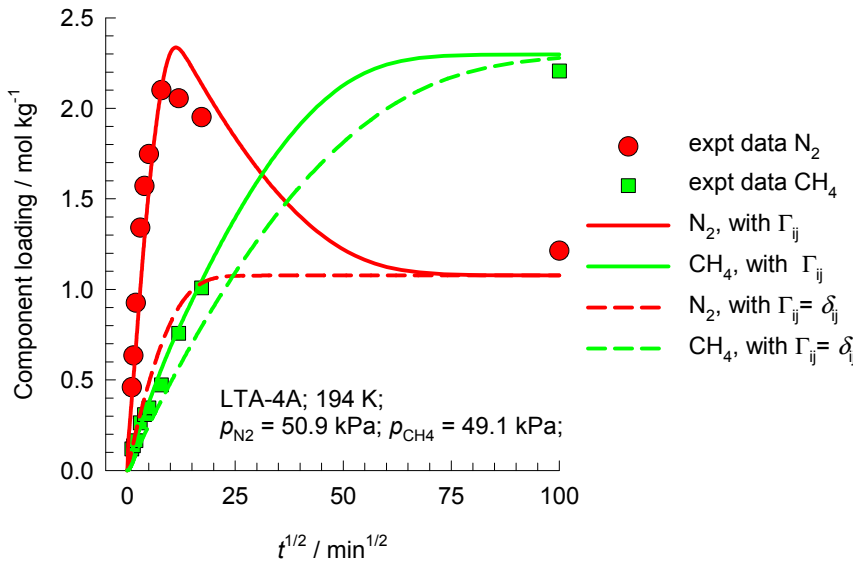


The continuous solid lines are simulations including the thermodynamic correction factor, Γ_i . These simulations capture the asymmetry in the adsorption and desorption cycles.

The dashed lines are simulations in which $\Gamma_i = 1$. These simulations anticipate that the adsorption and desorption cycles are symmetric.

The simulations assume a constant, loading independent M-S diffusivity, D_i . We take $D_i/r_c^2 = 0.0002 \text{ s}^{-1}$ where r_c is the crystal radius.

LTA-4A: Transient uptake of N₂ and CH₄



The experimental data are re-plotted using the information contained in
 Habgood, H. W. The kinetics of molecular sieve action. Sorption of nitrogen-methane mixtures by Linde molecular sieve 4A, Canad. J. Chem. 1958, 36, 1384-1397.

In these simulations, both the M-S diffusivities are assumed to be independent of loading. The overshoot in N₂ is not, therefore, a result of the loading dependence of its M-S diffusivity.

The overshoot in the N₂ uptake is a direct consequence of thermodynamic coupling caused by the off-diagonal elements of

$$\begin{bmatrix} \Gamma_{11} & \Gamma_{12} \\ \Gamma_{21} & \Gamma_{22} \end{bmatrix} \quad \text{where} \quad \Gamma_{ij} = \frac{q_i}{f_i} \frac{\partial f_j}{\partial q_i}$$

This has been demonstrated by

Krishna, R.; Baur, R. Modelling issues in zeolite based separation processes, Sep. Purif. Technol. 2003, 33, 213-254.

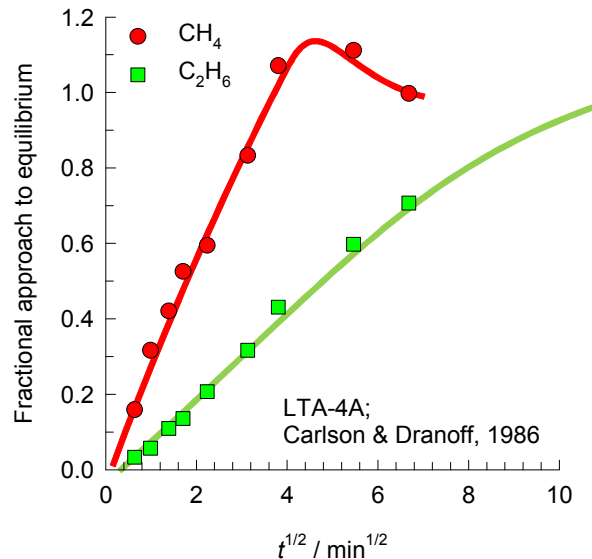
If the thermodynamic coupling is ignored, i.e. we assume

$$\Gamma_i = \delta_{ij}; \quad \text{Kronecker delta}$$

$$\begin{bmatrix} \Gamma_{11} & \Gamma_{12} \\ \Gamma_{21} & \Gamma_{22} \end{bmatrix} = \begin{bmatrix} 1 & 0 \\ 0 & 1 \end{bmatrix}$$

the N₂ overshoot disappears.

LTA-4A: Transient uptake of CH₄ and C₂H₆



The data are re-plotted using the information contained in
Carlson, N. W.; Dranoff, J. S. Competitive adsorption of methane and ethane on 4A zeolite. Fundamentals of Adsorption; Edited by A.I. Liapis, AIChE: New York, 1986.

In these simulations, both the M-S diffusivities are assumed to be independent of loading. The overshoot in CH₄ is not, therefore, a result of the loading dependence of its M-S diffusivity.

The overshoot in the CH₄ uptake is a direct consequence of thermodynamic coupling caused by the off-diagonal elements of

$$\begin{bmatrix} \Gamma_{11} & \Gamma_{12} \\ \Gamma_{21} & \Gamma_{21} \end{bmatrix} \quad \text{where} \quad \Gamma_{ij} = \frac{q_i}{f_i} \frac{\partial f_j}{\partial q_i}$$

This has been demonstrated by

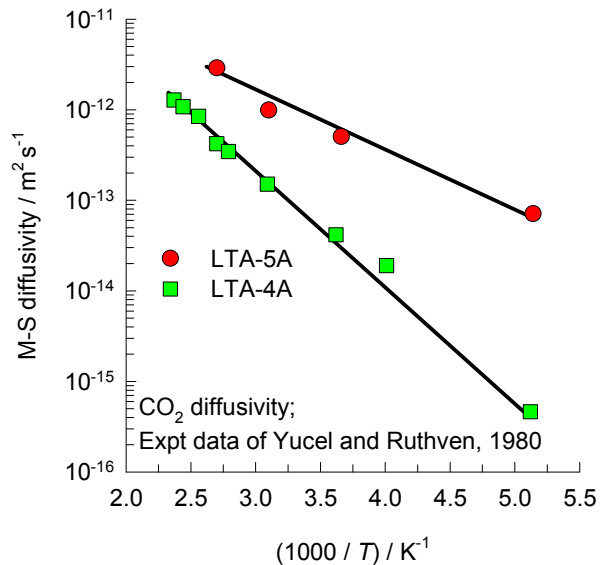
Krishna, R. Diffusion of binary mixtures in microporous materials: Overshoot and roll-up phenomena, Int. Commun. Heat Mass Transf. 2000, 27, 893-902.

If the thermodynamic coupling is ignored, i.e. we assume

$$\begin{bmatrix} \Gamma_{11} & \Gamma_{12} \\ \Gamma_{21} & \Gamma_{21} \end{bmatrix} = \begin{bmatrix} 1 & 0 \\ 0 & 1 \end{bmatrix}$$

the CH₄ overshoot disappears.

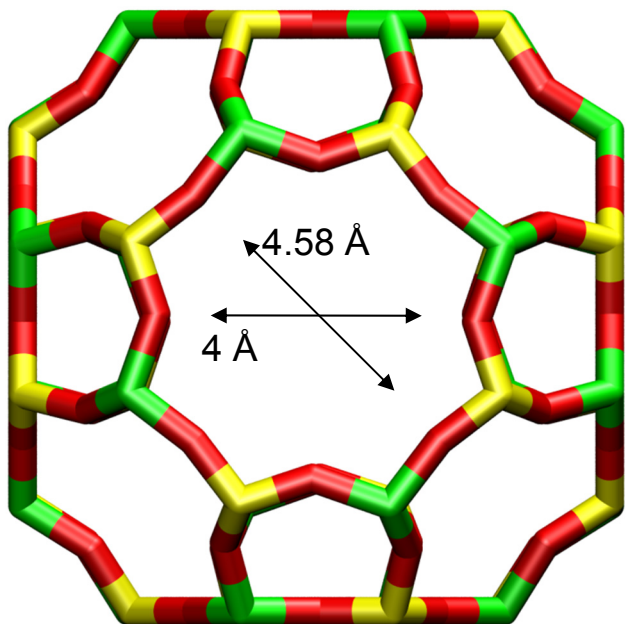
LTA-4A vs LTA-5A diffusivities of CO₂



The experimental data are from
Yucel, H.; Ruthven, D.M. Diffusion of CO₂ in 4A and 5A zeolite crystals. Journal of Colloid and Interface Science 1980, 74, 186-195.

Note that no MD simulation results are presented for LTA-4A because the diffusivities are too low to be determined accurately.

LTA-5A

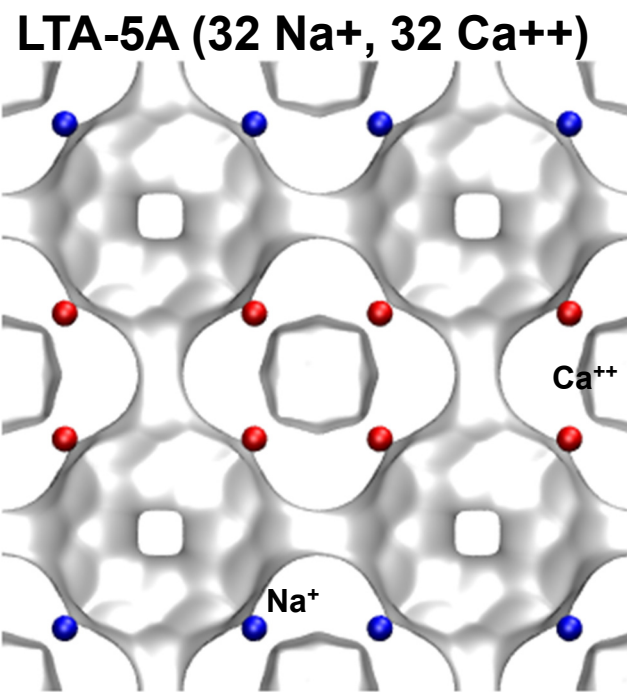


LTA-5A

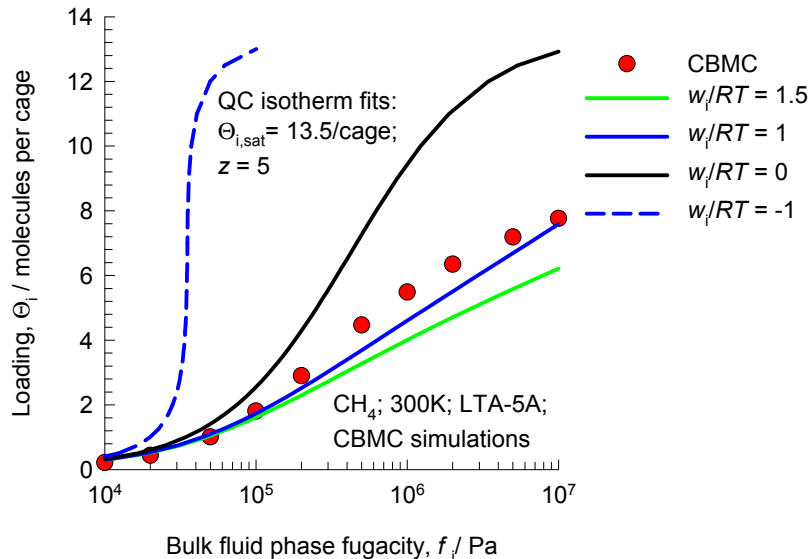
The window dimension calculated using the van der Waals diameter of framework atoms = 2.7 Å is indicated above by the arrow.

| LTA-5A | |
|--|----------|
| $a / \text{\AA}$ | 24.555 |
| $b / \text{\AA}$ | 24.555 |
| $c / \text{\AA}$ | 24.555 |
| Cell volume / \AA^3 | 14805.39 |
| conversion factor for [molec/uc] to [mol per kg Framework] | 0.0744 |
| conversion factor for [molec/uc] to [kmol/m ³] | 0.2955 |
| $\rho [\text{kg/m}^3]$ (with cations) | 1508.376 |
| MW unit cell [g/mol(framework+cations)] | 13448.48 |
| ϕ , fractional pore volume | 0.380 |
| open space / $\text{\AA}^3/\text{uc}$ | 5620.4 |
| Pore volume / cm^3/g | 0.252 |
| Surface area / m^2/g | |
| DeLaunay diameter / \AA | 4.00 |

LTA-5A



LTA-5A Modeling the loading dependence of CH₄ diffusivity at 300 K



Quasi - Chemical isotherm

$$b_i f_i = \frac{\theta_i}{(1-\theta_i)} \left(\frac{2(1-\theta_i)}{\varsigma_i + 1 - 2\theta_i} \right)^z$$

$$\theta_i = c_i / c_{i,sat} = q_i / q_{i,sat} = \Theta_i / \Theta_{i,sat}$$

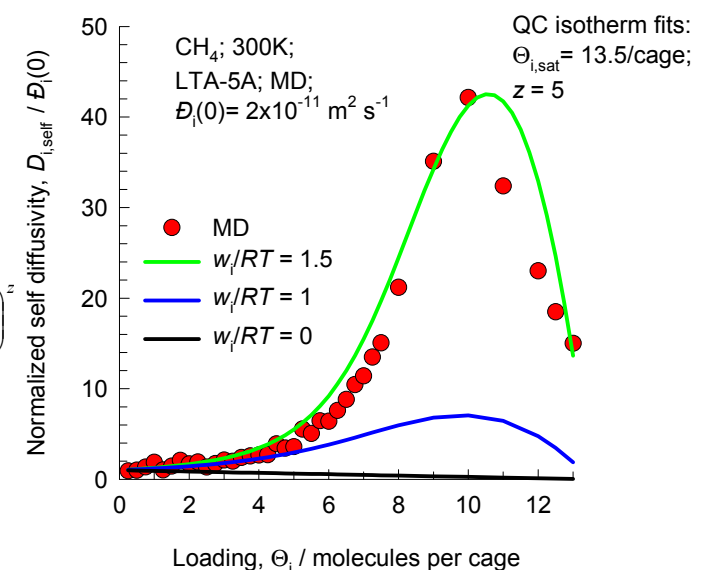
$$\varsigma_i = \sqrt{1 - 4\theta_i(1-\theta_i)(1 - \exp(-w_i/RT))}$$

$$\Gamma_i = \frac{1}{(1-\theta_i)} \left(1 + \frac{z}{2} \frac{(1-\varsigma_i)}{\varsigma_i} \right)$$

Krishna, Paschek and Baur (2004) model

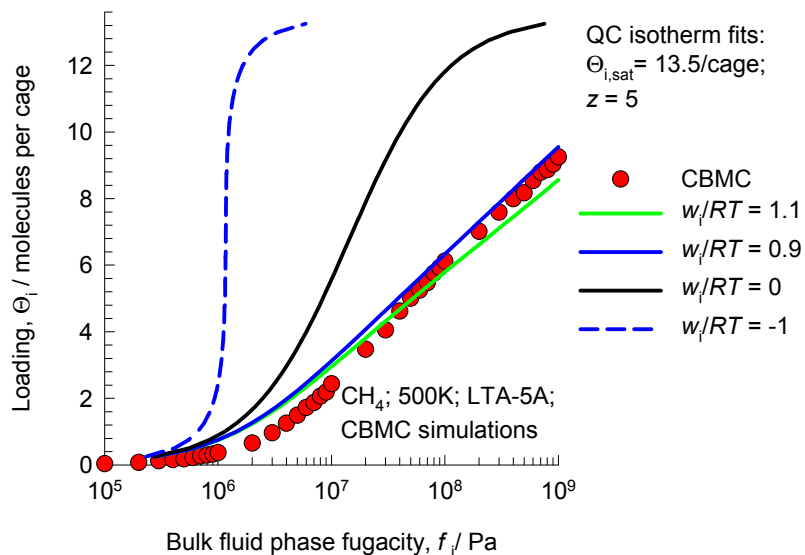
$$D_i = D_i(0) \left(\frac{1+\varsigma_i}{2(1-\theta_i)} \right)^{-z} \left(1 + \frac{(\varsigma_i - 1 + 2\theta_i)\exp(w_i/RT)}{2(1-\theta_i)} \right)^z$$

$$\varsigma_i = \sqrt{1 - 4\theta_i(1-\theta_i)(1 - \exp(-w_i/RT))}$$



The model used to describe the concentration dependence of D_i is described in detail in
 Krishna, R.; Paschek, D.; Baur, R. Modelling the occupancy dependence of diffusivities in zeolites, Microporous Mesoporous Mater. 2004, 76, 233-246.

LTA-5A Modeling the loading dependence of CH₄ diffusivity at 500 K



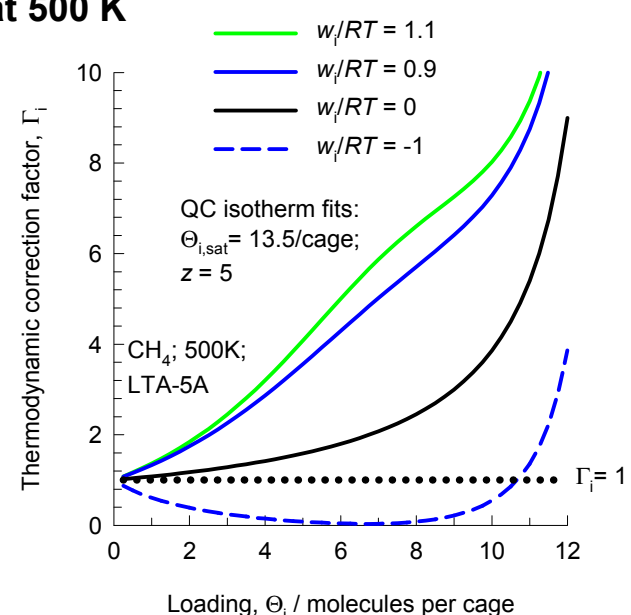
Quasi - Chemical isotherm

$$\beta_i f_i = \frac{\theta_i}{(1-\theta_i)} \left(\frac{2(1-\theta_i)}{\varsigma_i + 1 - 2\theta_i} \right)^z$$

$$\theta_i = c_i / c_{i,sat} = q_i / q_{i,sat} = \Theta_i / \Theta_{i,sat}$$

$$\varsigma_i = \sqrt{1 - 4\theta_i(1-\theta_i)(1 - \exp(-w_i/RT))}$$

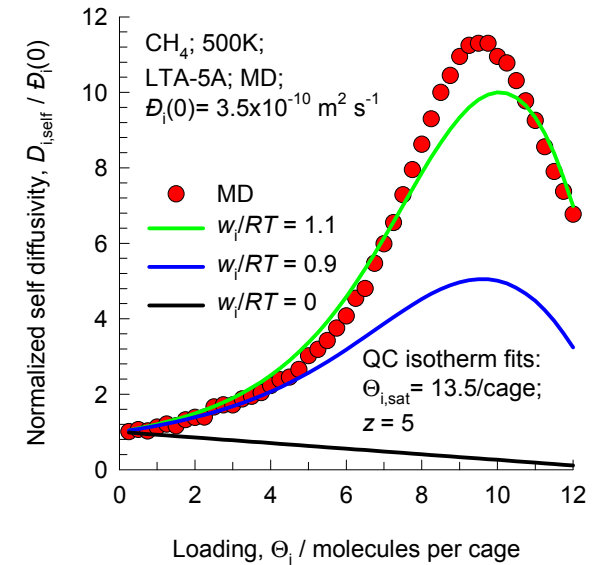
$$\Gamma_i = \frac{1}{(1-\theta_i)} \left(1 + \frac{z}{2} \frac{(1-\varsigma_i)}{\varsigma_i} \right)$$



Krishna, Paschek and Baur (2004) model

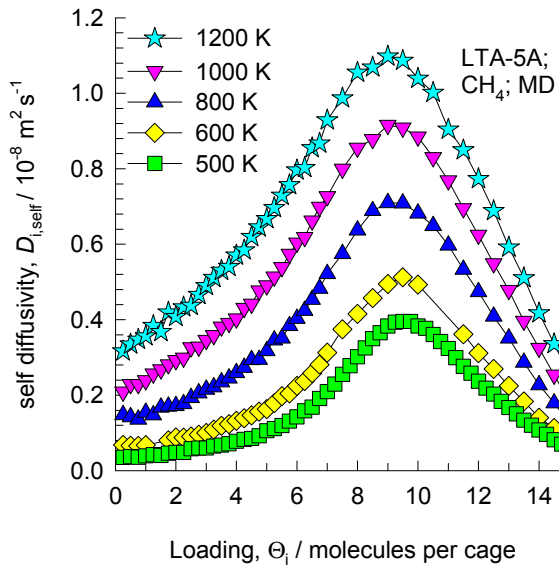
$$D_i = D_i(0) \left(\frac{1 + \varsigma_i}{2(1 - \theta_i)} \right)^{-z} \left(1 + \frac{(\varsigma_i - 1 + 2\theta_i) \exp(w_i/RT)}{2(1 - \theta_i)} \right)^{z-1}$$

$$\varsigma_i = \sqrt{1 - 4\theta_i(1-\theta_i)(1 - \exp(-w_i/RT))}$$

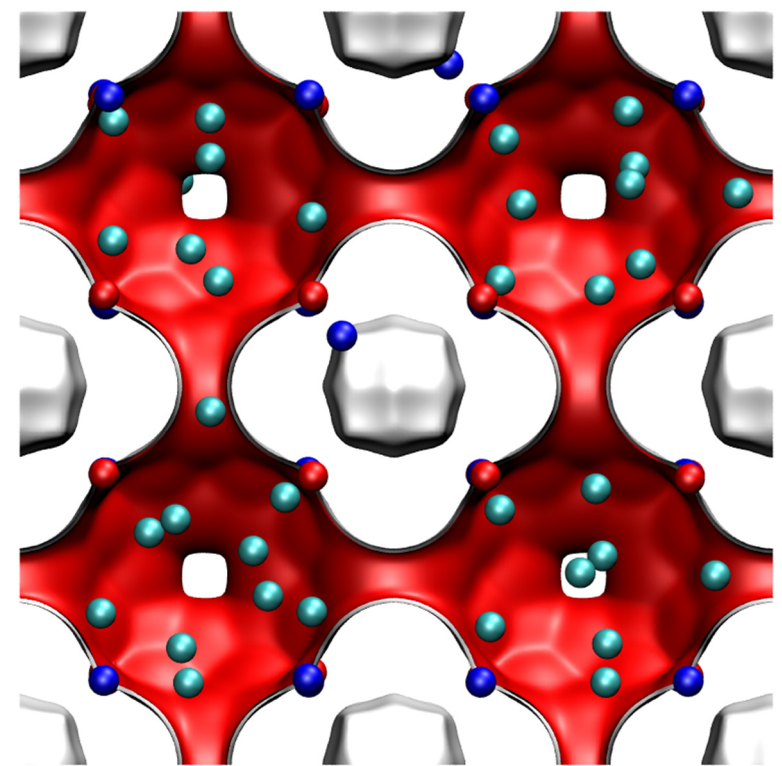
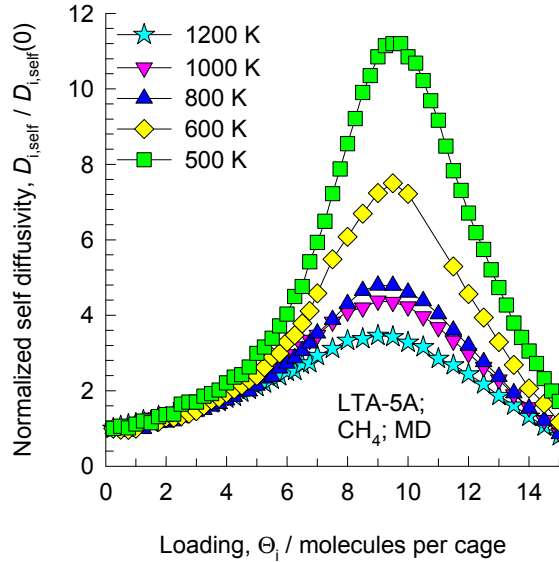


The model used to describe the concentration dependence of D_i is described in detail in Krishna, R.; Paschek, D.; Baur, R. Modelling the occupancy dependence of diffusivities in zeolites, *Microporous Mesoporous Mater.* 2004, 76, 233-246.

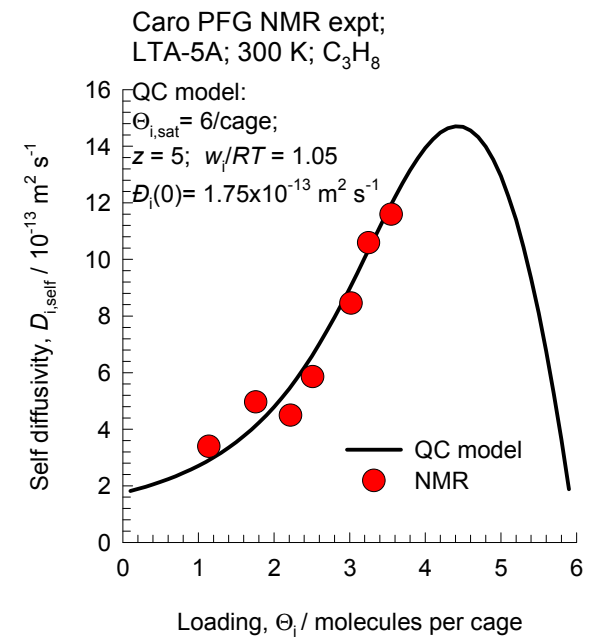
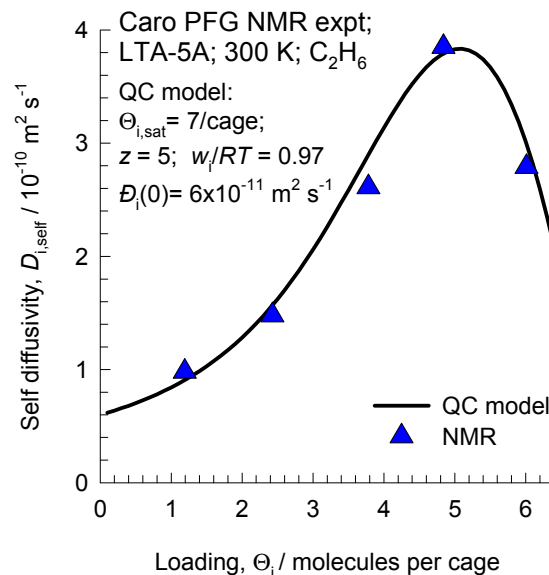
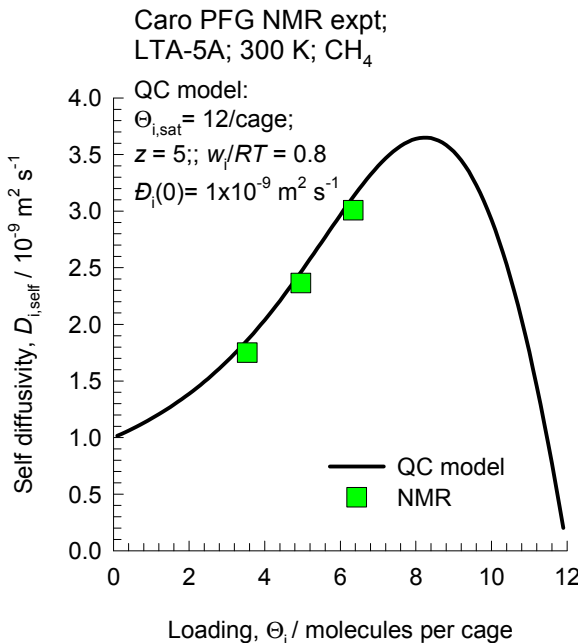
LTA-5A, diffusivity of CH₄



These data are for rigid frameworks



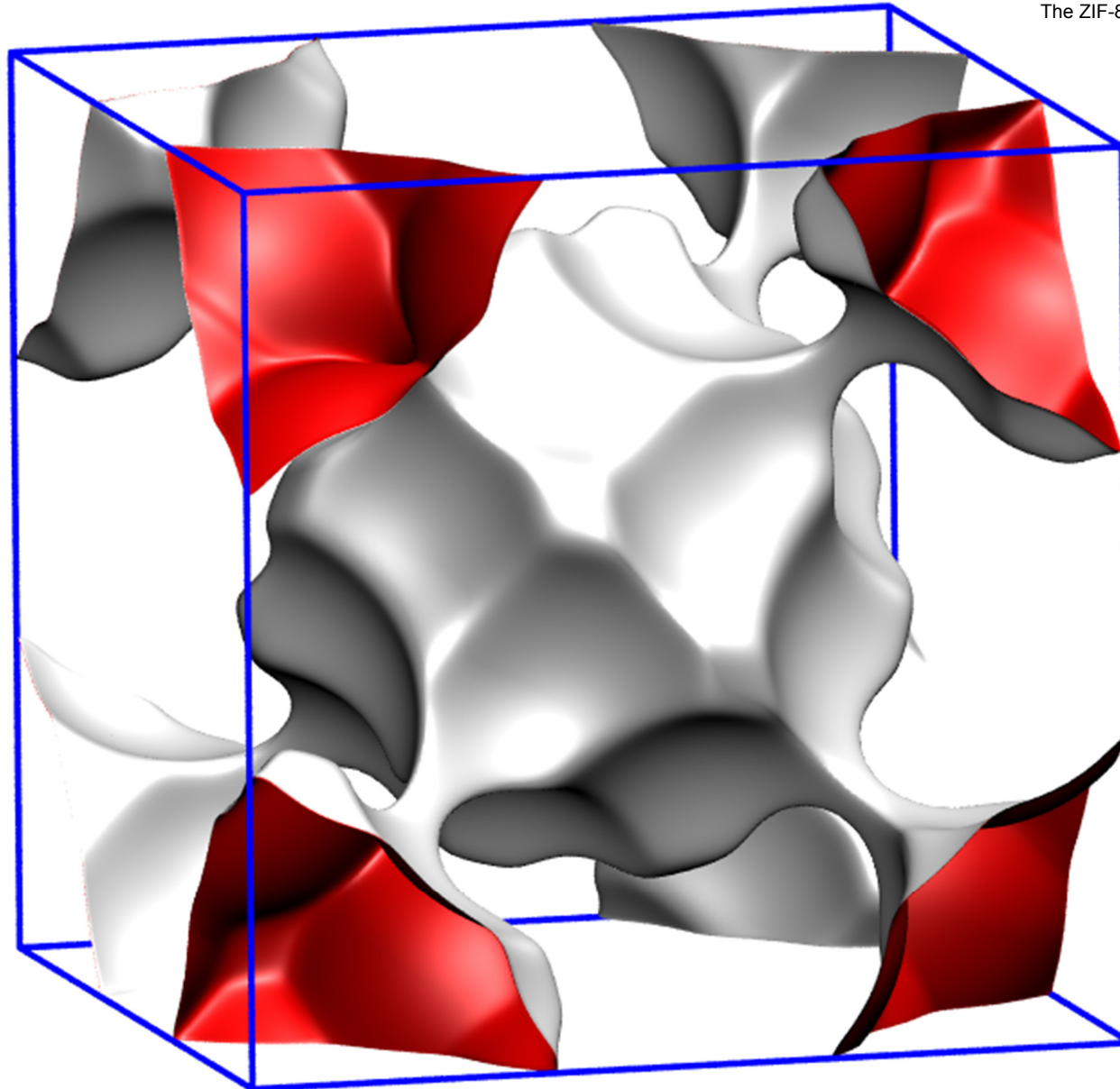
LTA-5A Modeling the MR experiments of Caro



The experimental data are from

Caro, J.; Bülow, M.; Schirmer, W.; Kärger, J.; Heink, W.; Pfeifer, H. Microdynamics of methane, ethane and propane in ZSM-5 type zeolites. Journal of the Chemical Society, Faraday Transactions 1985, 81, 2541-2550.

SOD-Si pore landscape



The ZIF-8 structure is analogous to that of SOD.

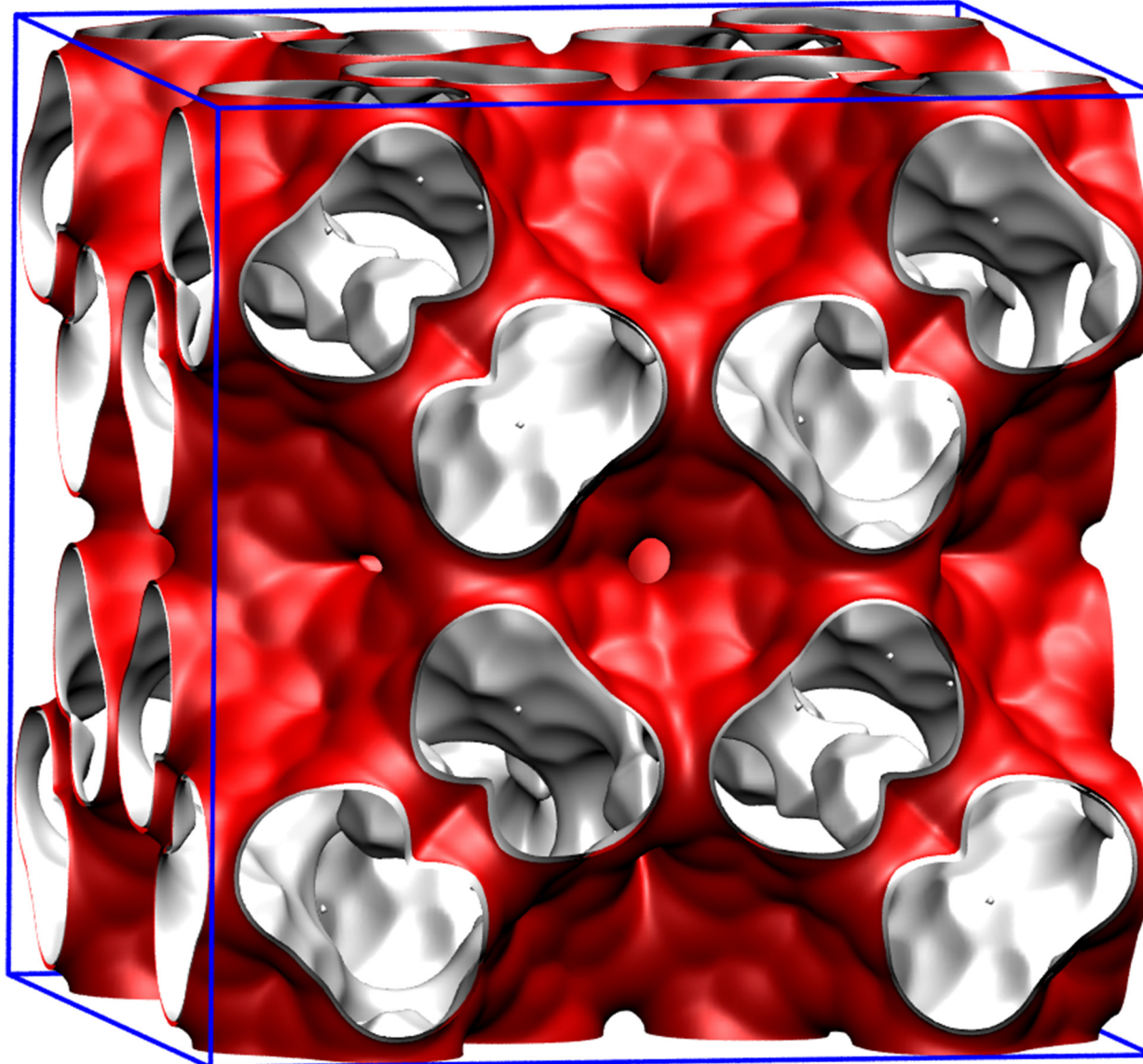
There are 2 cages per unit cell. The volume of one SOD cage is 84.8 \AA^3 , significantly smaller than that of ZIF-8 (1168 \AA^3), its structural analog.

Structural information from: C. Baerlocher, L.B. McCusker, Database of Zeolite Structures, International Zeolite Association, <http://www.iza-structure.org/databases/>

SOD-Si dimensions

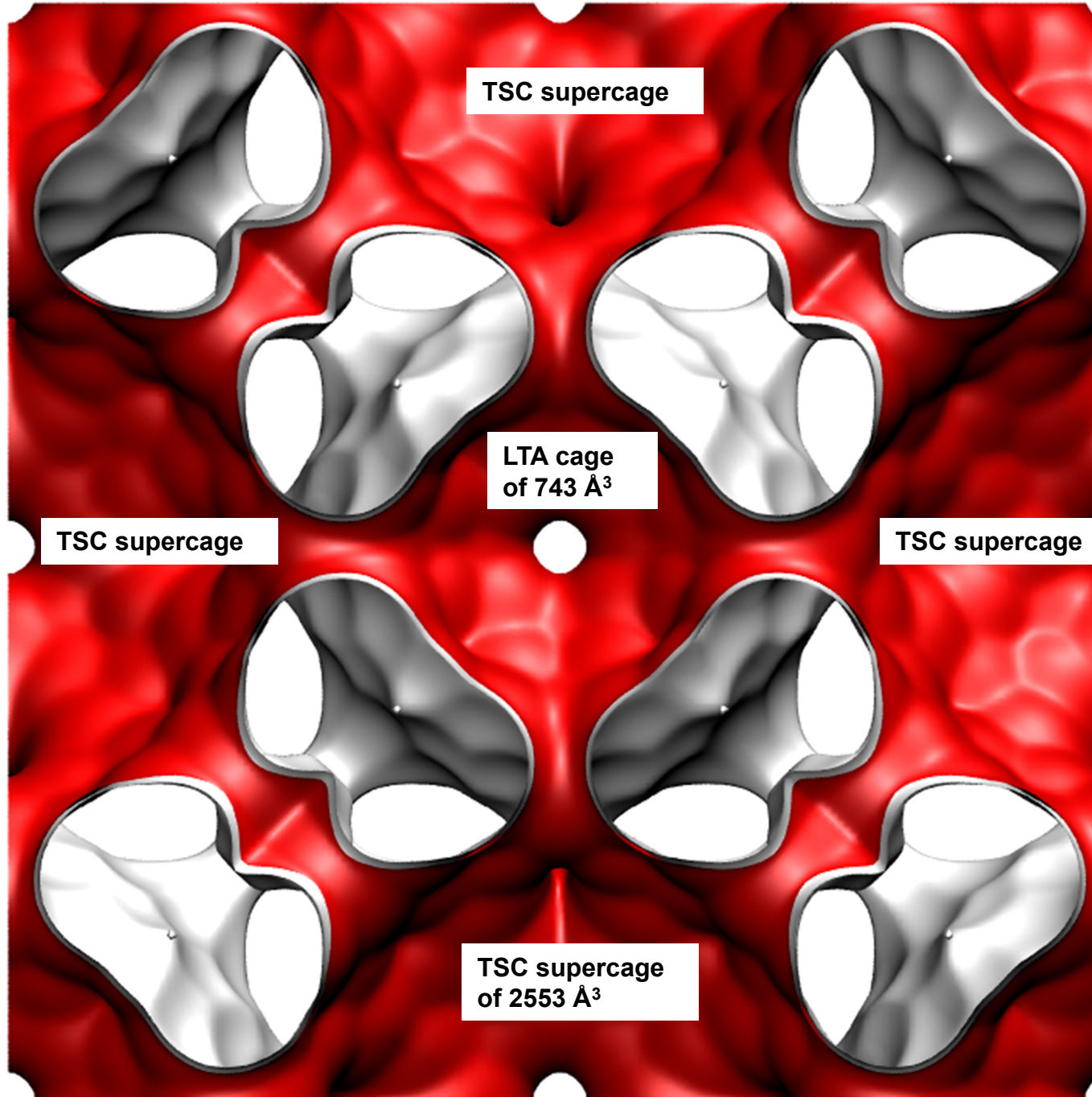
| | SOD-Si |
|--|----------|
| a /Å | 8.89 |
| b /Å | 8.89 |
| c /Å | 8.89 |
| Cell volume / Å ³ | 702.5954 |
| conversion factor for [molec/uc] to [mol per kg Framework] | 1.3869 |
| conversion factor for [molec/uc] to [kmol/m ³] | 9.7908 |
| ρ [kg/m ³] | 1704.106 |
| MW unit cell [g/mol(framework)] | 721.0176 |
| ϕ , fractional pore volume | 0.241 |
| open space / Å ³ /uc | 169.6 |
| Pore volume / cm ³ /g | 0.142 |
| Surface area /m ² /g | |
| DeLaunay diameter /Å | 2.47 |

TSC landscape



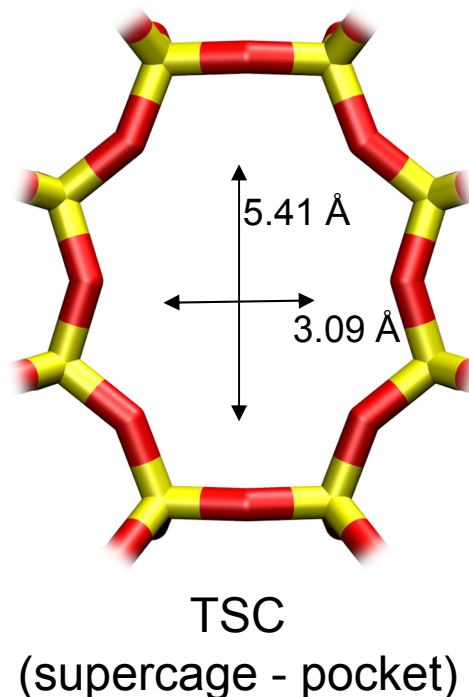
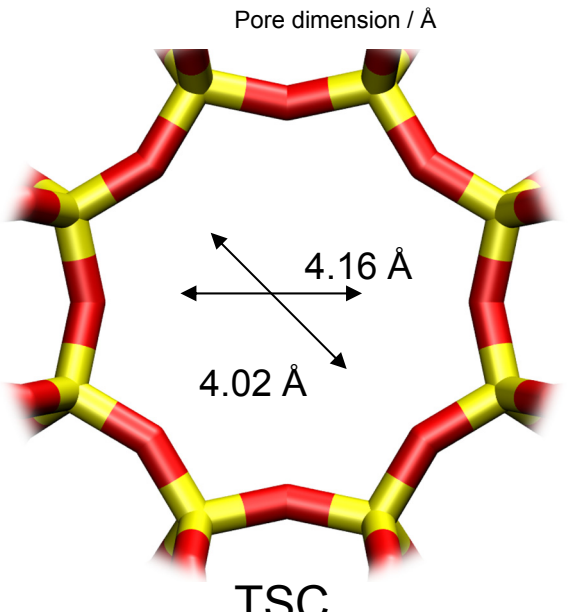
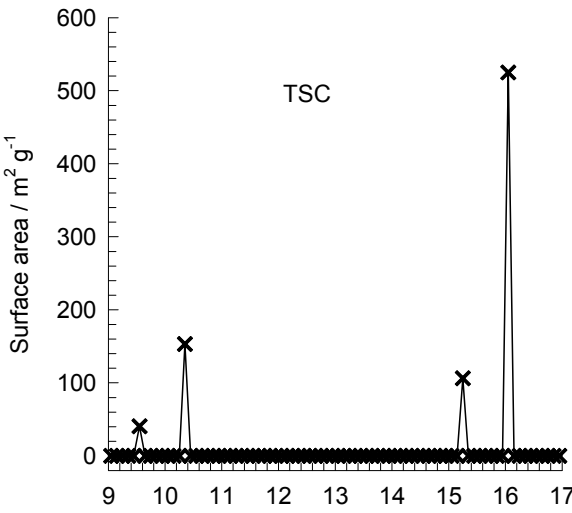
**Unit cell
of TSC**

Structural information from: C. Baerlocher, L.B. McCusker, Database of Zeolite Structures, International Zeolite Association,
<http://www.iza-structure.org/databases/>



8-ring windows of two sizes:
 $4.2 \times 4.2 \text{ \AA}$ along [100]
 $3.1 \times 5.6 \text{ \AA}$ along [110]

**Front
plane of
unit cell
of TSC**

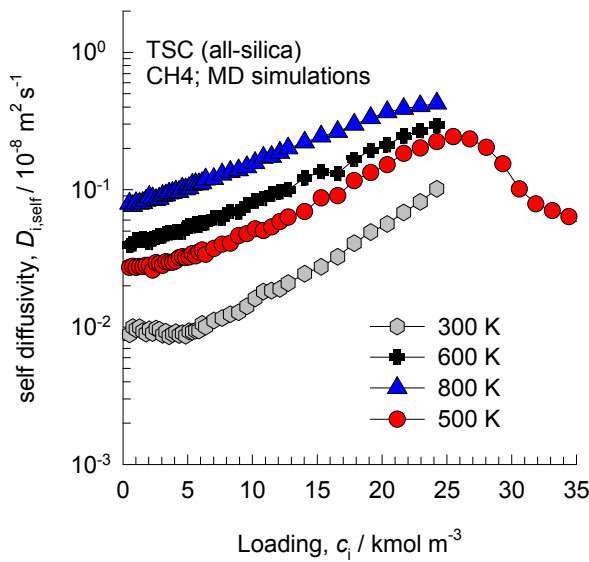
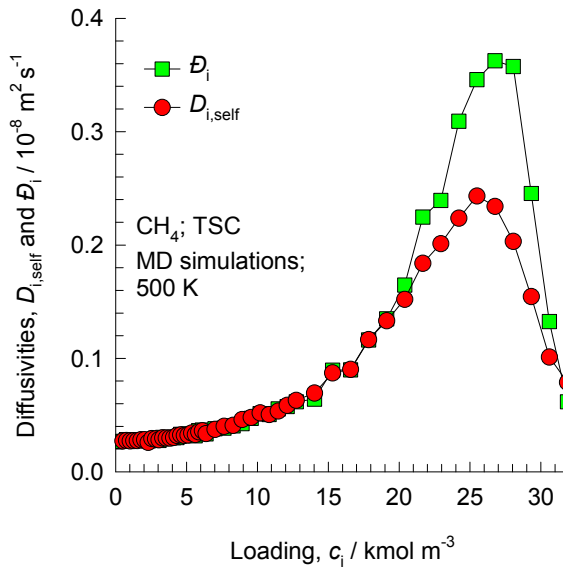


TSC window and pore dimensions

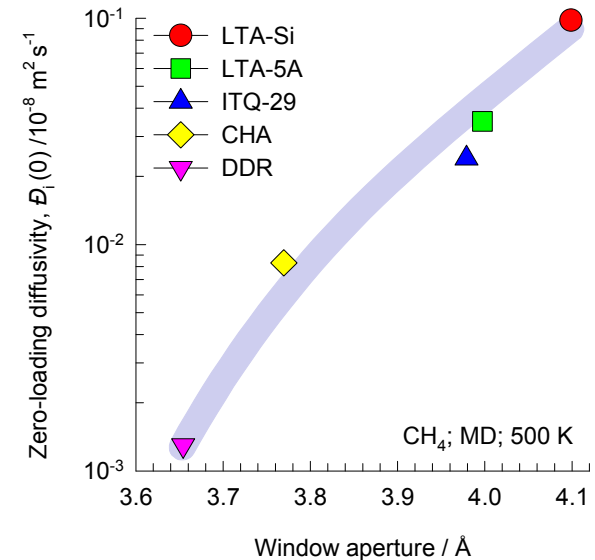
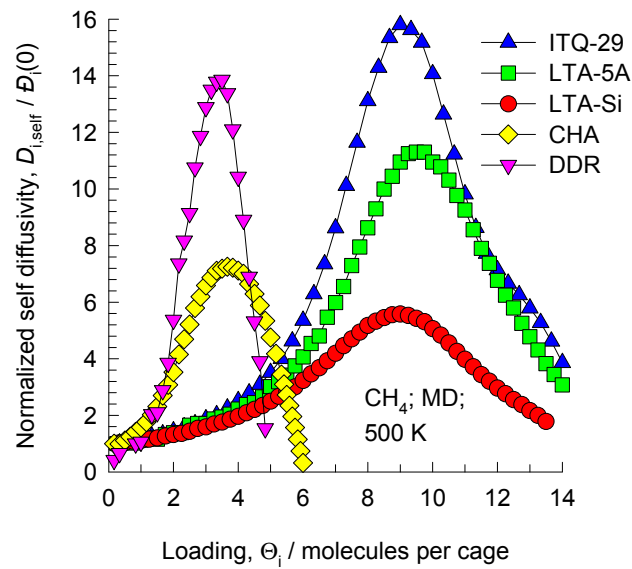
| | TSC |
|--|----------|
| $a / \text{\AA}$ | 30.742 |
| $b / \text{\AA}$ | 30.742 |
| $c / \text{\AA}$ | 30.742 |
| Cell volume / \AA^3 | 29053.36 |
| conversion factor for [molec/uc] to [mol per kg Framework] | 0.0433 |
| conversion factor for [molec/uc] to [kmol/m^3] | 0.1260 |
| $\rho / \text{kg/m}^3$ | 1318.729 |
| MW unit cell [g/mol(framework)] | 23072.56 |
| ϕ , fractional pore volume | 0.454 |
| open space / $\text{\AA}^3/\text{uc}$ | 13182.6 |
| Pore volume / cm^3/g | 0.344 |
| Surface area / m^2/g | 829.0 |
| DeLaunay diameter / \AA | 4.02 |

The window dimension calculated using the van der Waals diameter of framework atoms = 2.7 Å are indicated above by the arrows. It is likely that the pockets are inaccessible due to the narrow constriction of 3.092 Å. Another point to note is that the dimensions provided in the IZA website do not appear to be correct for the window on the left.

TSC MD simulations of unary self-diffusivities



Comparing CH₄ diffusivities in 8-ring zeolites

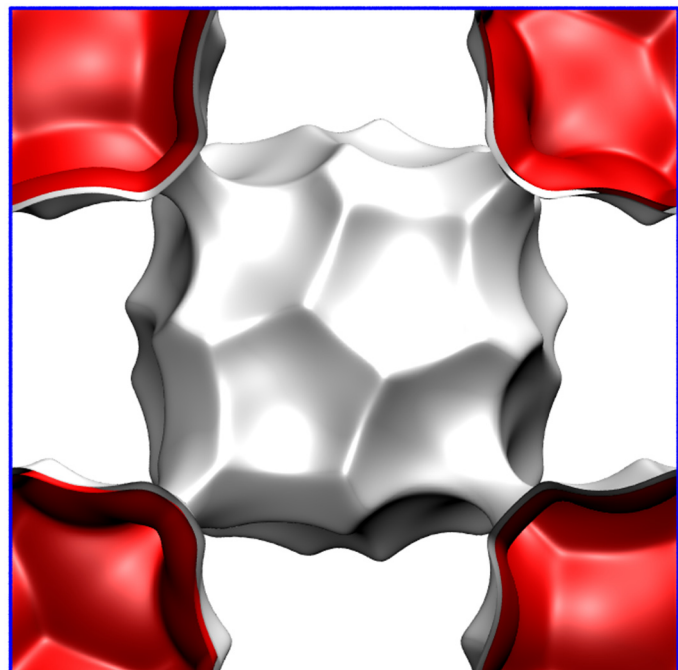


ZIF-8 pore landscapes

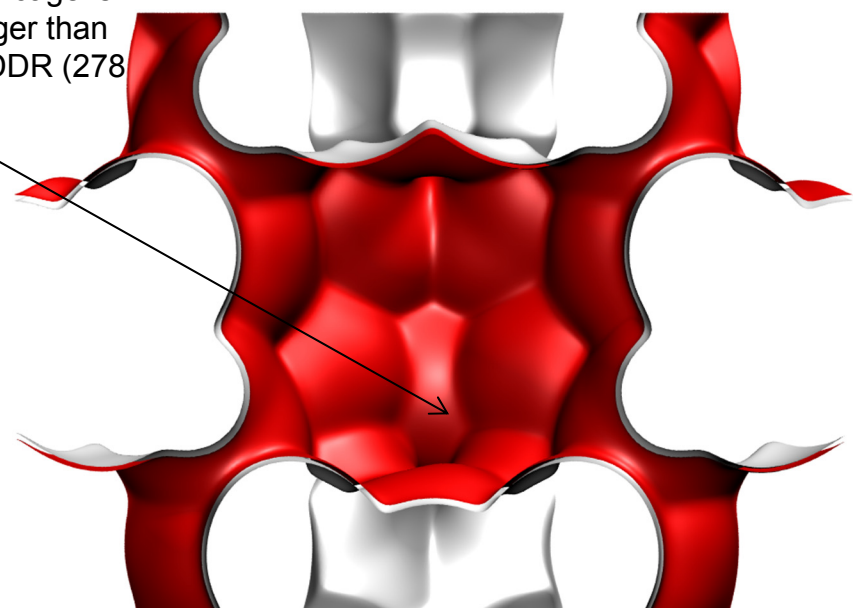
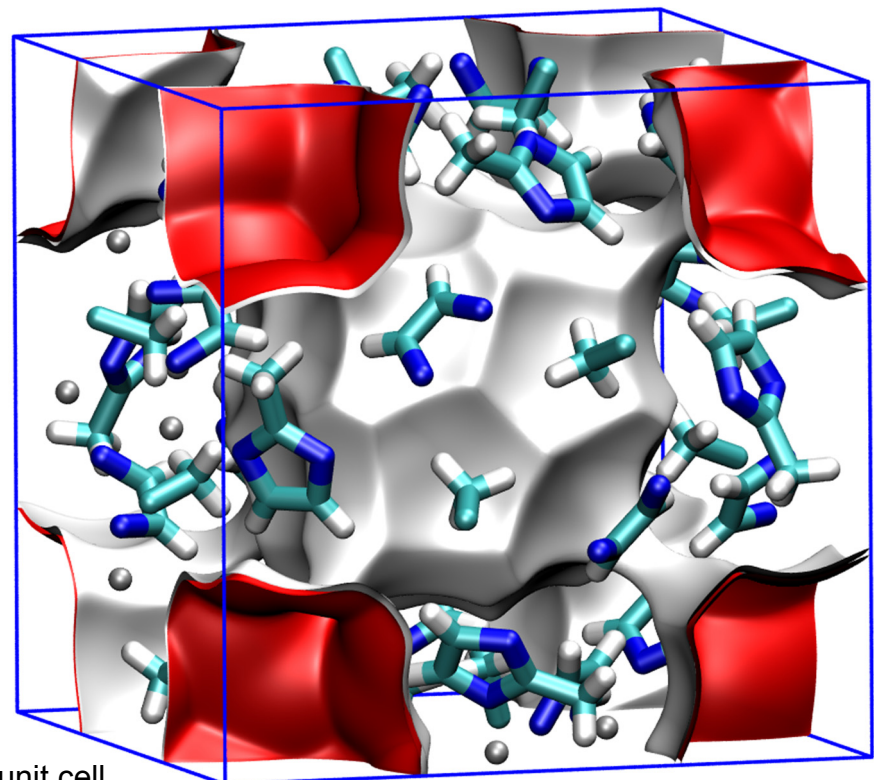
The ZIF-8 = $\text{Zn}(\text{methylimidazole})_2$ structure was taken from

R. Banerjee, A. Phan, B. Wang, C. Knobler, H. Furukawa, M. O'Keeffe, O.M. Yaghi, High-Throughput Synthesis of Zeolitic Imidazolate Frameworks and Application to CO_2 Capture, *Science* 319 (2008) 939-943.

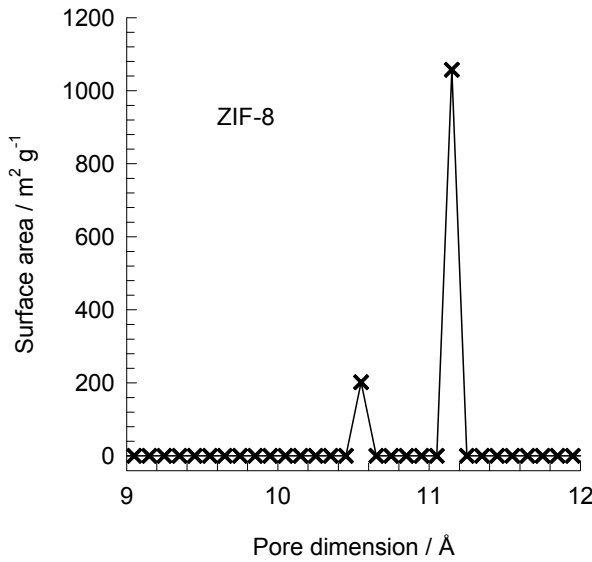
The original structural data (cif file) contains solvent molecules; these were removed and the solvent-free structures were simulated.



There are 2 cages per unit cell.
The volume of one ZIF-8 cage is
 1168 \AA^3 , significantly larger than
that of a single cage of DDR (278 \AA^3), or FAU (786 \AA^3).



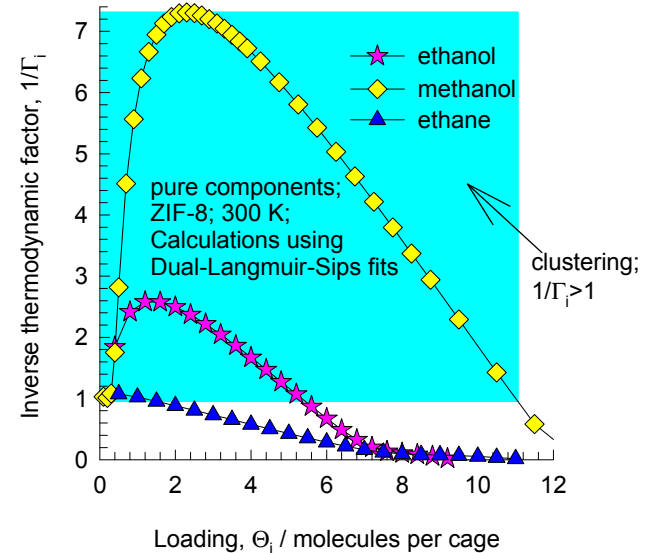
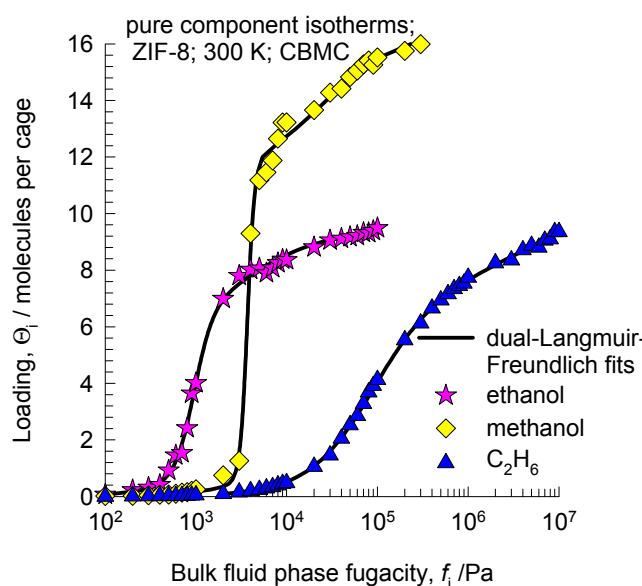
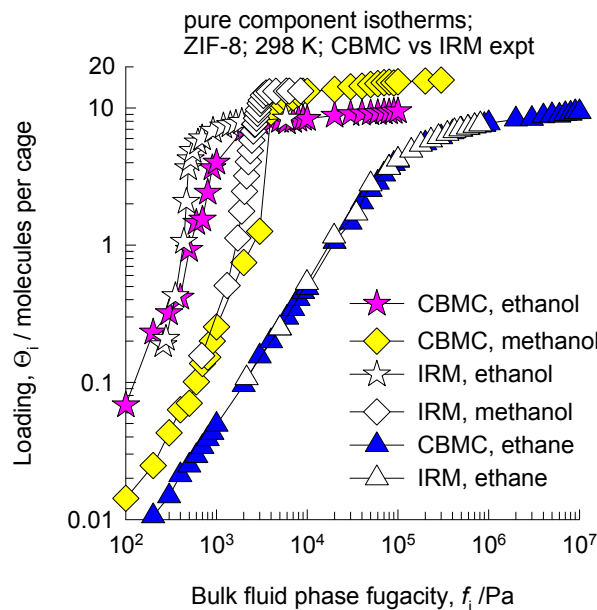
ZIF-8 dimensions



This plot of surface area versus pore dimension is determined using a combination of the DeLaunay triangulation method for pore dimension determination, and the procedure of Duren for determination of the surface area.

| ZIF-8 | |
|--|----------|
| a /Å | 16.991 |
| b /Å | 16.991 |
| c /Å | 16.991 |
| Cell volume / Å³ | 4905.201 |
| conversion factor for [molec/uc] to [mol per kg Framework] | 0.36663 |
| conversion factor for [molec/uc] to [kmol/m³] | 0.7106 |
| ρ [kg/m³] | 924.253 |
| MW unit cell [g/mol(framework)] | 2730.182 |
| ϕ , fractional pore volume | 0.476 |
| open space / Å³/uc | 2337.0 |
| Pore volume / cm³/g | 0.515 |
| Surface area /m²/g | 1164.7 |
| DeLaunay diameter /Å | 3.26 |

ZIF-8 methanol, ethanol, and ethane isotherms at 298 K

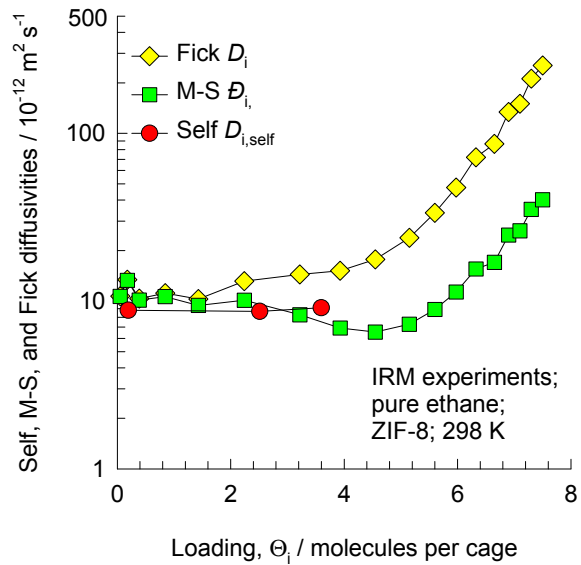
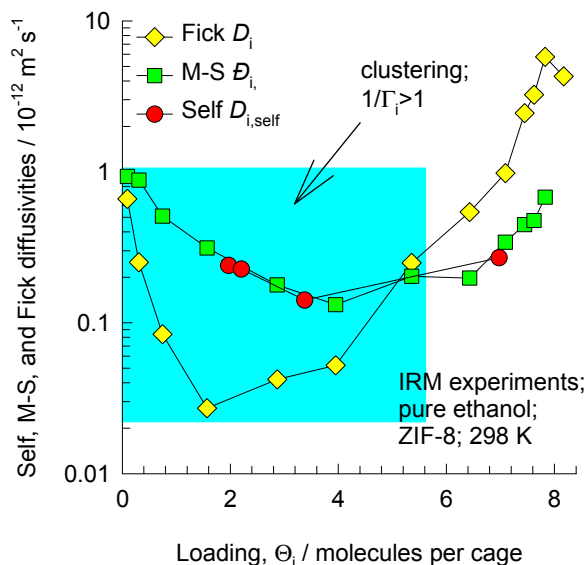
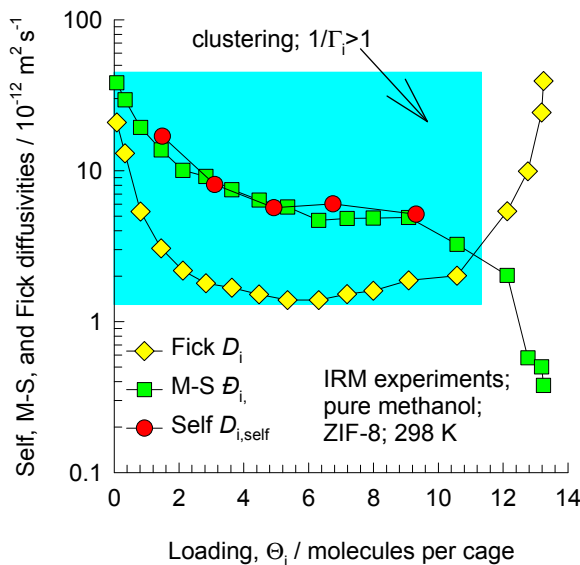


The experimental data are re-plotted using the information in:

C. Chmelik, H. Bux, J. Caro, L. Heinke, F. Hibbe, T. Titze, J. Kärger, Mass transfer in a nanoscale material enhanced by an opposing flux, Phys. Rev. Lett. 104 (2010) 085902.

The steep isotherms for methanol and ethanol are indicative of molecular clustering. This is confirmed by the inverse thermodynamic factors that significantly exceed unity for a range of molecular loadings. We should therefore expect the hierarchy of diffusivities to be “abnormal” for methanol, and ethanol.

ZIF-8 methanol, ethanol, and ethane diffusivities at 298 K

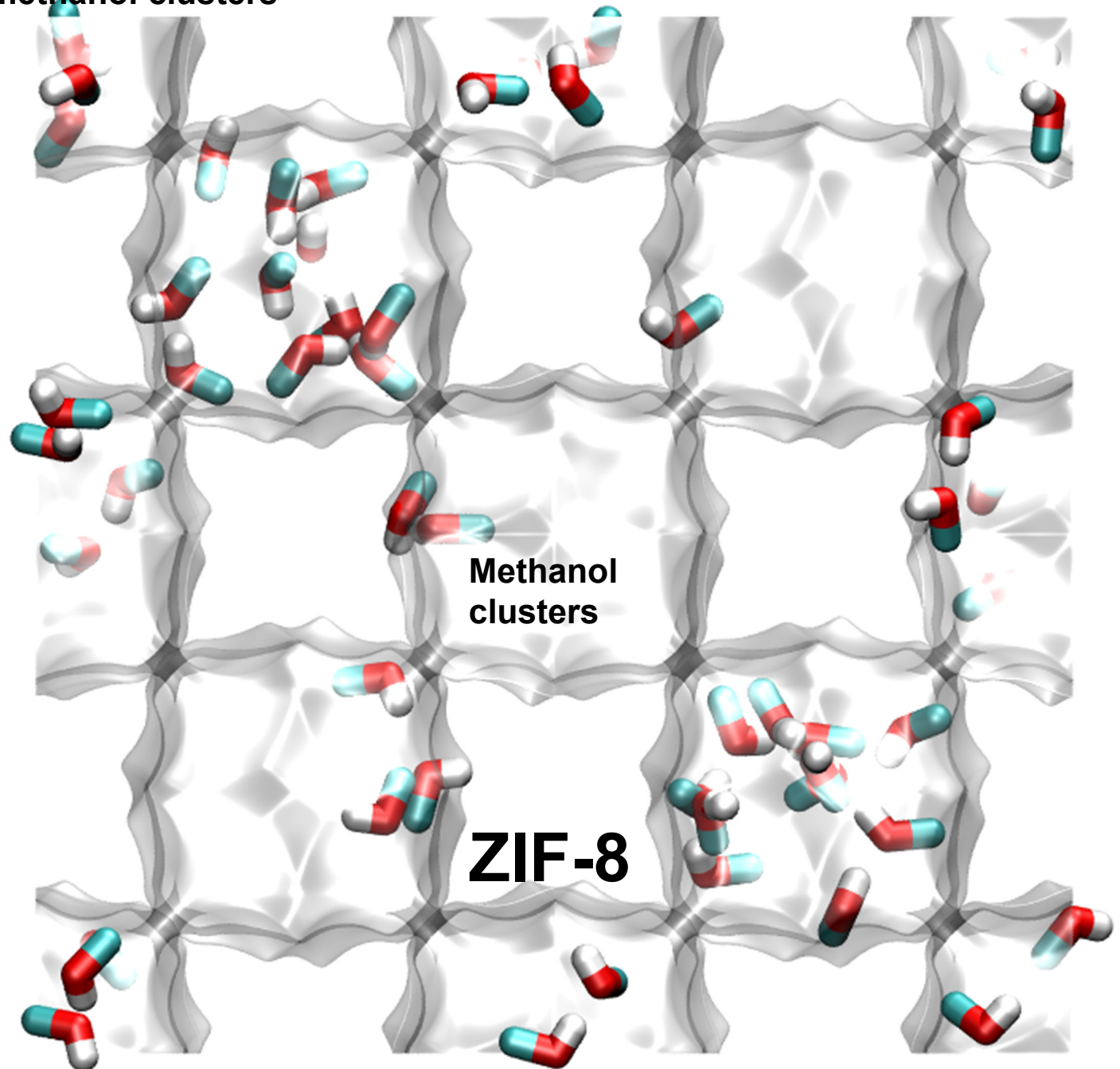


The experimental data are re-plotted using the information in:

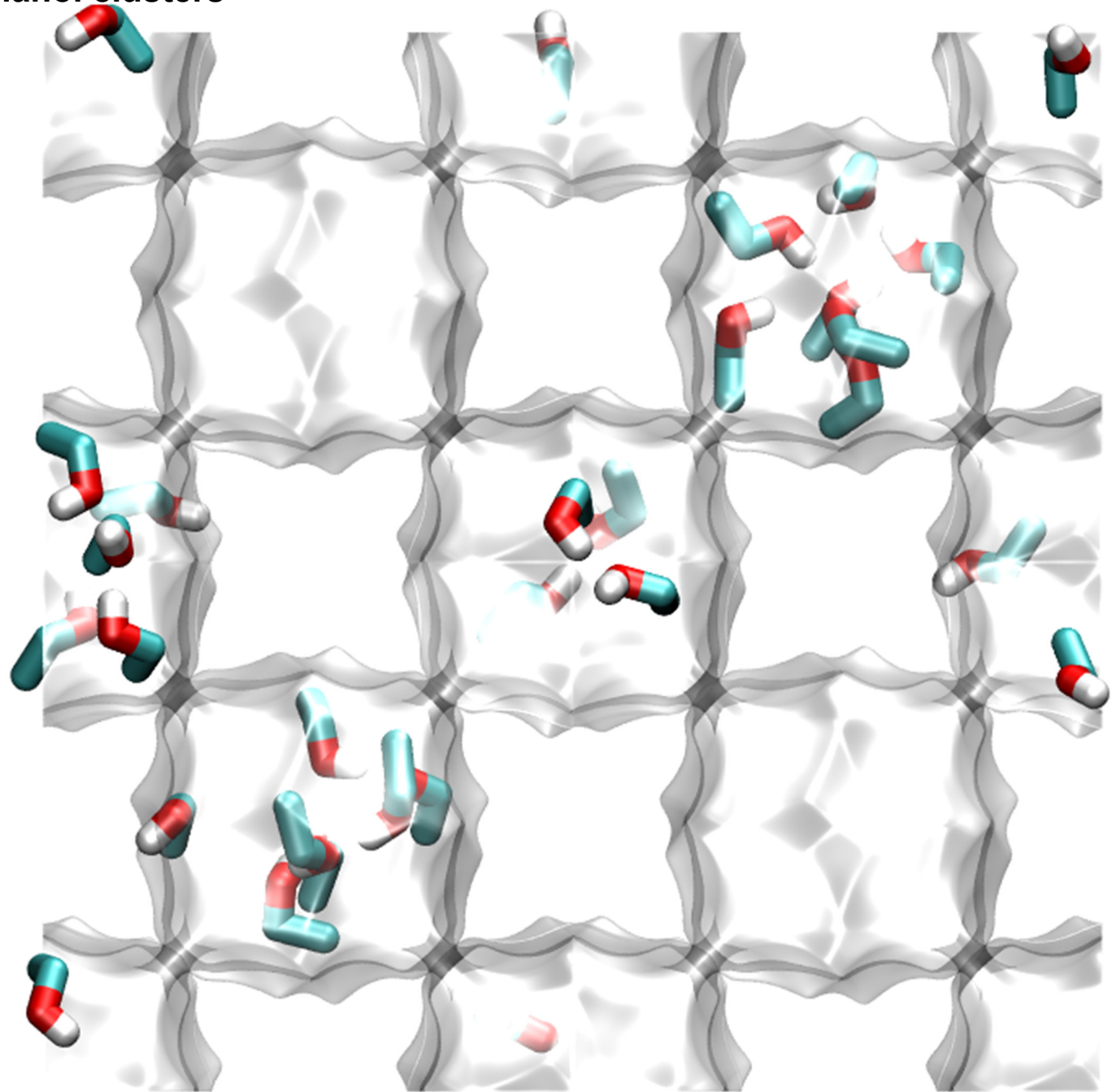
C. Chmelik, H. Bux, J. Caro, L. Heinke, F. Hibbe, T. Titze, J. Kärger, Mass transfer in a nanoscale material enhanced by an opposing flux, Phys. Rev. Lett. 104 (2010) 085902.

The hierarchy of diffusivities is M-S = Self > Fick in regions where molecular clustering occurs.

ZIF-8 snapshot of methanol clusters

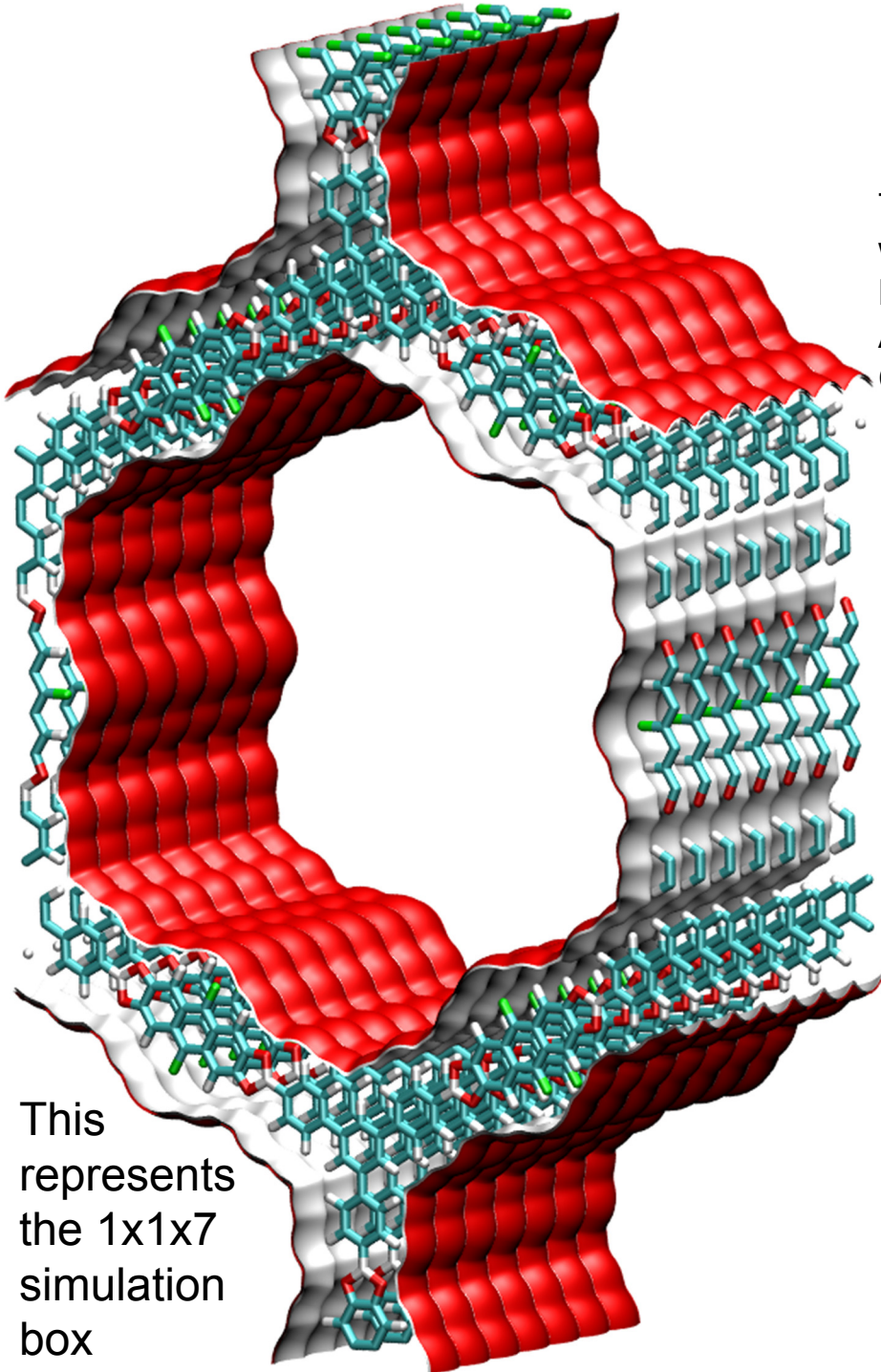


ZIF-8 snapshot of ethanol clusters



1D mesoporous channels

BTP-COF landscape

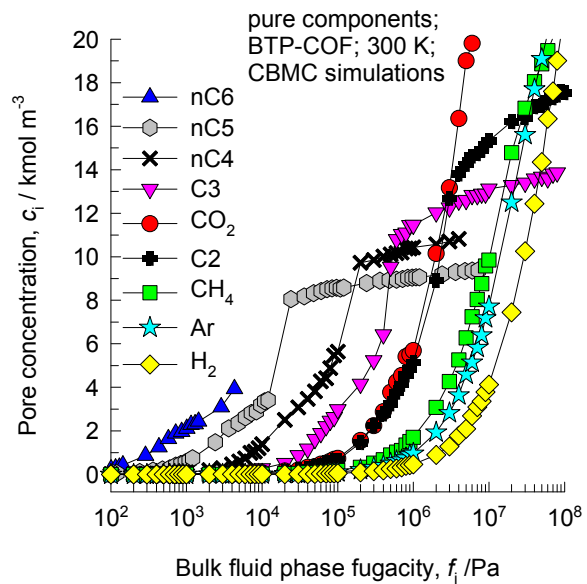


The crystallographic structural information for BTP-COF was obtained from

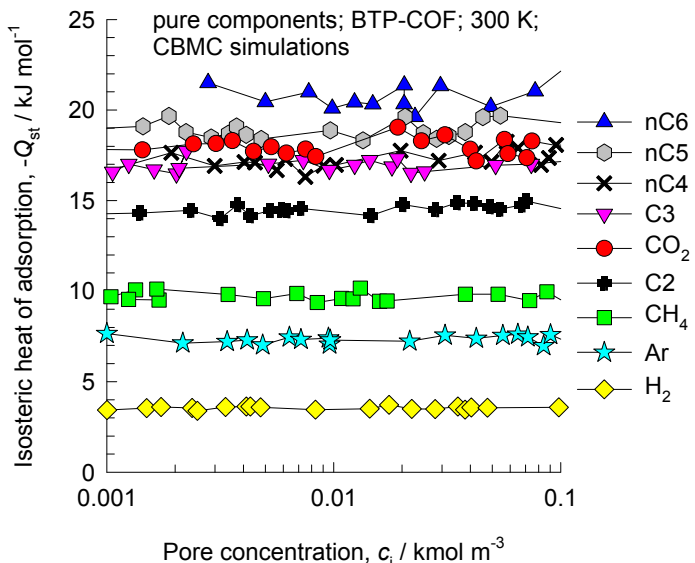
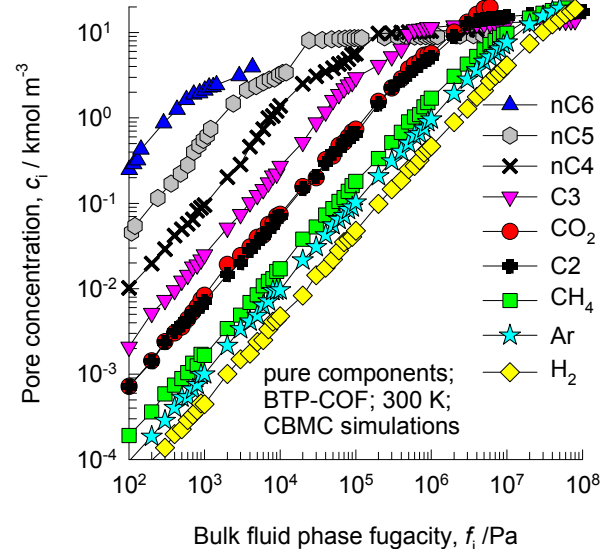
M. Dogru, A. Sonnauer, A. Gavryushin, P. Knochel, T. Bein,
A Covalent Organic Framework with 4 nm open pores,
Chem. Commun. 47 (2011) 1707-1709.

| | BTP-COF |
|--|----------|
| $a / \text{\AA}$ | 43.65 |
| $b / \text{\AA}$ | 75.604 |
| $c / \text{\AA}$ | 3.52 |
| Cell volume / \AA^3 | 11616.4 |
| conversion factor for [molec/uc] to [mol per kg Framework] | 0.3403 |
| conversion factor for [molec/uc] to [kmol/m ³] | 0.1900 |
| $\rho / \text{kg/m}^3$ | 420.0831 |
| MW unit cell [g/mol(framework)] | 2938.67 |
| ϕ , fractional pore volume | 0.752 |
| open space / $\text{\AA}^3/\text{uc}$ | 8738.7 |
| Pore volume / cm^3/g | 1.791 |
| Surface area / m^2/g | |
| DeLaunay diameter / \AA | 34.26 |

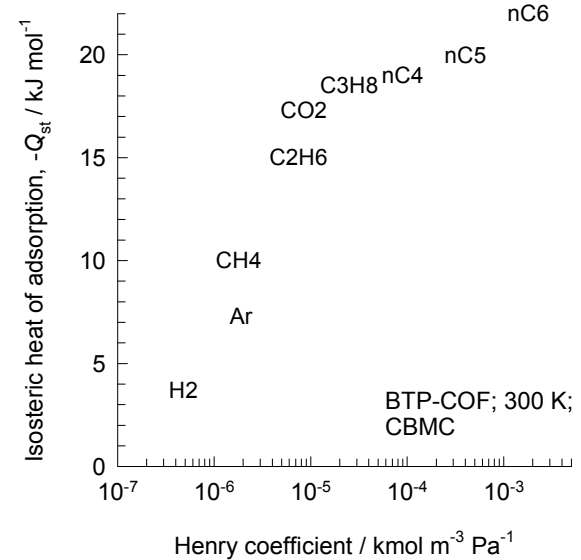
BTP-COF CBMC simulations of isotherms, and isosteric heats of adsorption



Note that C₂ and C₃ refer to saturated alkanes

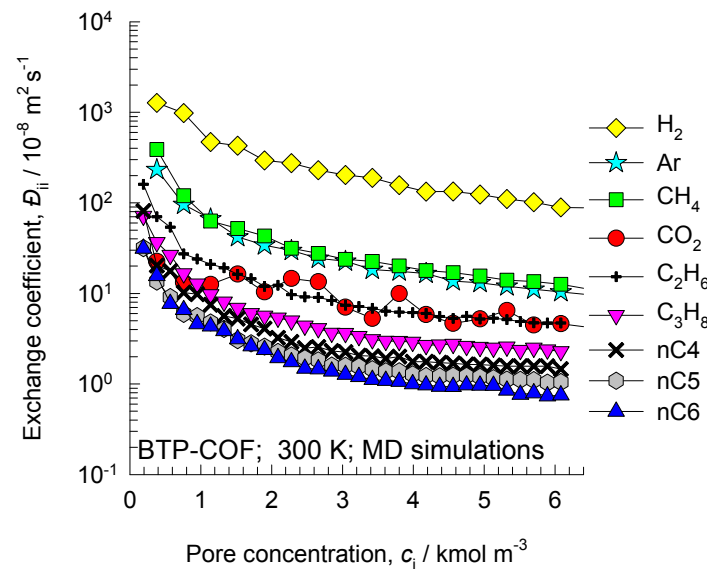
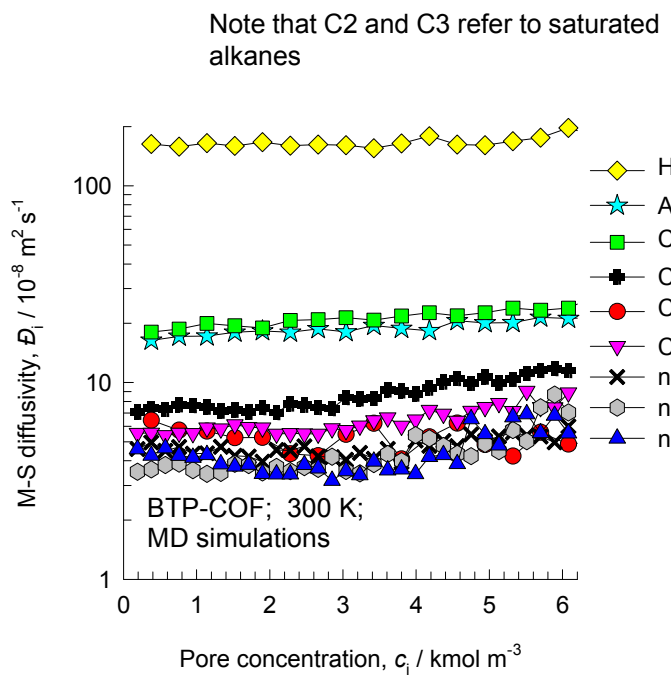
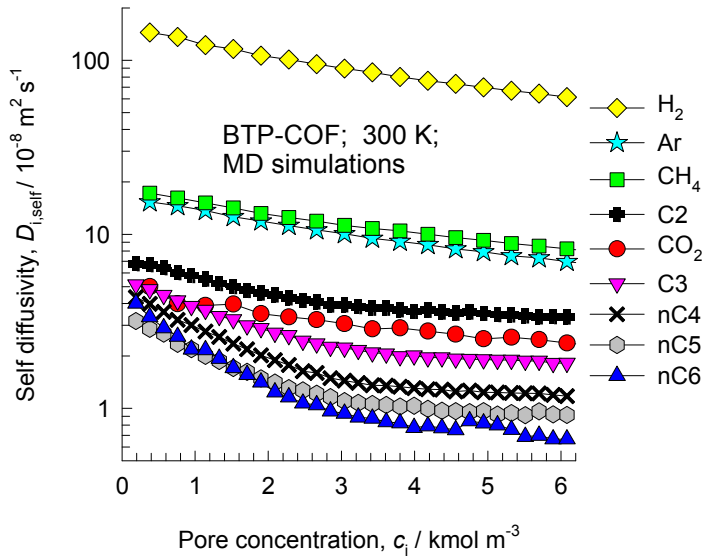


The isosteric heats of adsorption correlate with the Henry coefficients determined from CBMC



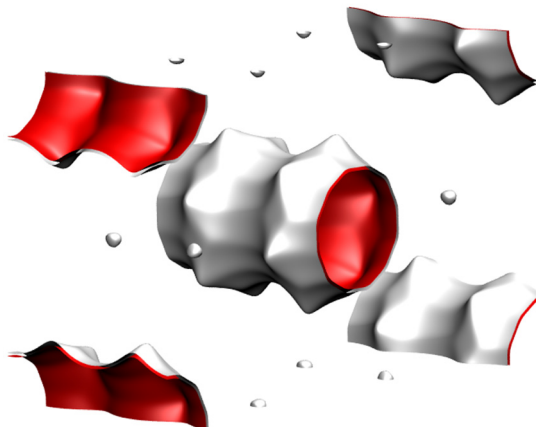
BTP-COF

MD simulations of unary self-, and M-S diffusivities



1D micro-porous channels

AFI landscapes



12-ring
1D channel of AFI

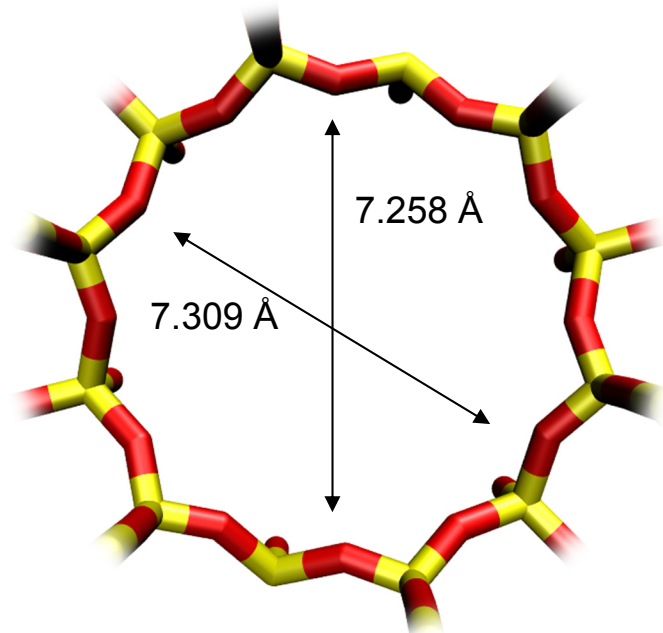


Snapshots showing location of CH₄ and CO₂

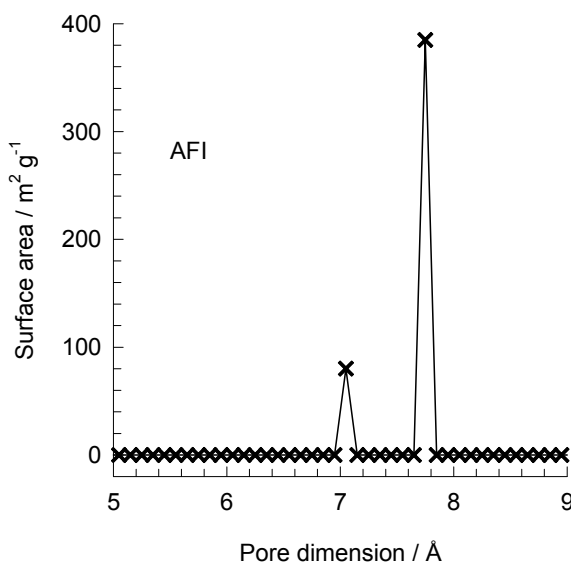


Structural information from: C. Baerlocher, L.B. McCusker, Database of Zeolite Structures, International Zeolite Association, <http://www.iza-structure.org/databases/>

AFI pore dimensions

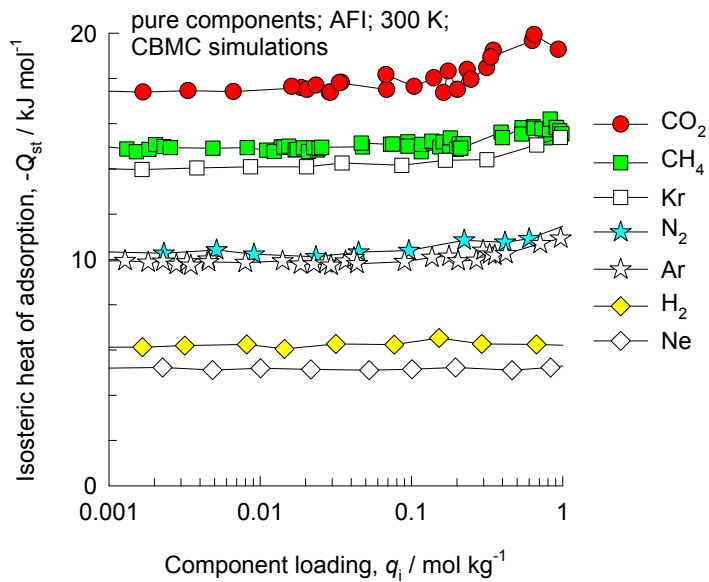
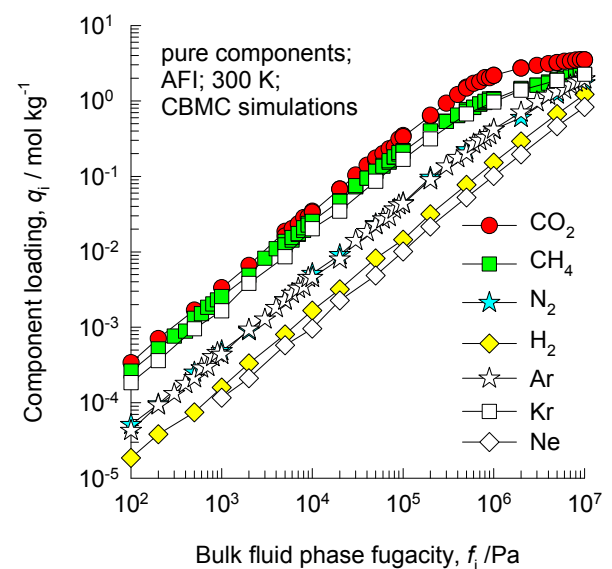
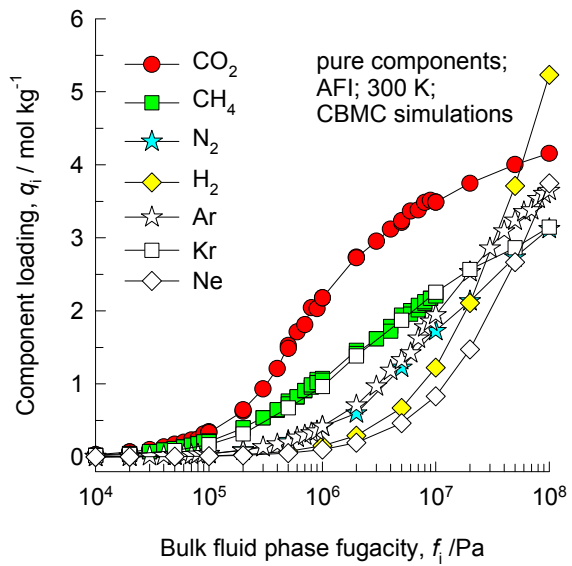


| | AFI |
|--|----------|
| $a / \text{\AA}$ | 23.774 |
| $b / \text{\AA}$ | 13.726 |
| $c / \text{\AA}$ | 8.484 |
| Cell volume / \AA^3 | 2768.515 |
| conversion factor for [molec/uc] to [mol per kg Framework] | 0.3467 |
| conversion factor for [molec/uc] to [kmol/m ³] | 2.1866 |
| $\rho / [\text{kg}/\text{m}^3]$ | 1729.876 |
| MW unit cell [g/mol(framework)] | 2884.07 |
| ϕ , fractional pore volume | 0.274 |
| open space / $\text{\AA}^3/\text{uc}$ | 759.4 |
| Pore volume / cm^3/g | 0.159 |
| Surface area / m^2/g | 466.0 |
| DeLaunay diameter / \AA | 7.26 |

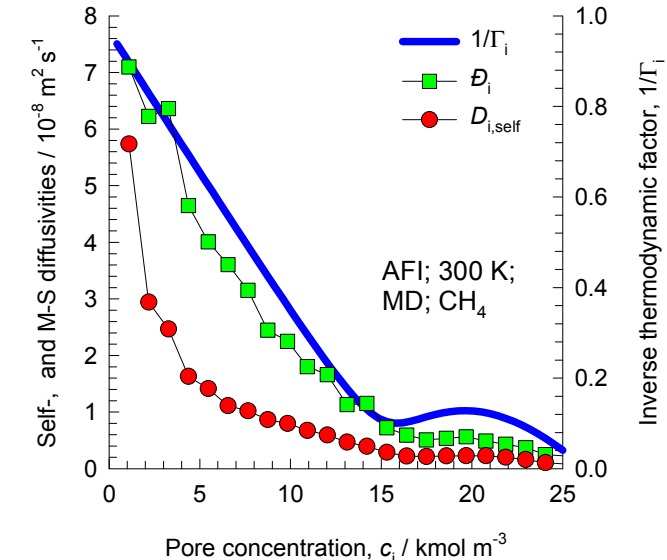
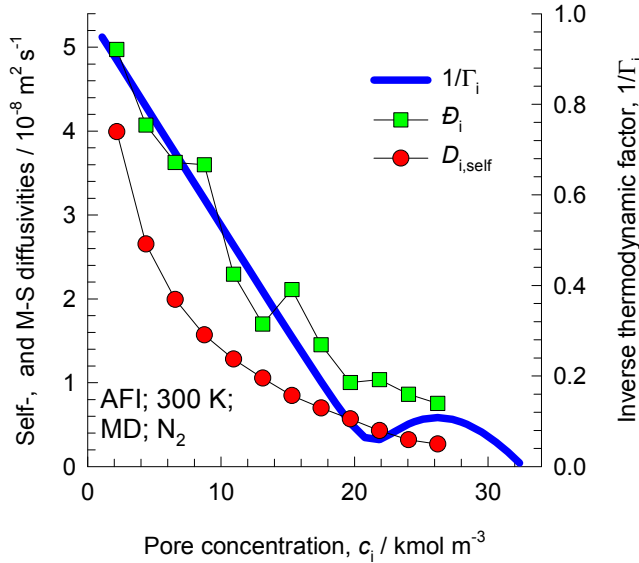
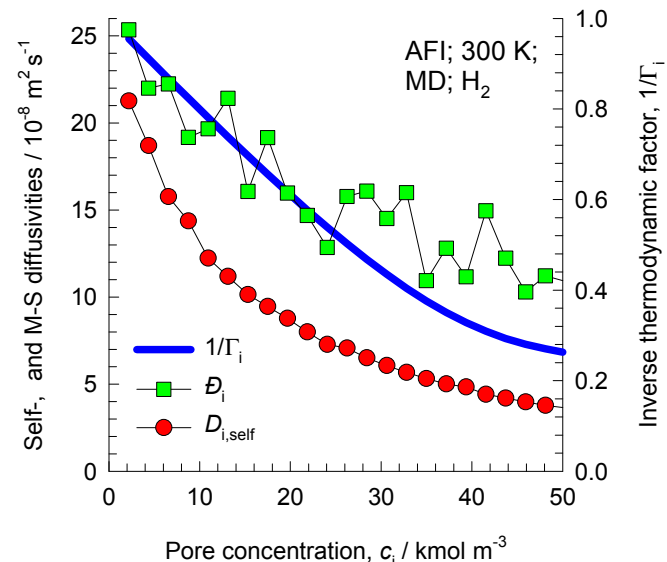
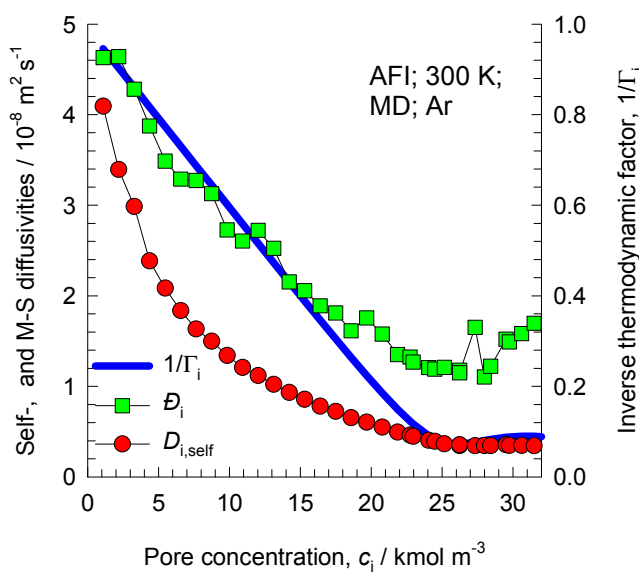


This plot of surface area versus pore dimension is determined using a combination of the DeLaunay triangulation method for pore dimension determination, and the procedure of Düren for determination of the surface area.

AFI CBMC simulations of isotherms, and isosteric heats of adsorption



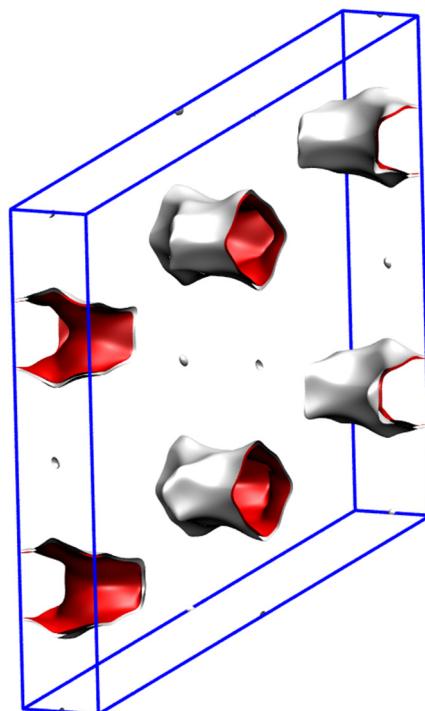
Influence of Inverse Thermodynamic Factor on diffusivities



MTW pore landscape



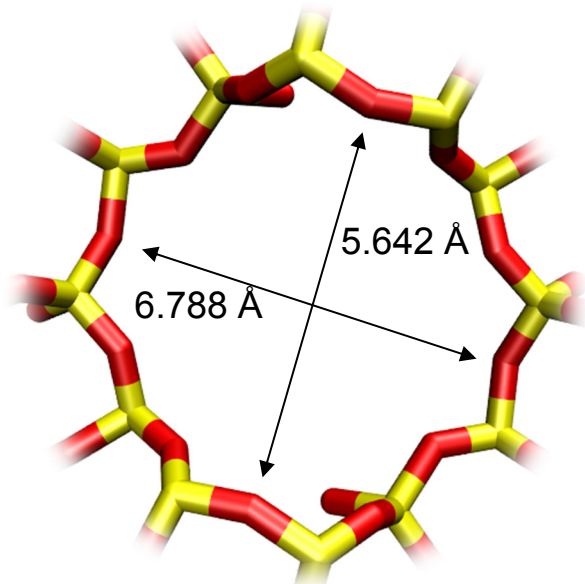
MTW has 1D 12-ring channels



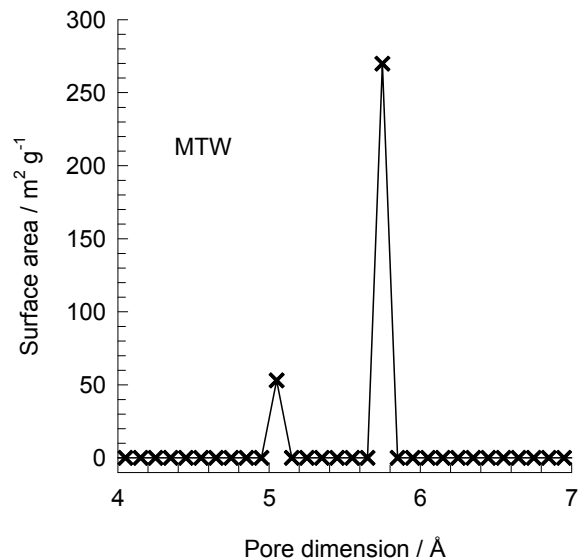
Structural information from: C. Baerlocher, L.B. McCusker,
Database of Zeolite Structures, International Zeolite Association,
<http://www.iza-structure.org/databases/>

MTW pore dimensions

MTW has 1D, 12-ring channels



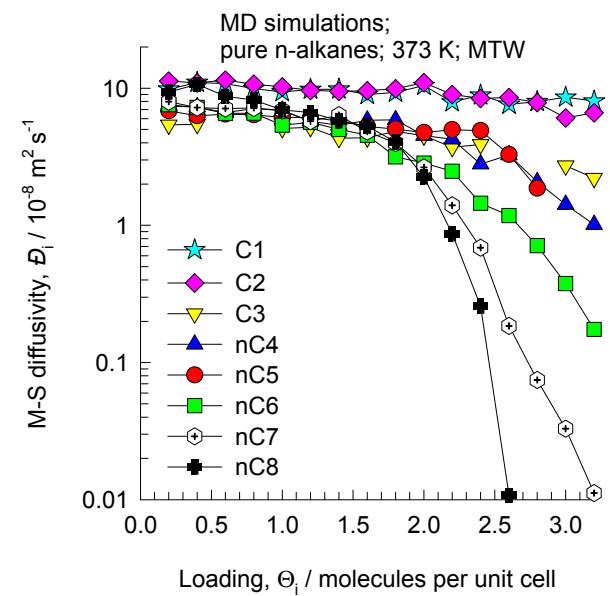
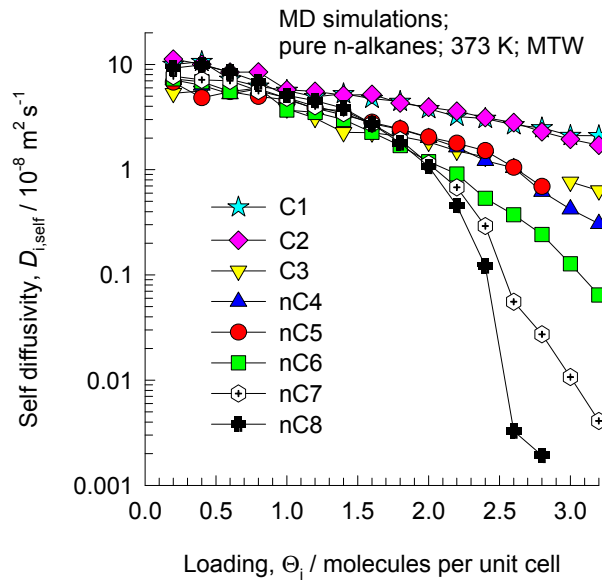
This plot of surface area versus pore dimension is determined using a combination of the DeLaunay triangulation method for pore dimension determination, and the procedure of Düren for determination of the surface area.



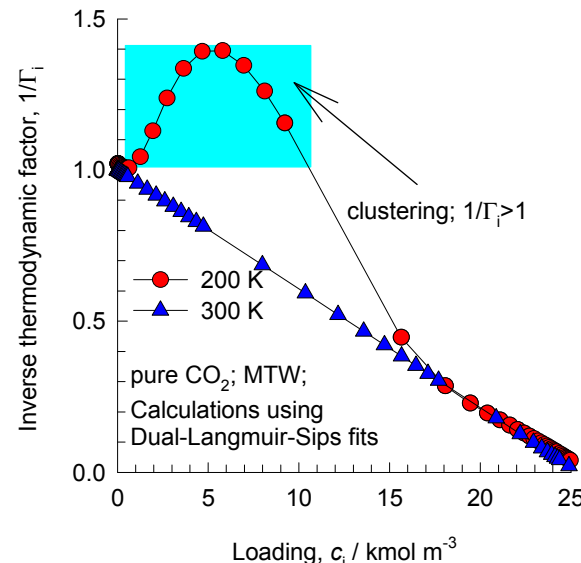
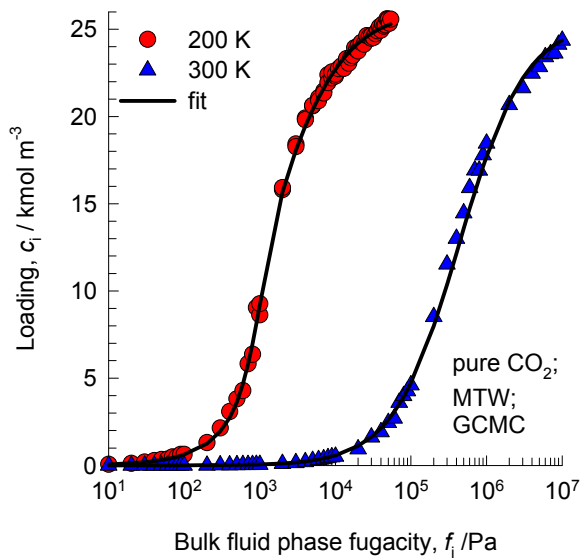
| MTW | |
|--|----------|
| a / Å | 24.863 |
| b / Å | 5.012 |
| c / Å | 24.326 |
| Cell volume / Å ³ | 2887.491 |
| conversion factor for [molec/uc] to [mol per kg Framework] | 0.2972 |
| conversion factor for [molec/uc] to [kmol/m ³] | 2.6759 |
| ρ [kg/m ³] | 1935.031 |
| MW unit cell [g/mol(framework)] | 3364.749 |
| ϕ , fractional pore volume | 0.215 |
| open space / Å ³ /uc | 620.6 |
| Pore volume / cm ³ /g | 0.111 |
| Surface area / m ² /g | 323.0 |
| DeLaunay diameter / Å | 5.69 |

MTW

MD simulations of unary self- , and M-S diffusivities



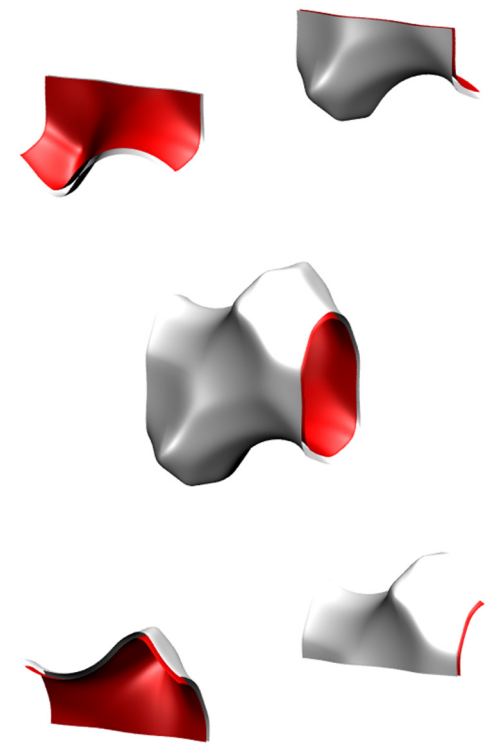
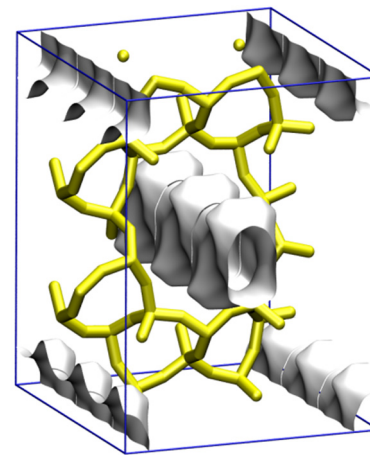
MTW adsorption of CO₂



TON pore landscape



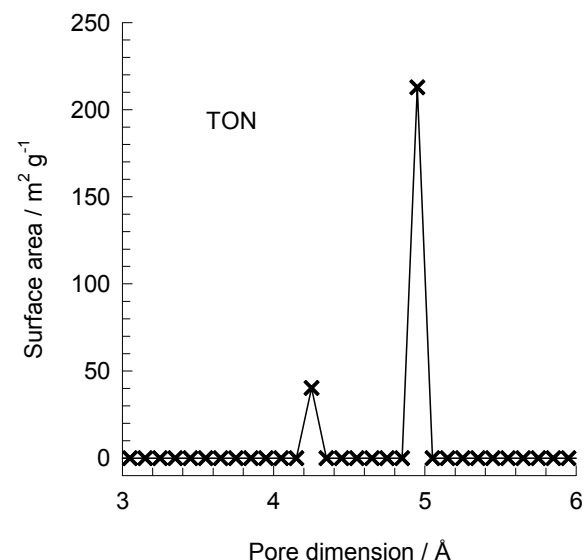
10-ring 1D channel of TON



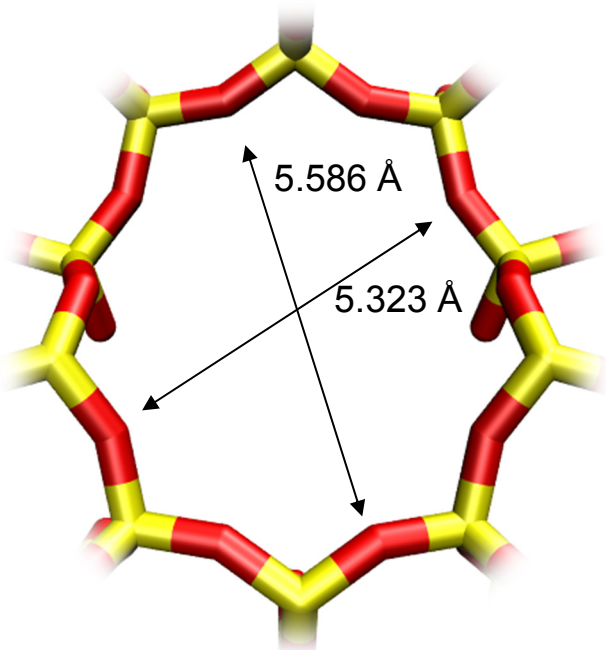
Structural information from: C. Baerlocher, L.B. McCusker, Database of Zeolite Structures, International Zeolite Association,
<http://www.iza-structure.org/databases/>

TON pore dimensions

This plot of surface area versus pore dimension is determined using a combination of the DeLaunay triangulation method for pore dimension determination, and the procedure of Dürren for determination of the surface area.



10-ring channel of TON

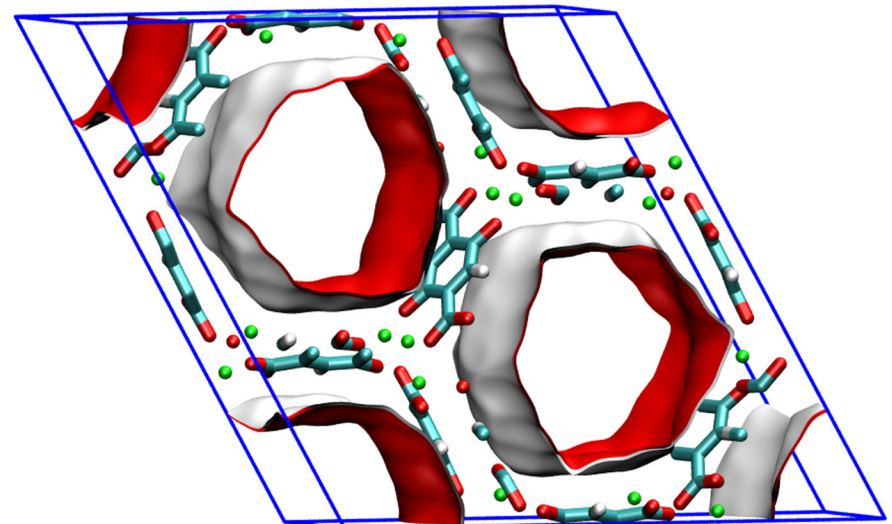
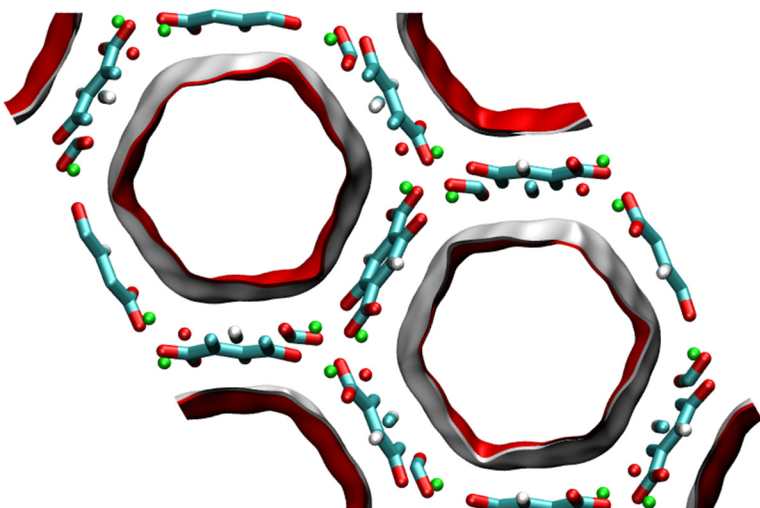


| TON | |
|--|----------|
| a /Å | 13.859 |
| b /Å | 17.42 |
| c /Å | 5.038 |
| Cell volume / Å³ | 1216.293 |
| conversion factor for [molec/uc] to [mol per kg Framework] | 0.6935 |
| conversion factor for [molec/uc] to [kmol/m³] | 7.1763 |
| ρ [kg/m³] | 1968.764 |
| MW unit cell [g/mol(framework)] | 1442.035 |
| ϕ , fractional pore volume | 0.190 |
| open space / Å³/uc | 231.4 |
| Pore volume / cm³/g | 0.097 |
| Surface area /m²/g | 253.0 |
| DeLaunay diameter /Å | 4.88 |

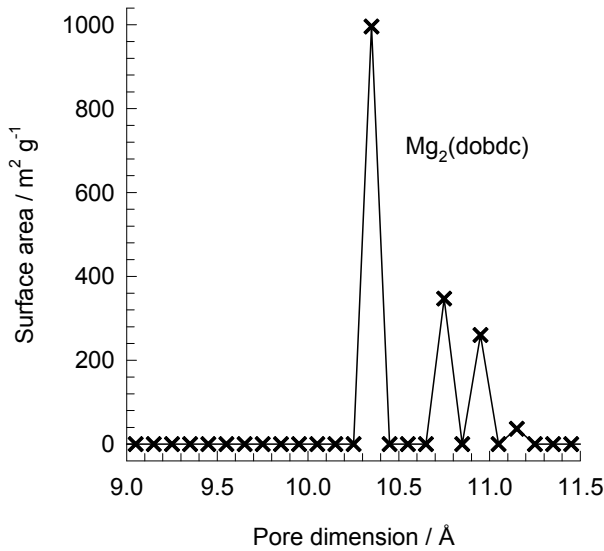
MgMOF-74 pore landscapes

The structural information on MgMOF-74 ($= \text{Mg}_2(\text{dobdc}) = \text{Mg}(\text{dobdc} = \text{CPO-27-Mg})$ with dobdc = (dobdc⁴⁻ = 2,5-dioxido-1,4-benzenedicarboxylate)) were obtained from

- A.Ö. Yazaydin, R.Q. Snurr, T.H. Park, K. Koh, J. Liu, M.D. LeVan, A.I. Benin, P. Jakubczak, M. Lanuza, D.B. Galloway, J.J. Low, R.R. Willis, Screening of Metal-Organic Frameworks for Carbon Dioxide Capture from Flue Gas using a Combined Experimental and Modeling Approach, *J. Am. Chem. Soc.* 131 (2009) 18198-18199.
- D. Britt, H. Furukawa, B. Wang, T.G. Glover, O.M. Yaghi, Highly efficient separation of carbon dioxide by a metal-organic framework replete with open metal sites, *Proc. Natl. Acad. Sci. U.S.A.* 106 (2009) 20637-20640.
- N.L. Rosi, J. Kim, M. Eddaoudi, B. Chen, M. O'Keeffe, O.M. Yaghi, Rod Packings and Metal-Organic Frameworks Constructed from Rod-Shaped Secondary Building Units, *J. Am. Chem. Soc.* 127 (2005) 1504-1518.
- P.D.C. Dietzel, B. Panella, M. Hirscher, R. Blom, H. Fjellvåg, Hydrogen adsorption in a nickel based coordination polymer with open metal sites in the cylindrical cavities of the desolvated framework, *Chem. Commun.* (2006) 959-961.
- P.D.C. Dietzel, V. Besikiotis, R. Blom, Application of metal-organic frameworks with coordinatively unsaturated metal sites in storage and separation of methane and carbon dioxide, *J. Mater. Chem.* 19 (2009) 7362-7370.
- S.R. Caskey, A.G. Wong-Foy, A.J. Matzger, Dramatic Tuning of Carbon Dioxide Uptake via Metal Substitution in a Coordination Polymer with Cylindrical Pores, *J. Am. Chem. Soc.* 130 (2008) 10870-10871.



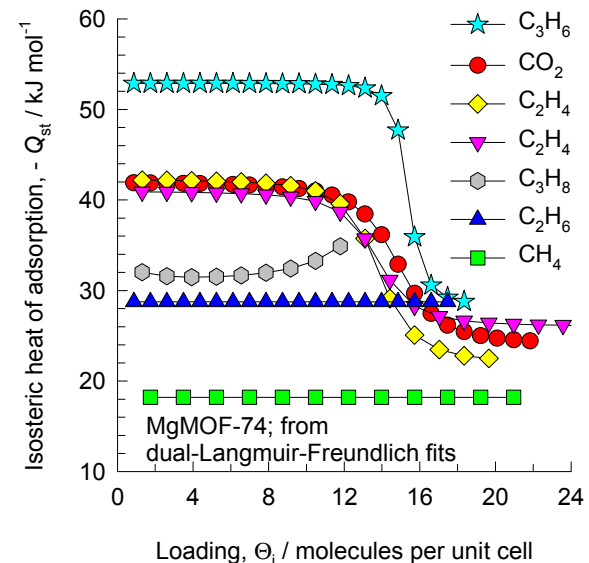
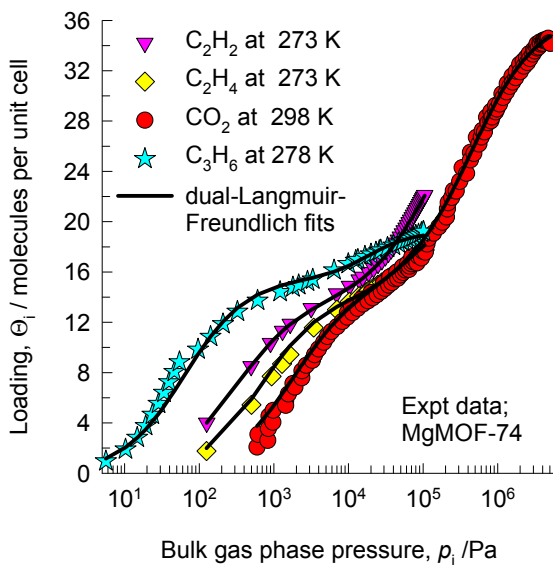
MgMOF-74 pore dimensions



This plot of surface area versus pore dimension is determined using a combination of the DeLaunay triangulation method for pore dimension determination, and the procedure of Düren for determination of the surface area.

| MgMOF-74 | |
|--|----------|
| $a / \text{\AA}$ | 25.8621 |
| $b / \text{\AA}$ | 25.8621 |
| $c / \text{\AA}$ | 6.91427 |
| Cell volume / \AA^3 | 4005.019 |
| conversion factor for [molec/uc] to [mol per kg Framework] | 0.4580 |
| conversion factor for [molec/uc] to [kmol/m³] | 0.5856 |
| $\rho / \text{kg/m}^3$ | 905.367 |
| MW unit cell [g/mol(framework)] | 2183.601 |
| ϕ , fractional pore volume | 0.708 |
| open space / $\text{\AA}^3/\text{uc}$ | 2835.6 |
| Pore volume / cm^3/g | 0.782 |
| Surface area / m^2/g | 1640.0 |
| DeLaunay diameter / \AA | 10.66 |

MgMOF-74 isotherms and isosteric heats of adsorption from experiments

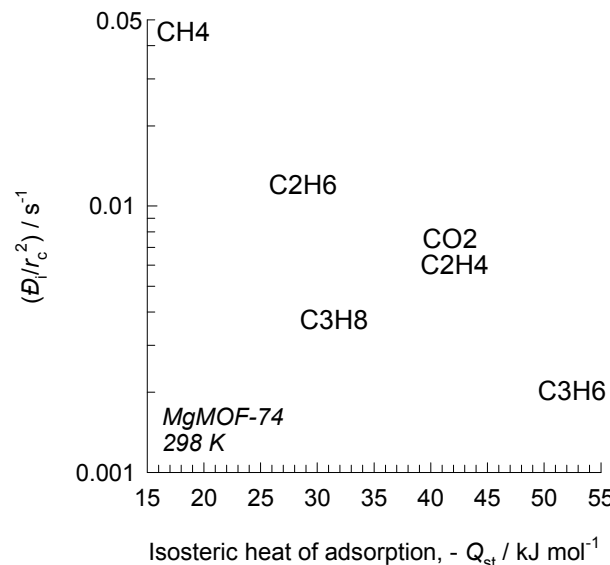


The pure component isotherms, with fits, and isosteric heats of adsorption are those reported by:
 He, Y.; Krishna, R.; Chen, B. Metal-Organic Frameworks with Potential for Energy-Efficient Adsorptive Separation of Light Hydrocarbons. *Energy Environ. Sci.* 2012, 5, 9107-9120.

The unary diffusivities are taken to be identical to those in MgMOF-74; the Maxwell-Stefan diffusivities are the ones presented by:

Krishna, R.; van Baten, J.M. Investigating the Relative Influences of Molecular Dimensions and Binding Energies on Diffusivities of Guest Species Inside Nanoporous Crystalline Materials. *J. Phys. Chem. C* 2012, 116, 23556-23568.

MgMOF-74 dependence of diffusivity on the isosteric heats of adsorption



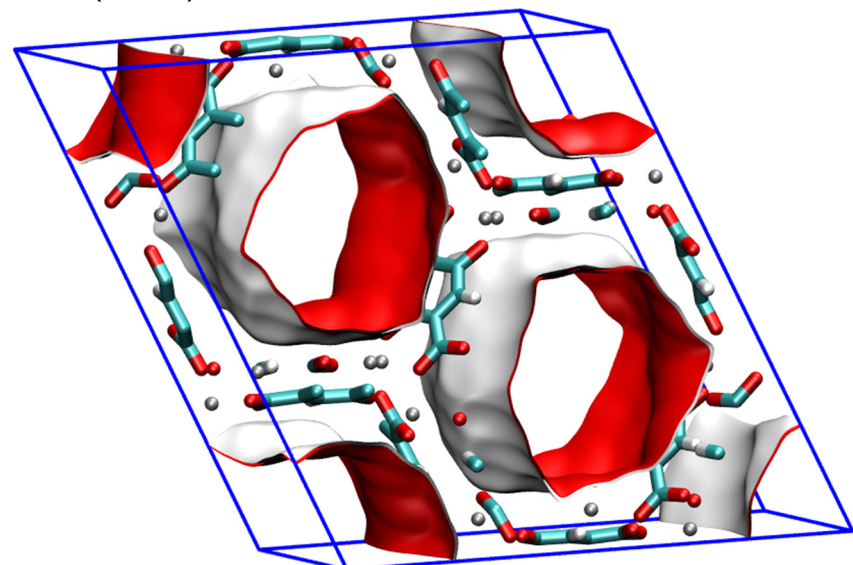
The pure component isotherms, with fits, and isosteric heats of adsorption are those reported by:
He, Y.; Krishna, R.; Chen, B. Metal-Organic Frameworks with Potential for Energy-Efficient Adsorptive Separation of Light Hydrocarbons. *Energy Environ. Sci.* 2012, 5, 9107-9120.

The unary diffusivities Maxwell-Stefan diffusivities are the ones presented by:
Krishna, R.; van Baten, J.M. Investigating the Relative Influences of Molecular Dimensions and Binding Energies on Diffusivities of Guest Species Inside Nanoporous Crystalline Materials. *J. Phys. Chem. C* 2012, 116, 23556-23568.

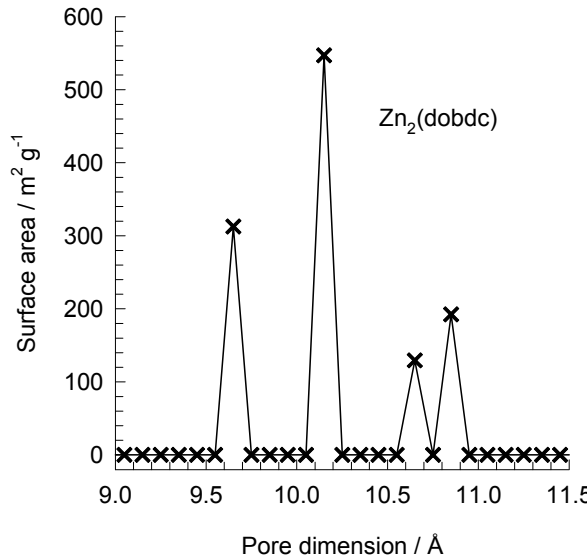
ZnMOF-74 pore landscapes

The structural information on ZnMOF-74 (= $\text{Zn}_2(\text{dobdc}) = \text{Zn}(\text{dobdc} = \text{CPO-27-Zn})$ with dobdc = (dobdc⁴⁻ = 2,5-dioxido-1,4-benzenedicarboxylate)) were obtained from

- A.Ö. Yazaydin, R.Q. Snurr, T.H. Park, K. Koh, J. Liu, M.D. LeVan, A.I. Benin, P. Jakubczak, M. Lanuza, D.B. Galloway, J.J. Low, R.R. Willis, Screening of Metal-Organic Frameworks for Carbon Dioxide Capture from Flue Gas using a Combined Experimental and Modeling Approach, *J. Am. Chem. Soc.* 131 (2009) 18198-18199.
- D. Britt, H. Furukawa, B. Wang, T.G. Glover, O.M. Yaghi, Highly efficient separation of carbon dioxide by a metal-organic framework replete with open metal sites, *Proc. Natl. Acad. Sci. U.S.A.* 106 (2009) 20637-20640.
- N.L. Rosi, J. Kim, M. Eddaoudi, B. Chen, M. O'Keeffe, O.M. Yaghi, Rod Packings and Metal-Organic Frameworks Constructed from Rod-Shaped Secondary Building Units, *J. Am. Chem. Soc.* 127 (2005) 1504-1518.
- P.D.C. Dietzel, B. Panella, M. Hirscher, R. Blom, H. Fjellvåg, Hydrogen adsorption in a nickel based coordination polymer with open metal sites in the cylindrical cavities of the desolvated framework, *Chem. Commun.* (2006) 959-961.
- P.D.C. Dietzel, V. Besikiotis, R. Blom, Application of metal-organic frameworks with coordinatively unsaturated metal sites in storage and separation of methane and carbon dioxide, *J. Mater. Chem.* 19 (2009) 7362-7370.
- S.R. Caskey, A.G. Wong-Foy, A.J. Matzger, Dramatic Tuning of Carbon Dioxide Uptake via Metal Substitution in a Coordination Polymer with Cylindrical Pores, *J. Am. Chem. Soc.* 130 (2008) 10870-10871.



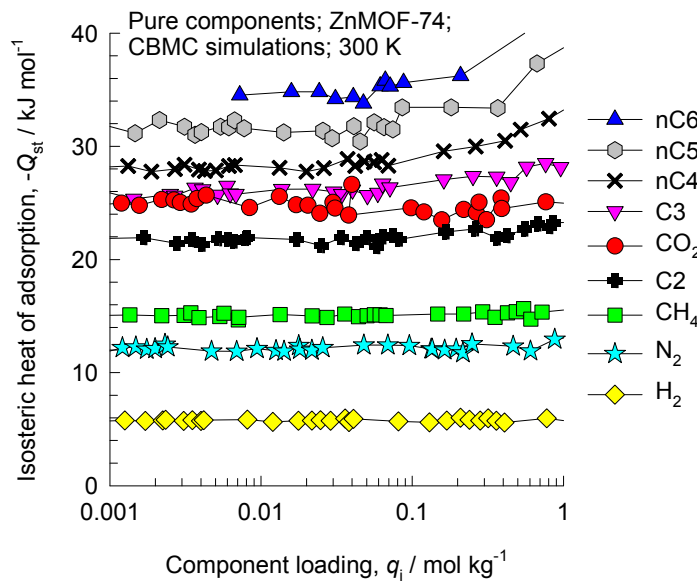
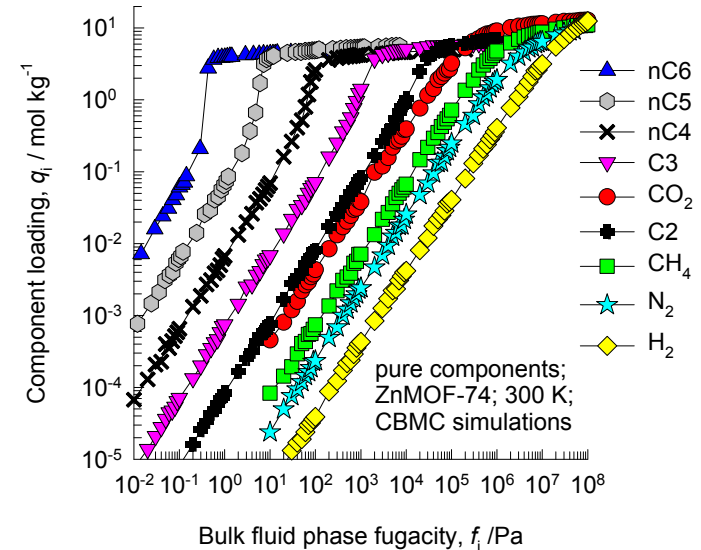
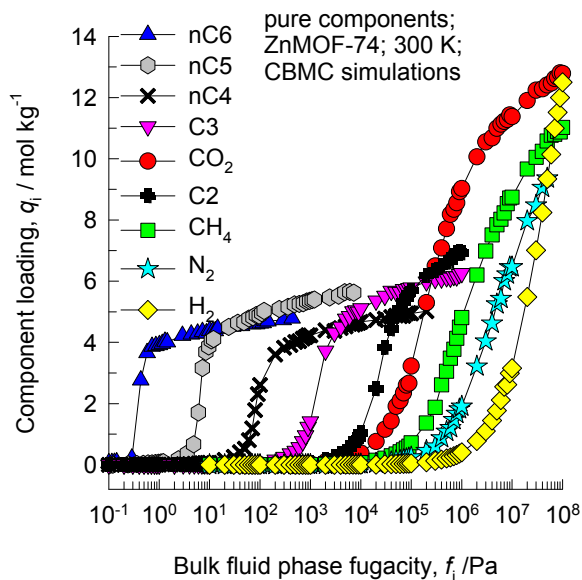
ZnMOF-74 pore dimensions



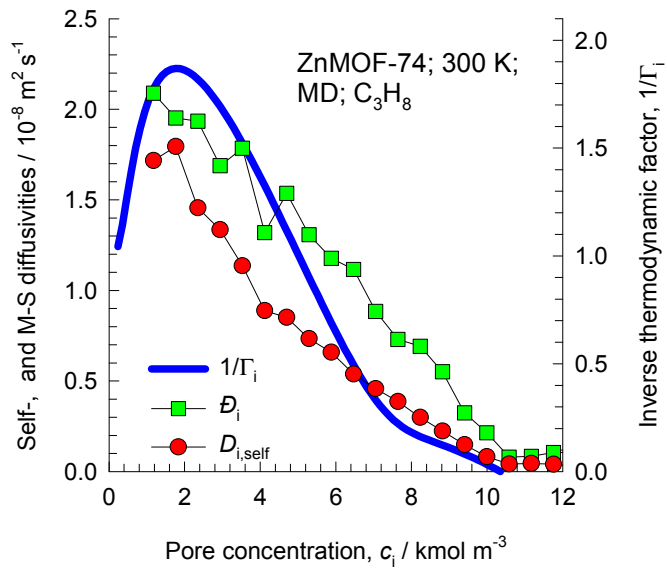
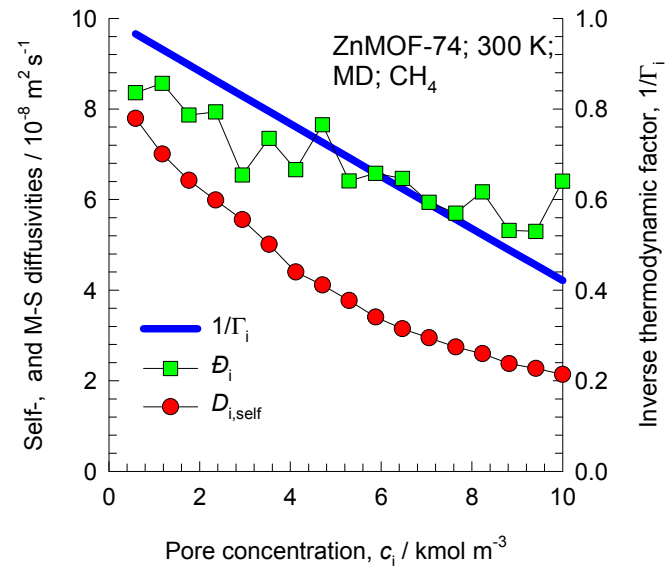
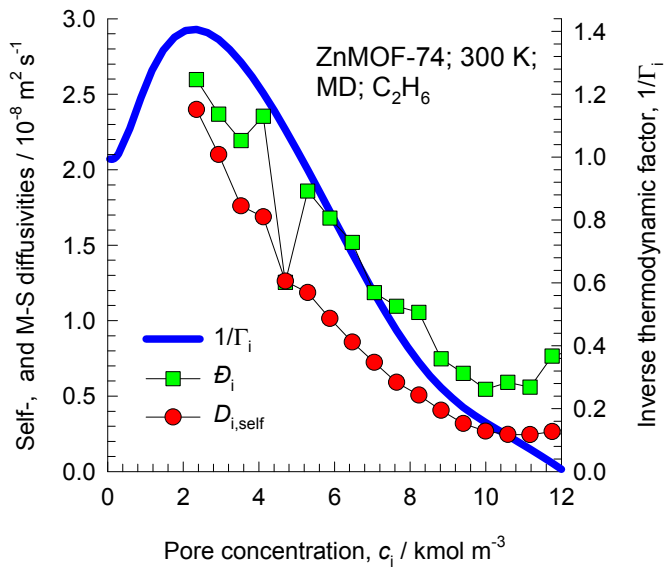
This plot of surface area versus pore dimension is determined using a combination of the DeLaunay triangulation method for pore dimension determination, and the procedure of Dürren for determination of the surface area.

| | ZnMOF-74 |
|--|----------|
| a / Å | 25.9322 |
| b / Å | 25.9322 |
| c / Å | 6.8365 |
| Cell volume / Å ³ | 3981.467 |
| conversion factor for [molec/uc] to [mol per kg Framework] | 0.3421 |
| conversion factor for [molec/uc] to [kmol/m ³] | 0.5881 |
| ρ [kg/m ³] | 1219.304 |
| MW unit cell [g/mol(framework)] | 2923.473 |
| ϕ , fractional pore volume | 0.709 |
| open space / Å ³ /uc | 2823.8 |
| Pore volume / cm ³ /g | 0.582 |
| Surface area / m ² /g | 1176.0 |
| DeLaunay diameter / Å | 9.49 |

ZnMOF-74 CBMC simulations of isotherms, and isosteric heats of adsorption



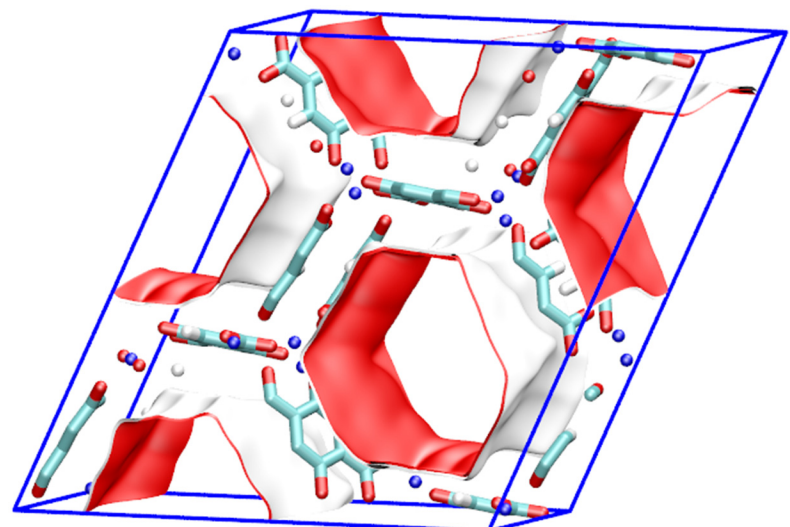
Influence of Inverse Thermodynamic Factor on diffusivities



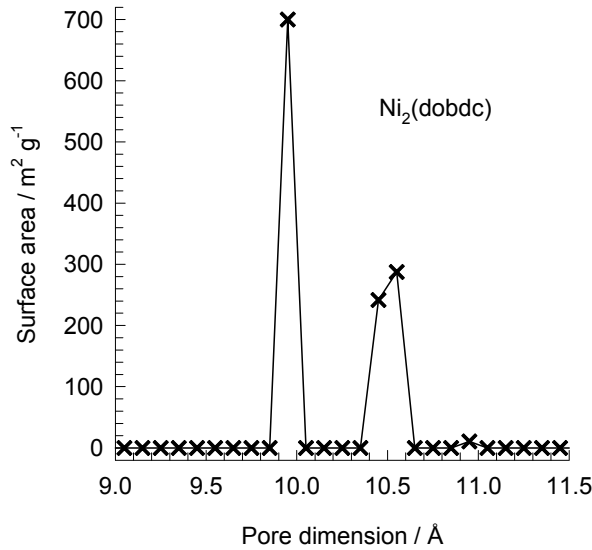
NiMOF-74 pore landscapes

The structural information on NiMOF-74 ($= \text{Ni}_2(\text{dobdc}) = \text{Ni}(\text{dobdc} = \text{CPO-27-Ni})$ with dobdc = (dobdc⁴⁻ = 2,5-dioxido-1,4-benzenedicarboxylate)) were obtained from

- A.Ö. Yazaydin, R.Q. Snurr, T.H. Park, K. Koh, J. Liu, M.D. LeVan, A.I. Benin, P. Jakubczak, M. Lanuza, D.B. Galloway, J.J. Low, R.R. Willis, Screening of Metal-Organic Frameworks for Carbon Dioxide Capture from Flue Gas using a Combined Experimental and Modeling Approach, *J. Am. Chem. Soc.* 131 (2009) 18198-18199.
- D. Britt, H. Furukawa, B. Wang, T.G. Glover, O.M. Yaghi, Highly efficient separation of carbon dioxide by a metal-organic framework replete with open metal sites, *Proc. Natl. Acad. Sci. U.S.A.* 106 (2009) 20637-20640.
- N.L. Rosi, J. Kim, M. Eddaoudi, B. Chen, M. O'Keeffe, O.M. Yaghi, Rod Packings and Metal-Organic Frameworks Constructed from Rod-Shaped Secondary Building Units, *J. Am. Chem. Soc.* 127 (2005) 1504-1518.
- P.D.C. Dietzel, B. Panella, M. Hirscher, R. Blom, H. Fjellvåg, Hydrogen adsorption in a nickel based coordination polymer with open metal sites in the cylindrical cavities of the desolvated framework, *Chem. Commun.* (2006) 959-961.
- P.D.C. Dietzel, V. Besikiotis, R. Blom, Application of metal-organic frameworks with coordinatively unsaturated metal sites in storage and separation of methane and carbon dioxide, *J. Mater. Chem.* 19 (2009) 7362-7370.
- S.R. Caskey, A.G. Wong-Foy, A.J. Matzger, Dramatic Tuning of Carbon Dioxide Uptake via Metal Substitution in a Coordination Polymer with Cylindrical Pores, *J. Am. Chem. Soc.* 130 (2008) 10870-10871.



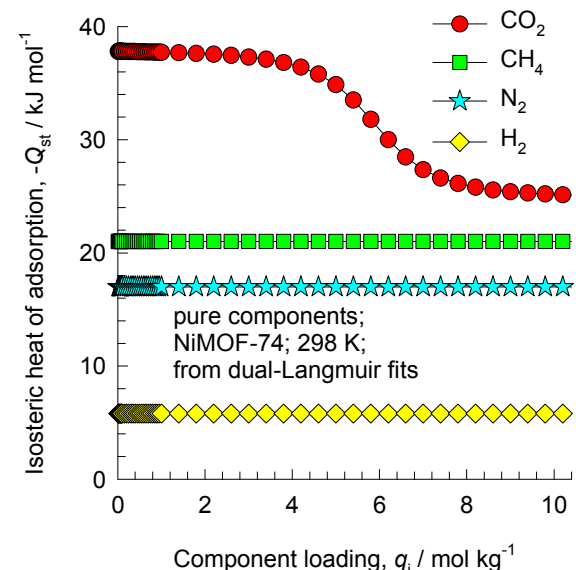
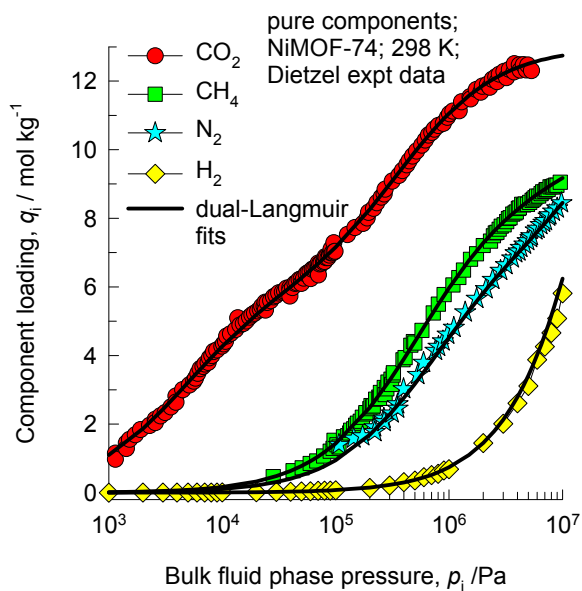
NiMOF-74 pore dimensions



This plot of surface area versus pore dimension is determined using a combination of the DeLaunay triangulation method for pore dimension determination, and the procedure of Düren for determination of the surface area.

| NiMOF-74 | |
|--|----------|
| a /Å | 25.7856 |
| b /Å | 25.7856 |
| c /Å | 6.7701 |
| Cell volume / Å ³ | 3898.344 |
| conversion factor for [molec/uc] to [mol per kg Framework] | 0.3568 |
| conversion factor for [molec/uc] to [kmol/m ³] | 0.6133 |
| ρ [kg/m ³] | 1193.811 |
| MW unit cell [g/mol(framework)] | 2802.592 |
| ϕ, fractional pore volume | 0.695 |
| open space / Å ³ /uc | 2707.6 |
| Pore volume / cm ³ /g | 0.582 |
| Surface area /m ² /g | 1239.0 |
| DeLaunay diameter /Å | 9.80 |

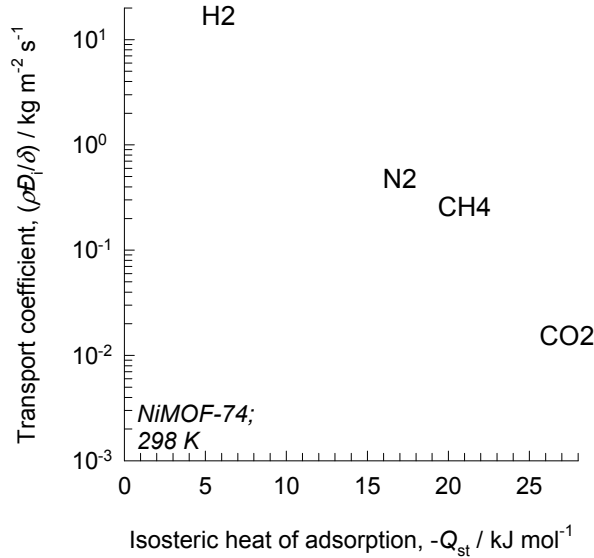
NiMOF-74 isotherms and isosteric heats of adsorption from experiments



The pure component isotherms, with fits, and isosteric heats of adsorption are those reported by:

Krishna, R.; van Baten, J.M. Investigating the Relative Influences of Molecular Dimensions and Binding Energies on Diffusivities of Guest Species Inside Nanoporous Crystalline Materials J. Phys. Chem. C 2012, 116, 23556-23568.

NiMOF-74: Analysis of membrane permeation experiments



The membrane transport coefficients are the ones presented by:

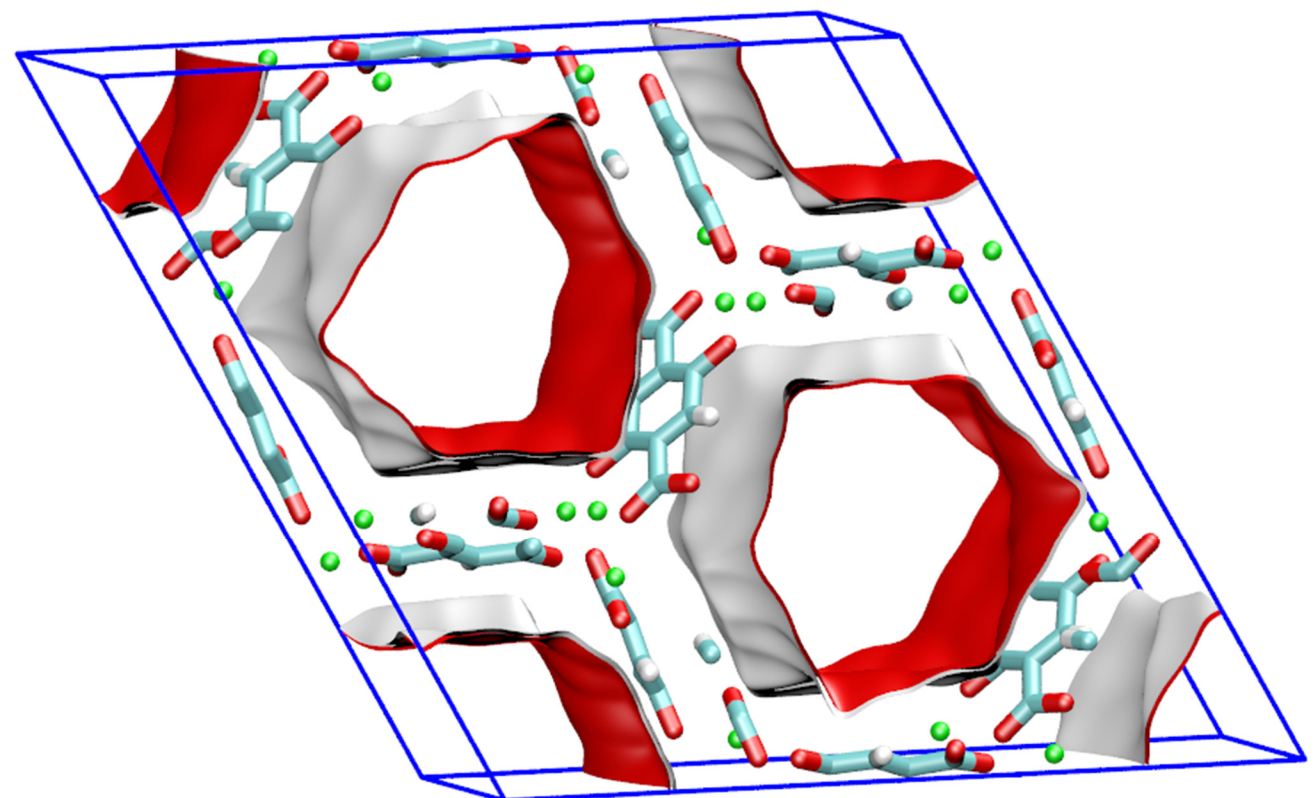
Krishna, R.; van Baten, J.M. Investigating the Relative Influences of Molecular Dimensions and Binding Energies on Diffusivities of Guest Species Inside Nanoporous Crystalline Materials J. Phys. Chem. C 2012, 116, 23556-23568.

FeMOF-74 pore landscapes

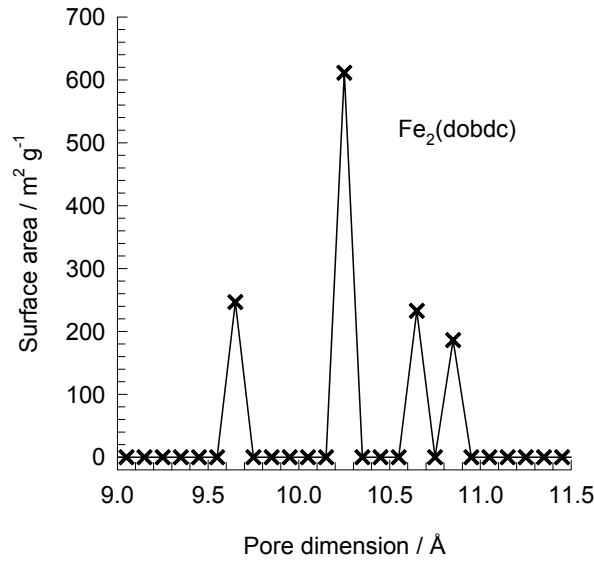
The structural information on FeMOF-74 ($= \text{Fe}_2(\text{dobdc}) = \text{Fe}\backslash(\text{dobdc} = \text{CPO-27-Fe})$ with dobdc = (dobdc⁴⁻ = 2,5-dioxido-1,4-benzenedicarboxylate)) was obtained from

Bloch et al. E.D. Bloch, L. Murray, W.L. Queen, S.M. Chavan, S.N. Maximoff, J.P. Bigi, R. Krishna, V.K. Peterson, F. Grandjean, G.J. Long, B. Smit, S. Bordiga, C.M. Brown, J.R. Long, Selective Binding of O₂ over N₂ in a Redox-Active Metal-Organic Framework with Open Iron(II) Coordination Sites, *J. Am. Chem. Soc.* 133 (2011) 14814-14822.

E.D. Bloch, W.L. Queen, R. Krishna, J.M. Zadrozny, C.M. Brown, J.R. Long, Hydrocarbon Separations in a Metal-Organic Framework with Open Iron(II) Coordination Sites, *Science* 335 (2012) 1606-1610.



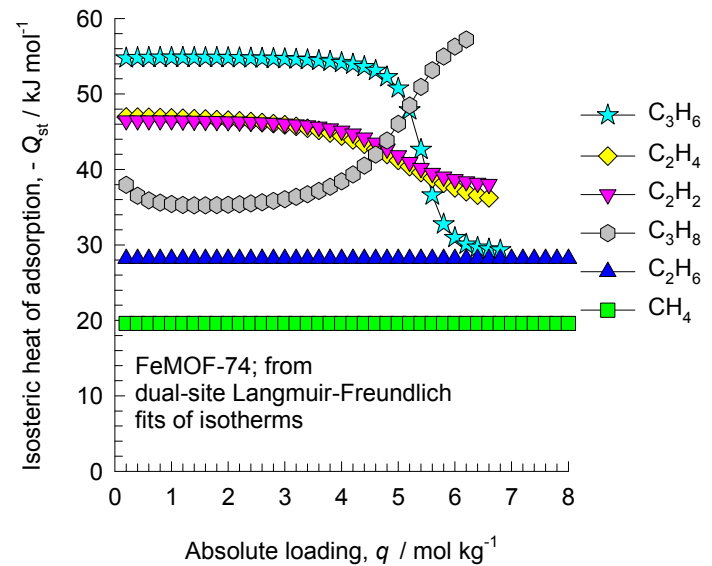
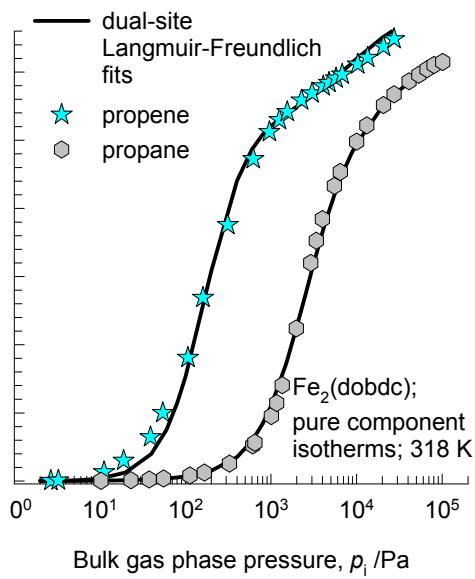
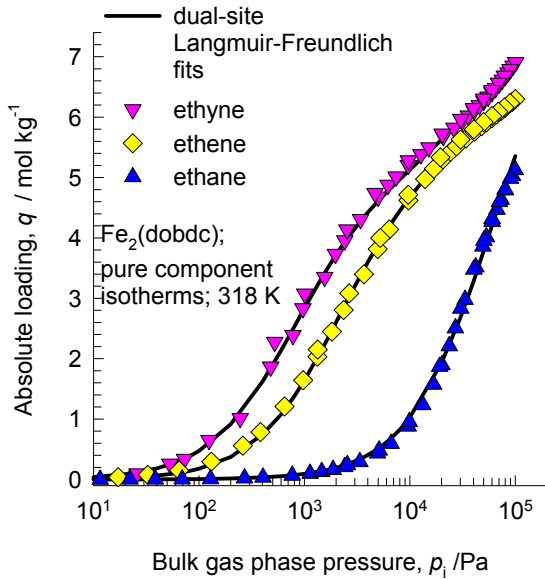
FeMOF-74 pore dimensions



This plot of surface area versus pore dimension is determined using a combination of the DeLaunay triangulation method for pore dimension determination, and the procedure of Düren for determination of the surface area.

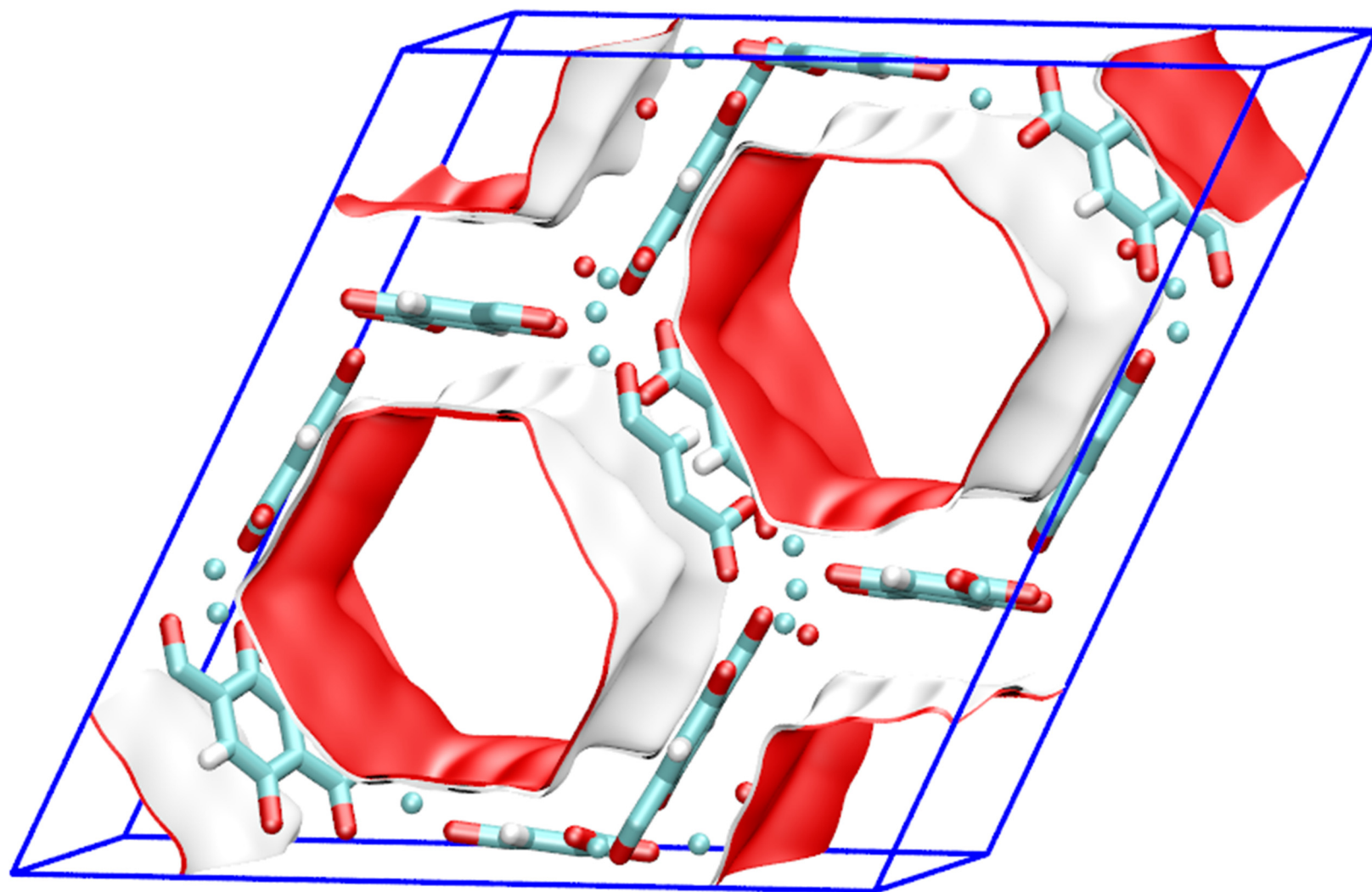
| FeMOF-74 | |
|--|----------|
| a /Å | 26.1627 |
| b /Å | 26.1627 |
| c /Å | 6.8422 |
| Cell volume / Å ³ | 4055.94 |
| conversion factor for [molec/uc] to [mol per kg Framework] | 0.3635 |
| conversion factor for [molec/uc] to [kmol/m ³] | 0.5807 |
| ρ [kg/m ³] | 1126.434 |
| MW unit cell [g/mol (framework)] | 2751.321 |
| ϕ , fractional pore volume | 0.705 |
| open space / Å ³ /uc | 2859.7 |
| Pore volume / cm ³ /g | 0.626 |
| Surface area /m ² /g | 1277.4 |
| DeLaunay diameter /Å | 11.12 |

FeMOF-74 isotherms and isosteric heats of adsorption from experiments

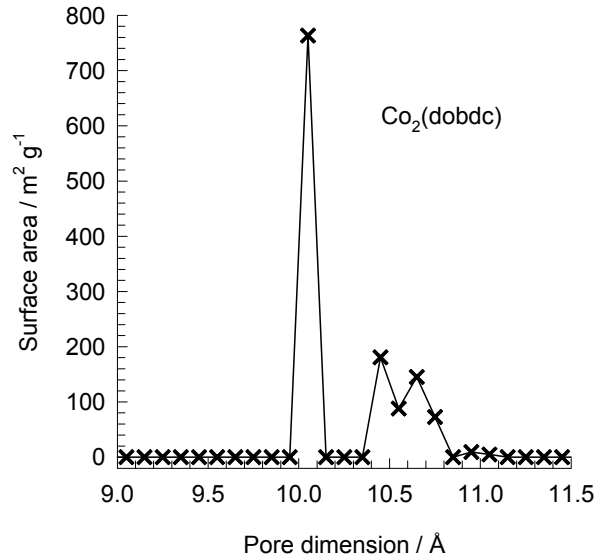


The pure component isotherms, with fits, and isosteric heats of adsorption are those reported by:
 He, Y.; Krishna, R.; Chen, B. Metal-Organic Frameworks with Potential for Energy-Efficient Adsorptive Separation of Light Hydrocarbons. *Energy Environ. Sci.* 2012, 5, 9107-9120.

CoMOF-74 pore landscapes



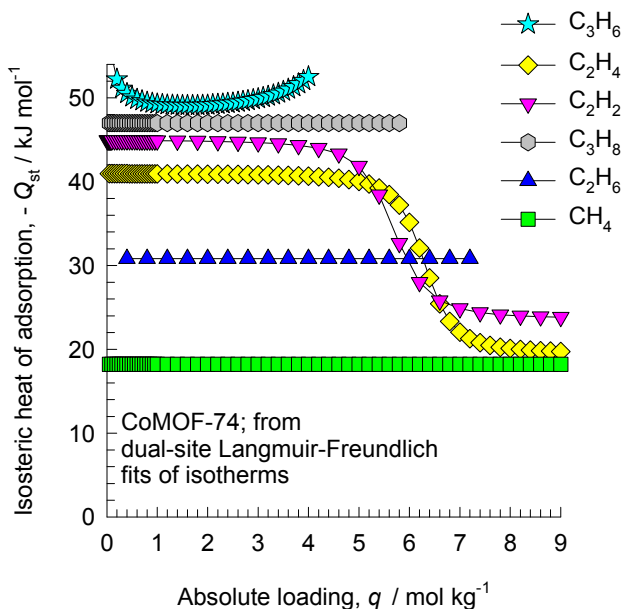
CoMOF-74 pore dimensions



This plot of surface area versus pore dimension is determined using a combination of the DeLaunay triangulation method for pore dimension determination, and the procedure of Düren for determination of the surface area. The computational details will be described in detail in a forthcoming publication.

| CoMOF-74 | |
|--|----------|
| a /Å | 25.885 |
| b /Å | 25.885 |
| c /Å | 6.8058 |
| Cell volume / Å ³ | 3949.173 |
| conversion factor for [molec/uc] to [mol per kg Framework] | 0.3563 |
| conversion factor for [molec/uc] to [kmol/m ³] | 0.5945 |
| ρ [kg/m ³] | 1180.261 |
| MW unit cell [g/mol(framework)] | 2806.908 |
| ϕ , fractional pore volume | 0.707 |
| open space / Å ³ /uc | 2793.1 |
| Pore volume / cm ³ /g | 0.599 |
| Surface area / m ² /g | 1274.0 |
| DeLaunay diameter /Å | 9.52 |

CoMOF-74 isotherms and isosteric heats of adsorption from experiments



The pure component isotherms, with fits, and isosteric heats of adsorption are those reported by:
He, Y.; Krishna, R.; Chen, B. Metal-Organic Frameworks with Potential for Energy-Efficient Adsorptive Separation of Light Hydrocarbons. *Energy Environ. Sci.* 2012, 5, 9107-9120.

MIL-47 pore landscape

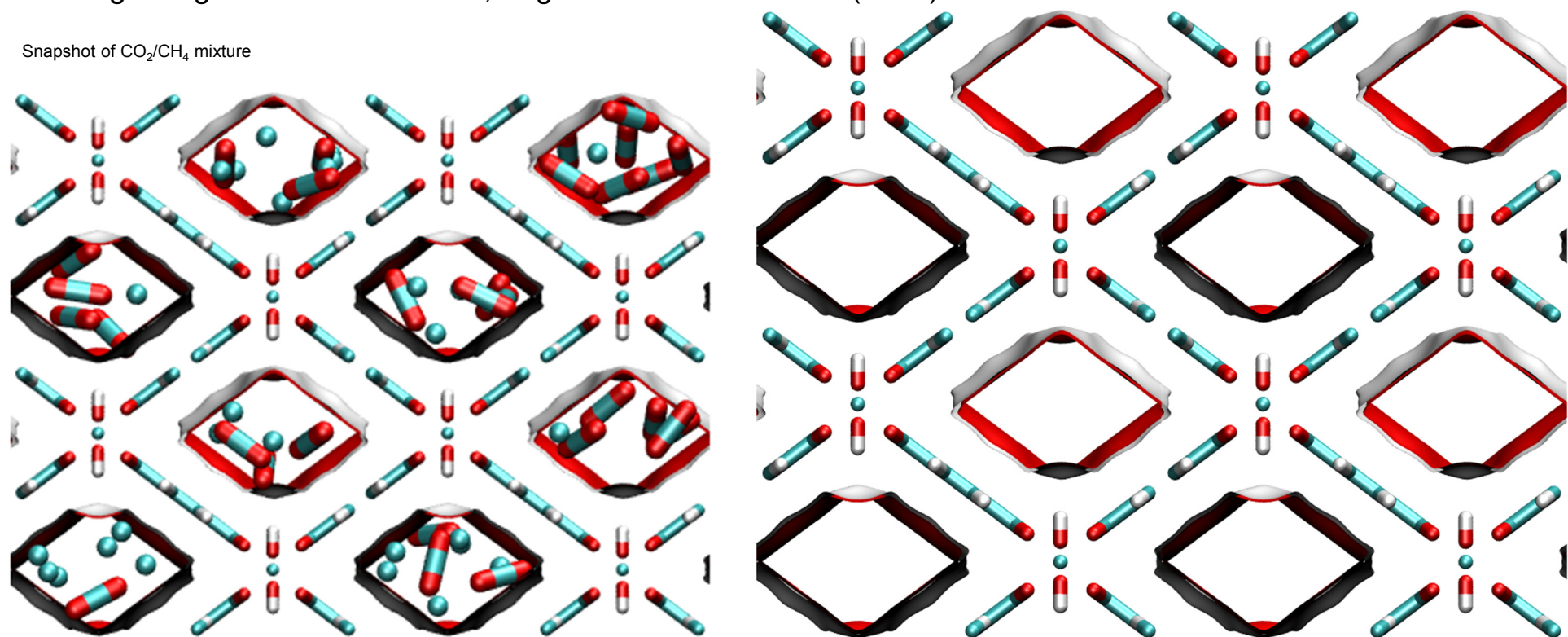
The structural information for MIL-47 was taken from

L. Alaerts, C.E.A. Kirschhock, M. Maes, M. van der Veen, V. Finsy, A. Depla, J.A. Martens, G.V. Baron, P.A. Jacobs, J.F.M. Denayer, D. De Vos, Selective Adsorption and Separation of Xylene Isomers and Ethylbenzene with the Microporous Vanadium(IV) Terephthalate MIL-47, *Angew. Chem. Int. Ed.* 46 (2007) 4293-4297.

V. Finsy, H. Verelst, L. Alaerts, D. De Vos, P.A. Jacobs, G.V. Baron, J.F.M. Denayer, Pore-Filling-Dependent Selectivity Effects in the Vapor-Phase Separation of Xylene Isomers on the Metal-Organic Framework MIL-47, *J. Am. Chem. Soc.* 130 (2008) 7110-7118.

K. Barthelet, J. Marrot, D. Riou, G. Férey, A Breathing Hybrid Organic - Inorganic Solid with Very Large Pores and High Magnetic Characteristics, *Angew. Chem. Int. Ed.* 41 (2007) 281-284.

Snapshot of CO₂/CH₄ mixture

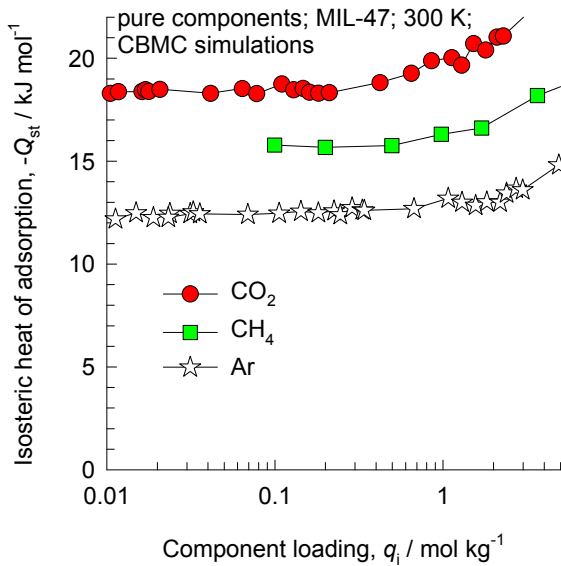
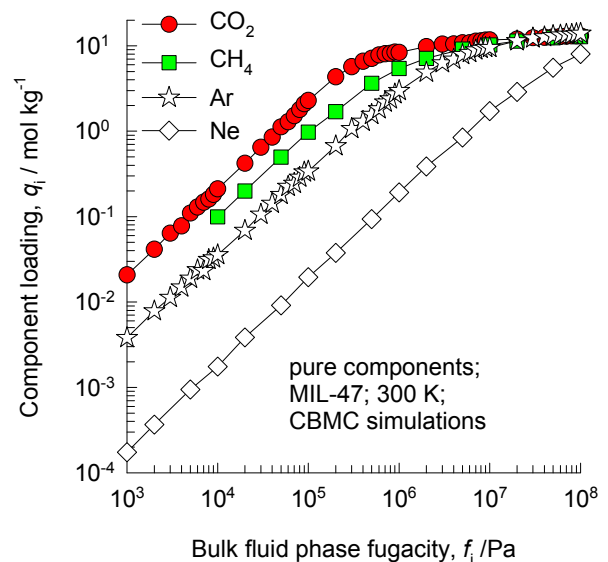
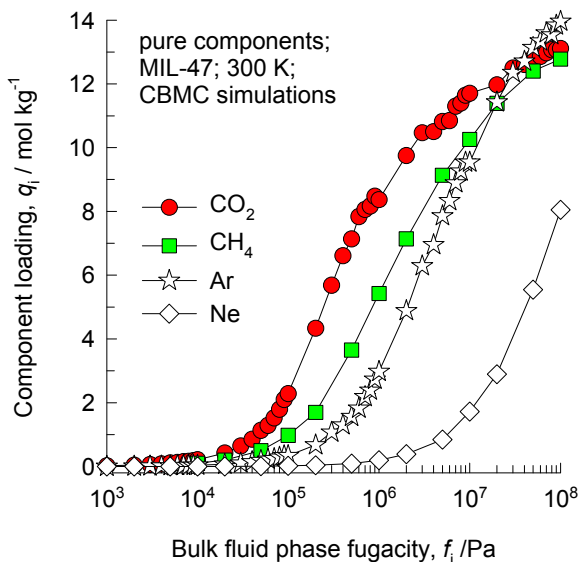


MIL-47 dimensions

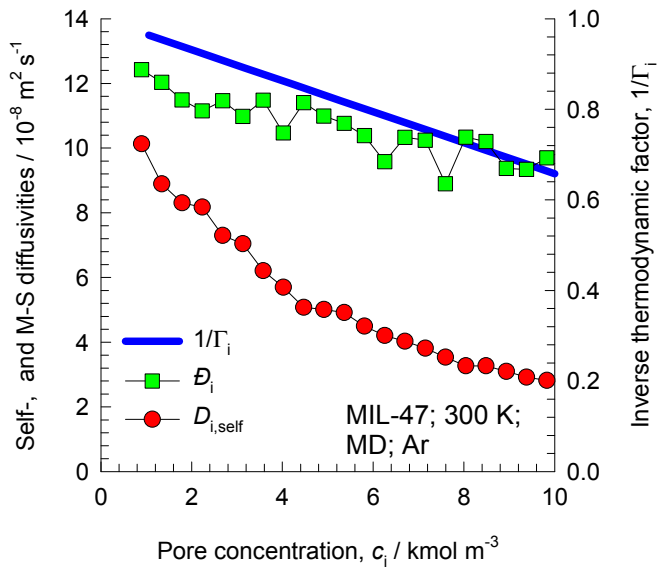
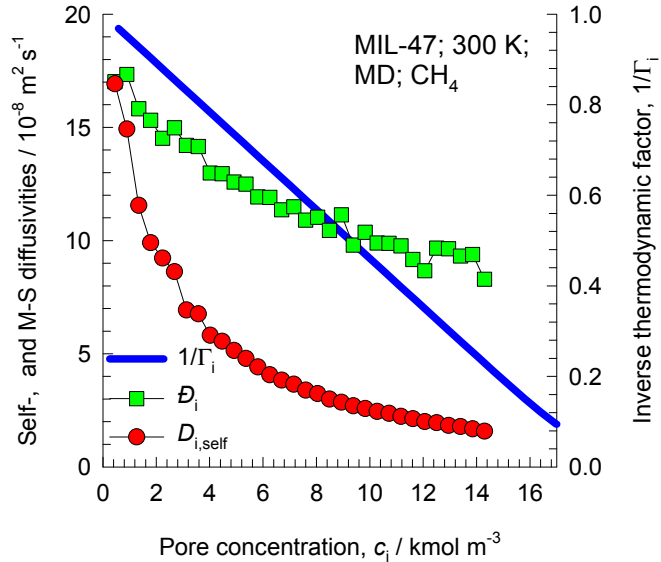
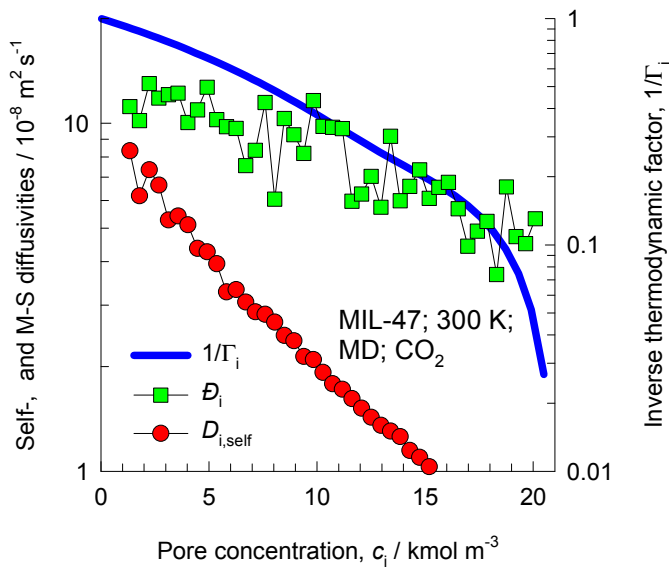
| | MIL-47 |
|--|----------|
| a /Å | 6.808 |
| b /Å | 16.12 |
| c /Å | 13.917 |
| Cell volume / Å ³ | 1527.321 |
| conversion factor for [molec/uc] to [mol per kg Framework] | 1.0824 |
| conversion factor for [molec/uc] to [kmol/m ³] | 1.7868 |
| ρ [kg/m ³] | 1004.481 |
| MW unit cell [g/mol(framework)] | 923.881 |
| ϕ , fractional pore volume | 0.608 |
| open space / Å ³ /uc | 929.3 |
| Pore volume / cm ³ /g | 0.606 |
| Surface area /m ² /g | 1472.8 |
| DeLaunay diameter /Å | 8.03 |

One-dimensional diamond-shaped channels with free internal diameter of 8Å

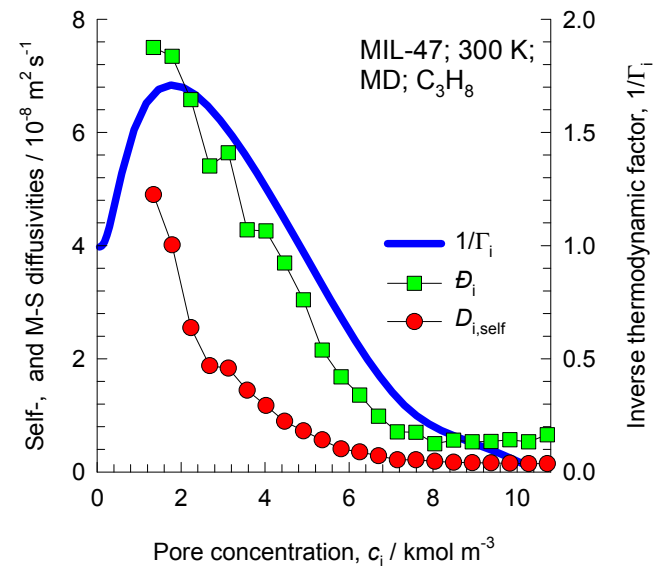
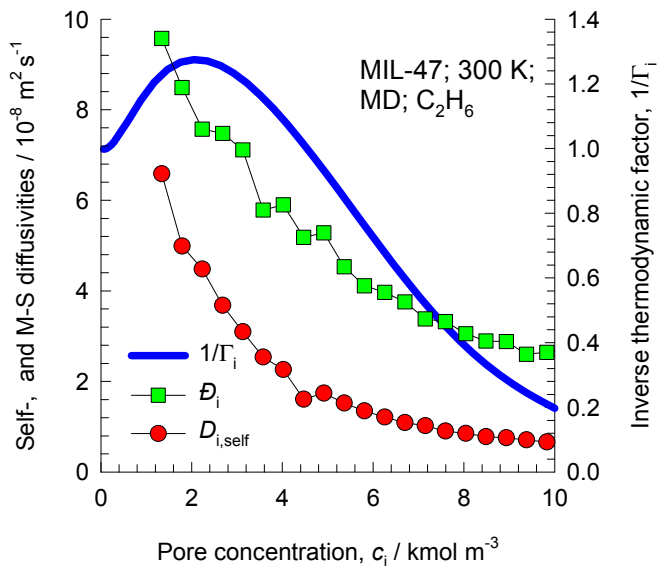
MIL-47 CBMC simulations of isotherms, and isosteric heats of adsorption



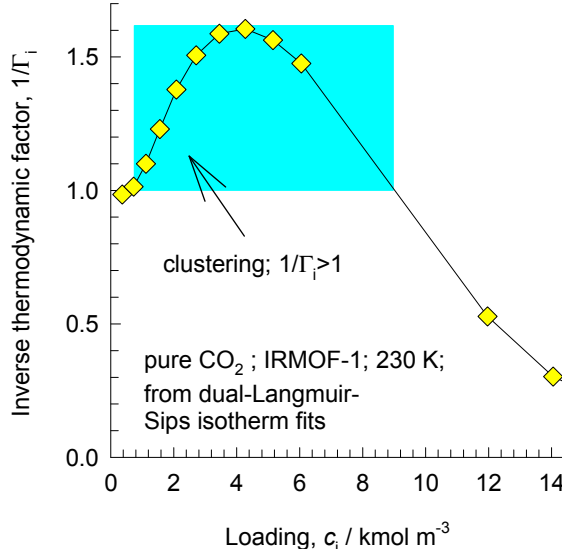
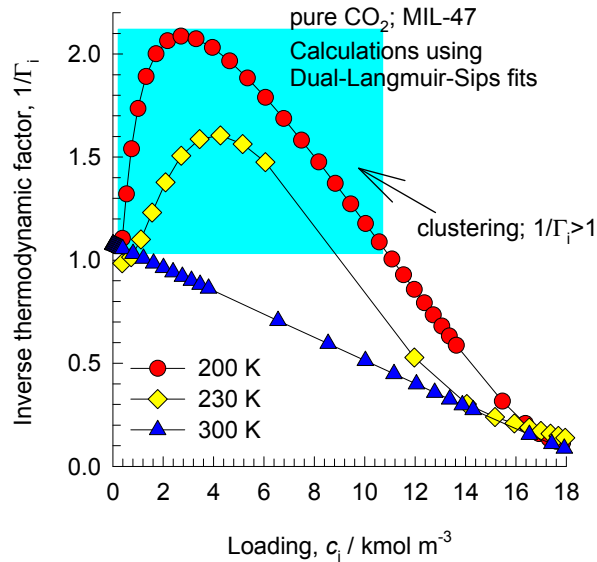
Influence of Inverse Thermodynamic Factor on diffusivities



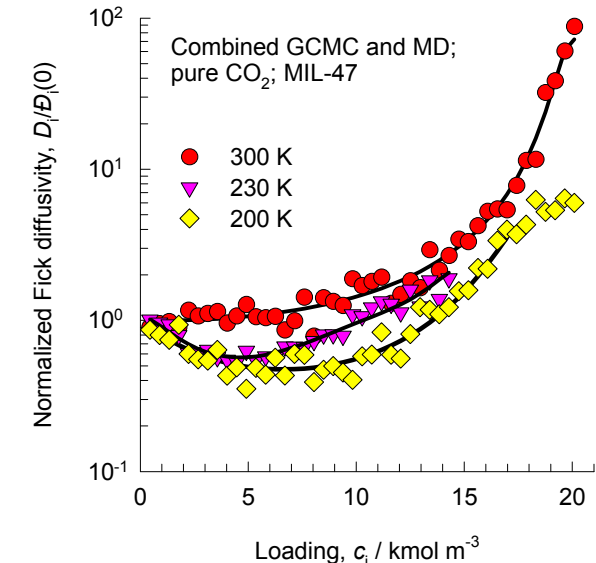
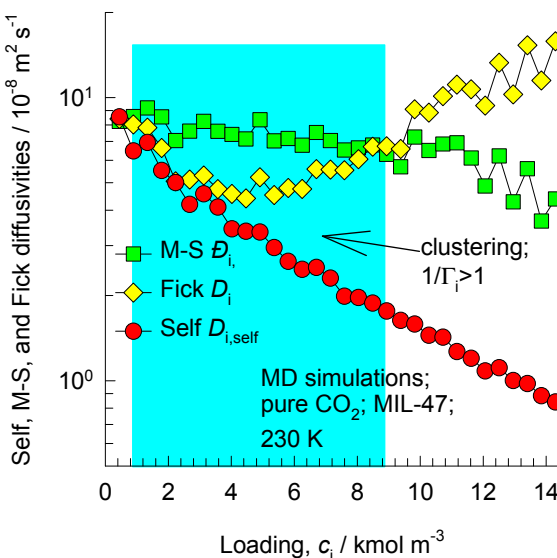
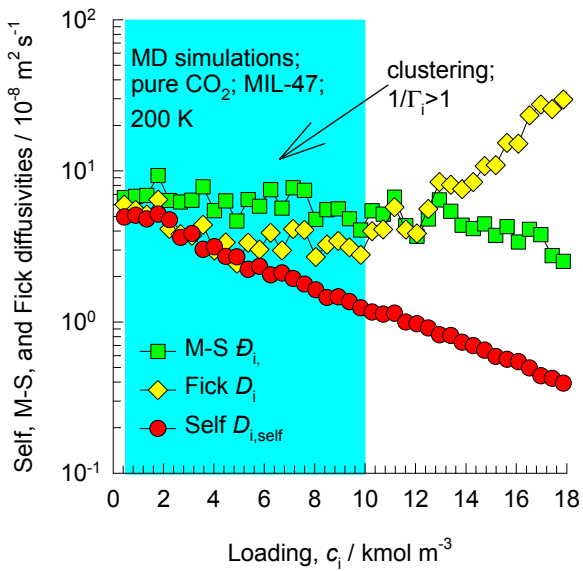
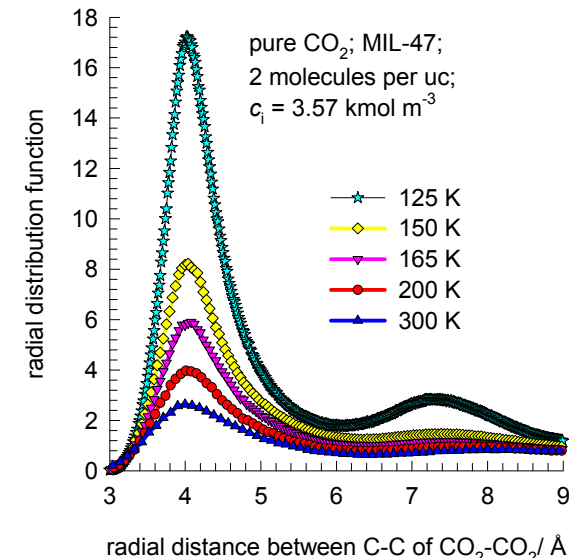
Influence of Inverse Thermodynamic Factor on diffusivities



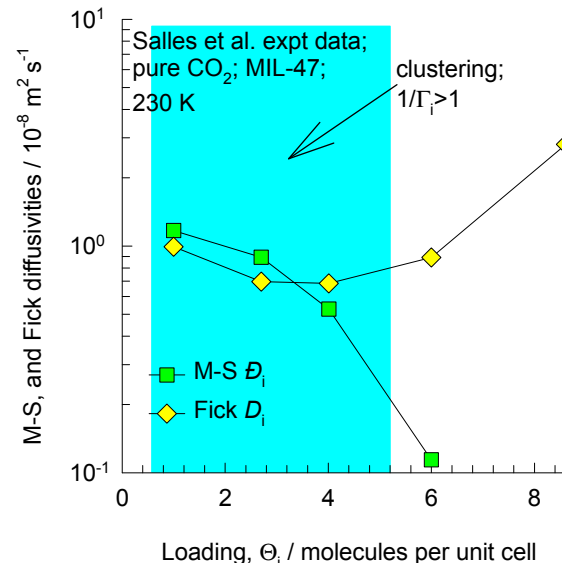
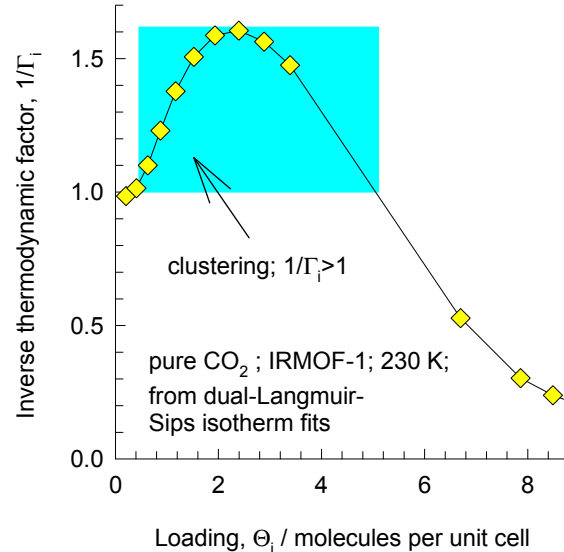
MIL-47 CO₂ adsorption and diffusion



The RDFs show that the degree of clustering increases as the temperature is decreased.



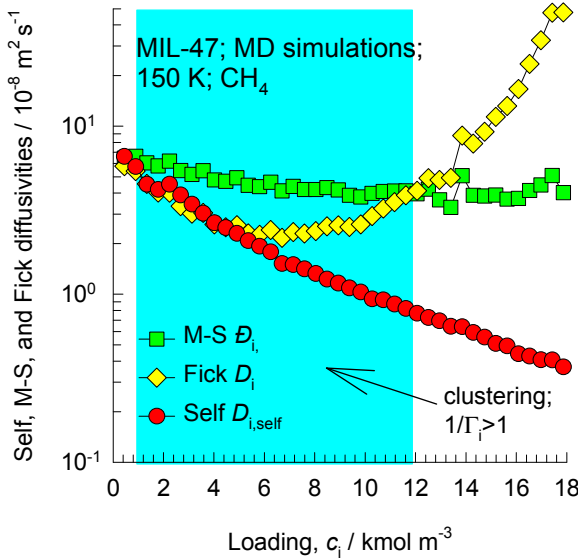
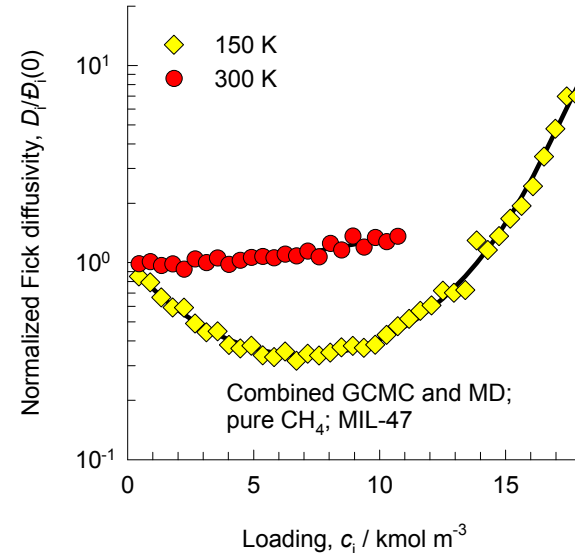
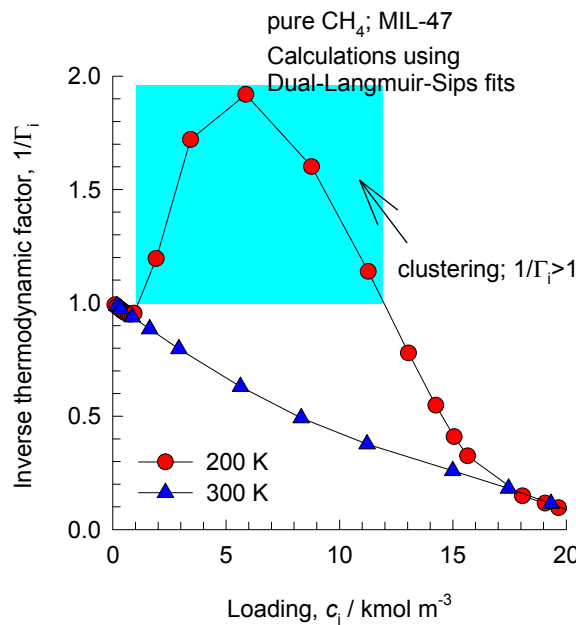
MIL-47 CO₂ adsorption and diffusion; analysis of Salles et al. expt data



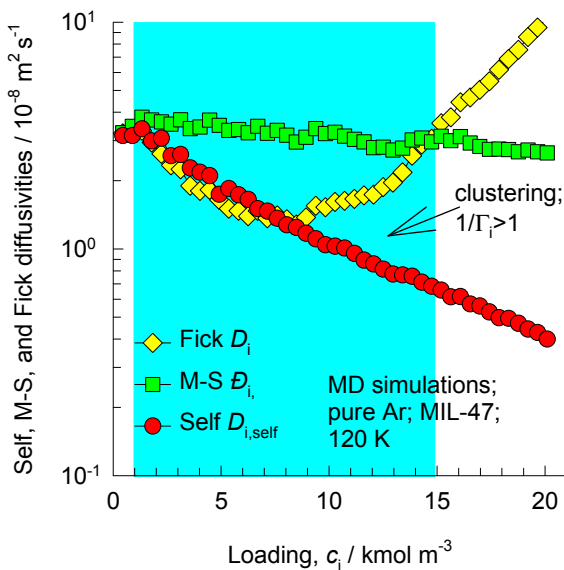
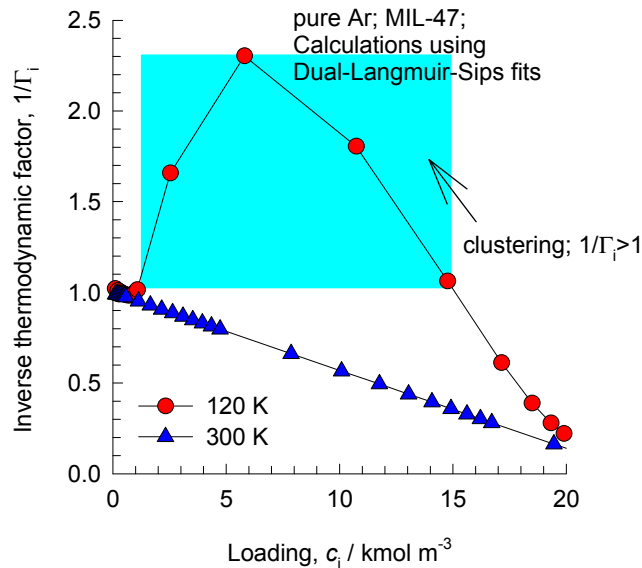
These are our CBMC simulation results, not those of Salles et al.

The experimental results of F. Salles, H. Jobic, T. Devic, P.L. Llewellyn, C. Serre, G. Férey, G. Maurin, Self and Transport Diffusivity of CO₂ in the Metal-Organic Framework MIL-47(V) Explored by Quasi-elastic Neutron Scattering Experiments and Molecular Dynamics Simulations, ACS Nano 2010, 4, 143-152, show that the Fick diffusivity can be lower than the Maxwell-Stefan diffusivity in regions where clustering of molecules occurs. The Fick diffusivity decreases with loading in the regions in which $1/\Gamma_i > 1$. Please also note that the Salles data on diffusivities is spatially averaged over x, y, and z directions. Our MD data in the previous slide is for diffusion in the x-direction. So our diffusivities are expected to be about 3 times higher.

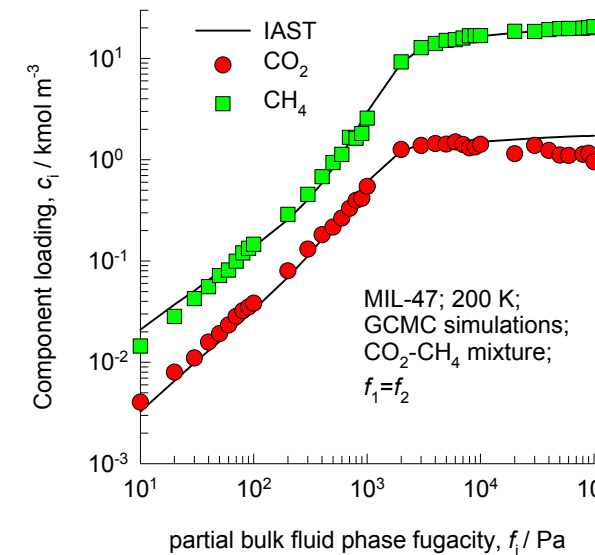
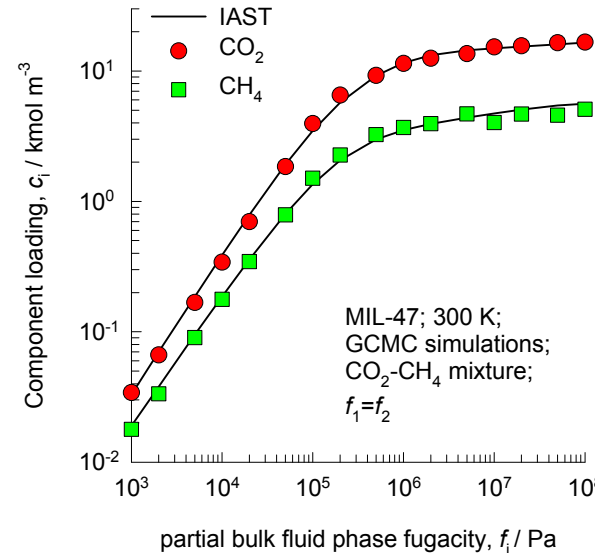
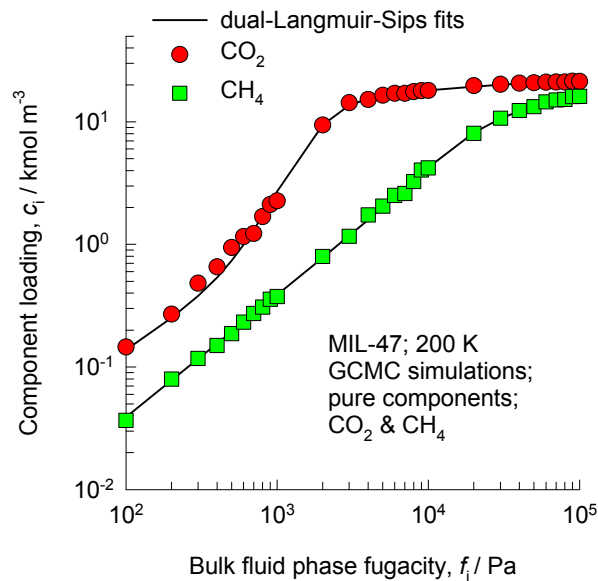
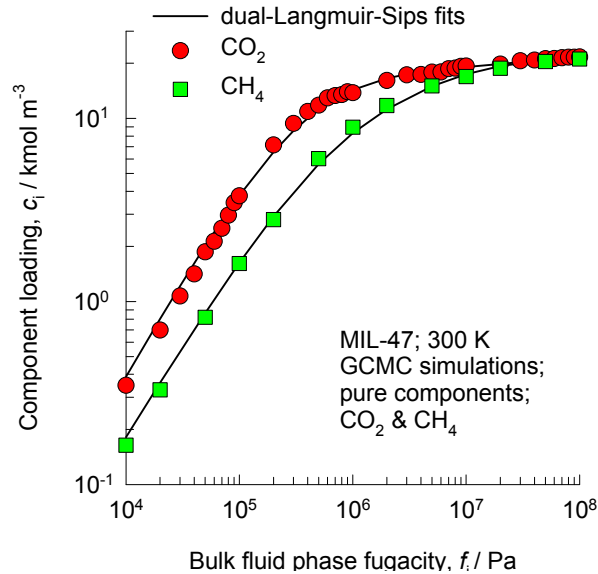
MIL-47 CH₄ adsorption and diffusion



MIL-47 Ar adsorption and diffusion



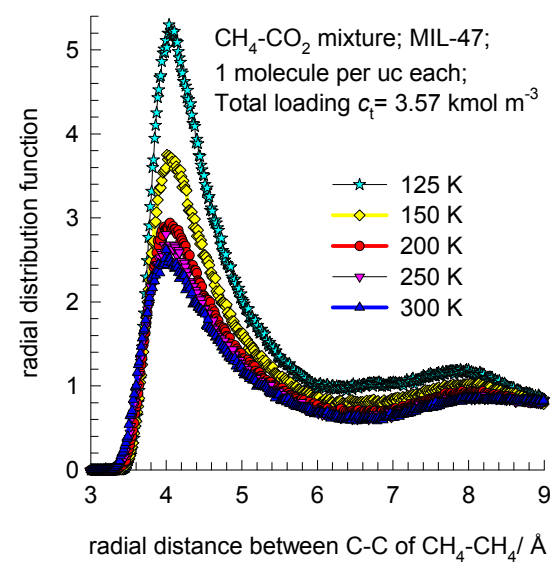
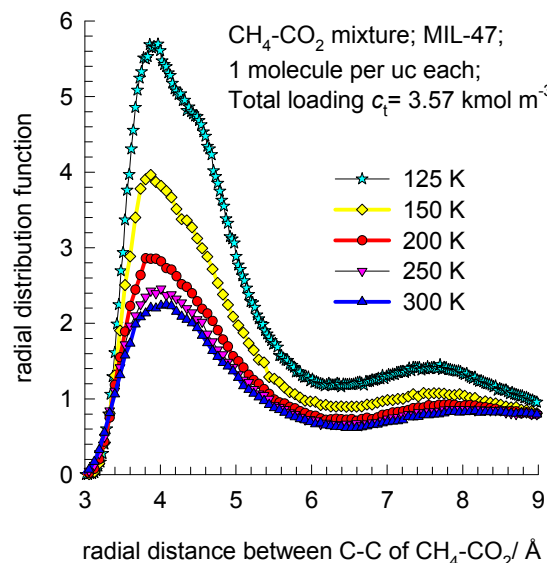
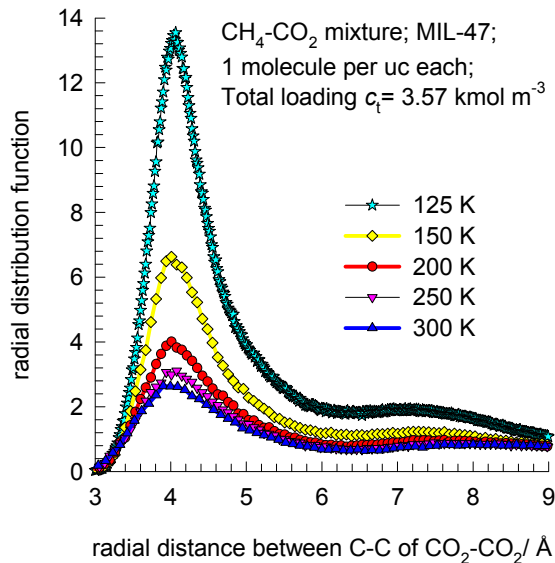
MIL-47 CBMC simulation results for CO₂-CH₄ mixtures



The IAST provides a good estimation of component loadings in the mixture.

MIL-47 RDFs for CO₂-CH₄ mixtures

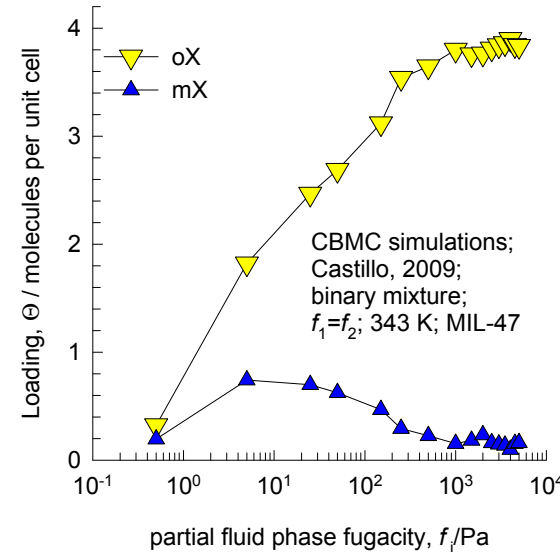
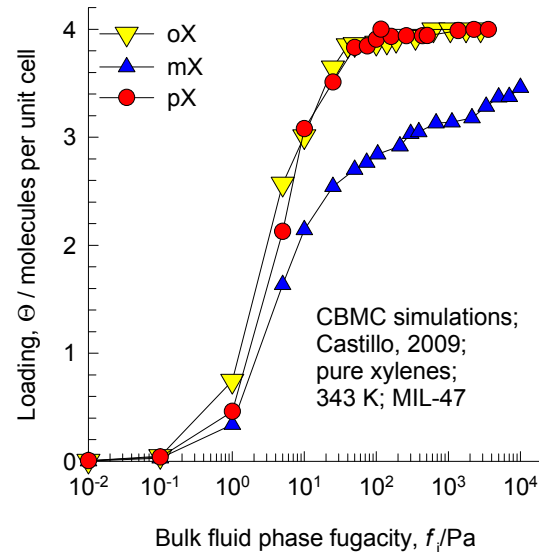
The RDFs are based on distances between the centres of mass of the molecules.



The RDFs demonstrate that clustering persists in mixtures, and increases with decreasing temperature

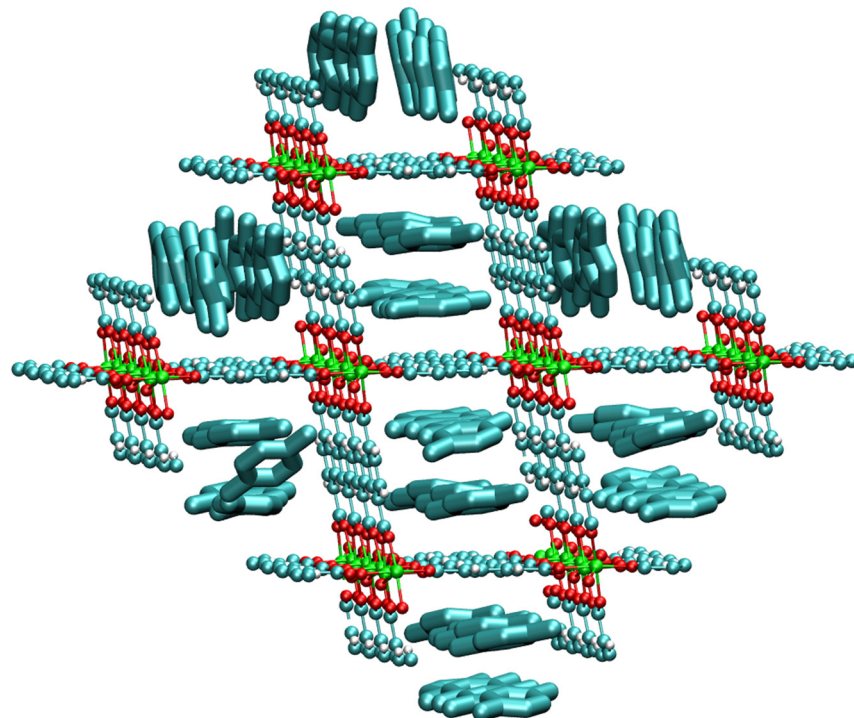
MIL-47 adsorption of xylene isomers

These simulation results are from Castillo, J. M.; Vlugt, T. J. H.; Calero, S. J. Phys. Chem. C 2009, 113, 20869-20874.

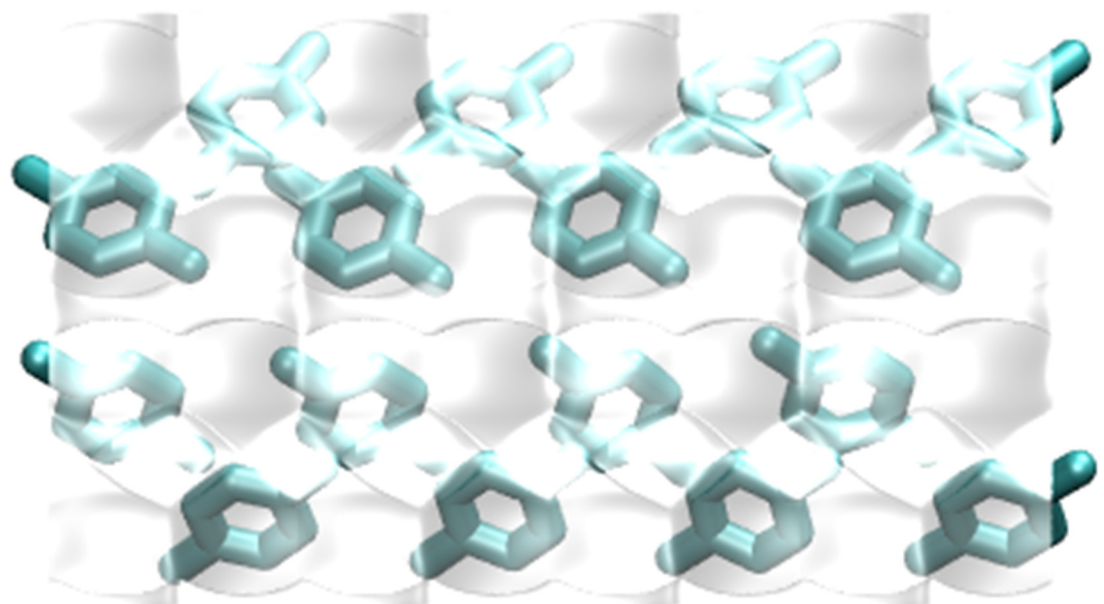
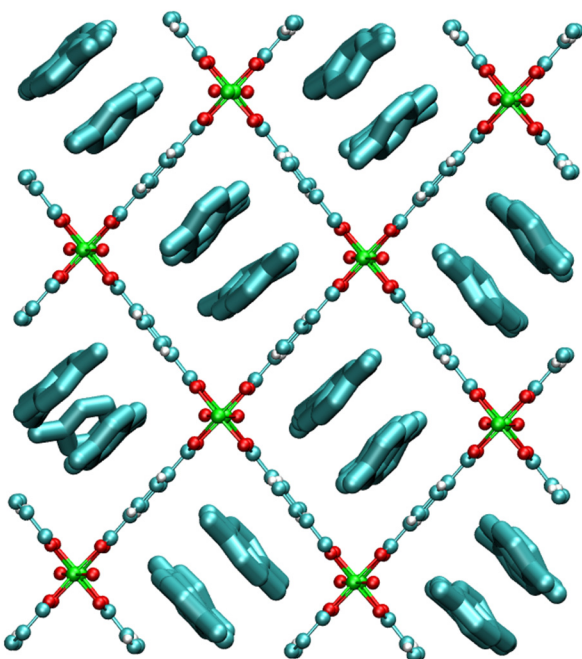


The adsorption selectivity hierarchy $\text{oX} > \text{mX}$ is dictated by the hierarchy of critical temperatures, i.e. degree of clustering. The degree of clustering has to be interpreted somewhat differently. As can be seen in the snapshots of the location of o-, p-, and m- xylenes in the following three slides, the xylene isomers stack nicely within the channels of MIL-47. The stacking efficiency for o- and p- isomers are significantly superior to that of the m- isomer, as evidenced from the snapshots.

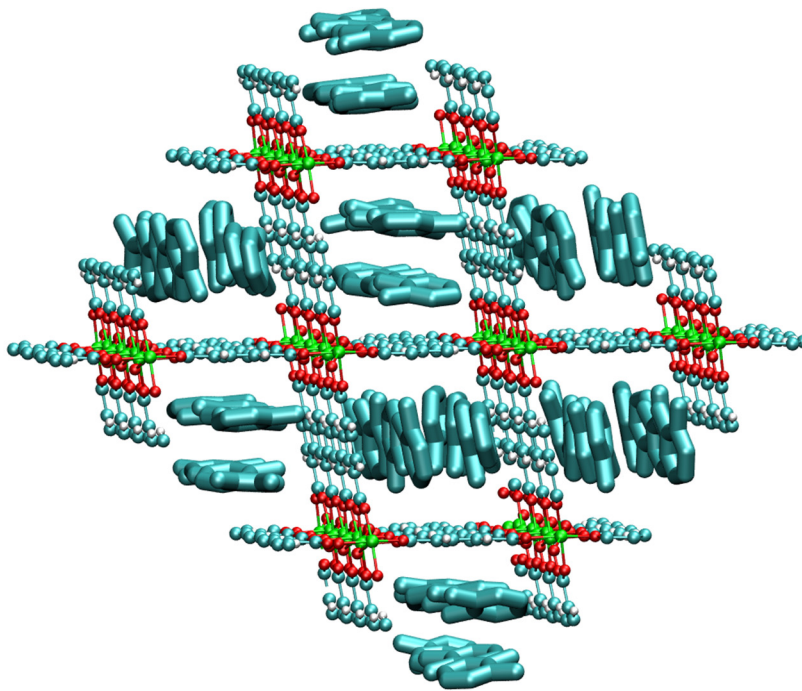
p-xylene



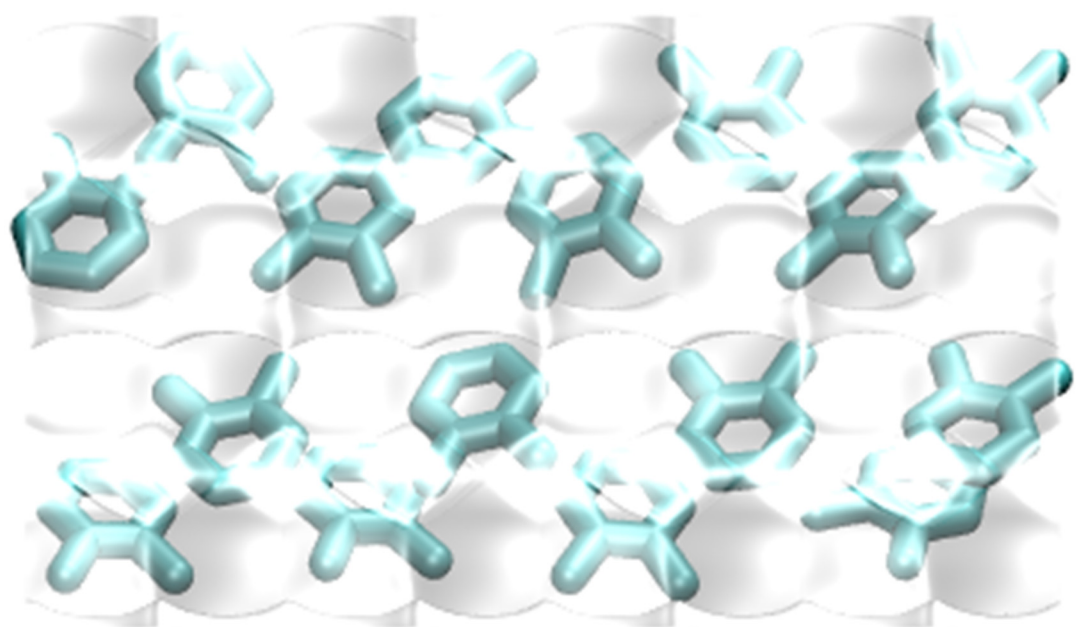
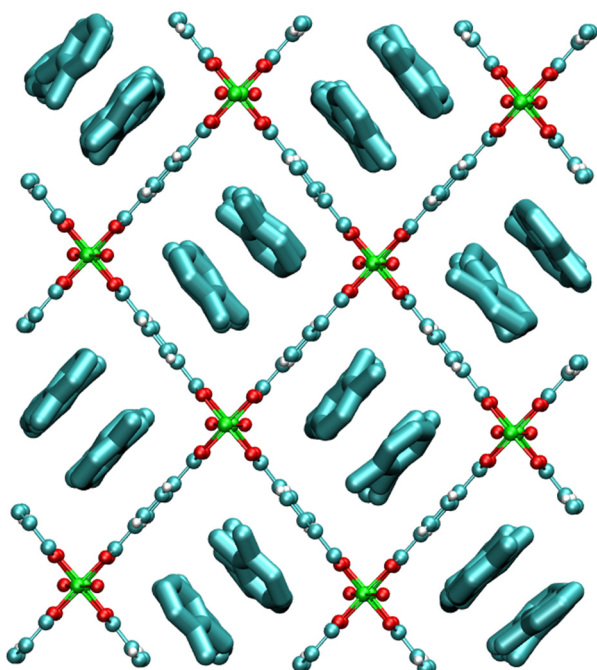
o-xylene and p-xylene
appear to pack the
channels very well



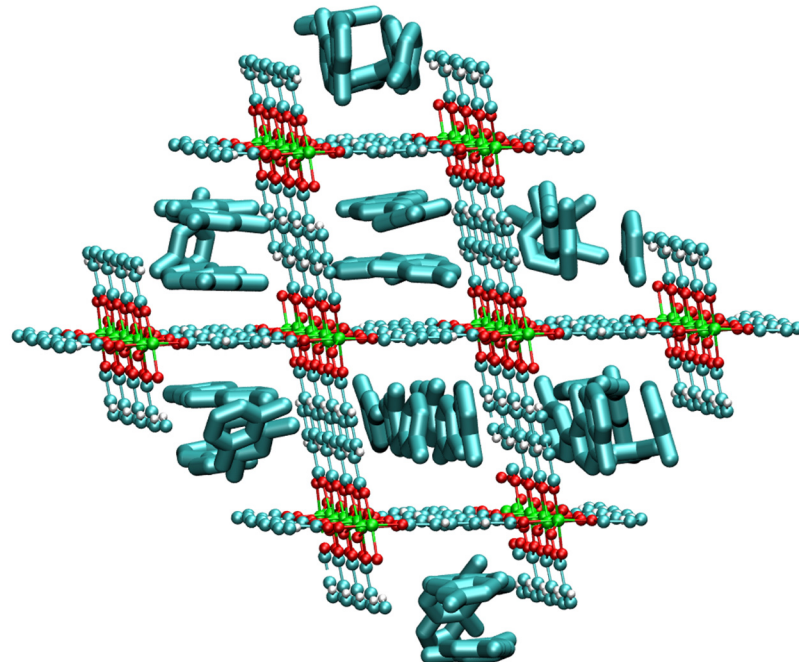
o-xylene



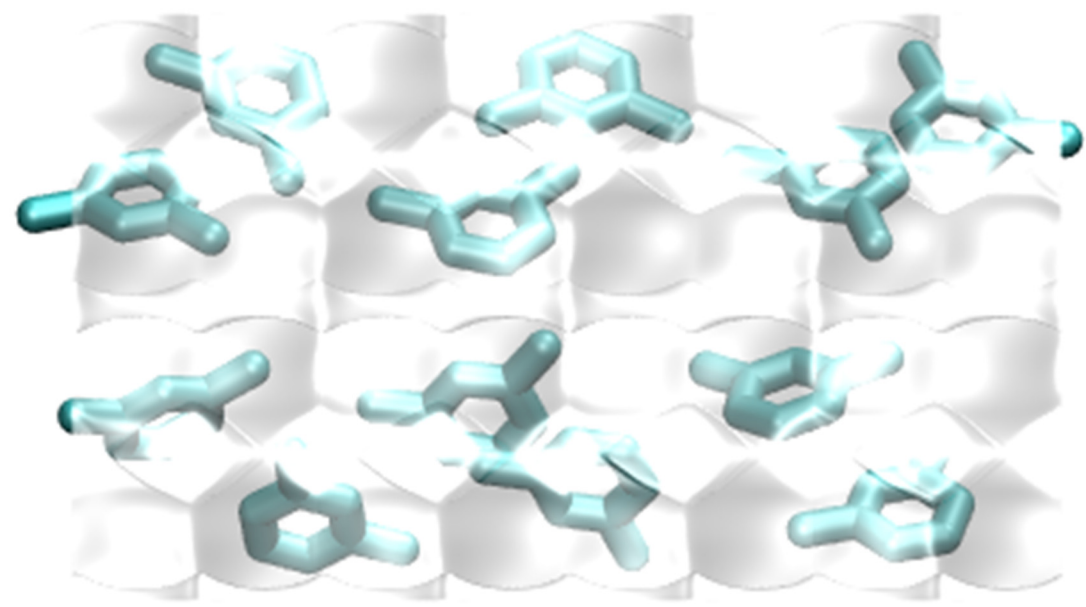
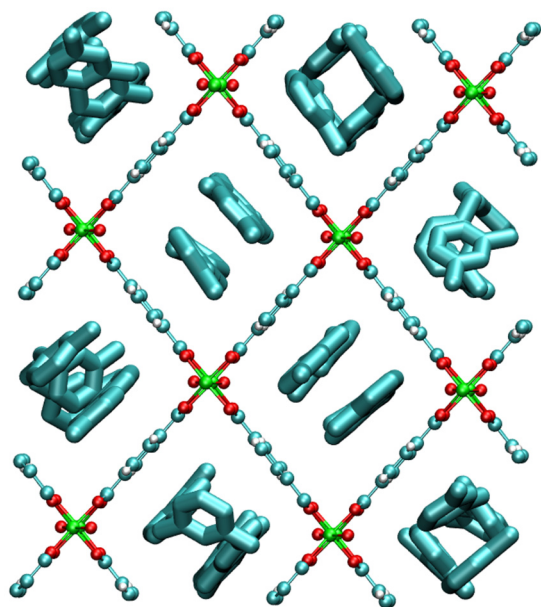
o-xylene and p-xylene
appear to pack the
channels very well



m-xylene



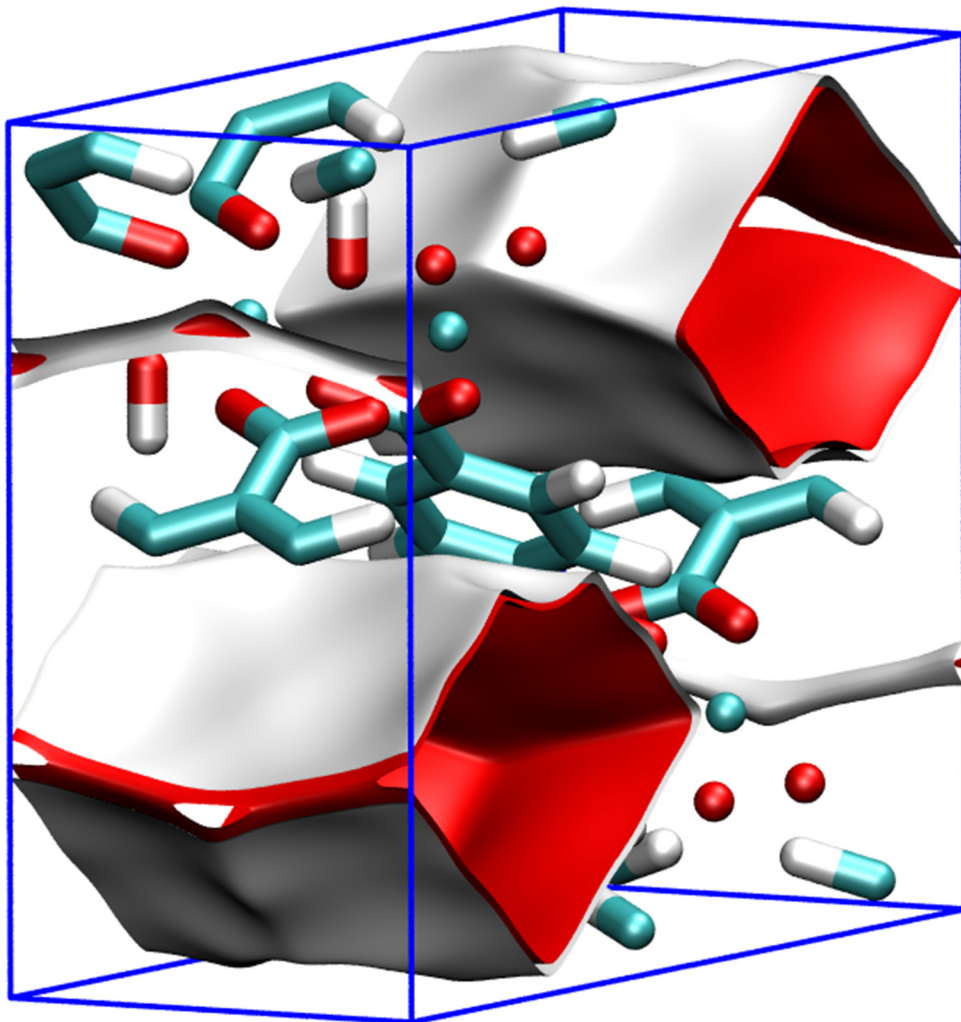
m-xylene does not pack the channels as well as o- and p-xylene. This is also evidenced in the snapshots.



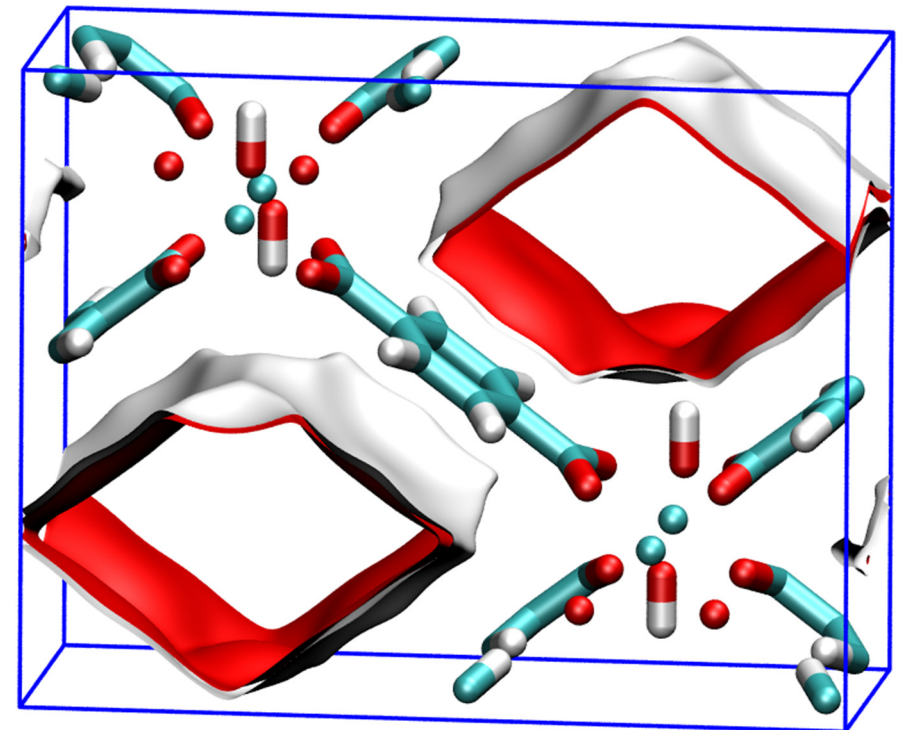
MIL – 53 (Cr) pore landscape

The structural data for MIL-53 (Cr) = Cr(OH)(O₂C-C₆H₄-CO₂) was taken from

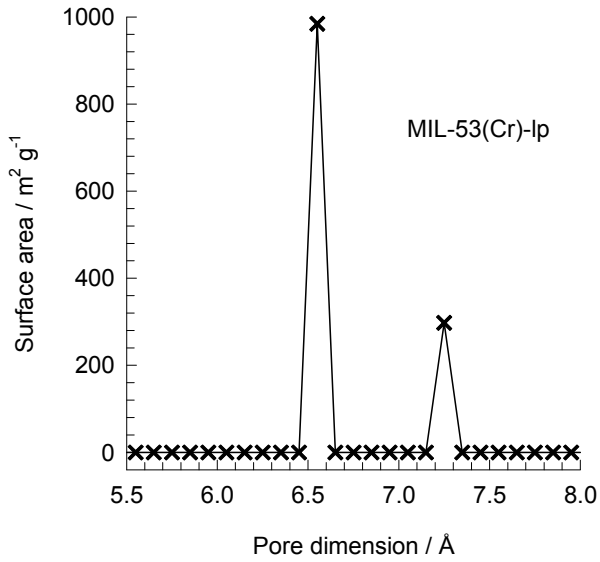
D.S. Coombes, F. Corà, C. Mellot-Draznieks, R.G. Bell, Sorption-Induced Breathing in the Flexible Metal Organic Framework CrMIL-53: Force-Field Simulations and Electronic Structure Analysis, J. Phys. Chem. C 113 (2009) 544-552.



Simulation results presented are for –Ip structure, i.e. large pore



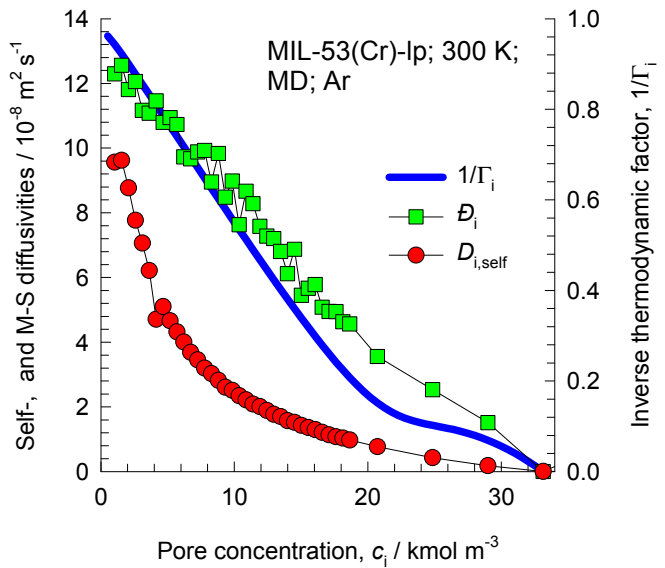
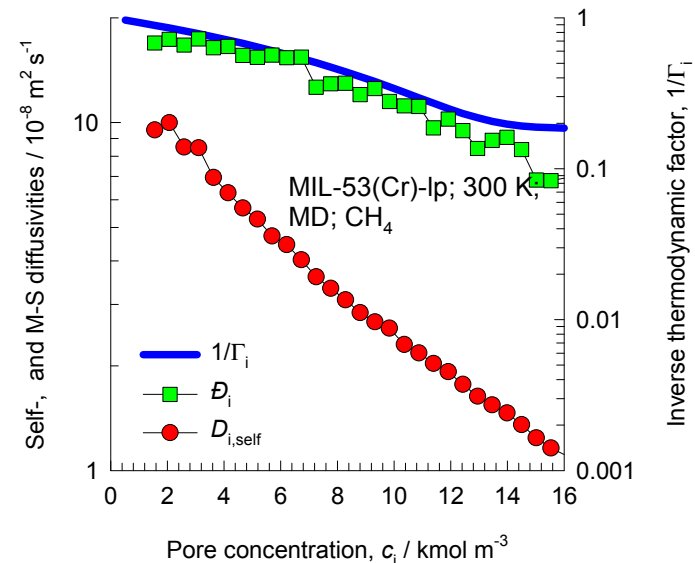
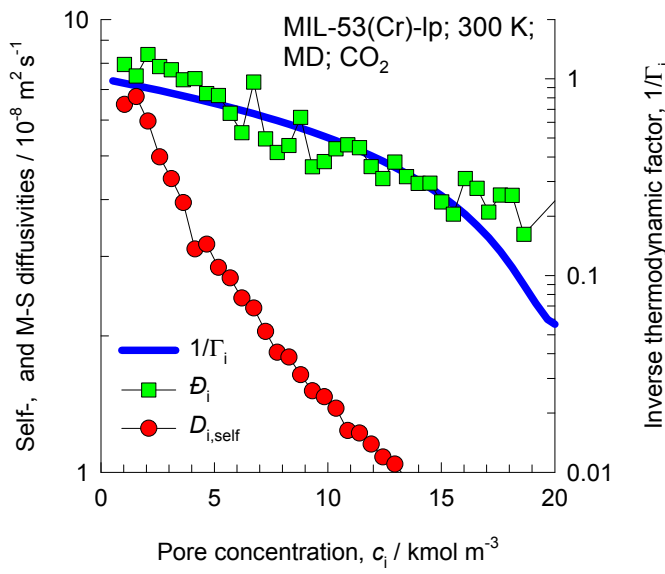
MIL-53 (Cr) pore dimensions



| MIL53(Cr)-Ip | |
|--|----------|
| $a / \text{\AA}$ | 16.733 |
| $b / \text{\AA}$ | 13.038 |
| $c / \text{\AA}$ | 6.812 |
| Cell volume / \AA^3 | 1486.139 |
| conversion factor for [molec/uc] to [mol per kg Framework] | 1.0728 |
| conversion factor for [molec/uc] to [kmol/m³] | 2.0716 |
| $\rho / [\text{kg}/\text{m}^3]$ | 1041.534 |
| MW unit cell [g/mol(framework)] | 932.1312 |
| ϕ , fractional pore volume | 0.539 |
| open space / $\text{\AA}^3/\text{uc}$ | 801.6 |
| Pore volume / cm^3/g | 0.518 |
| Surface area / m^2/g | 1280.5 |
| DeLaunay diameter / \AA | 7.40 |

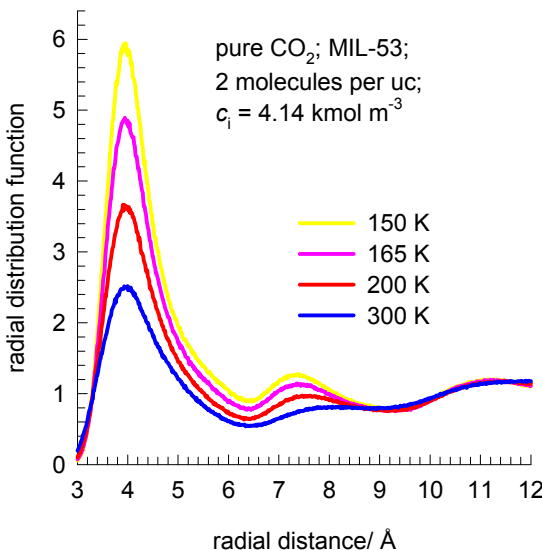
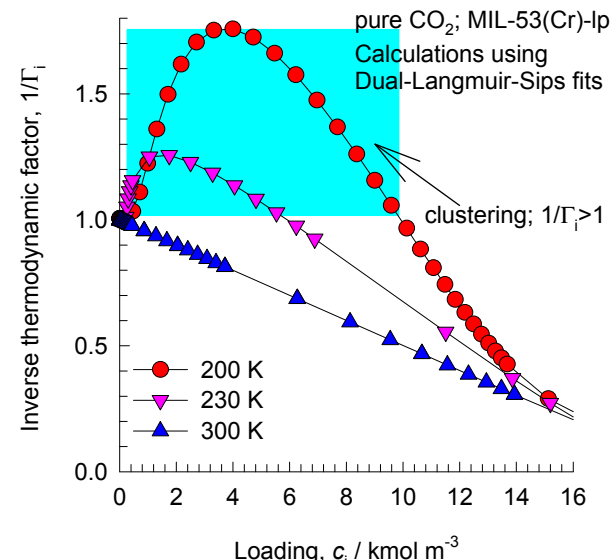
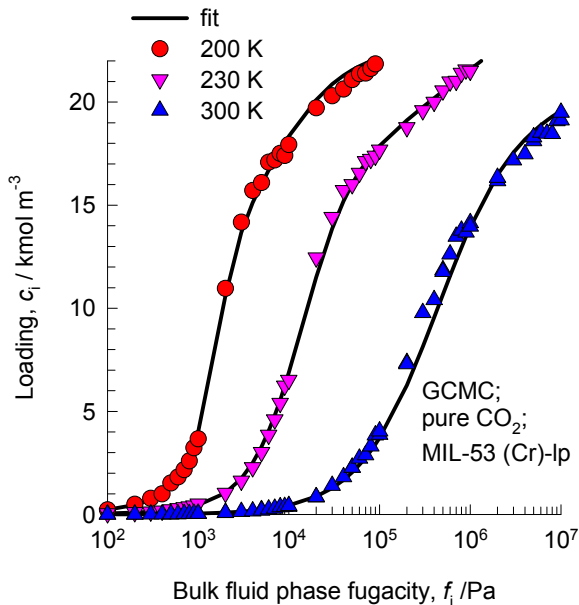
One-dimensional lozenge-shaped channels

Influence of Inverse Thermodynamic Factor on diffusivities



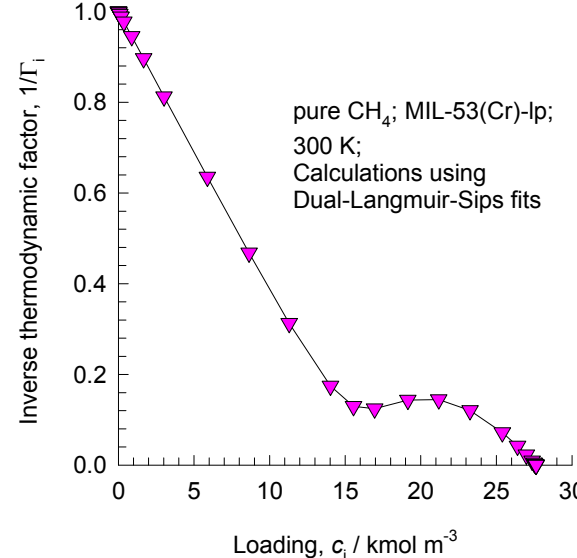
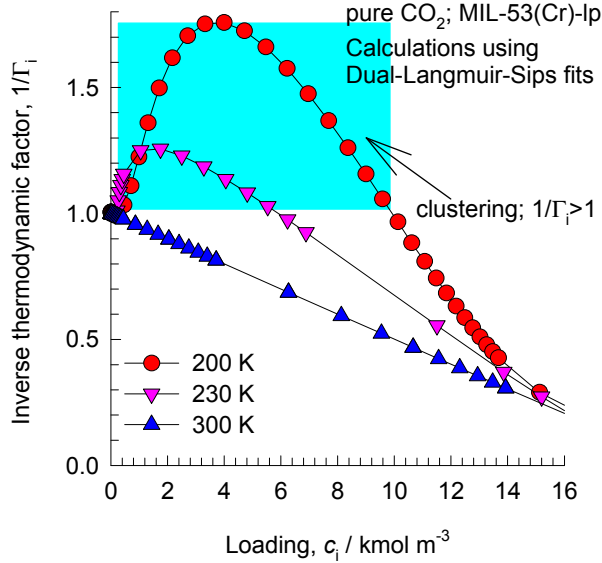
MIL-53 (Cr) -Ip

CBMC simulation results for adsorption of pure CO₂

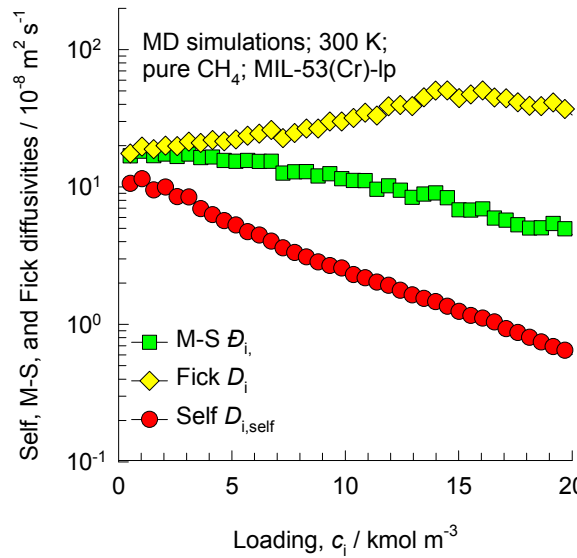
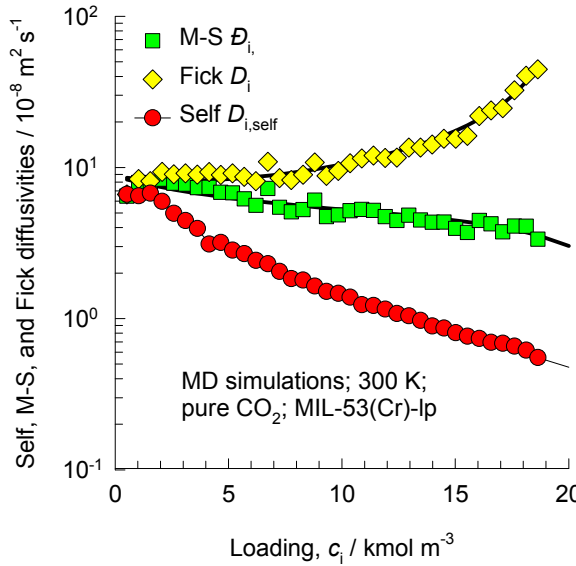


MIL-53 (Cr)-Ip

MD simulations for CO₂ and CH₄ diffusion at 300 K

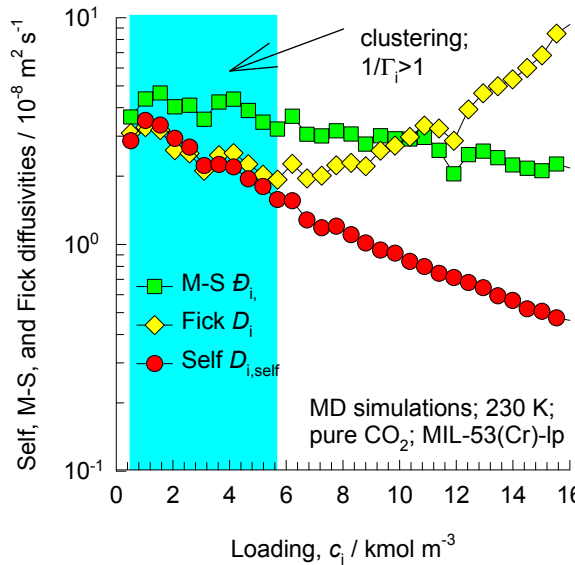
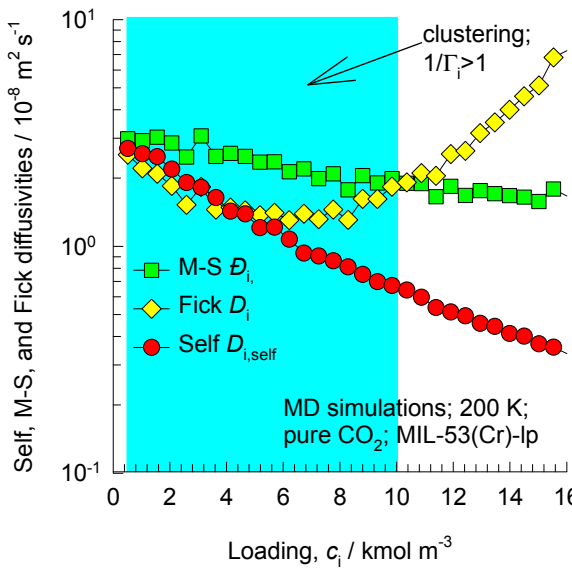
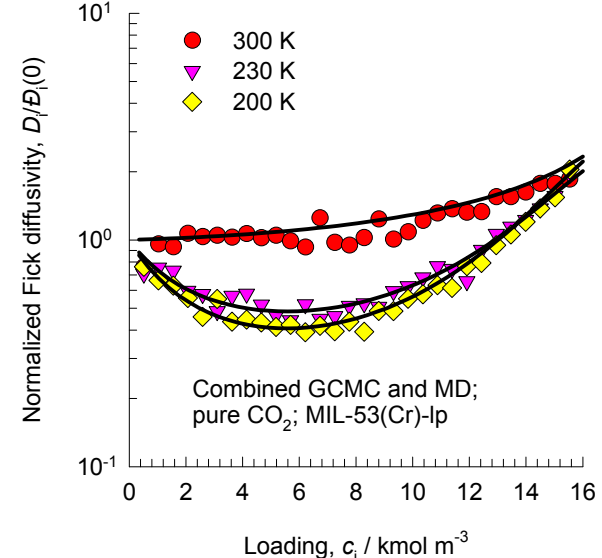
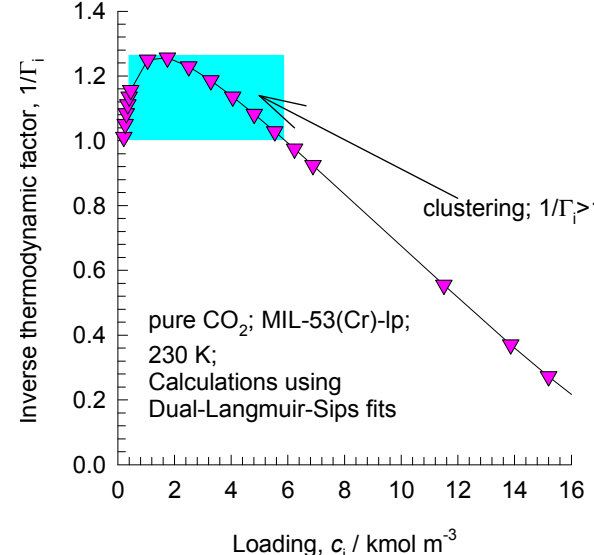
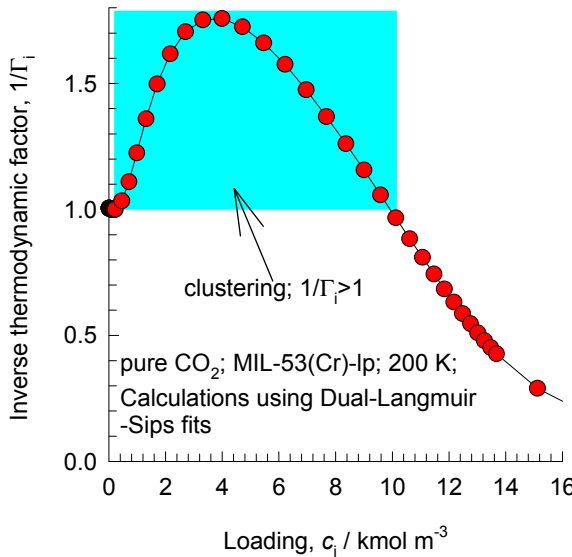


No clustering of either component at 300 K



MIL-53 (Cr)-Ip

MD simulations for CO₂ diffusion at 200 K and 230 K

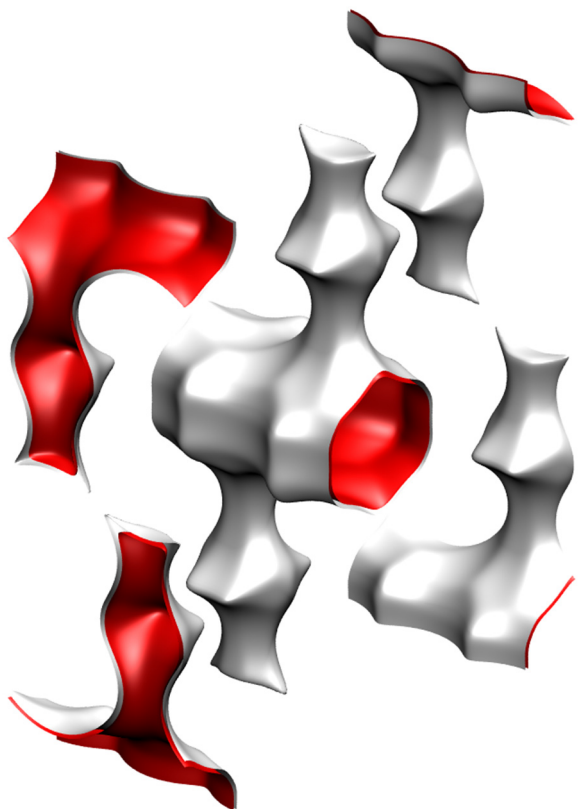


The experimental data of the Fick diffusivity at 230 K, published by Salles et al. (Angew. Chem. Int. Ed. 2009, 48, 8335-8339), shows that for the regions in which $1/\Gamma_i > 1$ the Fick diffusivity decreases with the loading.

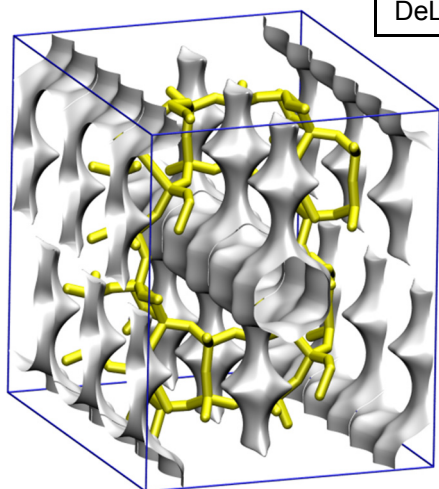
1D micro-porous channels

With side pockets

MOR pore landscape

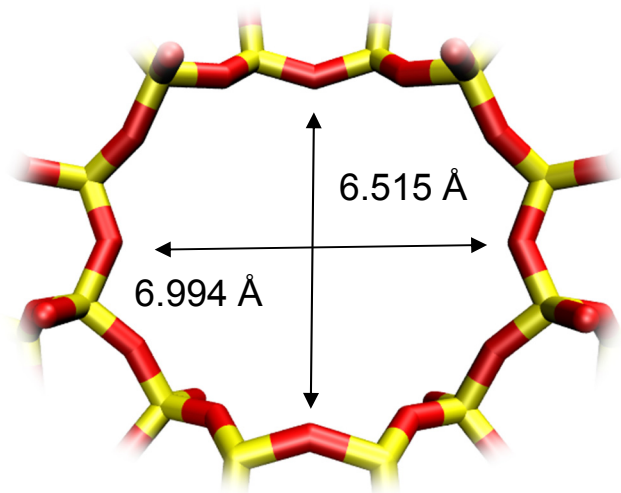


| | MOR |
|--|----------|
| $a / \text{\AA}$ | 18.094 |
| $b / \text{\AA}$ | 20.516 |
| $c / \text{\AA}$ | 7.524 |
| Cell volume / \AA^3 | 2793.033 |
| conversion factor for [molec/uc] to [mol per kg Framework] | 0.3467 |
| conversion factor for [molec/uc] to [kmol/m^3] | 2.0877 |
| $\rho [\text{kg}/\text{m}^3]$ | 1714.691 |
| MW unit cell [g/mol(framework)] | 2884.07 |
| ϕ , fractional pore volume | 0.285 |
| open space / $\text{\AA}^3/\text{uc}$ | 795.4 |
| Pore volume / cm^3/g | 0.166 |
| Surface area / m^2/g | 417.0 |
| DeLaunay diameter / \AA | 6.44 |

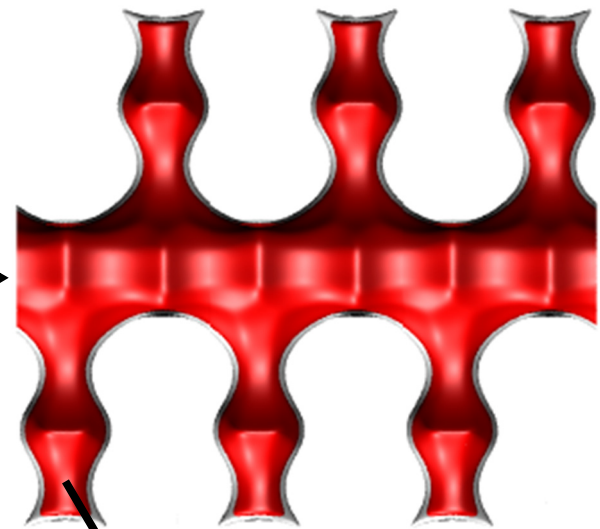


Structural information from: C. Baerlocher, L.B. McCusker, Database of Zeolite Structures, International Zeolite Association, <http://www.iza-structure.org/databases/>

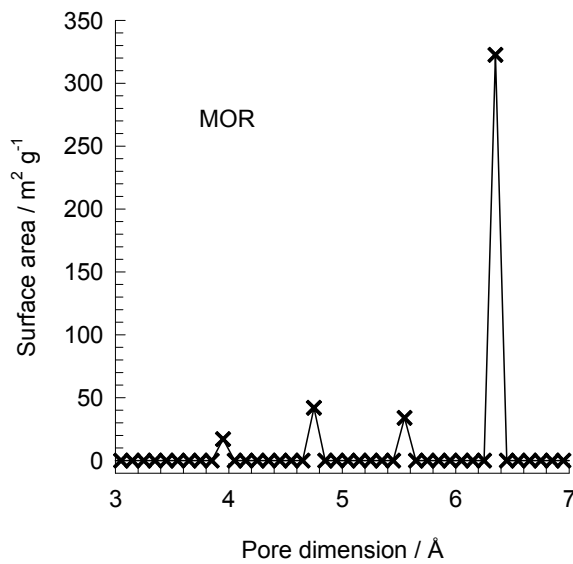
MOR pore dimensions



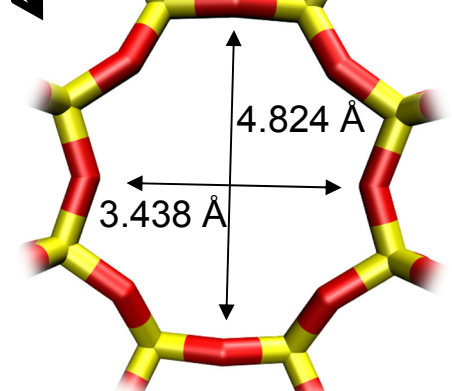
12-ring
main channels



MOR Channel [1 0 0]

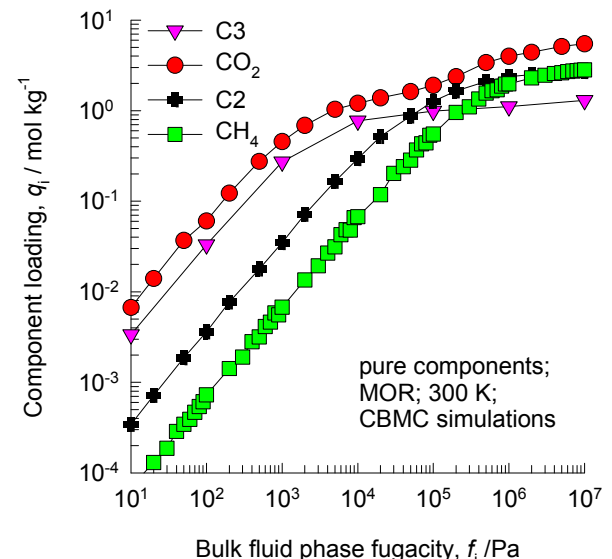
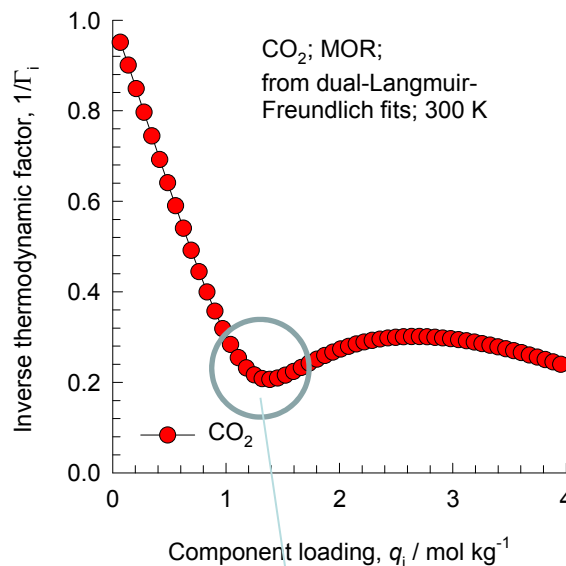
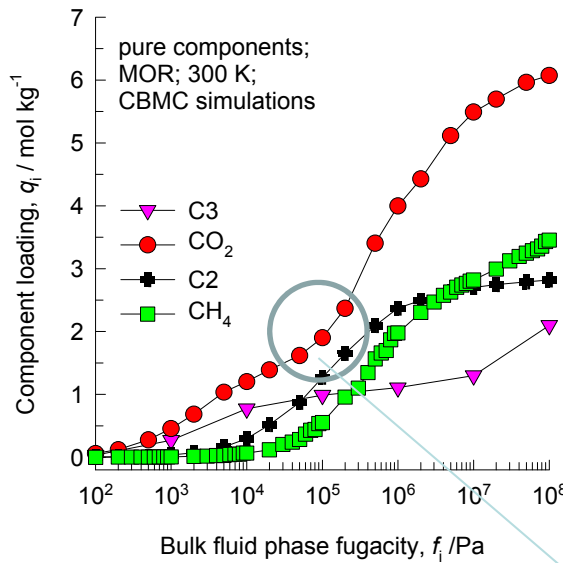


This plot of surface area versus pore dimension is determined using a combination of the DeLaunay triangulation method for pore dimension determination, and the procedure of Düren for determination of the surface area.

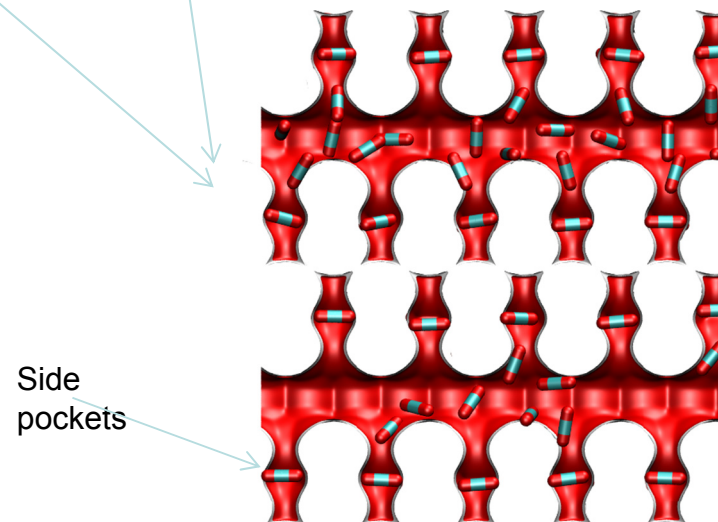
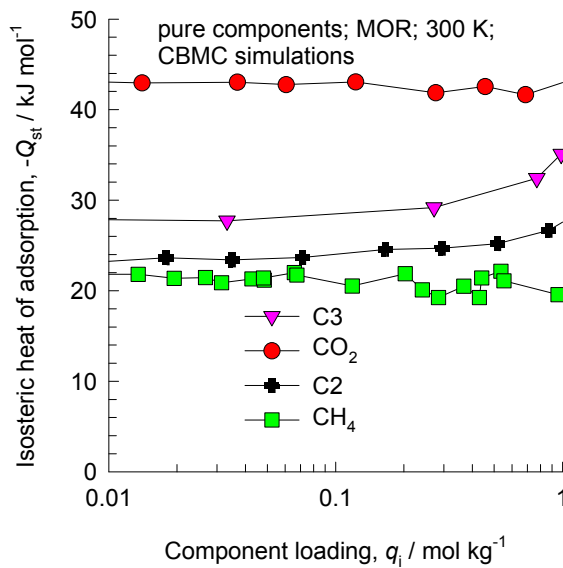


MOR [0 1 0]

MOR CBMC simulations of isotherms, and $-Q_{st}$; MD simulations of diffusivities



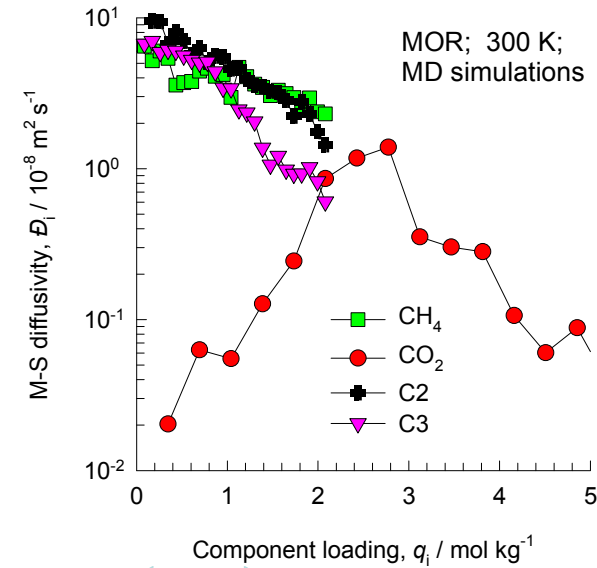
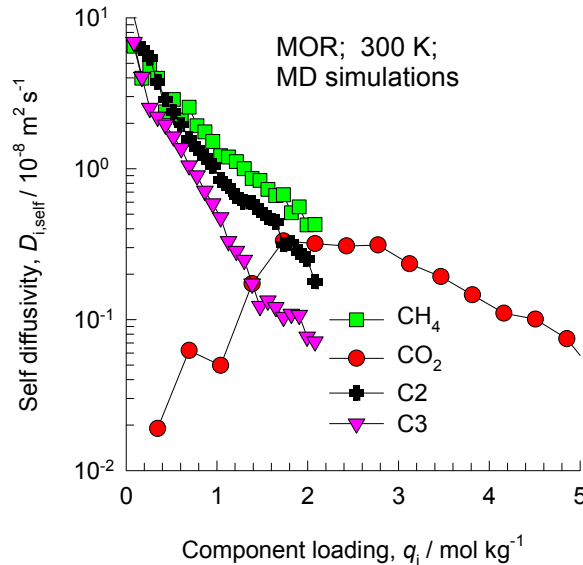
Note that C2 and C3 above refer to saturated alkanes.



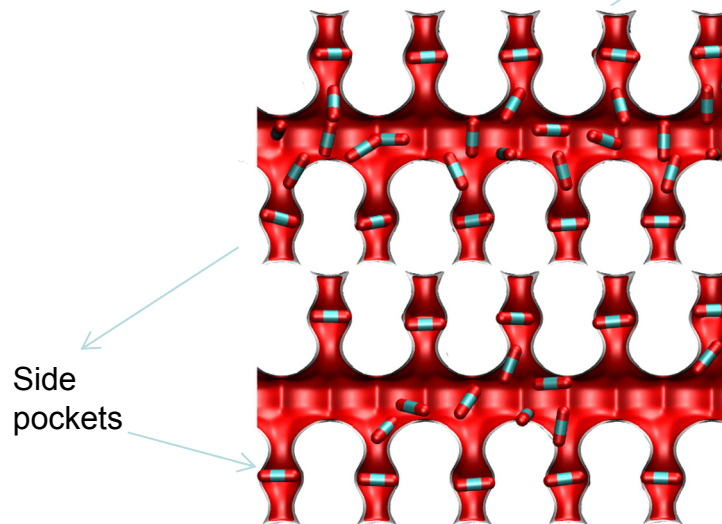
CO_2 preferentially locates in the side pockets as shown in snapshot. At a loading of $4/\text{uc} = 1.39 \text{ mol/kg}$, the pockets are full. This causes an infection. This also explains the high heat of adsorption due to snug fits in the side pockets

MOR

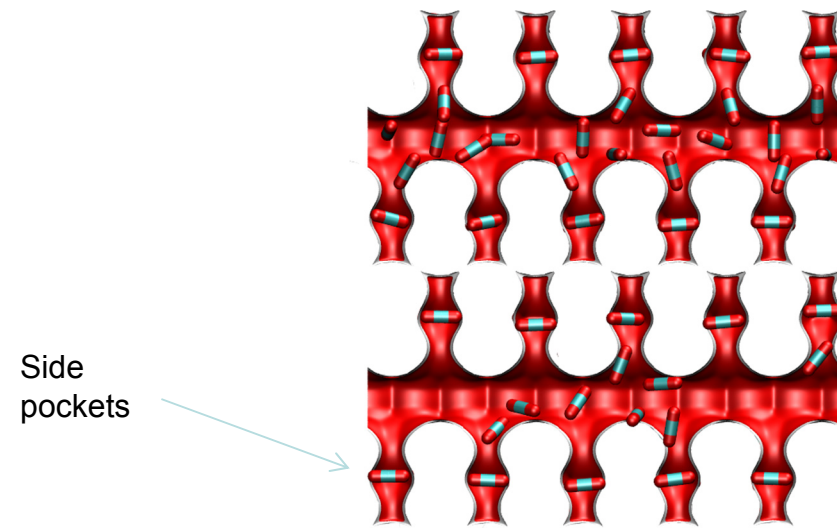
MD simulations of unary diffusivities



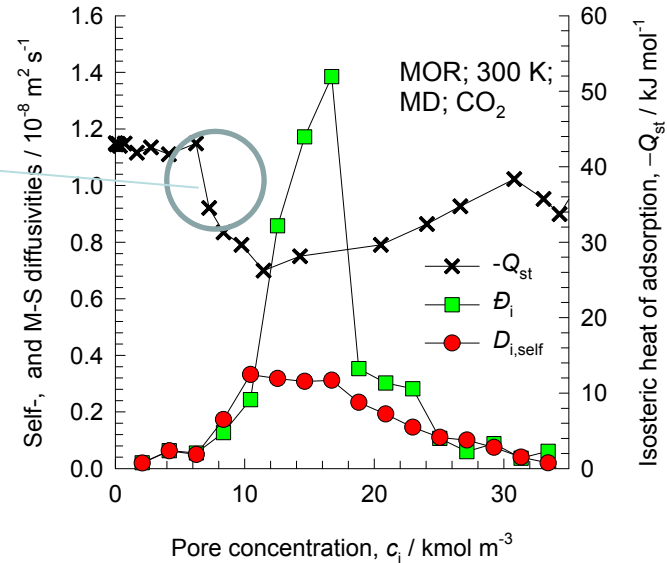
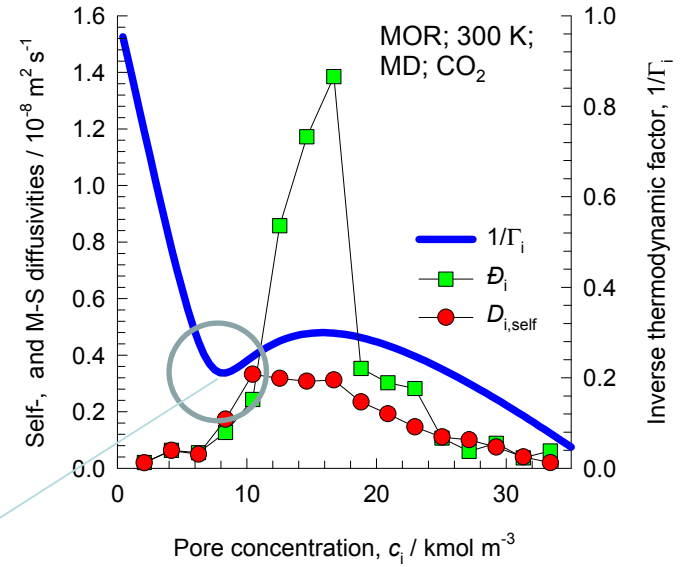
CO_2 preferentially locates in the side pockets in this loading range. This explains the low diffusivities.



Influence of $1/\Gamma_i$ and $-Q_{st}$ on diffusivities



CO_2 preferentially locates in the side pockets as shown in snapshot. At a loading of $4/\text{uc} = 8.35 \text{ kmol m}^{-3}$, the pockets are full. This causes an infection. This also explains the high heat of adsorption due to snug fits in the side pockets

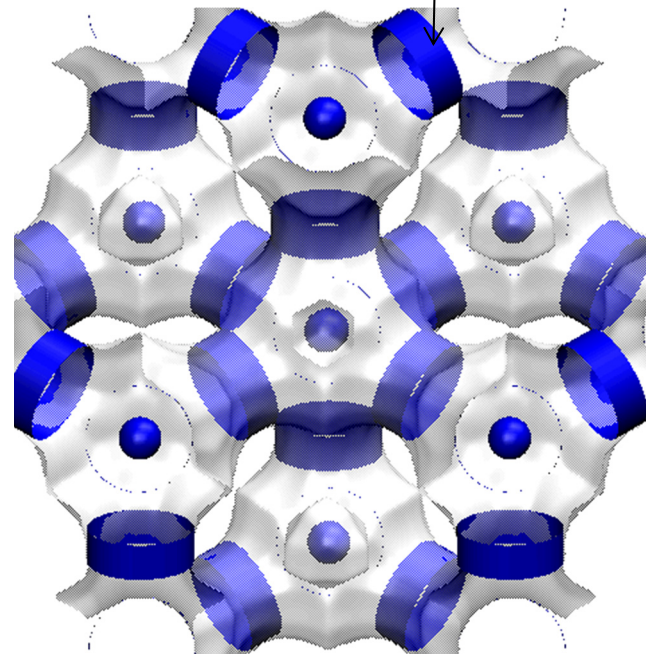


**“Open” structures with
large cavities**

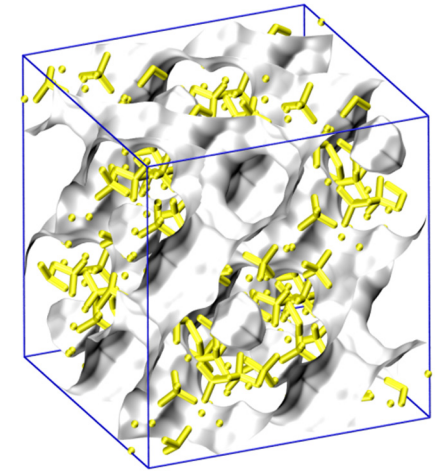
FAU-Si pore landscape

The sodalite cages are blocked in simulations and are not accessible to guest molecules; these are excluded for pore volume determination.

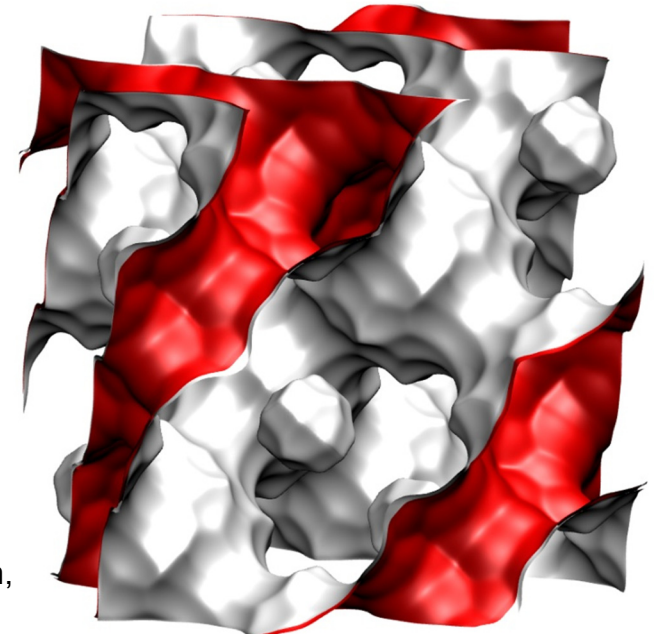
12-ring
window of FAU



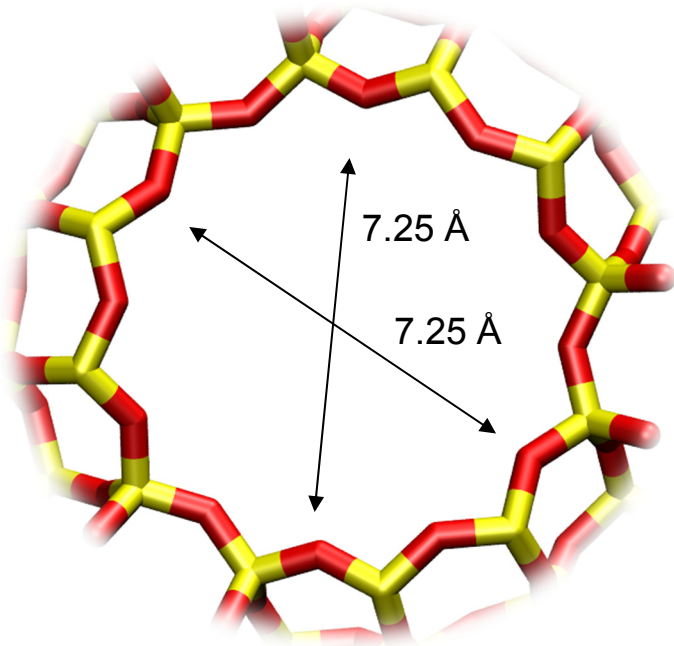
There are 8 cages per unit cell.
The volume of one FAU cage is
 786 \AA^3 , larger in size than that of
LTA (743 \AA^3) and DDR (278 \AA^3).



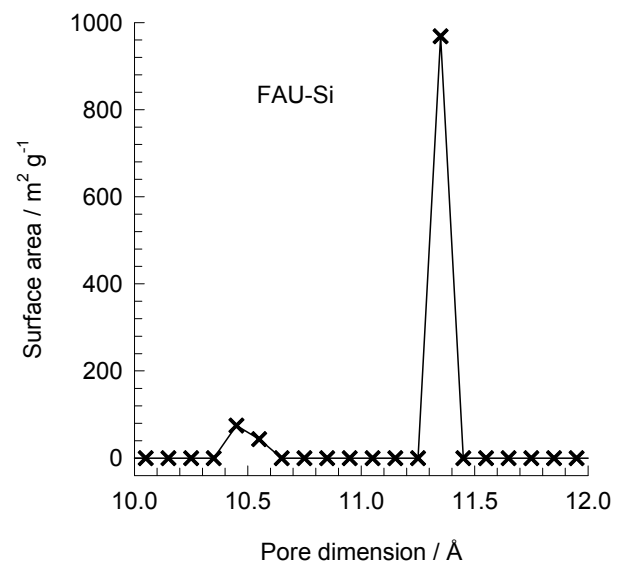
Structural information from: C. Baerlocher,
L.B. McCusker, Database of Zeolite
Structures, International Zeolite Association,
<http://www.iza-structure.org/databases/>



FAU-Si window and pore dimensions

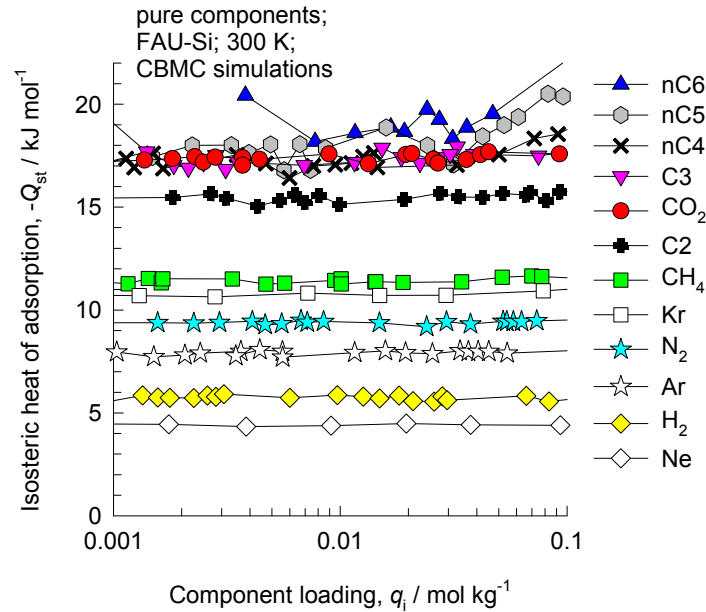
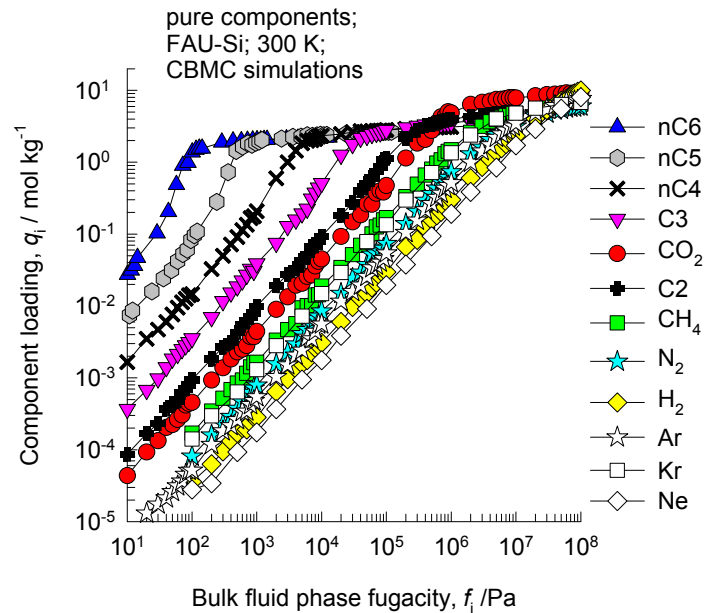
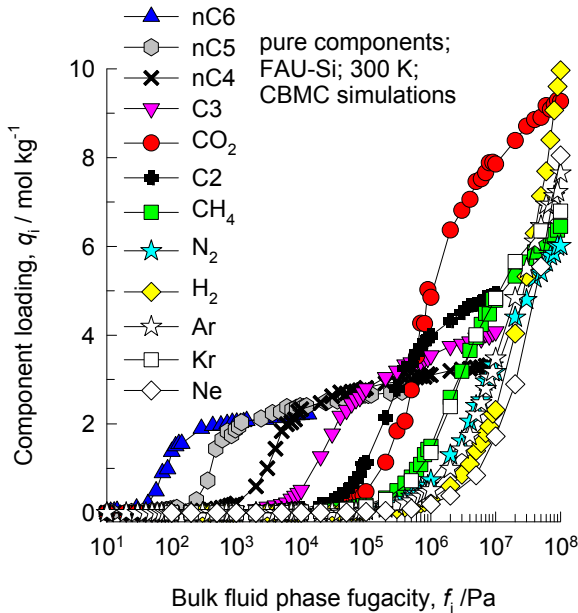


This plot of surface area versus pore dimension is determined using a combination of the DeLaunay triangulation method for pore dimension determination, and the procedure of Düren for determination of the surface area.



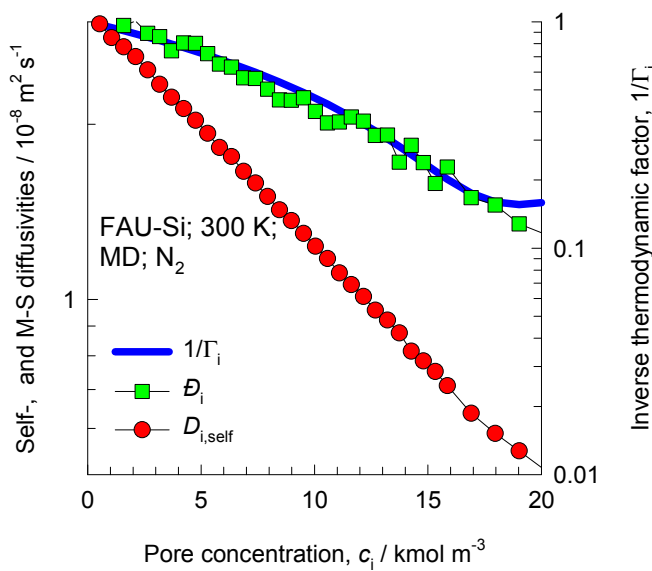
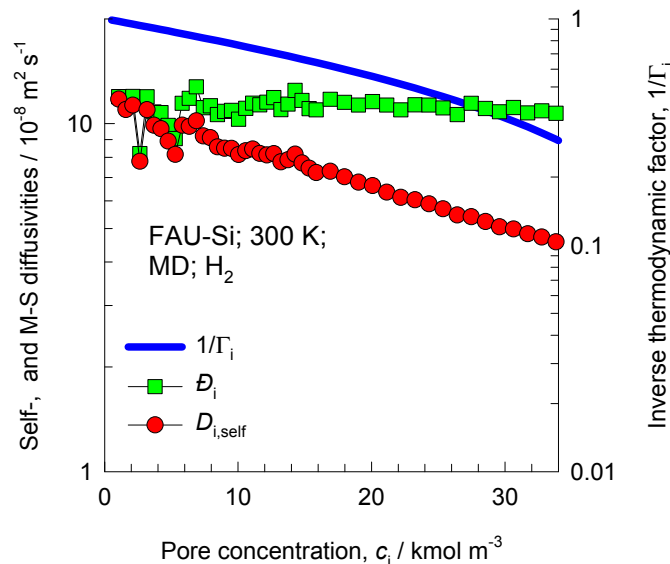
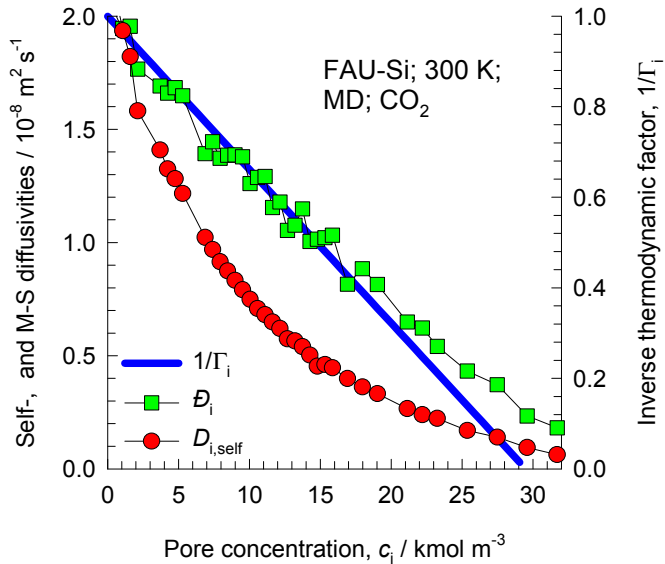
| | FAU-Si |
|--|----------|
| $a / \text{\AA}$ | 24.28 |
| $b / \text{\AA}$ | 24.28 |
| $c / \text{\AA}$ | 24.28 |
| Cell volume / \AA^3 | 14313.51 |
| conversion factor for [molec/uc] to [mol per kg Framework] | 0.0867 |
| conversion factor for [molec/uc] to [kmol/m ³] | 0.2642 |
| $\rho / [\text{kg}/\text{m}^3]$ | 1338.369 |
| MW unit cell [g/mol (framework)] | 11536.28 |
| ϕ , fractional pore volume | 0.439 |
| open space / $\text{\AA}^3/\text{uc}$ | 6285.6 |
| Pore volume / cm^3/g | 0.328 |
| Surface area / m^2/g | 1086.0 |
| DeLaunay diameter / \AA | 7.37 |

FAU-Si CBMC simulations of isotherms, and isosteric heats of adsorption

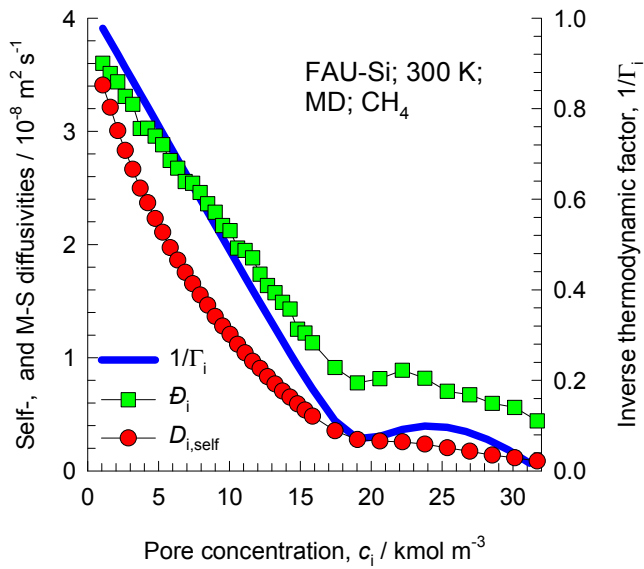


Note that C2 and C3 above refer to saturated alkanes

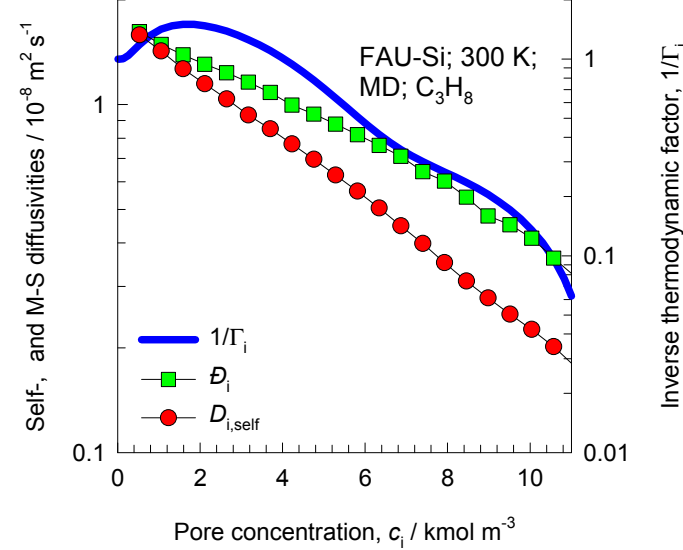
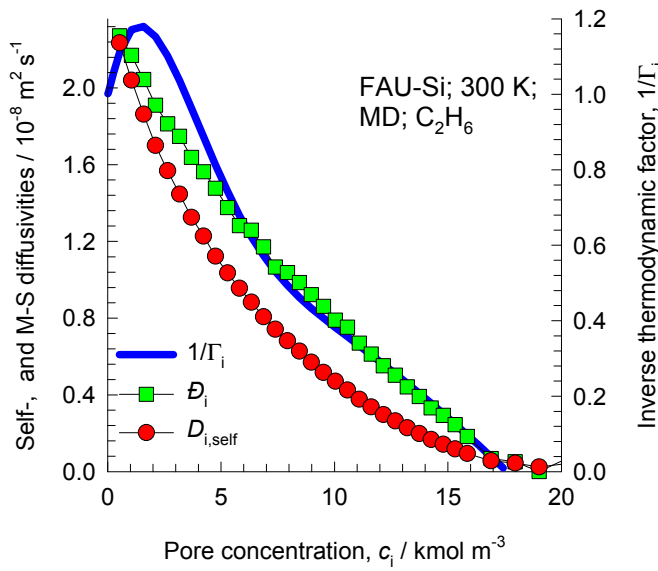
Influence of Inverse Thermodynamic Factor on diffusivities



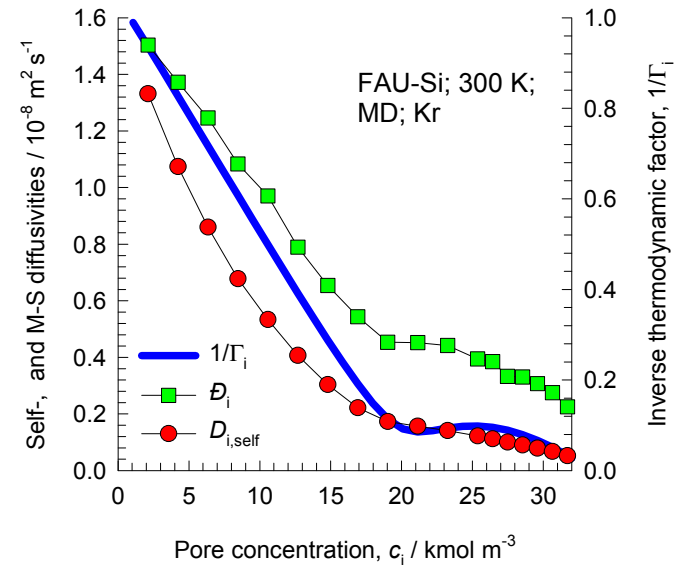
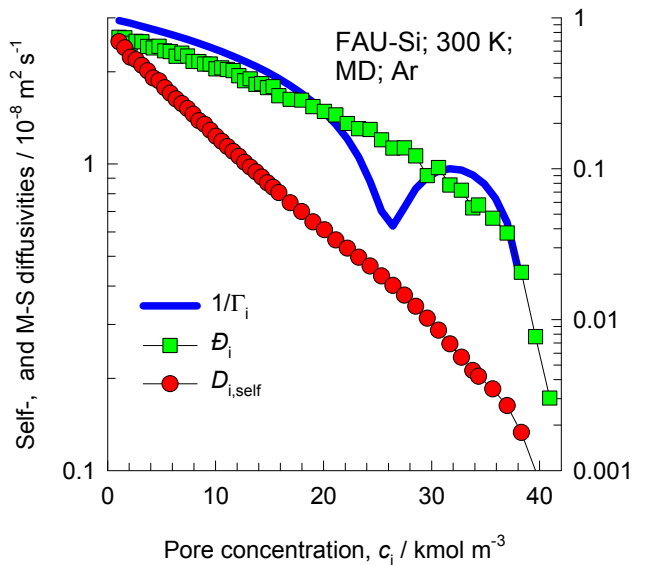
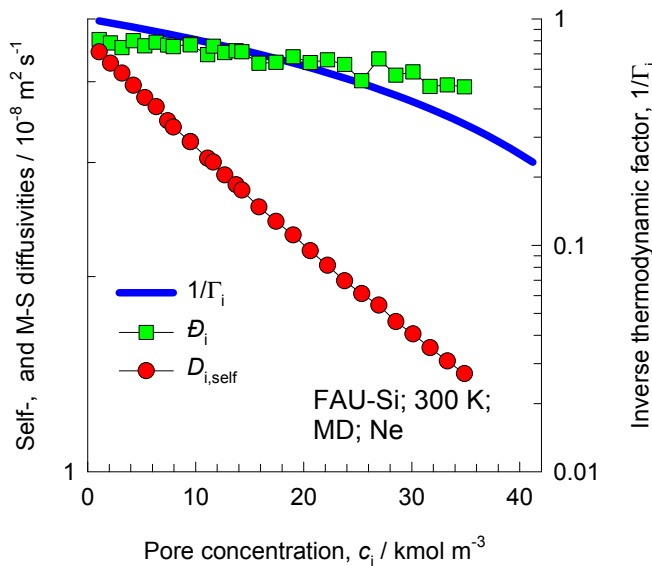
Influence of Inverse Thermodynamic Factor on diffusivities



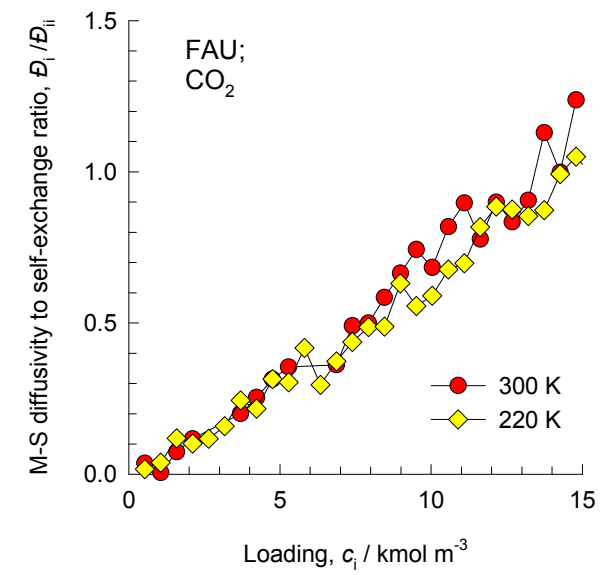
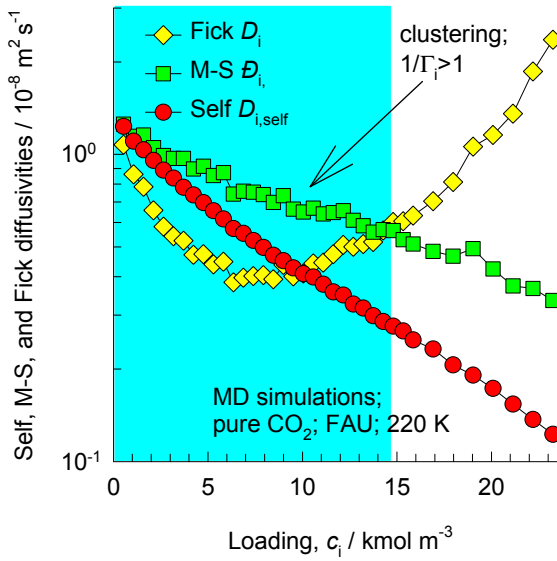
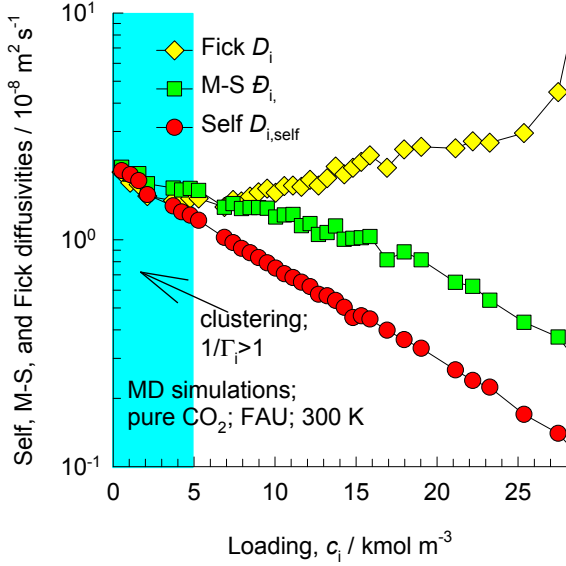
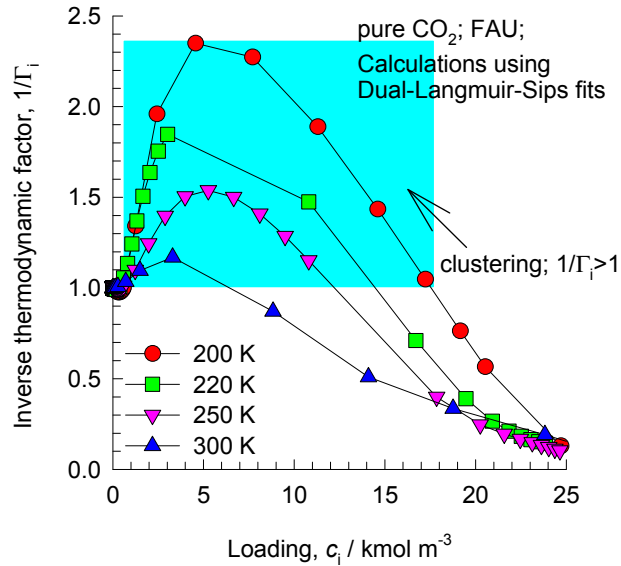
The isotherm inflection for methane gets reflected in the concentration dependence of the M-S diffusivity.



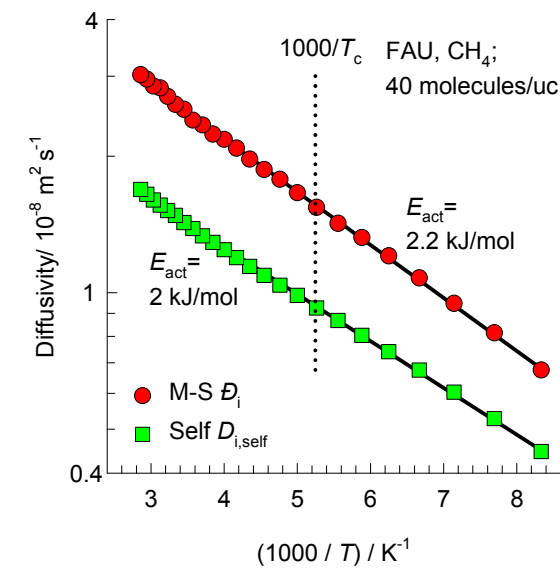
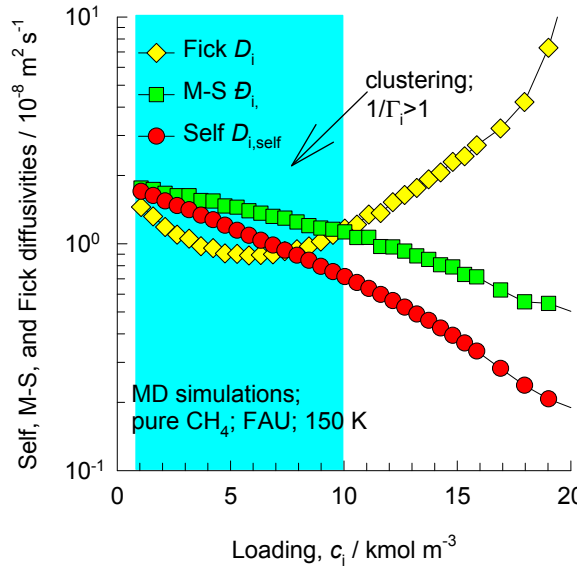
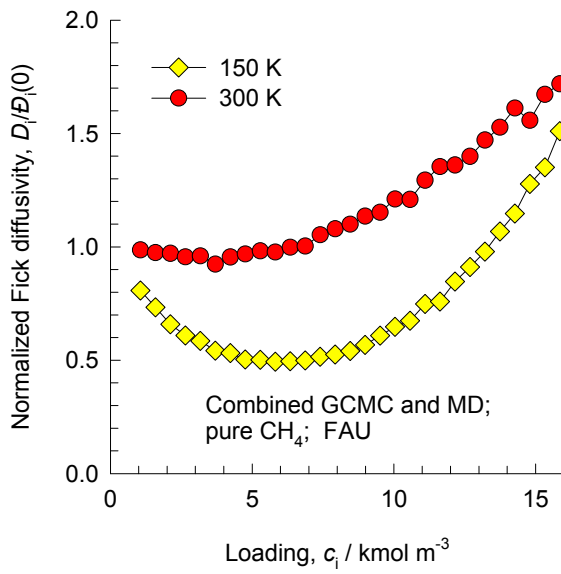
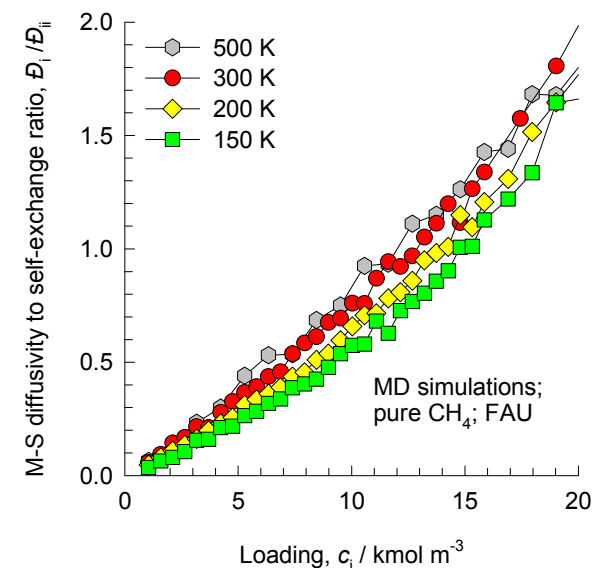
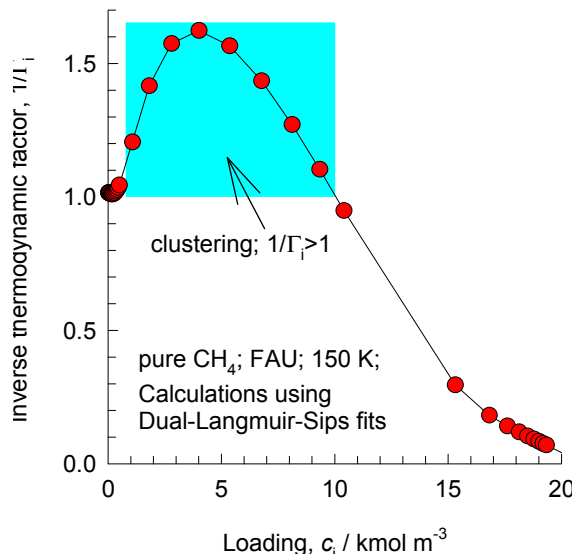
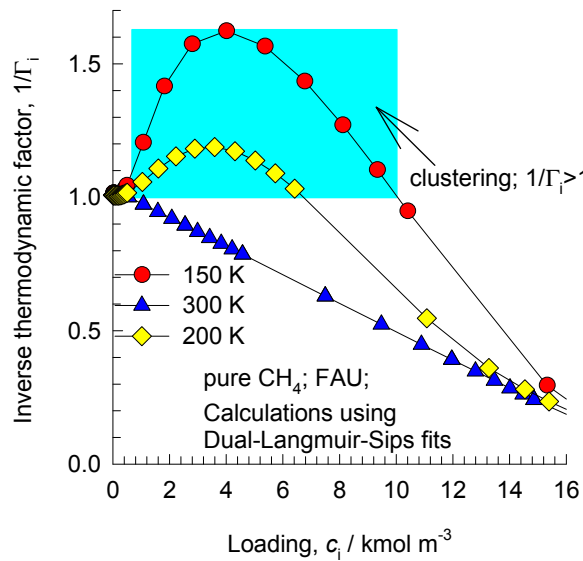
Influence of Inverse Thermodynamic Factor on diffusivities



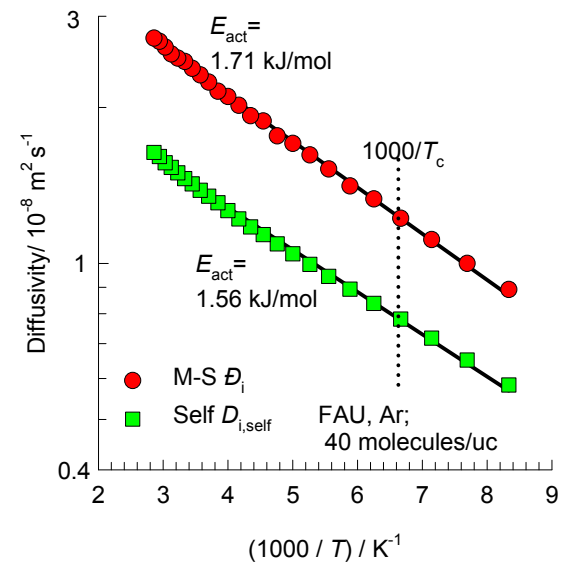
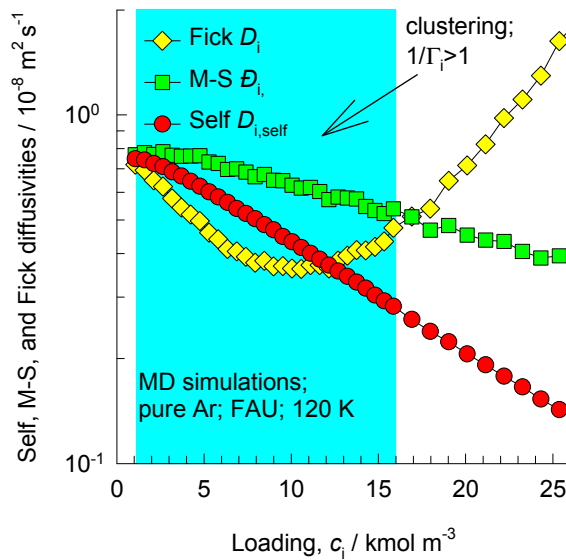
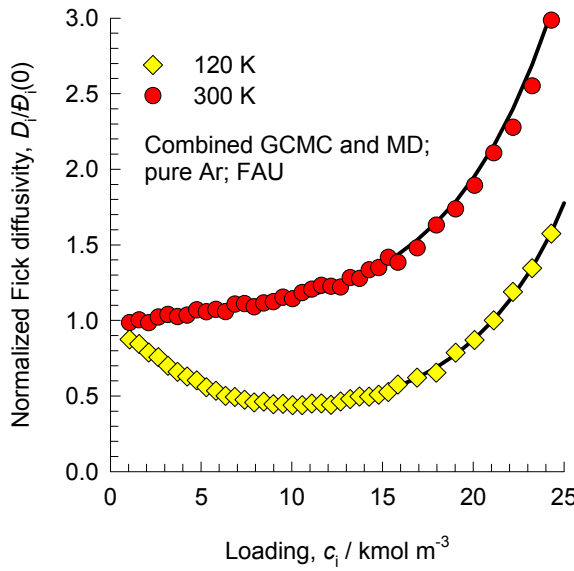
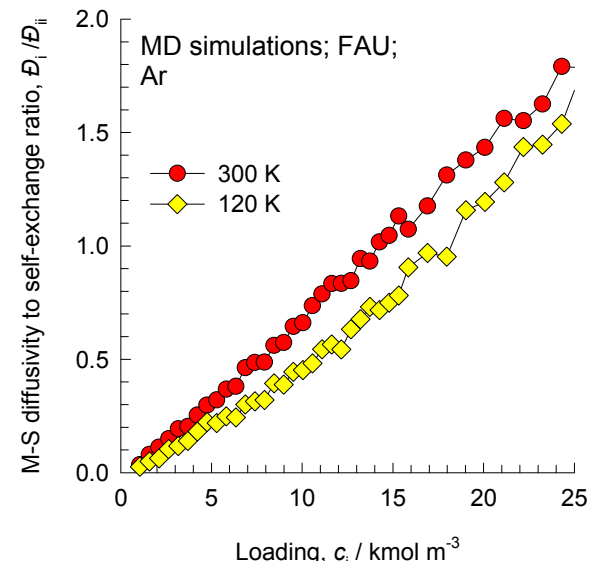
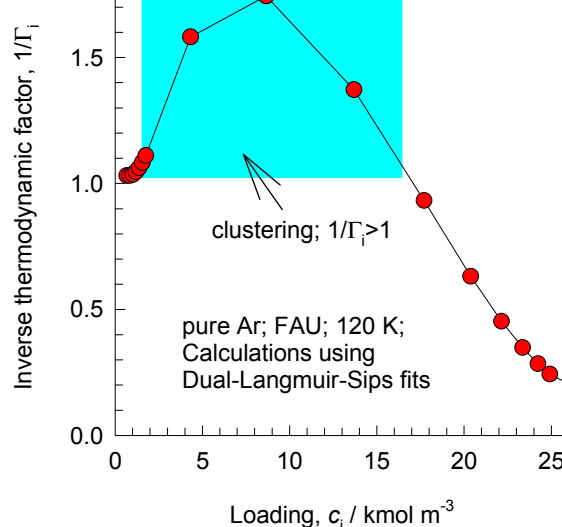
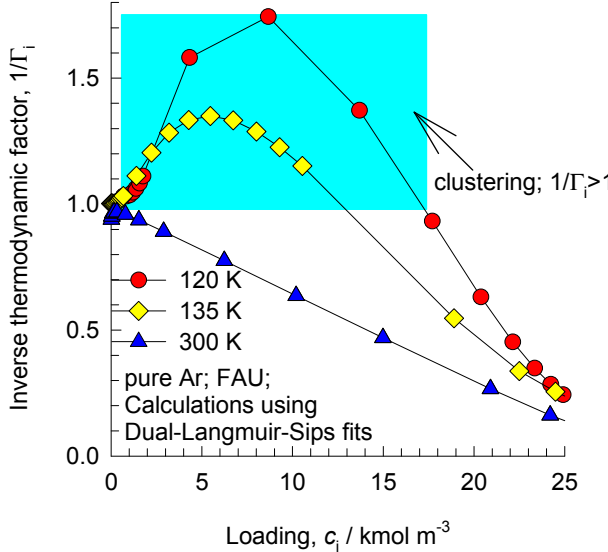
FAU-Si CO₂ adsorption and diffusion



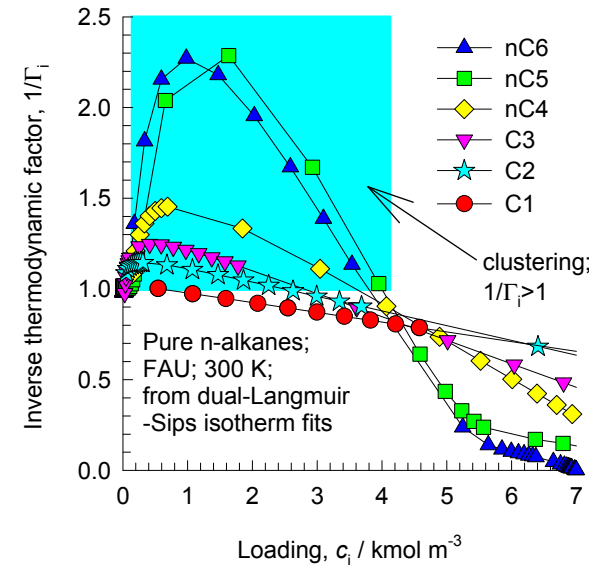
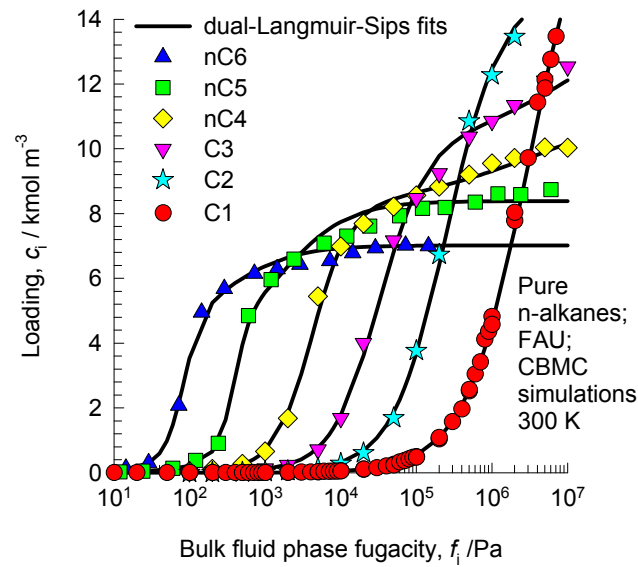
FAU-Si CH₄ adsorption and diffusion



FAU-Si Ar adsorption and diffusion

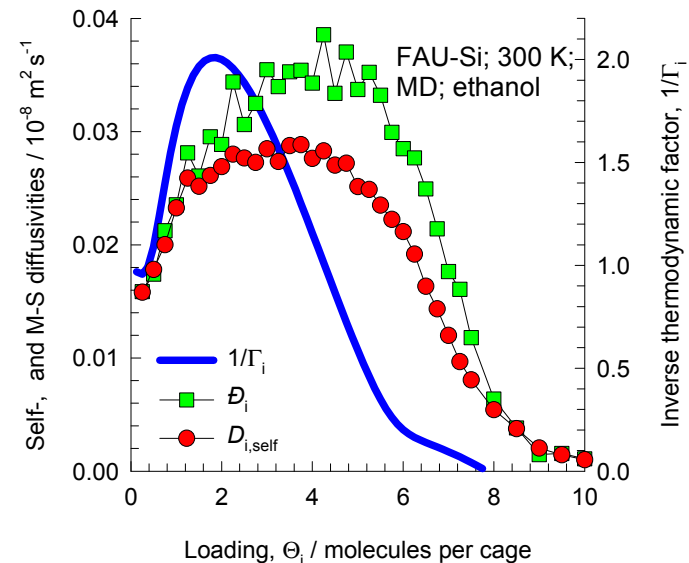
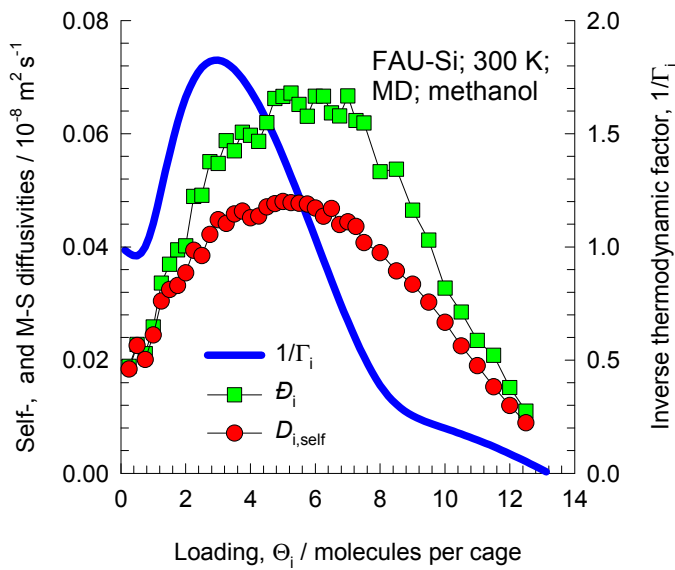


FAU-Si CBMC simulations of isotherms and thermodynamic factors for n-alkanes



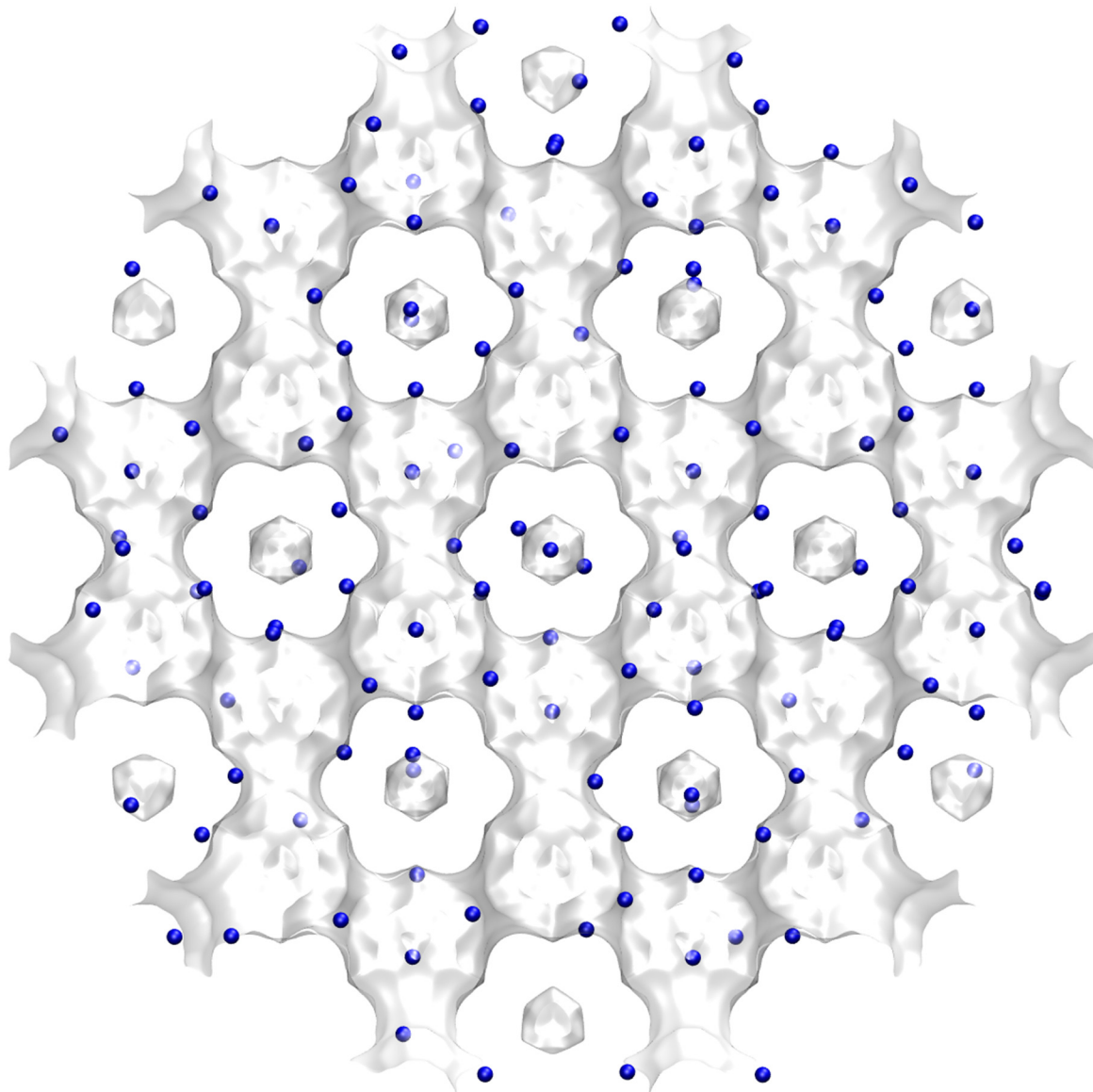
The degree of clustering increases with increasing chain length of n-alkanes.

Influence of Inverse Thermodynamic Factor on diffusivities



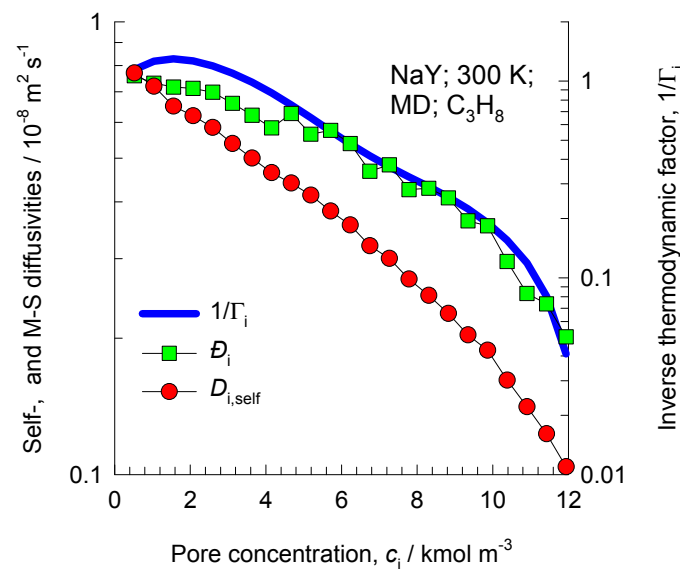
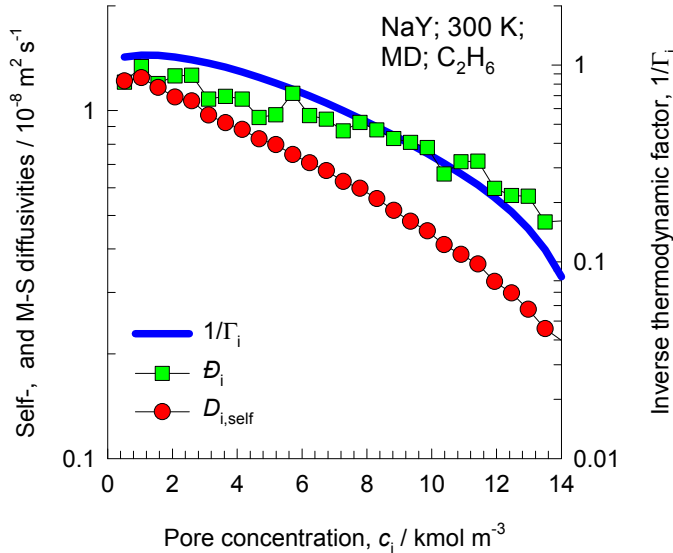
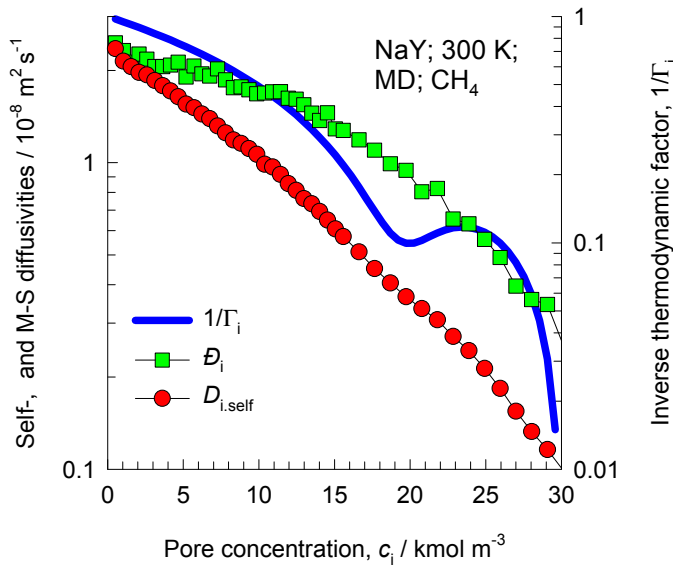
NaY (138 Si, 54 Al, 54 Na⁺, Si/Al=2.55)

Blue spheres are cations

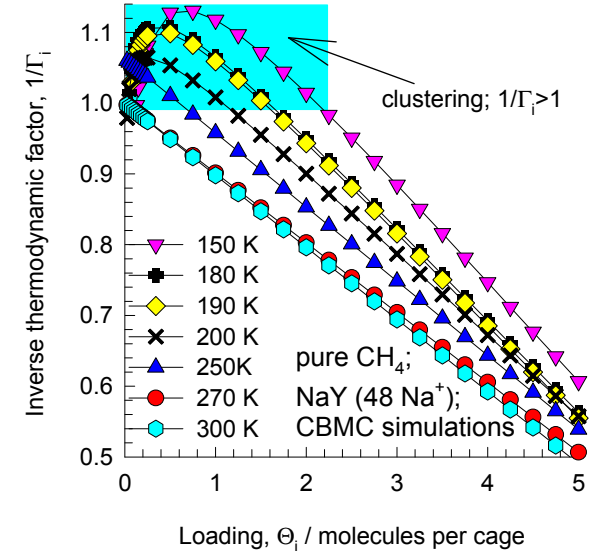
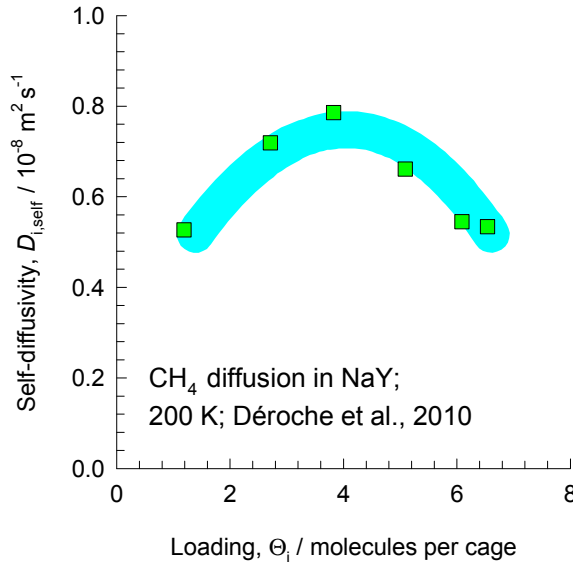


| | FAU-54Al |
|--|----------|
| a /Å | 25.028 |
| b /Å | 25.028 |
| c /Å | 25.028 |
| Cell volume / Å ³ | 15677.56 |
| conversion factor for [molec/uc] to [mol per kg Framework] | 0.0786 |
| conversion factor for [molec/uc] to [kmol/m ³] | 0.2596 |
| ρ [kg/m ³] (with cations) | 1347.1 |
| MW unit cell [g/mol(framework+cations)] | 12718.08 |
| ϕ , fractional pore volume | 0.408 |
| open space / Å ³ /uc | 6396.6 |
| Pore volume / cm ³ /g | 0.303 |
| Surface area /m ² /g | |
| DeLaunay diameter /Å | 7.37 |

Influence of Inverse Thermodynamic Factor on diffusivities



NaY CH₄ self-diffusivity at 200 K



The QENS experimental data are re-plotted using the information in:

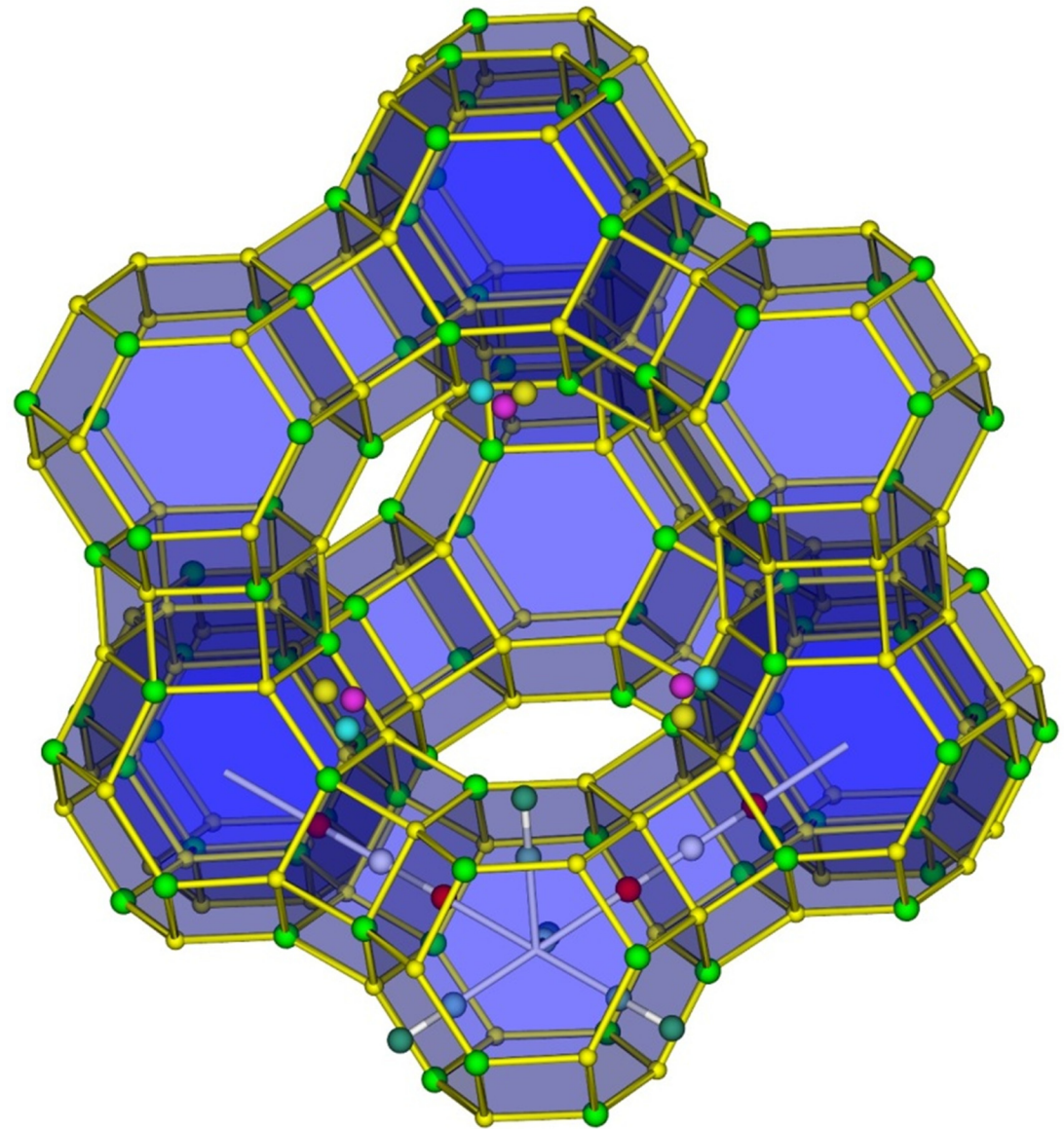
I. Deroche, G. Maurin, B.J. Borah, H. Jobic, S. Yashonath, Diffusion of pure CH₄ and its binary mixture with CO₂ in Faujasite NaY: A combination of neutron scattering experiments and Molecular Dynamics simulations, J. Phys. Chem. C 114 (2010) 5027-5034.

The CBMC simulations of the inverse thermodynamic factor are from our earlier works:

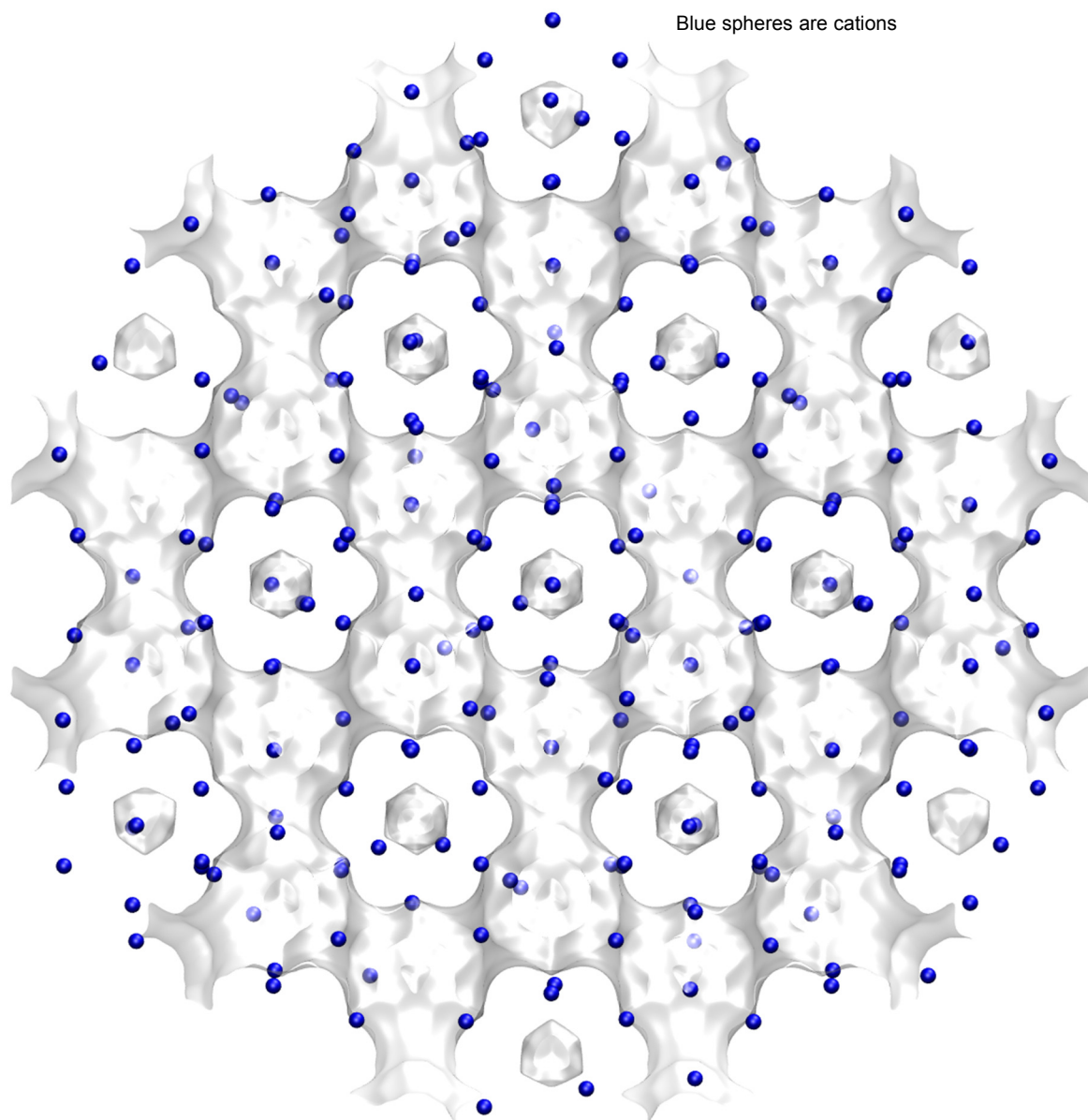
R. Krishna, J.M. van Baten, Investigating cluster formation in adsorption of CO₂, CH₄, and Ar in zeolites and metal organic frameworks at sub-critical temperatures, Langmuir 26 (2010) 3981-3992.

R. Krishna, J.M. van Baten, A rationalization of the Type IV loading dependence in the Kärger-Pfeifer classification of self-diffusivities, Microporous Mesoporous Mater. 142 (2011) 745-748.

NaX (106 Si, 86 Al, 86 Na+, Si/Al=1.23)

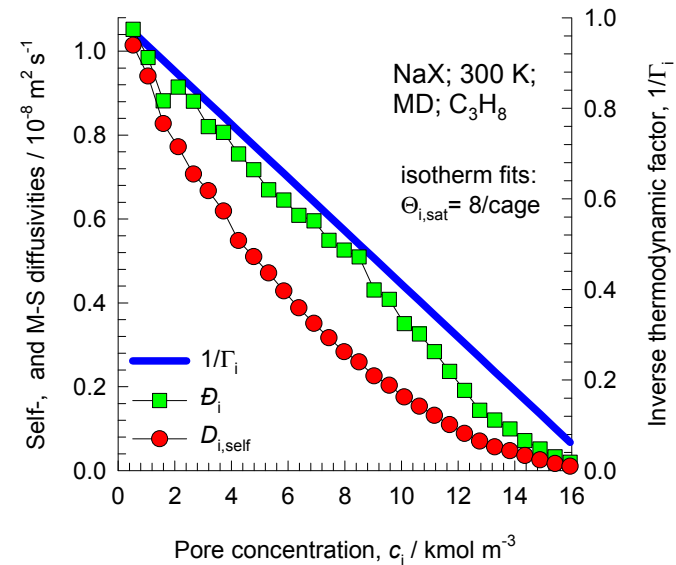
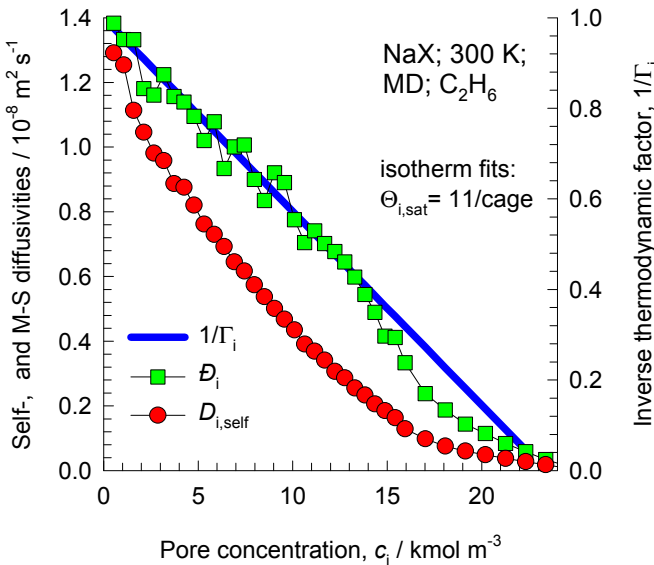
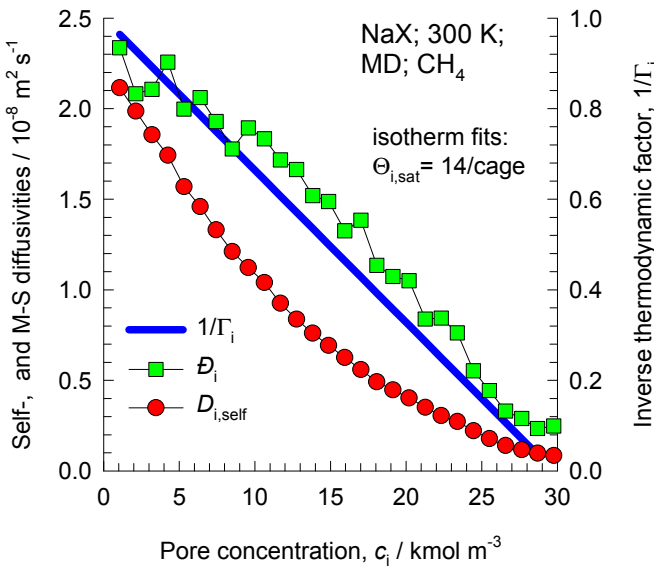


NaX (106 Si, 86 Al, 86 Na⁺, Si/Al=1.23)

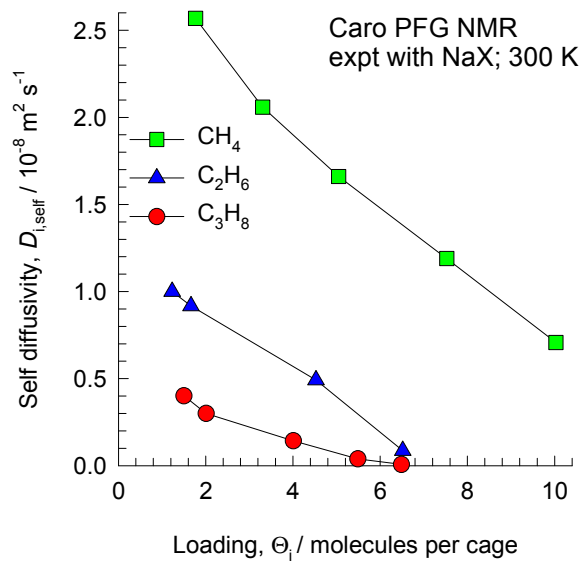


| | FAU- 86Al |
|---|--------------|
| a /Å | 25.028 |
| b /Å | 25.028 |
| c /Å | 25.028 |
| Cell volume / Å ³ | 15677.56 |
| conversion factor for [molec/uc] to [mol per kg Framework] | 0.0745 |
| conversion factor for [molec/uc] to [kmol/m ³] | 0.2658 |
| ρ [kg/m ³] (with cations) | 1421.277 |
| MW unit cell [g/mol(framework+cations)] | 13418.42 |
| ϕ, fractional pore volume | 0.399 |
| open space / Å ³ /uc | 6248.0 |
| Pore volume / cm ³ /g | 0.280 |
| Surface area /m ² /g | |
| DeLaunay diameter /Å | 7.37 |

Influence of Inverse Thermodynamic Factor on diffusivities



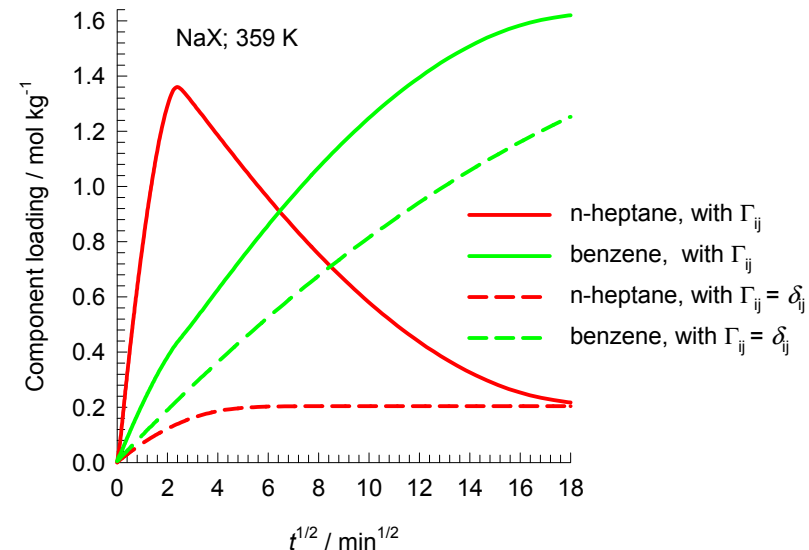
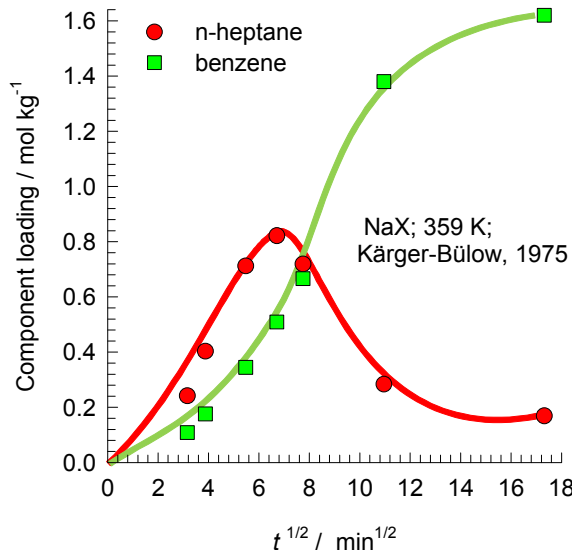
NaX NMR experiments of Caro



The experimental data are from

Caro, J.; Bülow, M.; Schirmer, W.; Kärger, J.; Heink, W.; Pfeifer, H. Microdynamics of methane, ethane and propane in ZSM-5 type zeolites. Journal of the Chemical Society, Faraday Transactions 1985, 81, 2541-2550.

NaX: Transient uptake of n-heptane and benzene



The data are re-plotted using the information contained in
Kärger, J.; Bülow, M. Theoretical prediction of uptake behaviour in adsorption kinetics of binary gas mixtures using irreversible thermodynamics, Chem. Eng. Sci. 1975, 30, 893-896.

The overshoot in the nC7 uptake is a direct consequence of thermodynamic coupling caused by the off-diagonal elements of

$$\begin{bmatrix} \Gamma_{11} & \Gamma_{12} \\ \Gamma_{21} & \Gamma_{21} \end{bmatrix} \quad \text{where} \quad \Gamma_{ij} = \frac{q_i}{f_i} \frac{\partial f_i}{\partial q_j}$$

This has been demonstrated by

Krishna, R. Multicomponent surface diffusion of adsorbed species - A description based on the generalized Maxwell-Stefan equations, Chem. Eng. Sci. 1990, 45, 1779-1791.

If the thermodynamic coupling is ignored, i.e. we assume

$$\begin{bmatrix} \Gamma_{11} & \Gamma_{12} \\ \Gamma_{21} & \Gamma_{21} \end{bmatrix} = \begin{bmatrix} 1 & 0 \\ 0 & 1 \end{bmatrix}$$

the nC7 overshoot disappears.

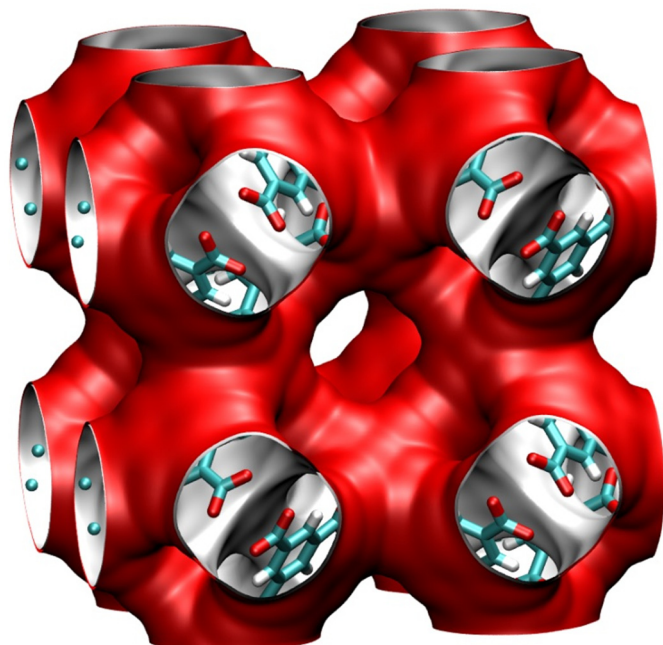
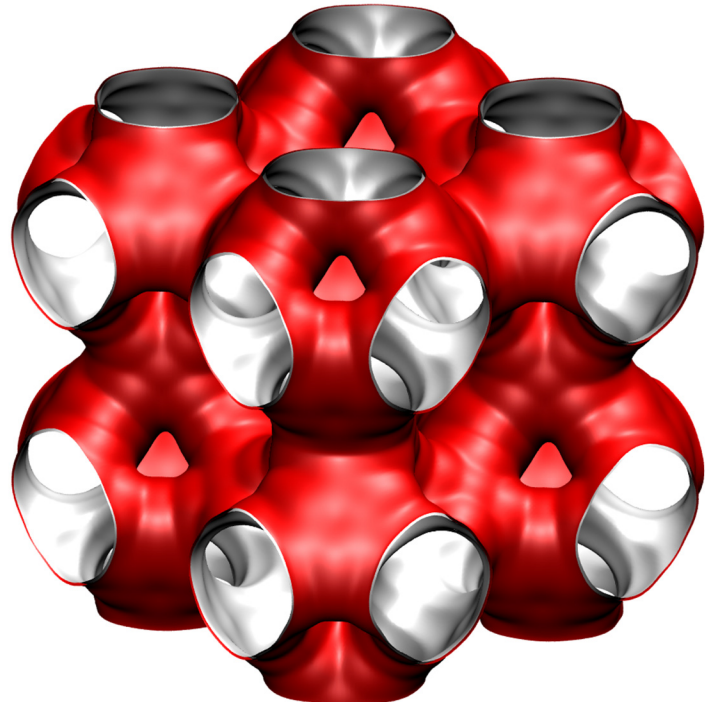
CuBTC pore landscapes

The structural information for CuBTC (= $\text{Cu}_3(\text{BTC})_2$ with BTC = 1,3,5-benzenetricarboxylate) have been taken from

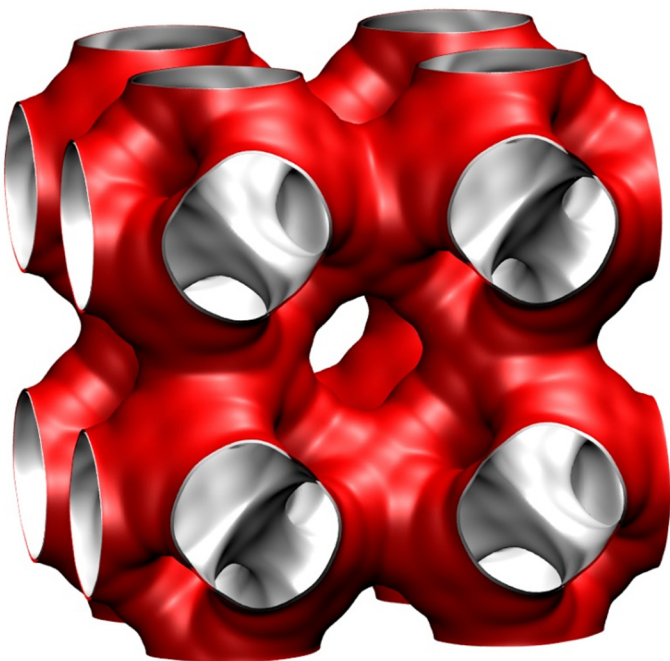
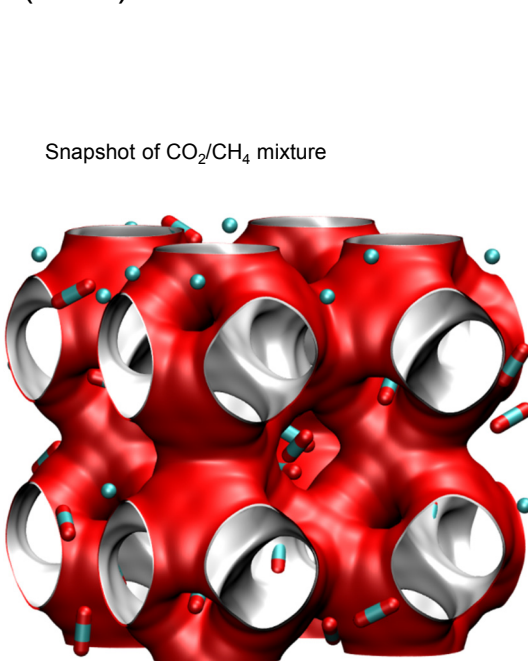
S.S.Y. Chui, S.M.F. Lo, J.P.H. Charmant, A.G. Orpen, I.D. Williams, A chemically functionalizable nanoporous material $[\text{Cu}_3(\text{TMA})_2(\text{H}_2\text{O})_3]_n$, *Science* 283 (1999) 1148-1150.

The crystal structure of Chui et al. includes axial oxygen atoms weakly bonded to the Cu atoms, which correspond to water ligands. Our simulations have been performed on the dry CuBTC with these oxygen atoms removed.

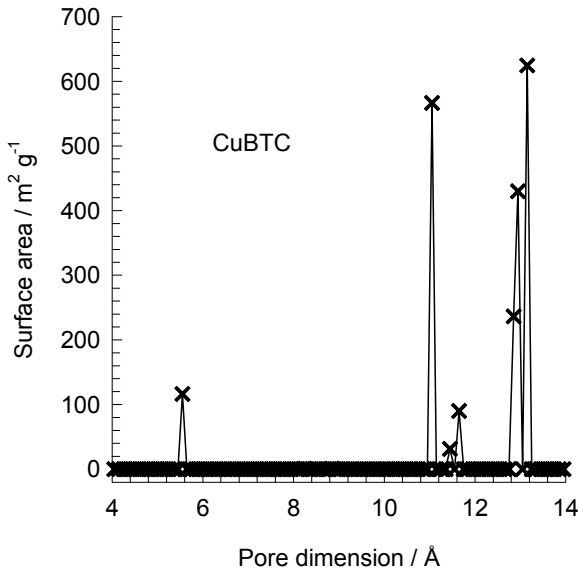
Q. Yang, C. Zhong, Electrostatic-Field-Induced Enhancement of Gas Mixture Separation in Metal-Organic Frameworks: A Computational Study, *ChemPhysChem* 7 (2006) 1417-1421.



Snapshot of CO₂/CH₄ mixture



CuBTC pore dimensions

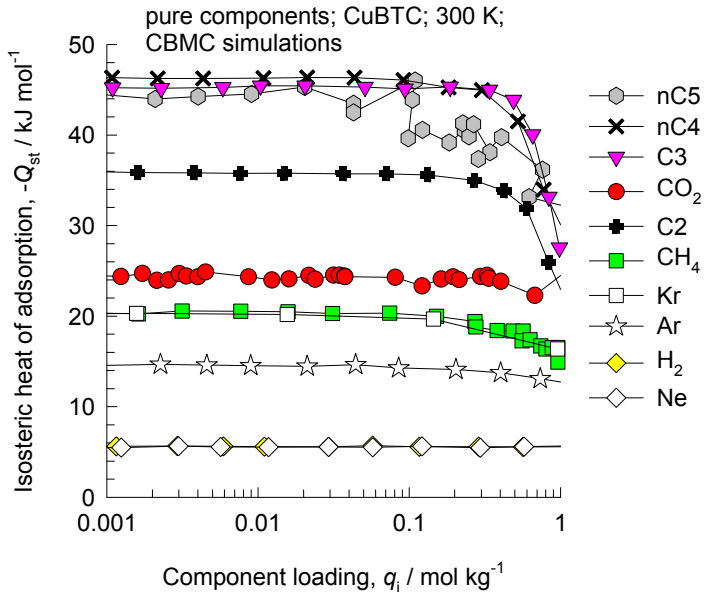
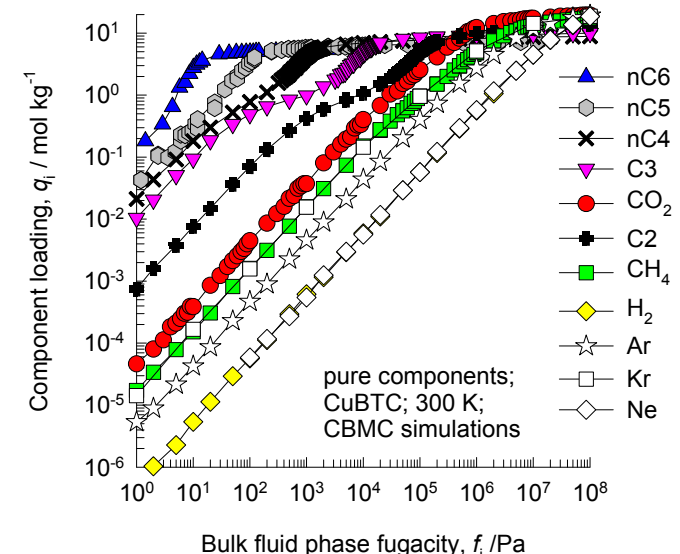
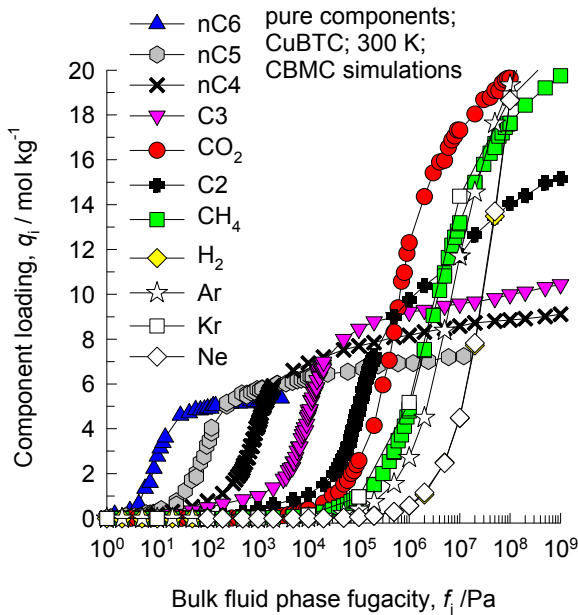


This plot of surface area versus pore dimension is determined using a combination of the DeLaunay triangulation method for pore dimension determination, and the procedure of Düren for determination of the surface area.

| | CuBTC |
|--|----------|
| $a / \text{\AA}$ | 26.343 |
| $b / \text{\AA}$ | 26.343 |
| $c / \text{\AA}$ | 26.343 |
| Cell volume / \AA^3 | 18280.82 |
| conversion factor for [molec/uc] to [mol per kg Framework] | 0.1034 |
| conversion factor for [molec/uc] to [kmol/m³] | 0.1218 |
| $\rho / \text{kg/m}^3$ | 878.8298 |
| MW unit cell [g/mol(framework)] | 9674.855 |
| ϕ , fractional pore volume | 0.746 |
| open space / $\text{\AA}^3/\text{uc}$ | 13628.4 |
| Pore volume / cm^3/g | 0.848 |
| Surface area / m^2/g | 2097.0 |
| DeLaunay diameter / \AA | 6.23 |

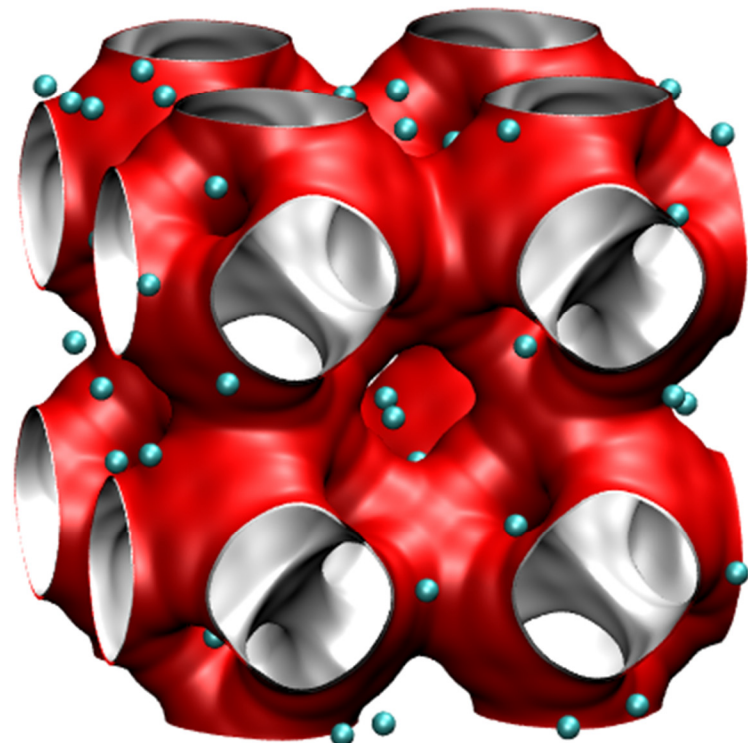
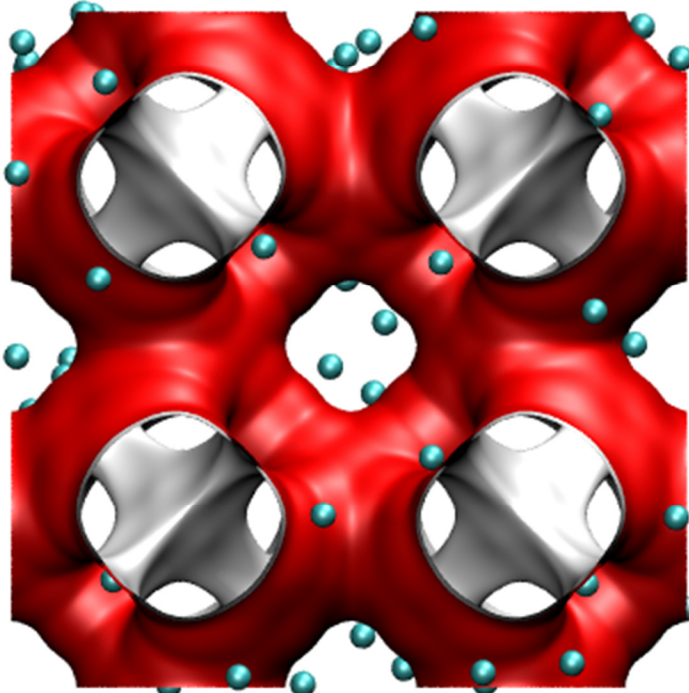
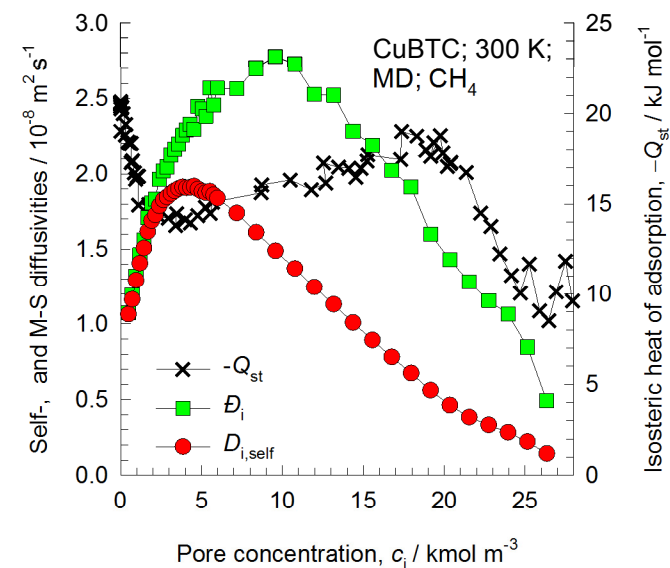
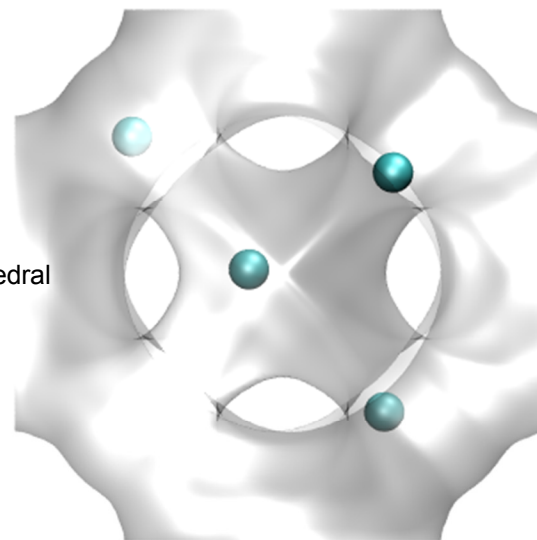
The CuBTC structure consists of two types of “cages” and two types of “windows” separating these cages. Large cages are inter-connected by 9 Å windows of square cross-section. The large cages are also connected to tetrahedral-shaped pockets of ca. 6 Å size through triangular-shaped windows of ca. 4.6 Å size

CuBTC CBMC simulations of isotherms, and isosteric heats of adsorption



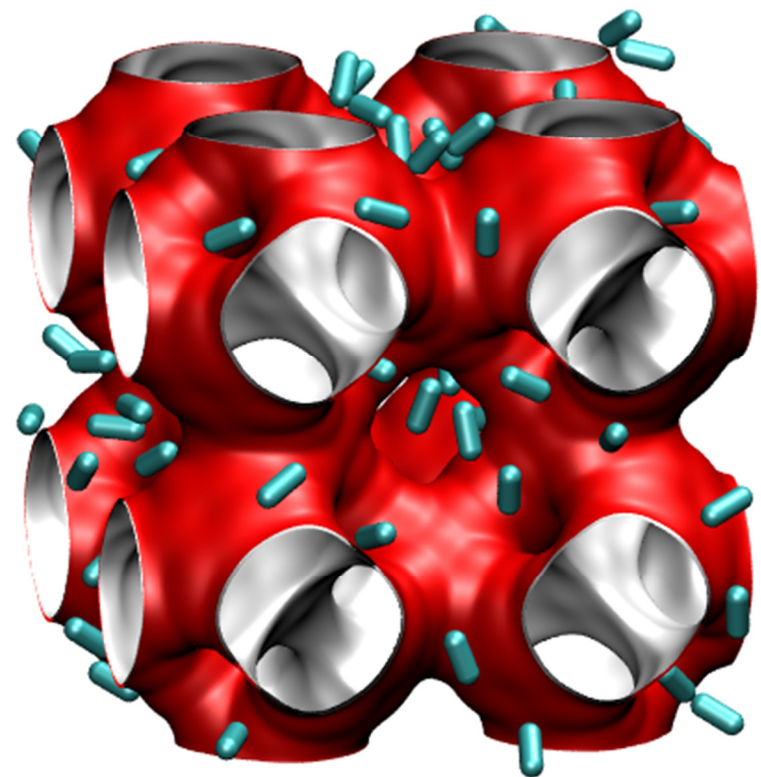
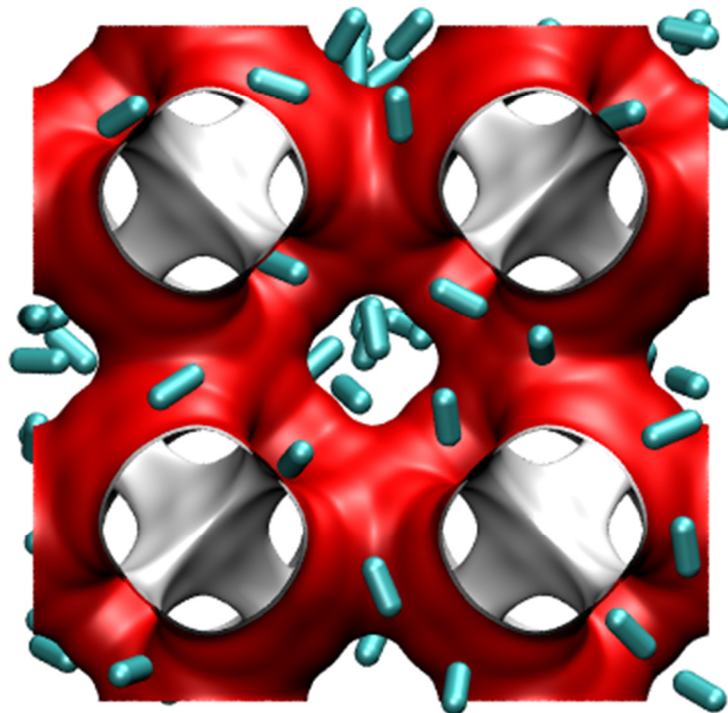
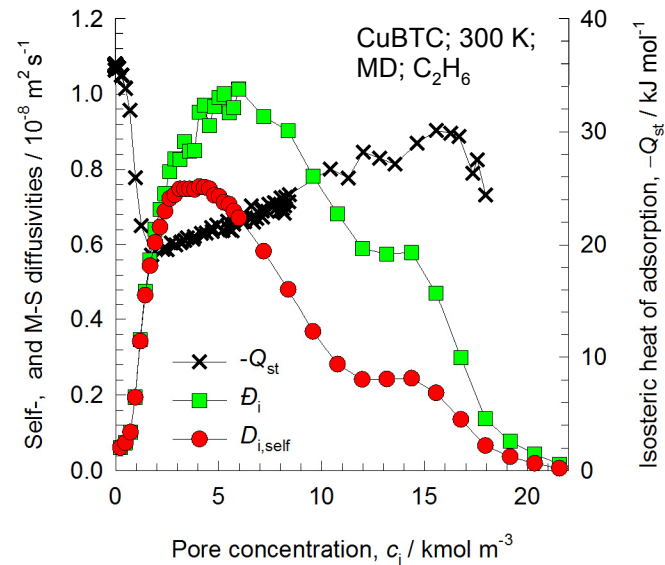
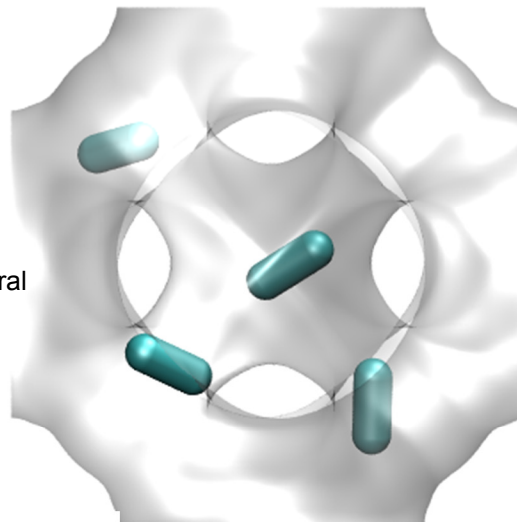
Influence of $-Q_{st}$ on diffusivities

Location of CH_4
inside the tetrahedral
pockets



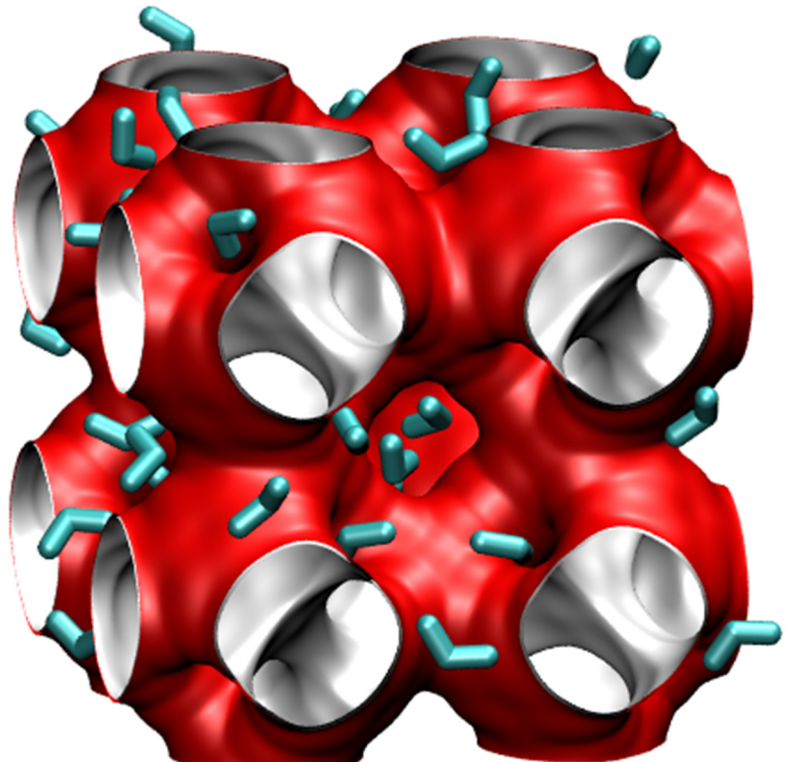
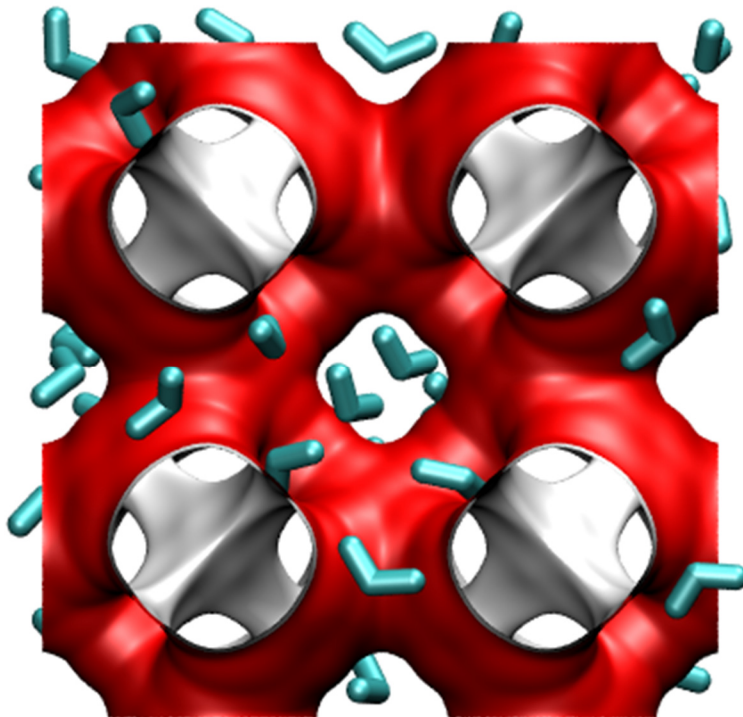
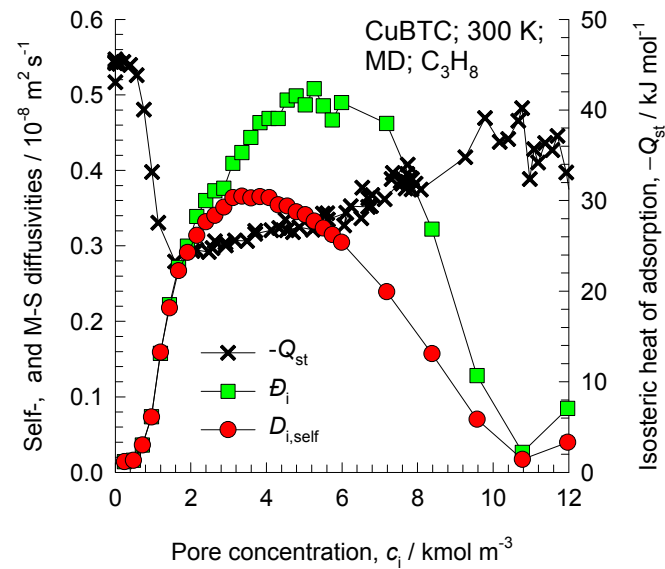
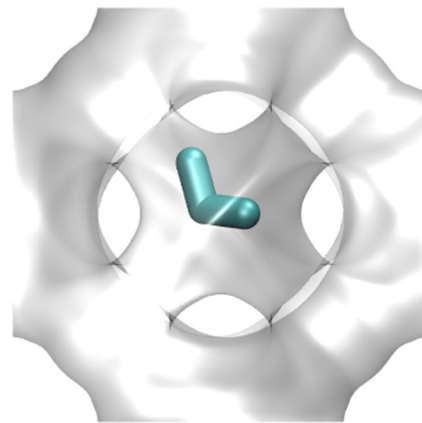
Influence of $-Q_{st}$ on diffusivities

Location of C_2H_6
inside the tetrahedral
pockets

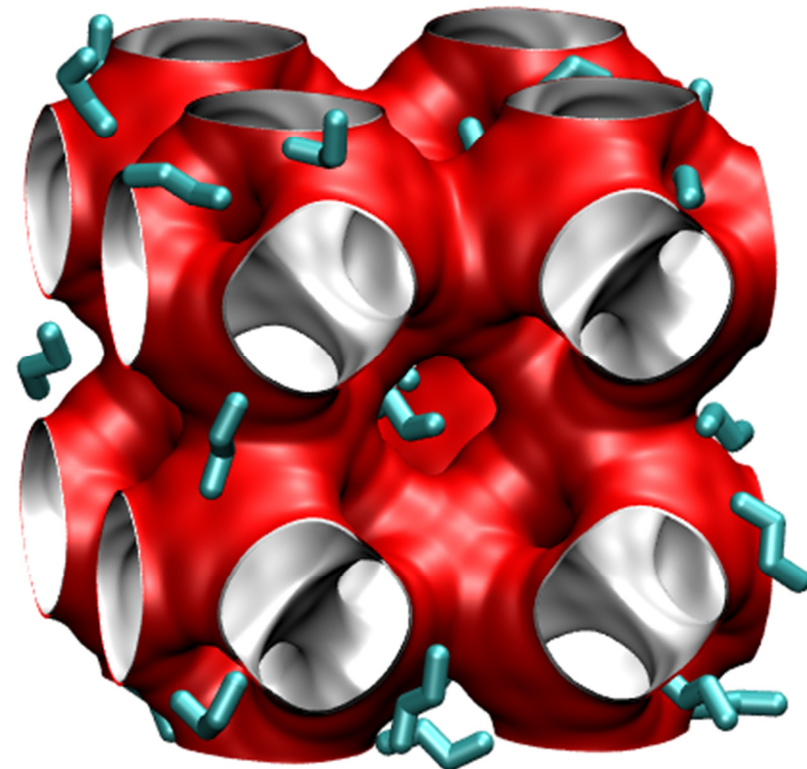
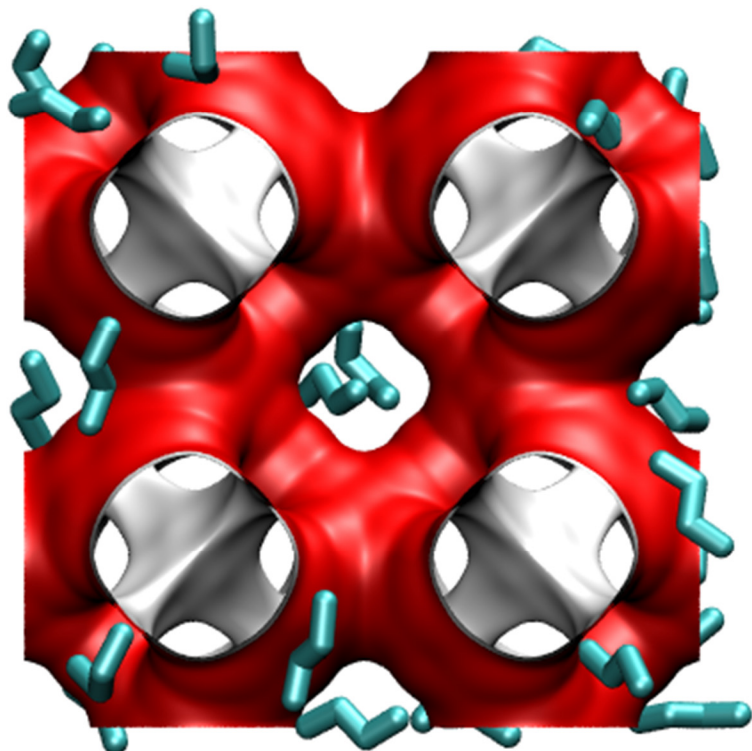
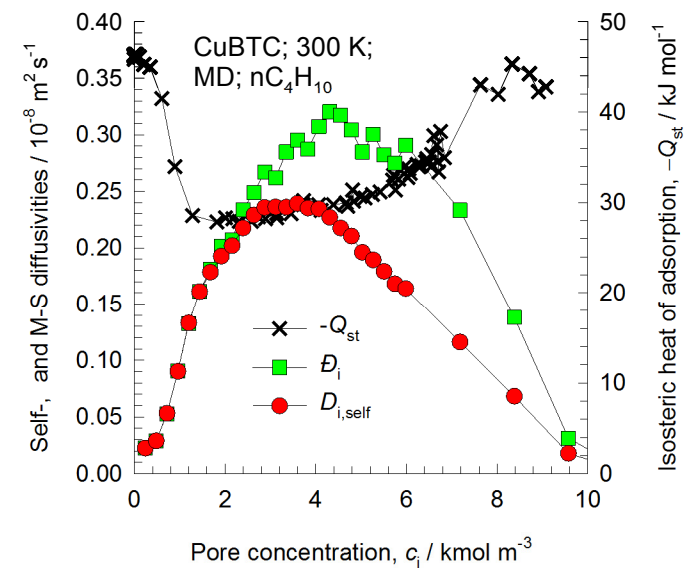
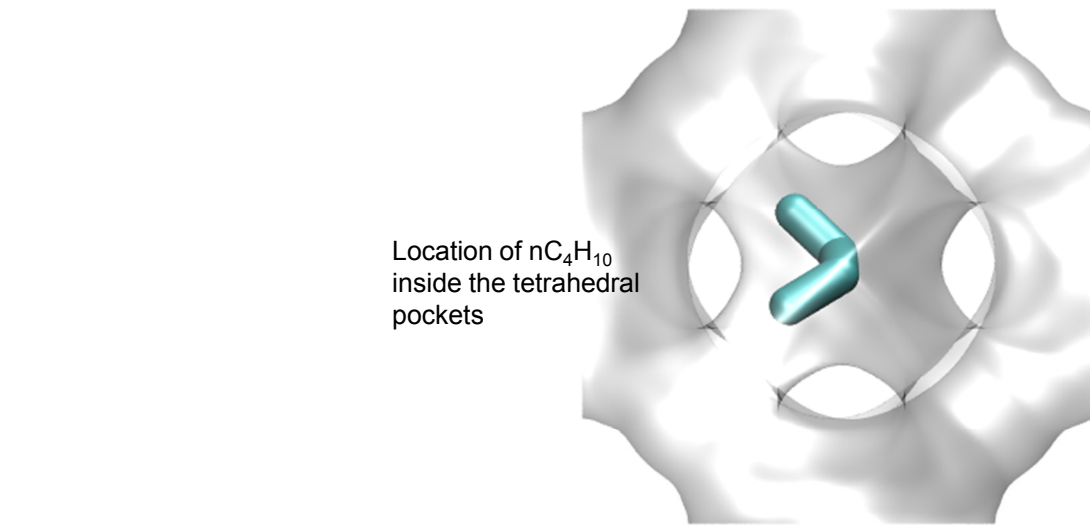


Influence of $-Q_{st}$ on diffusivities

Location of C_3H_8
inside the tetrahedral
pockets

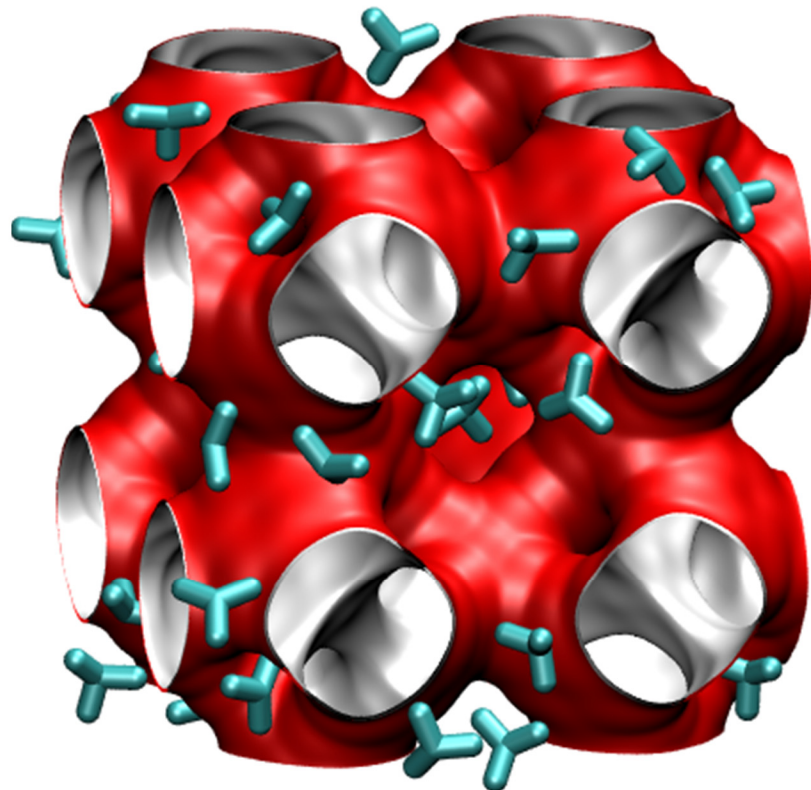
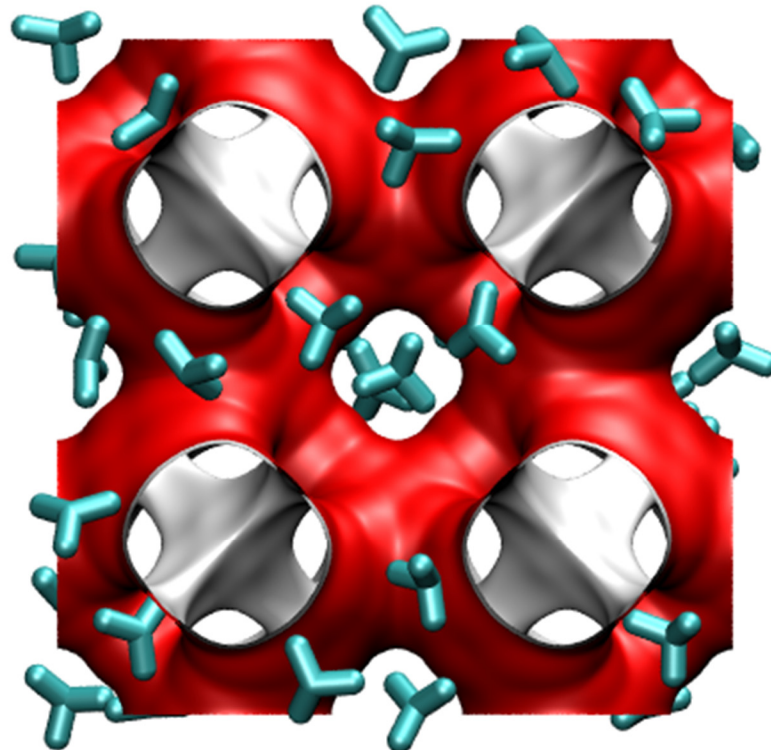
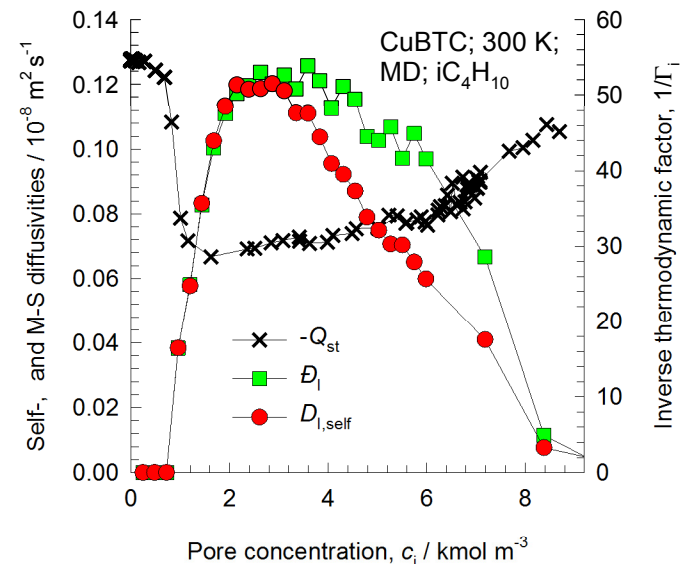
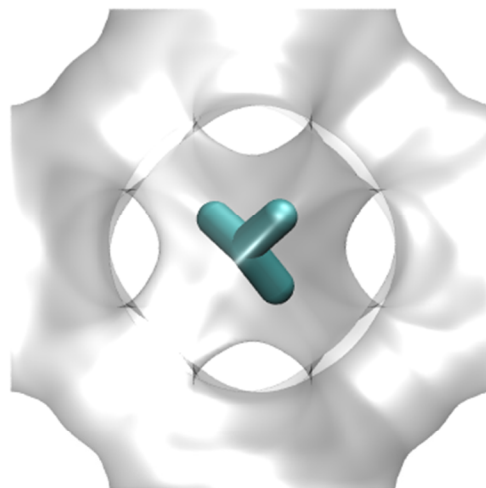


Influence of $-Q_{st}$ on diffusivities

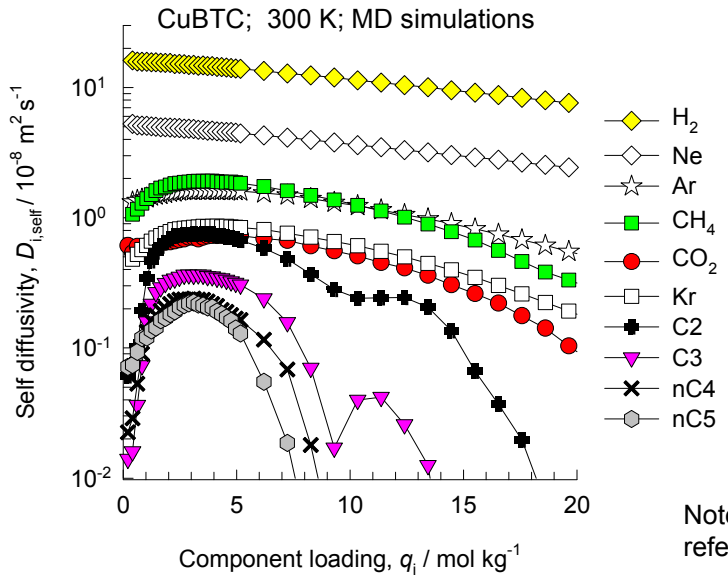


Influence of $-Q_{st}$ on diffusivities

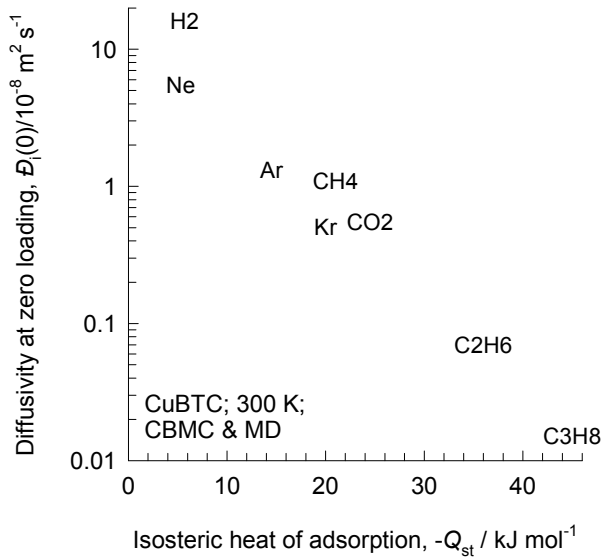
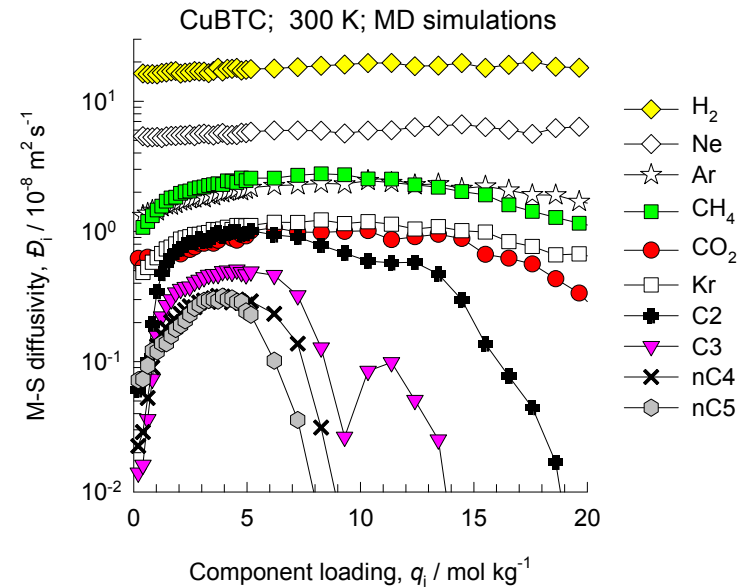
Location of iC_4H_{10}
inside the tetrahedral
pockets



CuBTC MD simulations of unary self- , and M-S diffusivities



Note that C2 and C3 refer to saturated alkanes

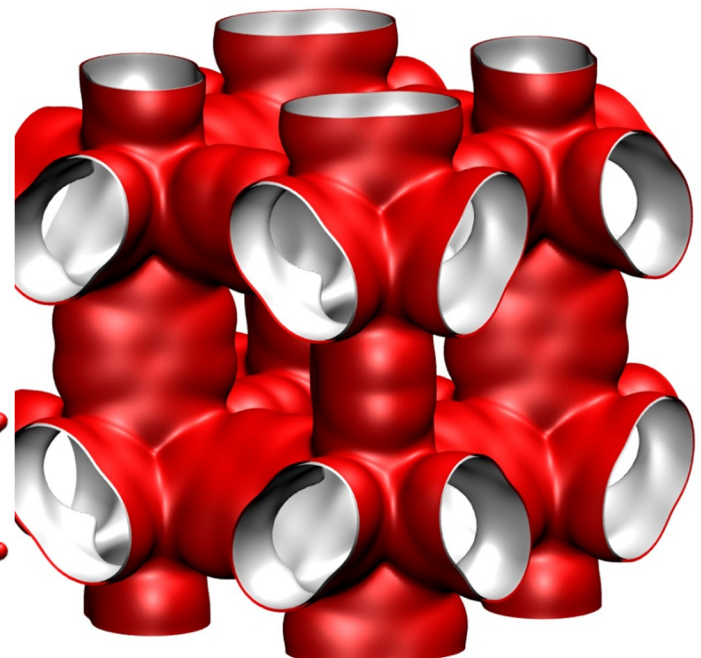
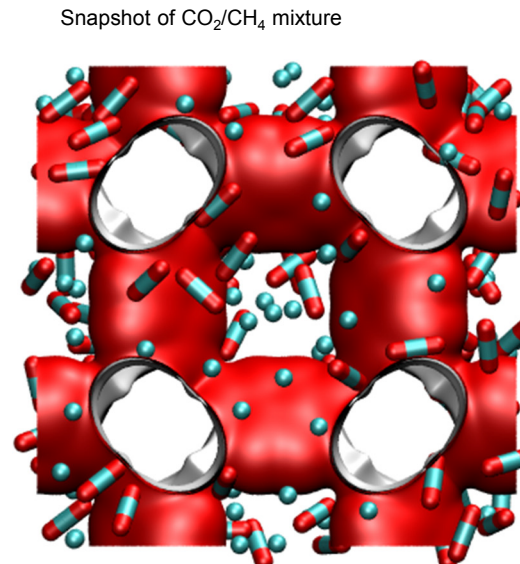
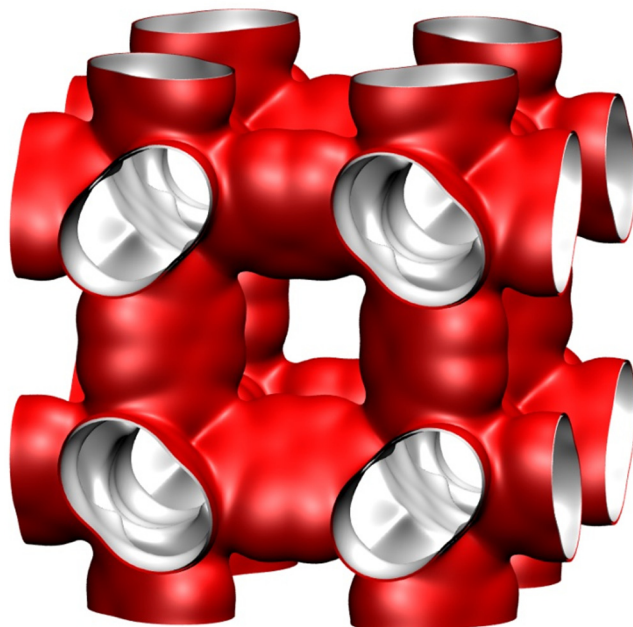
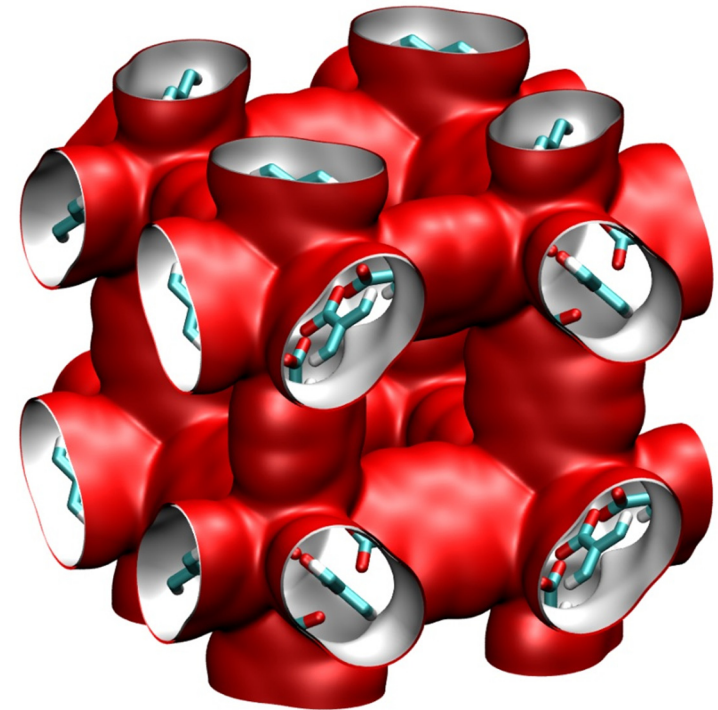


IRMOF-1 pore landscape

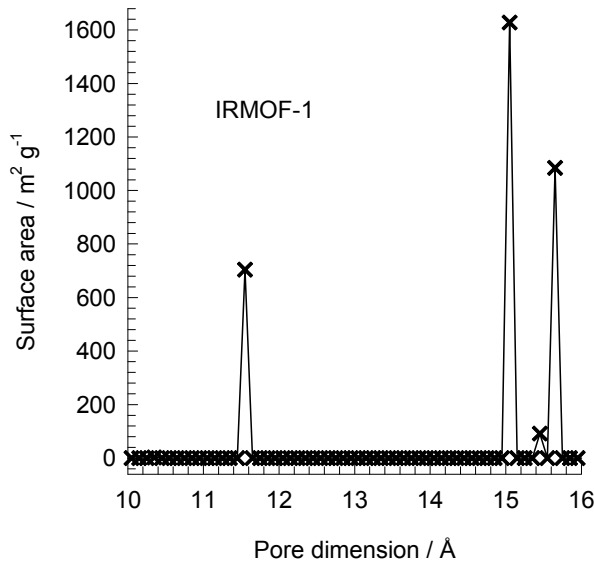
For IRMOF-1 (= MOF 5 = $Zn_4O(BDC)_3$ with BDC^{2-} = 1-4 benzenedicarboxylate) the structural information was obtained from

D. Dubbeldam, K.S. Walton, D.E. Ellis, R.Q. Snurr,
Exceptional Negative Thermal Expansion in Isoreticular Metal–Organic Frameworks, *Angew. Chem. Int. Ed.* 46 (2007) 4496-4499.

D. Dubbeldam, H. Frost, K.S. Walton, R.Q. Snurr,
Molecular simulation of adsorption sites of light gases in the metal-organic framework IRMOF-1, *Fluid Phase Equilib.* 261 (2007) 152-161.



IRMOF-1 pore dimensions

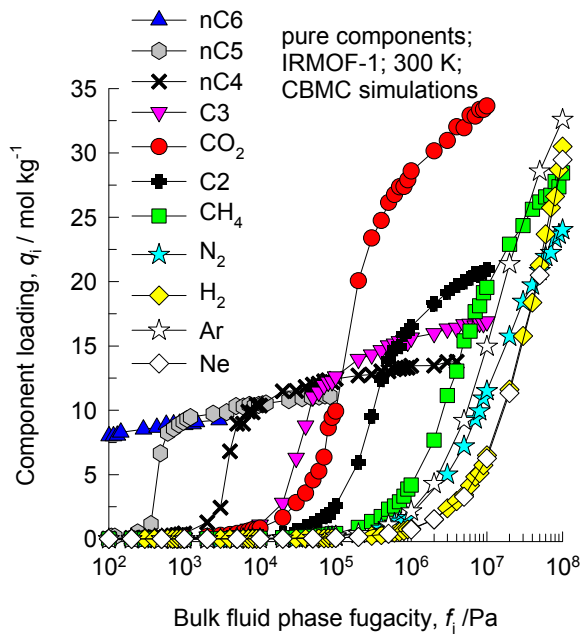


This plot of surface area versus pore dimension is determined using a combination of the DeLaunay triangulation method for pore dimension determination, and the procedure of Düren for determination of the surface area.

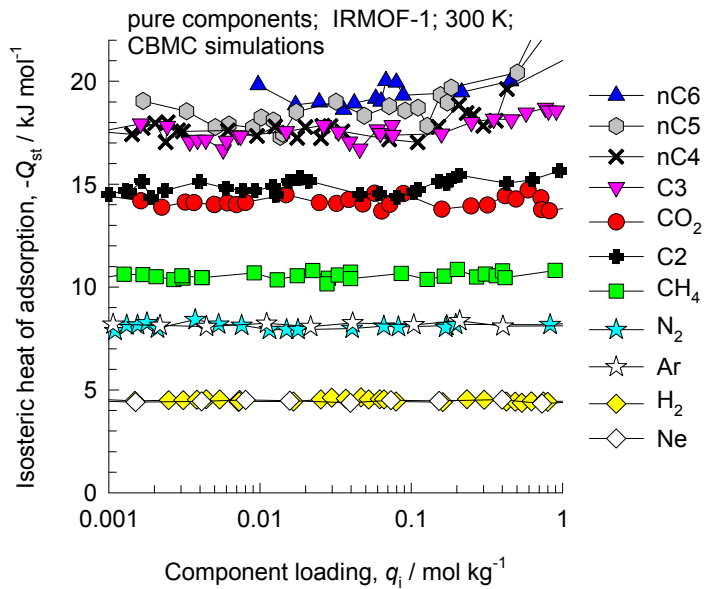
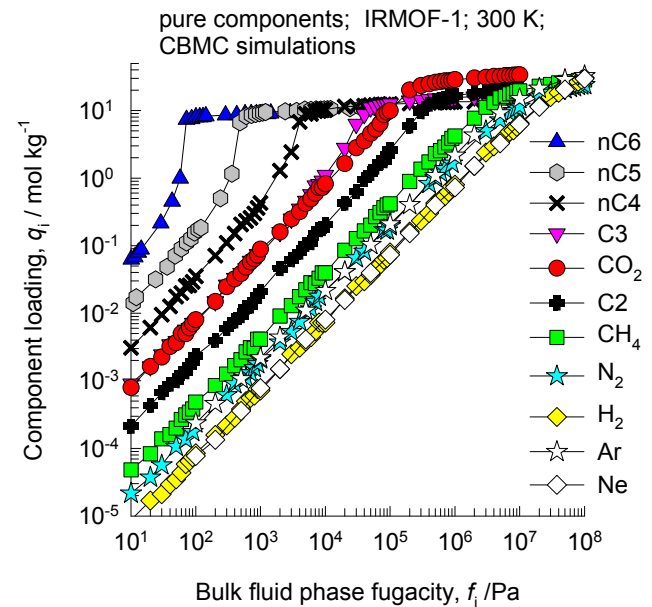
| IRMOF-1 | |
|--|----------|
| $a / \text{\AA}$ | 25.832 |
| $b / \text{\AA}$ | 25.832 |
| $c / \text{\AA}$ | 25.832 |
| Cell volume / \AA^3 | 17237.49 |
| conversion factor for [molec/uc] to [mol per kg Framework] | 0.1624 |
| conversion factor for [molec/uc] to [kmol/m^3] | 0.1186 |
| $\rho / [\text{kg/m}^3]$ | 593.2075 |
| MW unit cell [g/mol(framework)] | 6157.788 |
| ϕ , fractional pore volume | 0.812 |
| open space / $\text{\AA}^3/\text{uc}$ | 13996.3 |
| Pore volume / cm^3/g | 1.369 |
| Surface area / m^2/g | 3522.2 |
| DeLaunay diameter / \AA | 7.38 |

Two alternating, inter-connected, cavities of 11 \AA and 15 \AA with window size of 8 \AA .

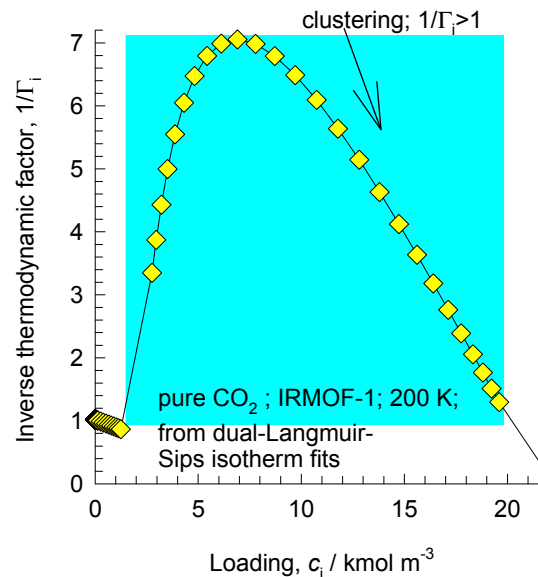
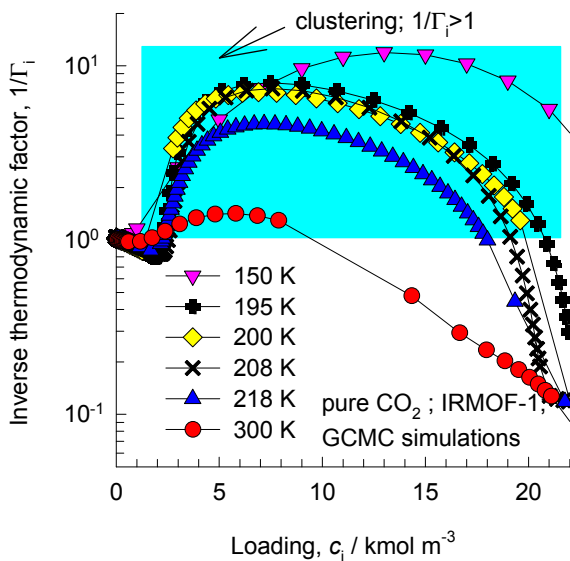
IRMOF-1 CBMC simulations of isotherms, and isosteric heats of adsorption



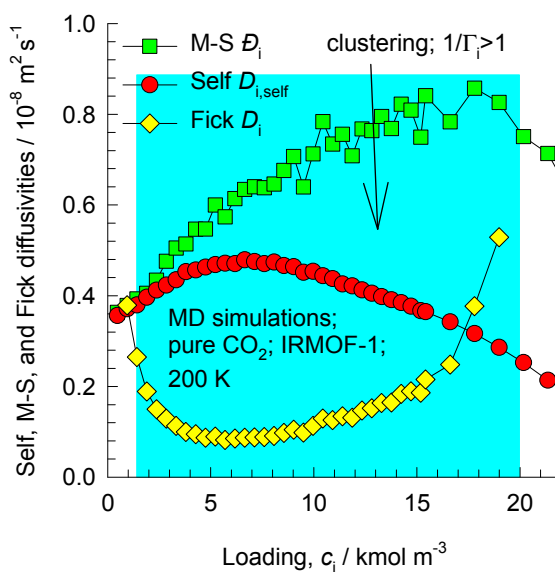
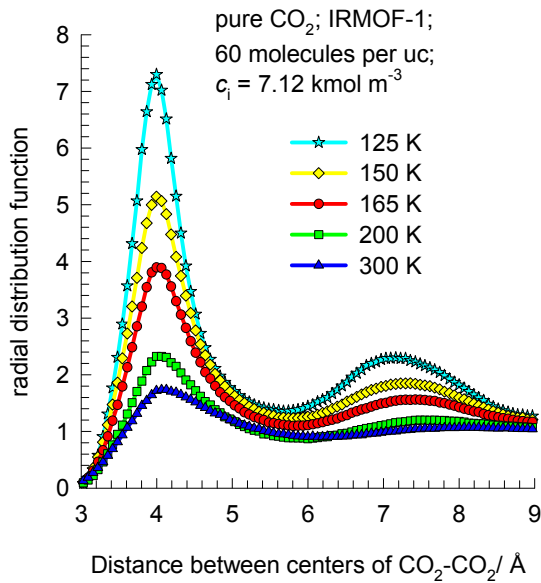
Note that C2 and C3 refer to saturated alkanes



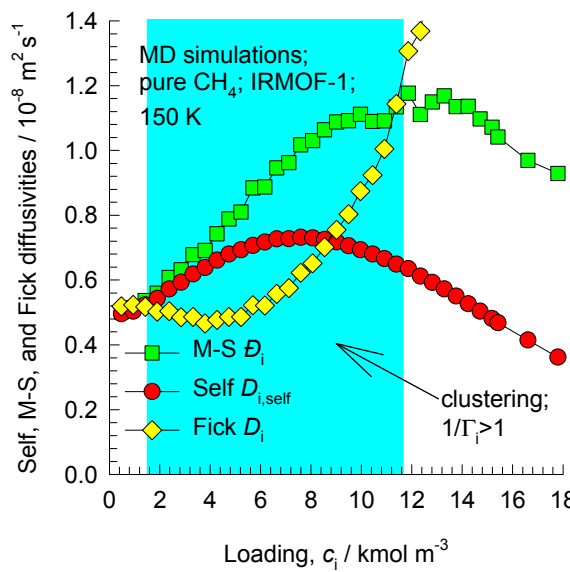
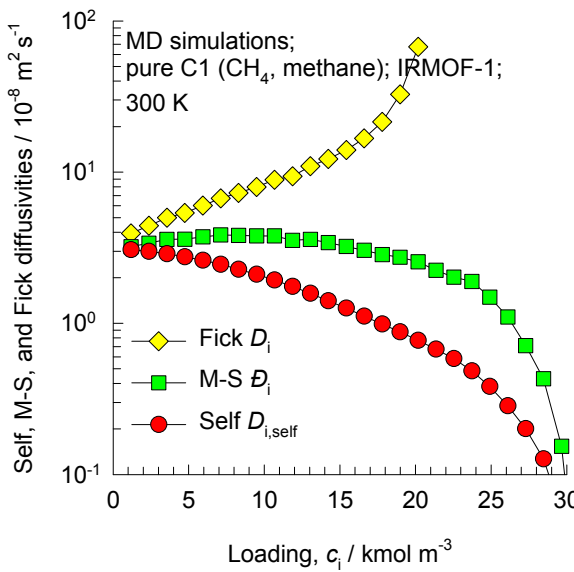
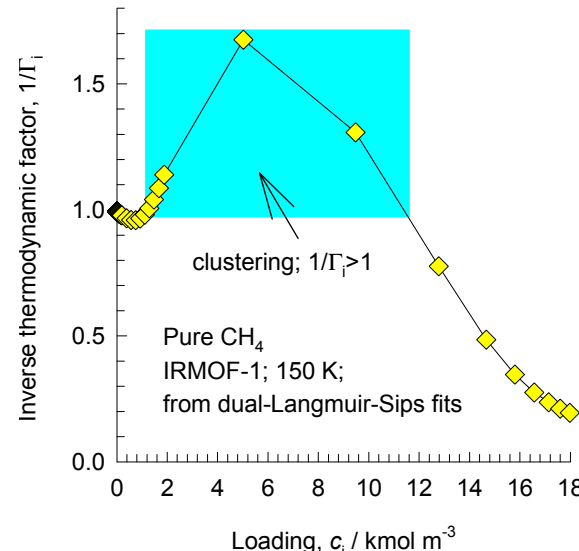
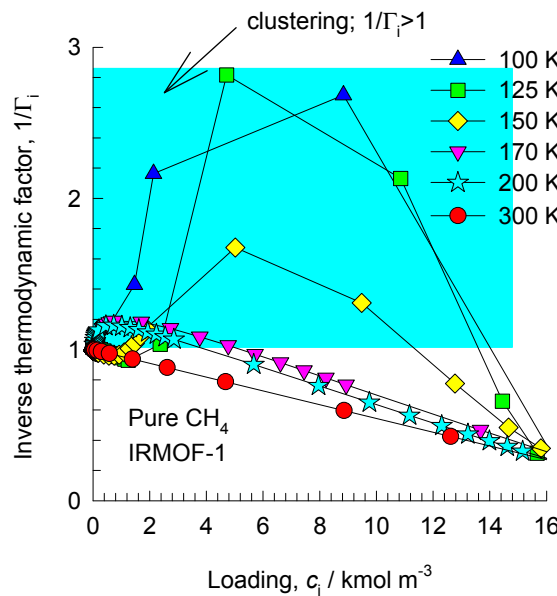
IRMOF-1 CO_2 adsorption and diffusion



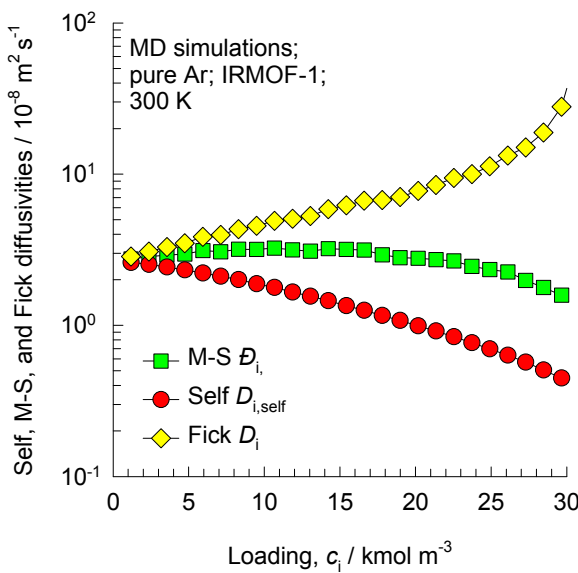
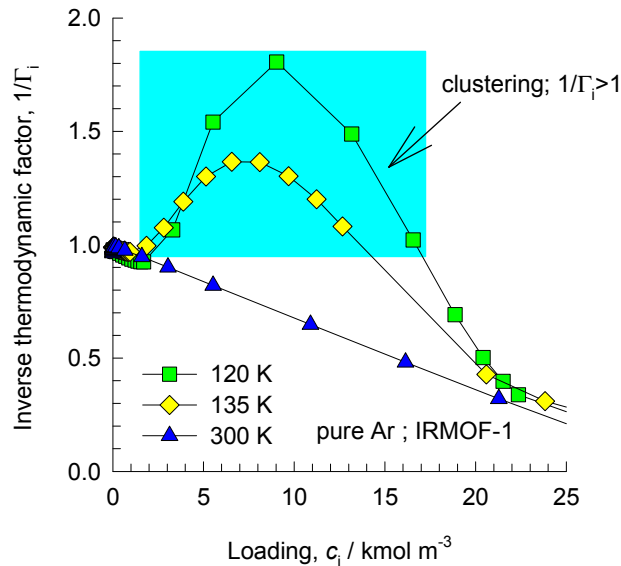
The RDFs show that the degree of clustering increases as the temperature is decreased.



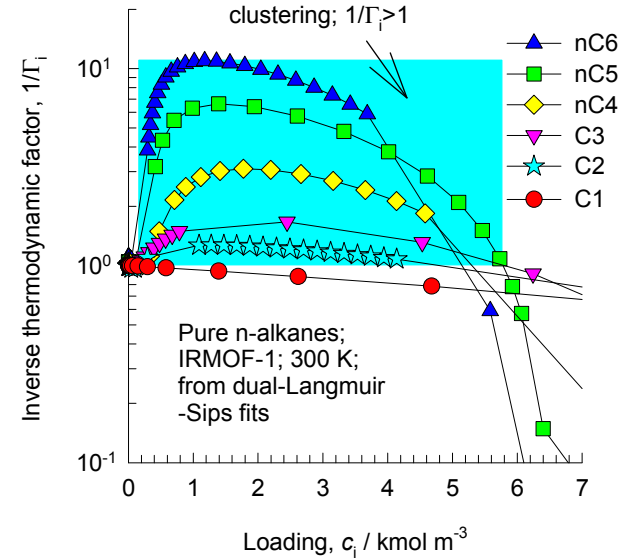
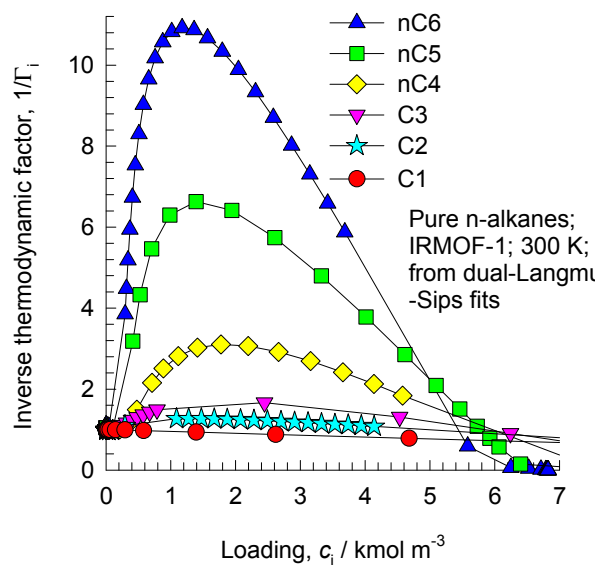
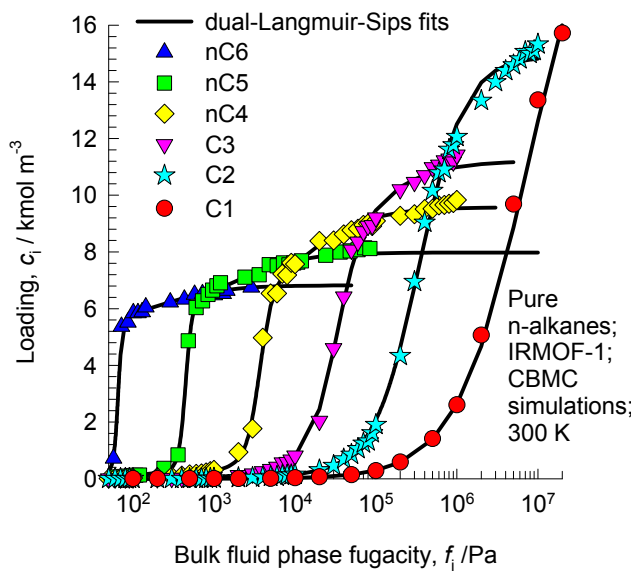
IRMOF-1 CH₄ adsorption and diffusion



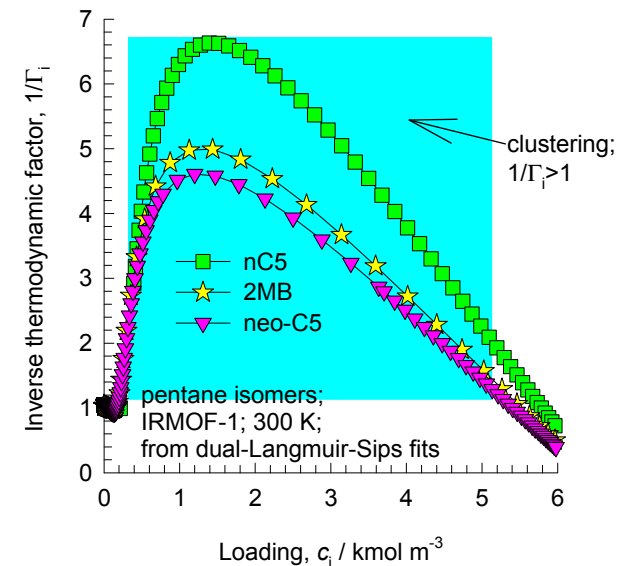
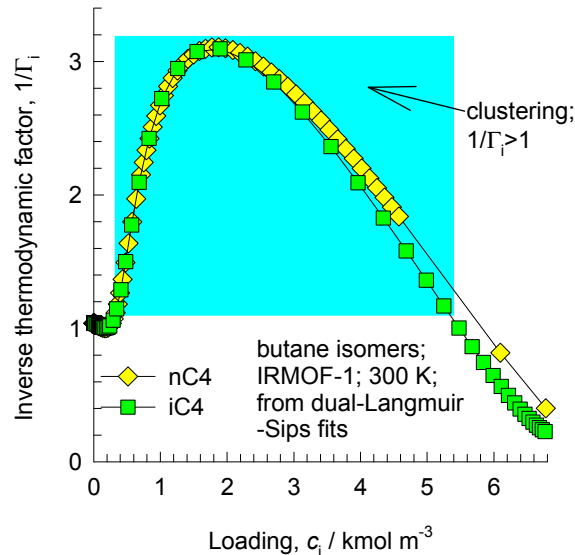
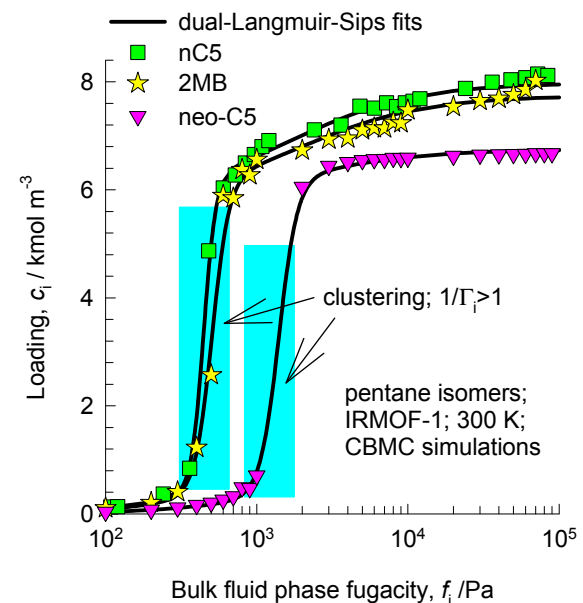
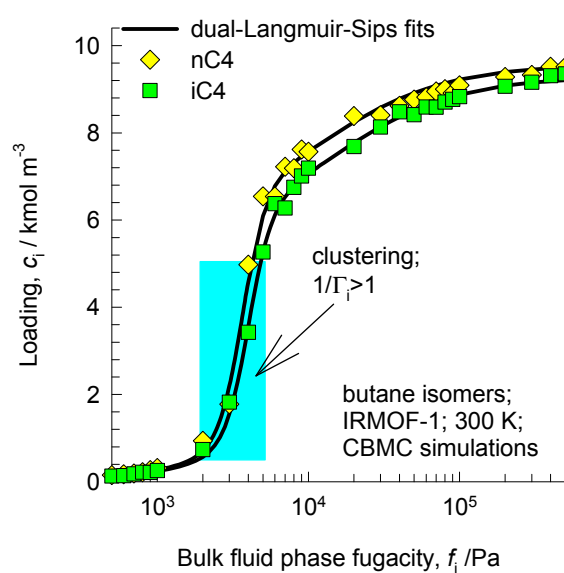
IRMOF-1 Ar adsorption and diffusion



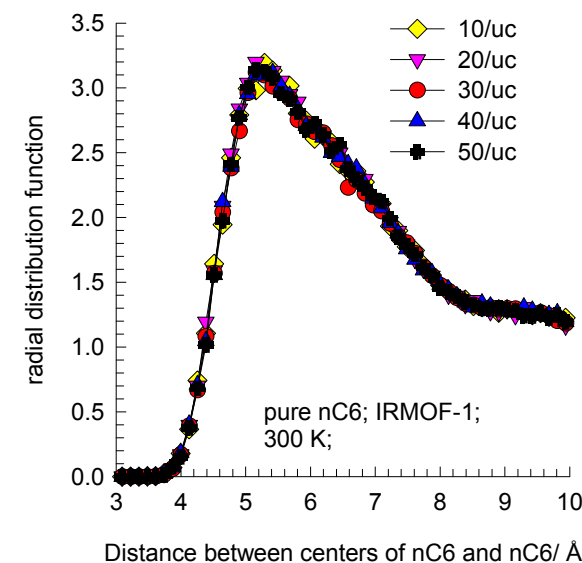
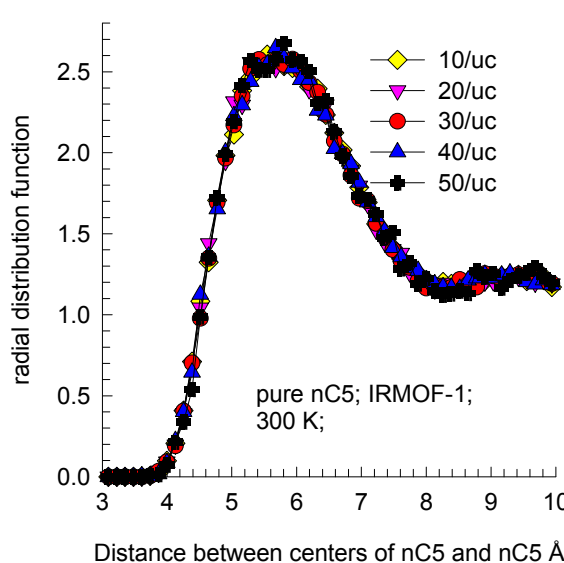
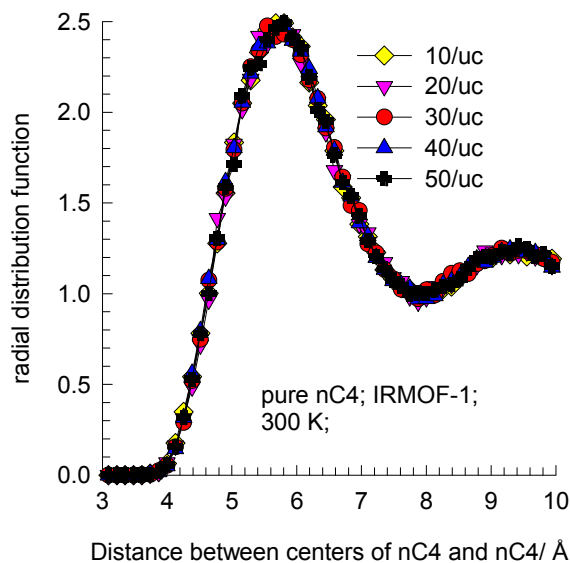
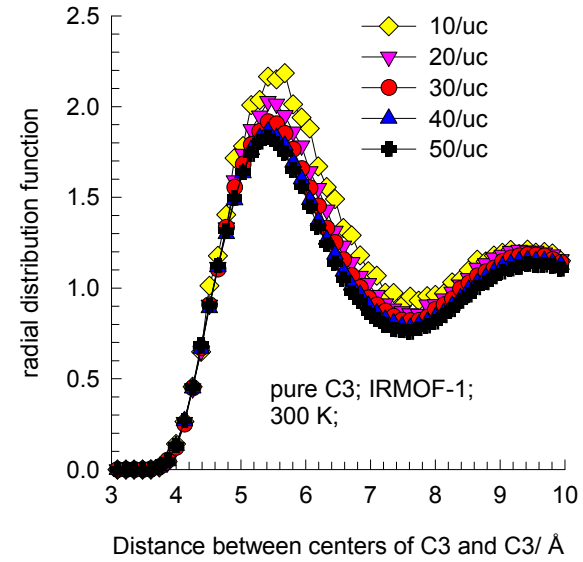
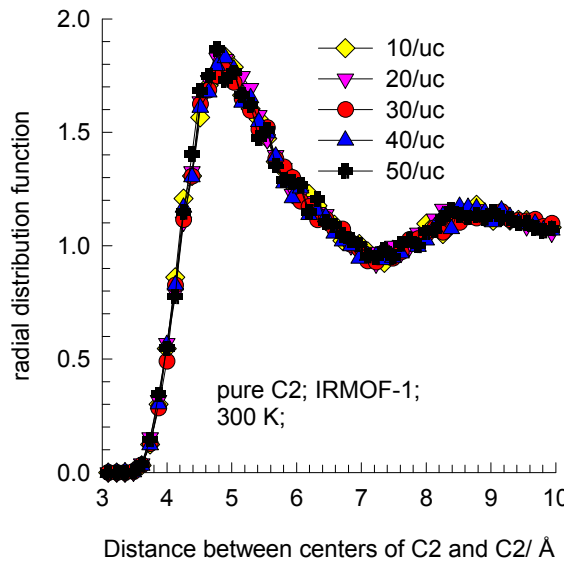
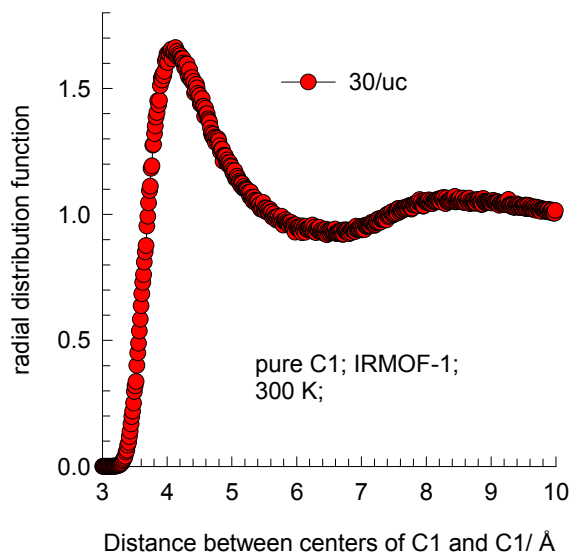
IRMOF-1 CBMC simulations for linear alkanes



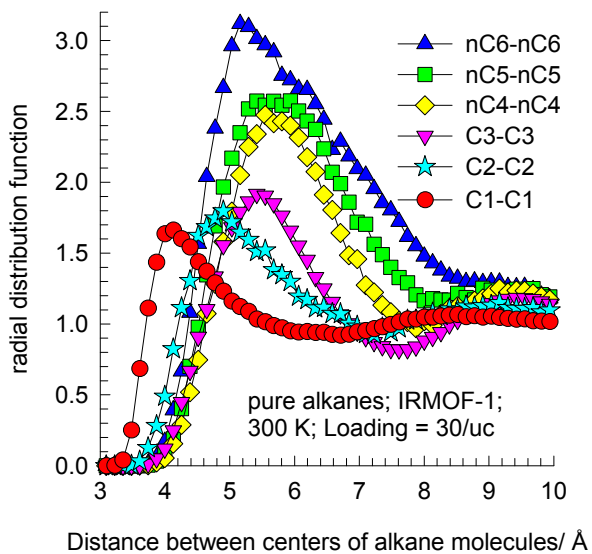
IRMOF-1 CBMC simulations for pure C4 and C5 isomers



IRMOF-1 RDFs for pure alkanes

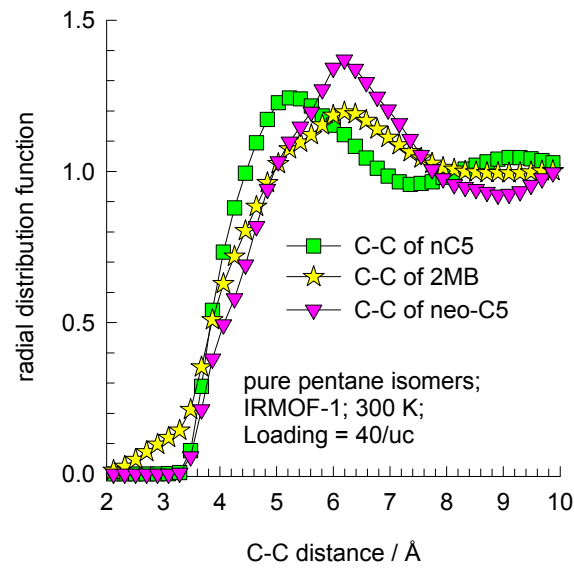
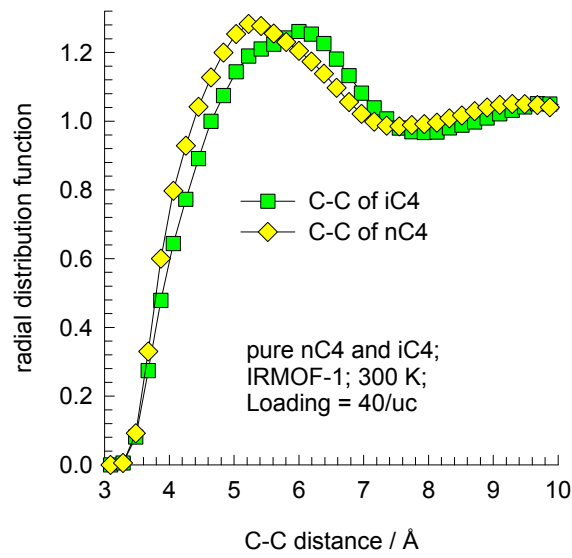


IRMOF-1 Comparison of RDFs of n-alkanes



These RDFs are constructed on the basis of distances between centers of mass of n-alkane molecules

IRMOF-1 RDF comparison of linear and branched alkanes

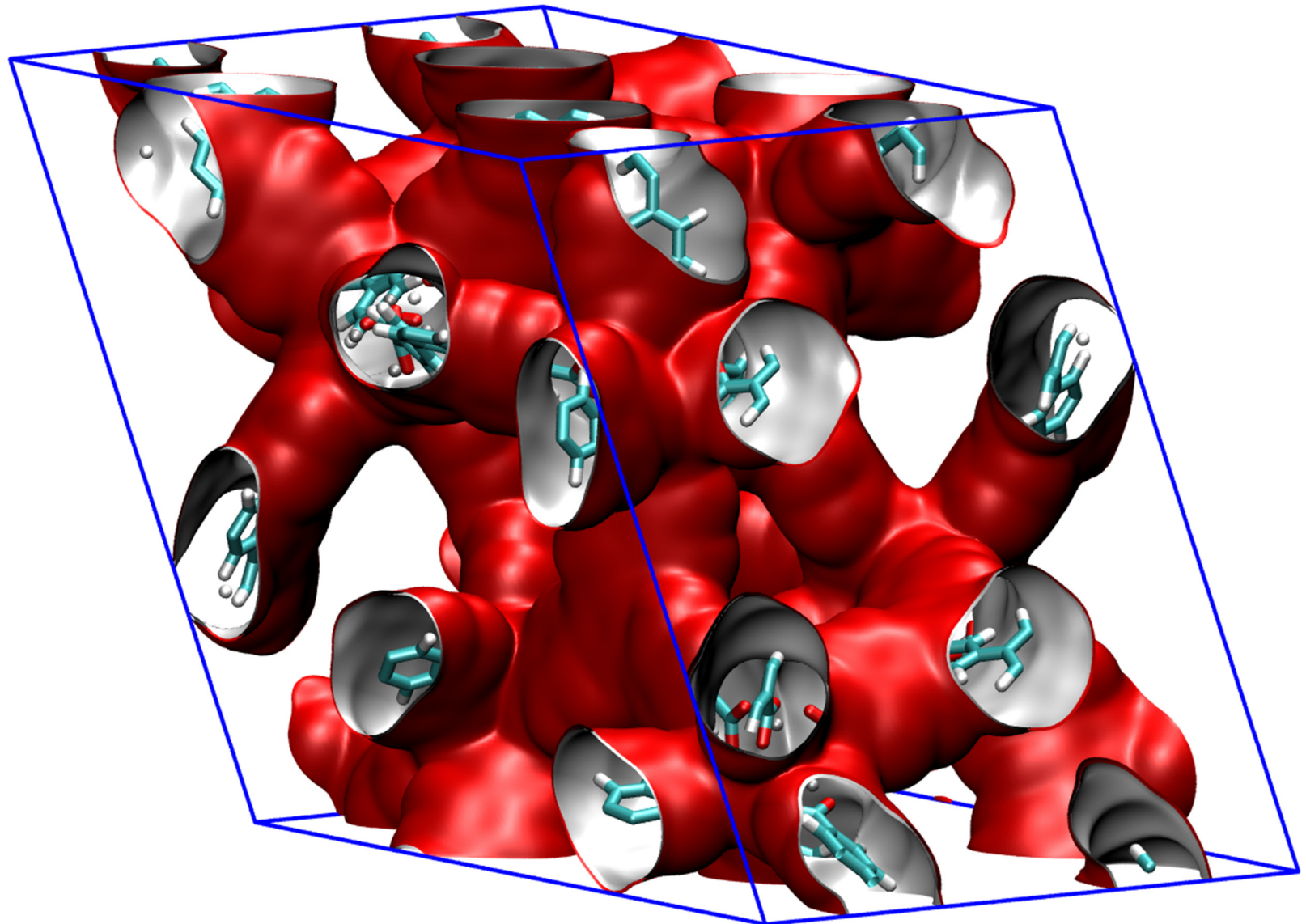


These RDFs are constructed
on the basis of distances
between every intermolecular
C-C pairs

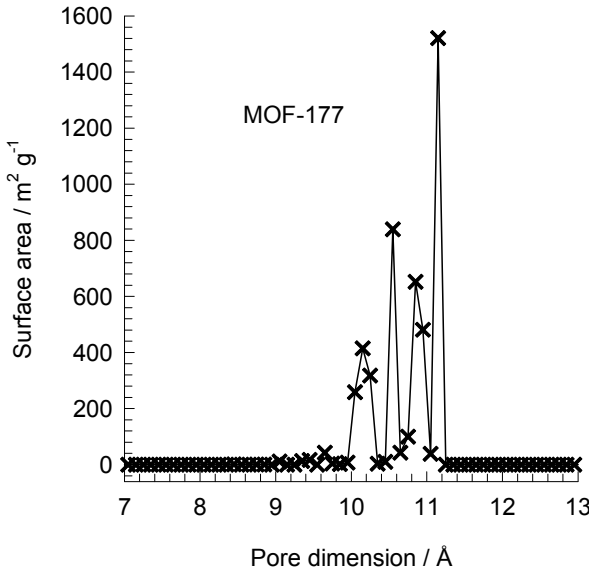
MOF-177 pore landscape

The structural information for MOF-177 (= $\text{Zn}_4\text{O}(\text{BTB})_2$ with (BTB^{3-} = 1,3,5-benzenetribenzoate)) is provided by

H.K. Chae, D.Y. Siberio-Pérez, J. Kim, Y.B. Go, M. Eddaoudi, A.J. Matzger, M. O'Keeffe, O.M. Yaghi, A route to high surface area, porosity and inclusion of large molecules in crystals, Nature 427 (2004) 523-527.



MOF-177 pore dimensions



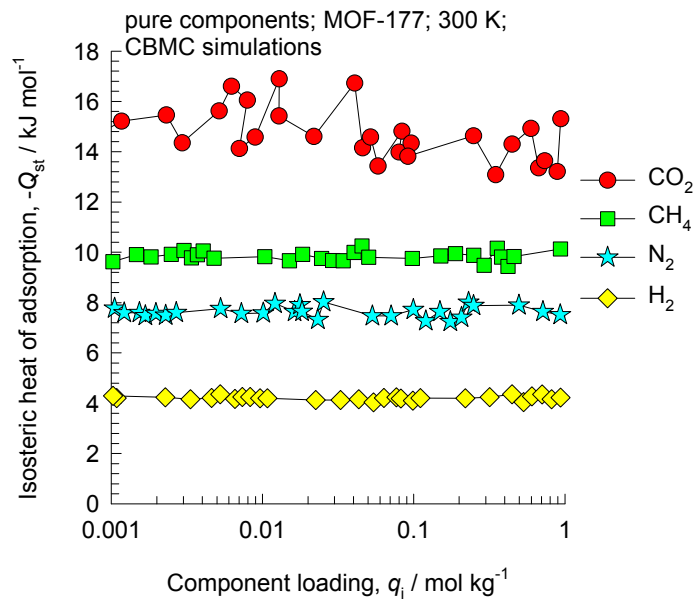
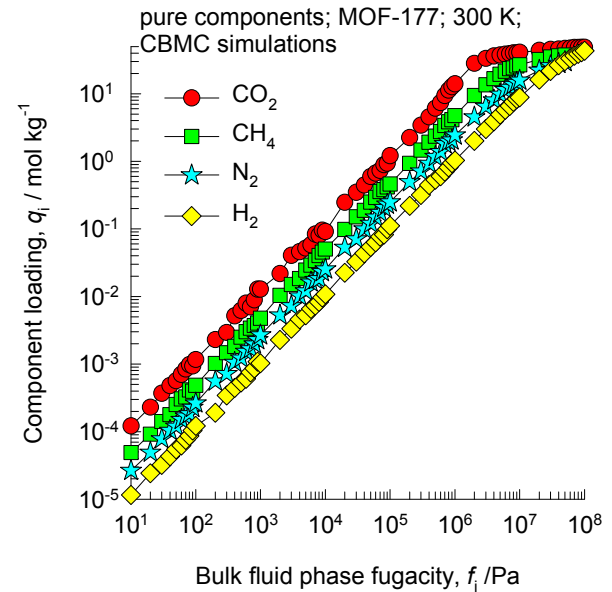
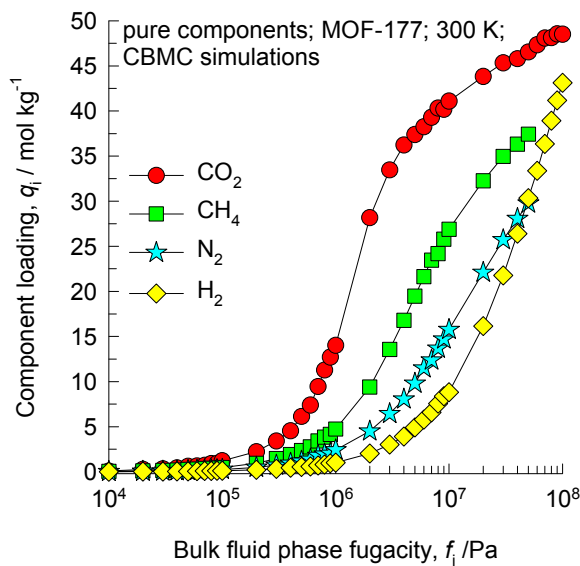
This plot of surface area versus pore dimension is determined using a combination of the DeLaunay triangulation method for pore dimension determination, and the procedure of Düren for determination of the surface area.

| MOF-177 | |
|--|----------|
| $a / \text{\AA}$ | 37.072 |
| $b / \text{\AA}$ | 37.072 |
| $c / \text{\AA}$ | 30.033 |
| Cell volume / \AA^3 | 35745.5 |
| conversion factor for [molec/uc] to [mol per kg Framework] | 0.1089 |
| conversion factor for [molec/uc] to [kmol/m^3] | 0.0553 |
| $\rho / [\text{kg/m}^3]$ | 426.5952 |
| MW unit cell [g/mol(framework)] | 9182.931 |
| ϕ , fractional pore volume | 0.840 |
| open space / $\text{\AA}^3/\text{uc}$ | 30010.9 |
| Pore volume / cm^3/g | 1.968 |
| Surface area / m^2/g | 4781.0 |
| DeLaunay diameter / \AA | 10.1 |

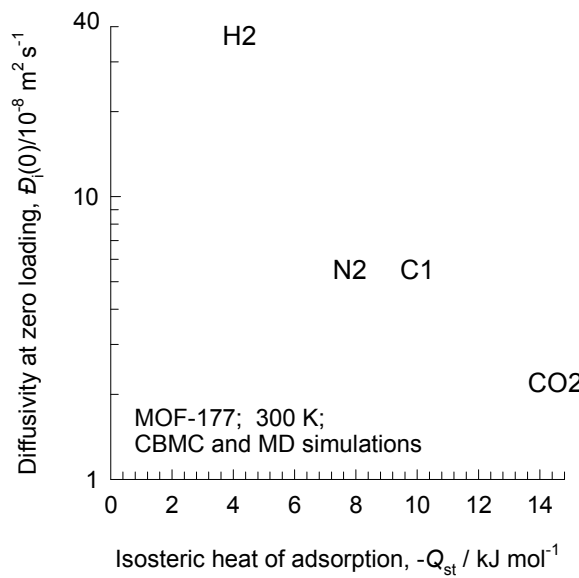
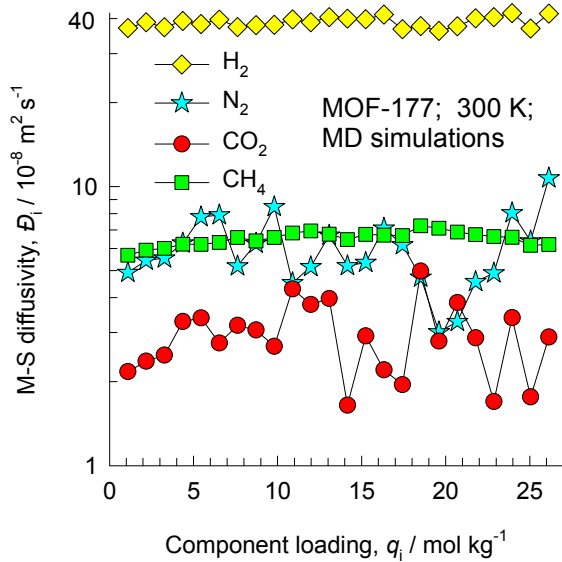
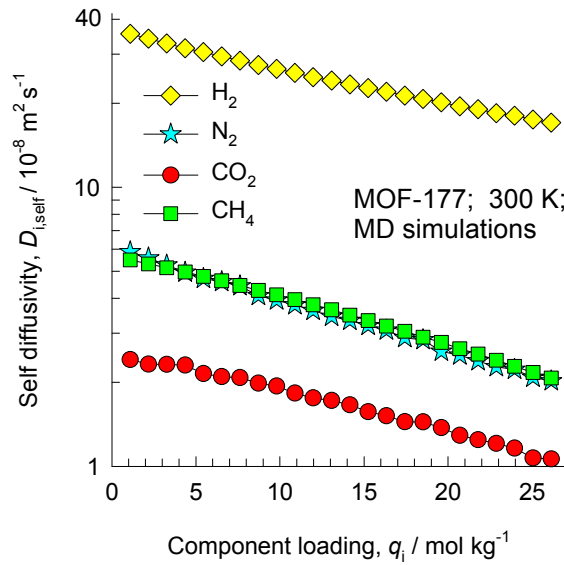
Tetrahedral $[\text{Zn}_4\text{O}]^{6+}$ units are linked by large, triangular tricarboxylate ligands. Six diamond-shaped channels (upper) with diameter of 10.8 Å surround a pore containing eclipsed BTB³⁻ moieties.

MOF-177

CBMC simulations of isotherms, and isosteric heats of adsorption

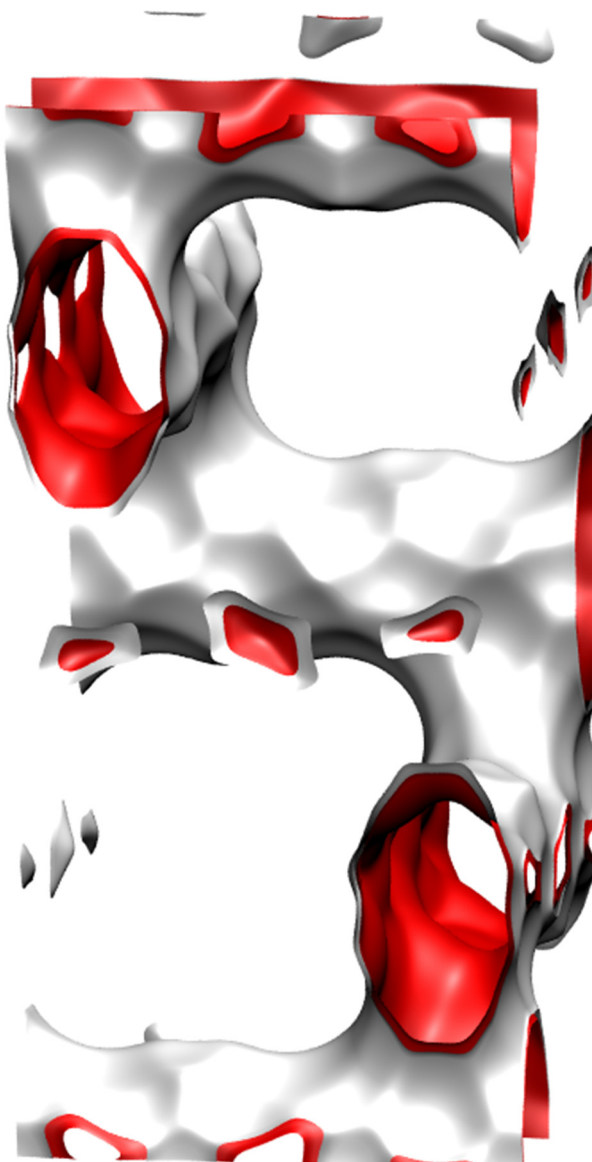


MOF-177 MD simulations of unary self-, and M-S diffusivities



Intersecting channels

BEA pore landscape



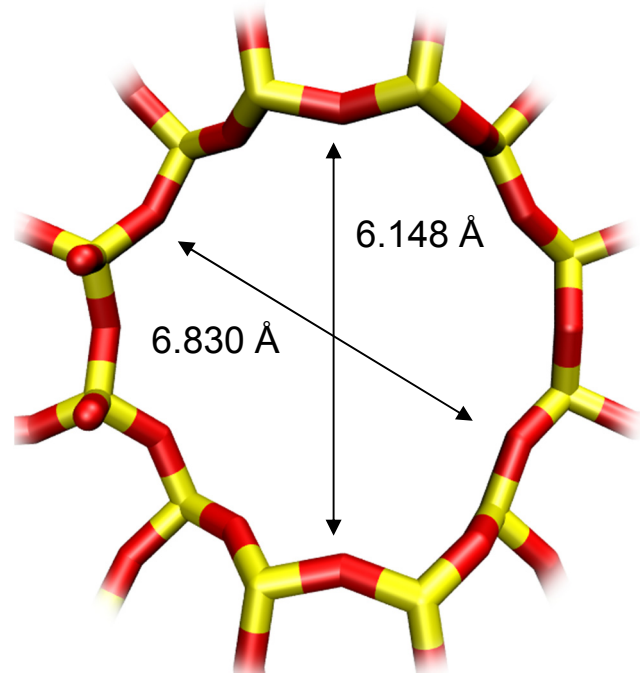
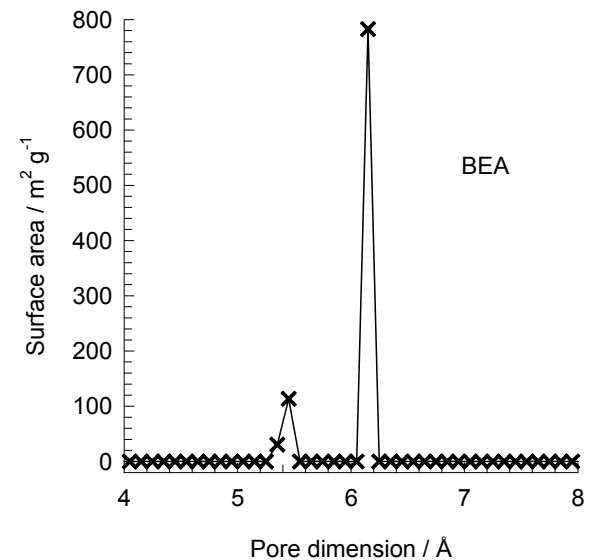
Intersecting channels of two sizes:
12-ring and 10-ring

| | BEA |
|--|----------|
| $a / \text{\AA}$ | 12.661 |
| $b / \text{\AA}$ | 12.661 |
| $c / \text{\AA}$ | 26.406 |
| Cell volume / \AA^3 | 4232.906 |
| conversion factor for [molec/uc] to [mol per kg Framework] | 0.2600 |
| conversion factor for [molec/uc] to [kmol/m ³] | 0.9609 |
| $\rho / \text{kg/m}^3$ | 1508.558 |
| MW unit cell [g/mol(framework)] | 3845.427 |
| ϕ , fractional pore volume | 0.408 |
| open space / $\text{\AA}^3/\text{uc}$ | 1728.1 |
| Pore volume / cm^3/g | 0.271 |
| Surface area / m^2/g | 923.0 |
| DeLaunay diameter / \AA | 5.87 |

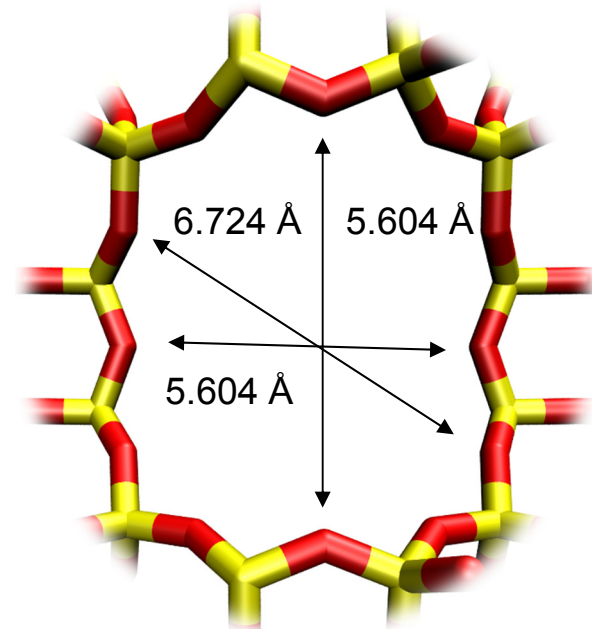
Structural information from: C. Baerlocher, L.B. McCusker, Database of Zeolite Structures, International Zeolite Association, <http://www.iza-structure.org/databases/>

BEA pore dimensions

This plot of surface area versus pore dimension is determined using a combination of the DeLaunay triangulation method for pore dimension determination, and the procedure of Düren for determination of the surface area.

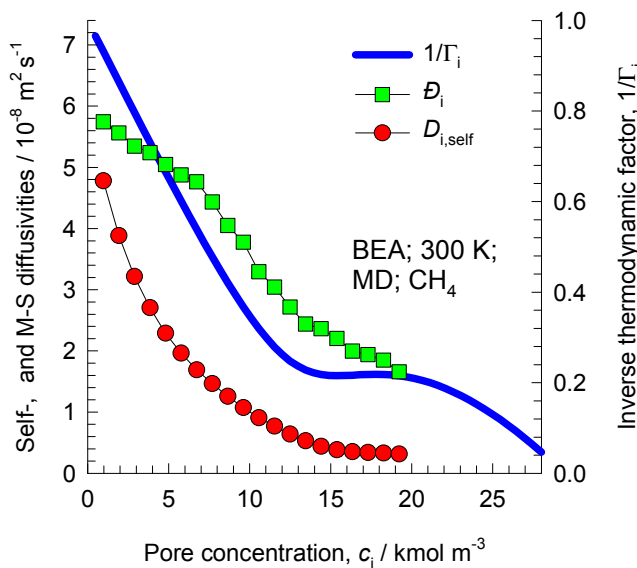


BEA [1 0 0]



BEA [0 0 1]

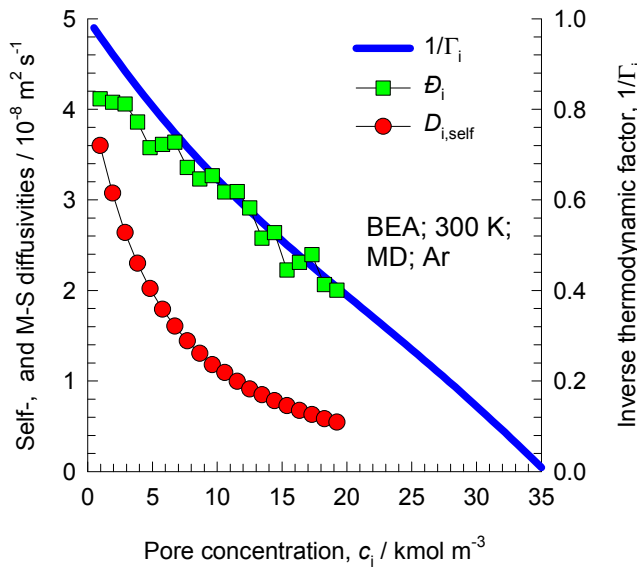
Influence of Inverse Thermodynamic Factor on diffusivities



A detailed analysis of the loading dependence of CH₄ in BEA is contained in

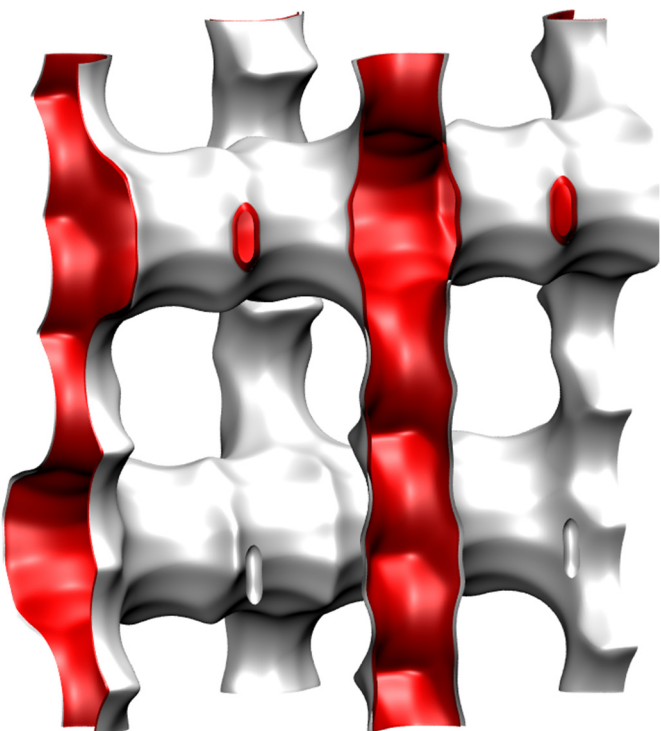
E. Beerdsen, D. Dubbeldam and B. Smit, J Phys Chem B, 2006, 110, 22754-22772.

E. Beerdsen, D. Dubbeldam and B. Smit, Phys. Rev. Lett., 2006, 96, 044501.



BOG pore landscape

Intersecting channels:
12-ring and 10-ring

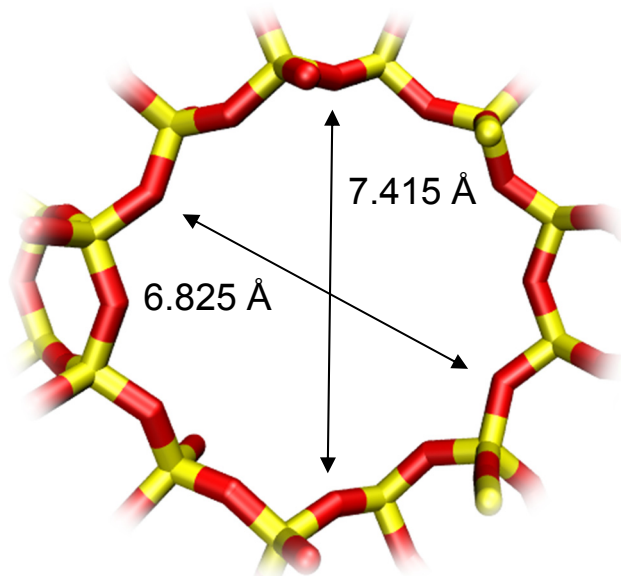


| | BOG |
|--|----------|
| $a / \text{\AA}$ | 20.236 |
| $b / \text{\AA}$ | 23.798 |
| $c / \text{\AA}$ | 12.798 |
| Cell volume / \AA^3 | 6163.214 |
| conversion factor for [molec/uc] to [mol per kg Framework] | 0.1734 |
| conversion factor for [molec/uc] to [kmol/m^3] | 0.7203 |
| $\rho [\text{kg}/\text{m}^3]$ | 1995.523 |
| MW unit cell [g/mol(framework)] | 5768.141 |
| ϕ , fractional pore volume | 0.374 |
| open space / $\text{\AA}^3/\text{uc}$ | 2305.4 |
| Pore volume / cm^3/g | 0.241 |
| Surface area / m^2/g | 758.0 |
| DeLaunay diameter / \AA | 5.02 |

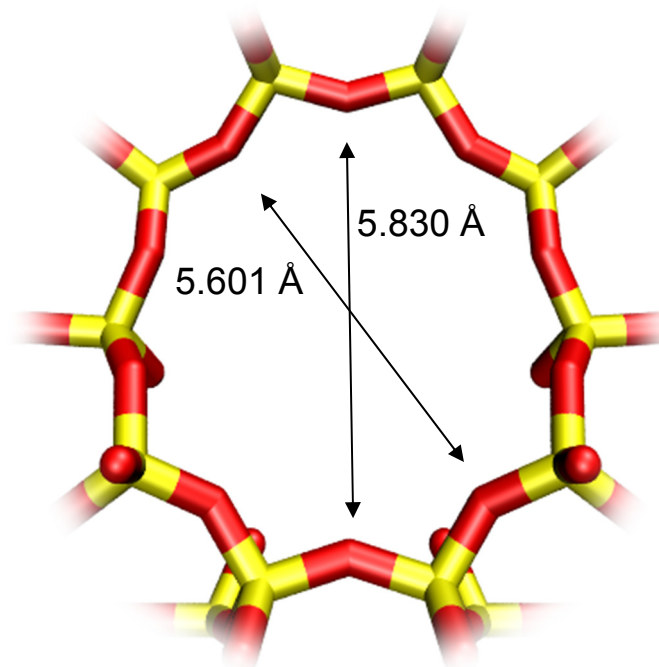
Structural information from: C. Baerlocher, L.B. McCusker, Database of Zeolite Structures, International Zeolite Association, <http://www.iza-structure.org/databases/>

BOG pore dimensions

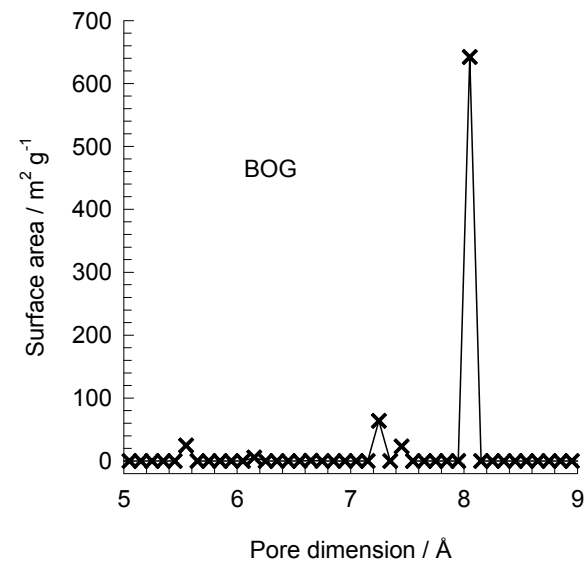
This plot of surface area versus pore dimension is determined using a combination of the DeLaunay triangulation method for pore dimension determination, and the procedure of Düren for determination of the surface area.



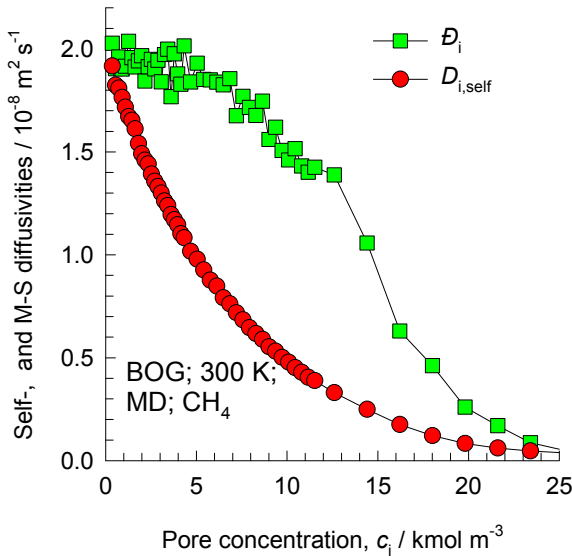
BOG [1 0 0]



BOG [0 1 0]



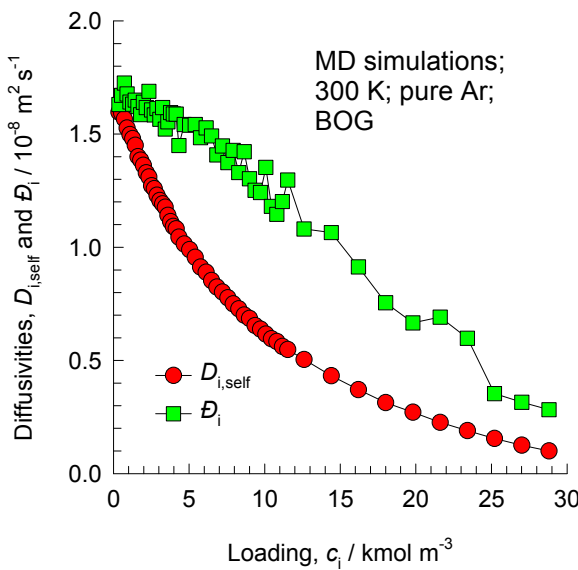
Loading dependence of diffusivities



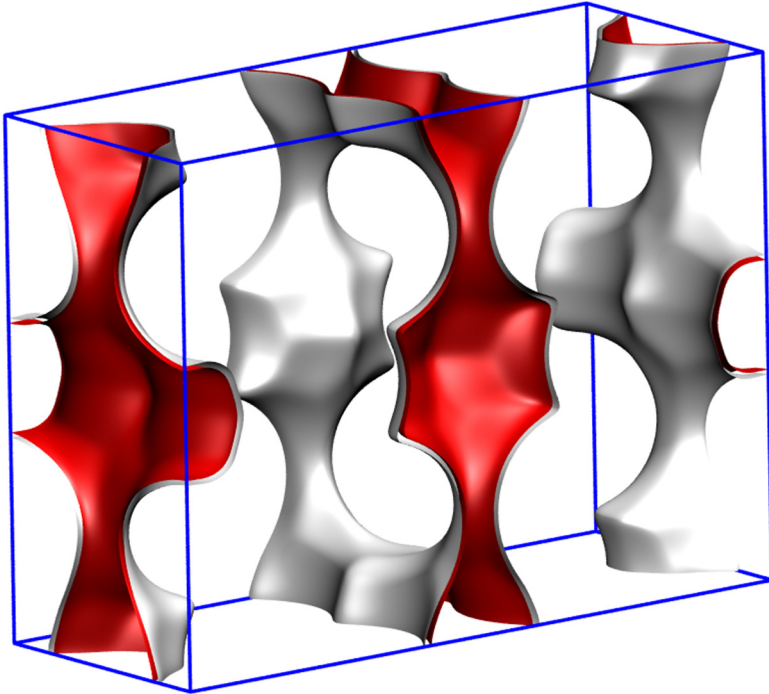
A detailed analysis of the loading dependence of CH_4 in BOG is contained in

E. Beerdsen, D. Dubbeldam
and B. Smit, J Phys Chem B,
2006, 110, 22754-22772.

E. Beerdsen, D. Dubbeldam
and B. Smit, Phys. Rev. Lett.,
2006, 96, 044501.

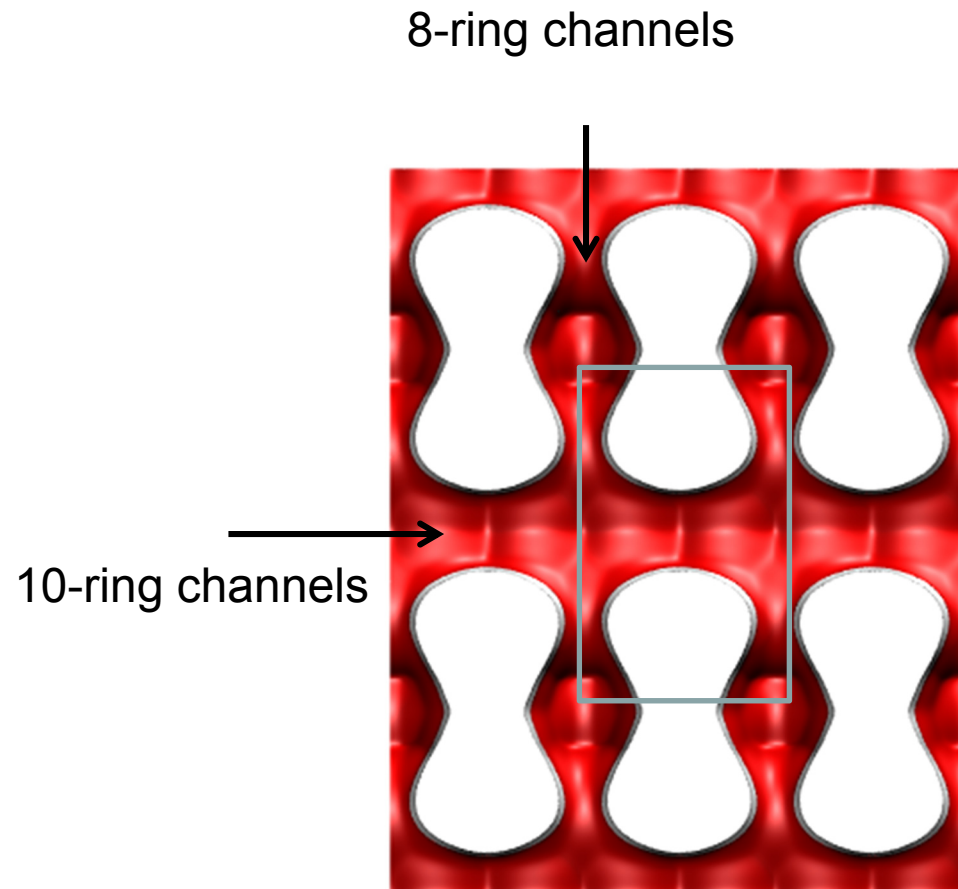


FER pore landscape



This is one unit cell

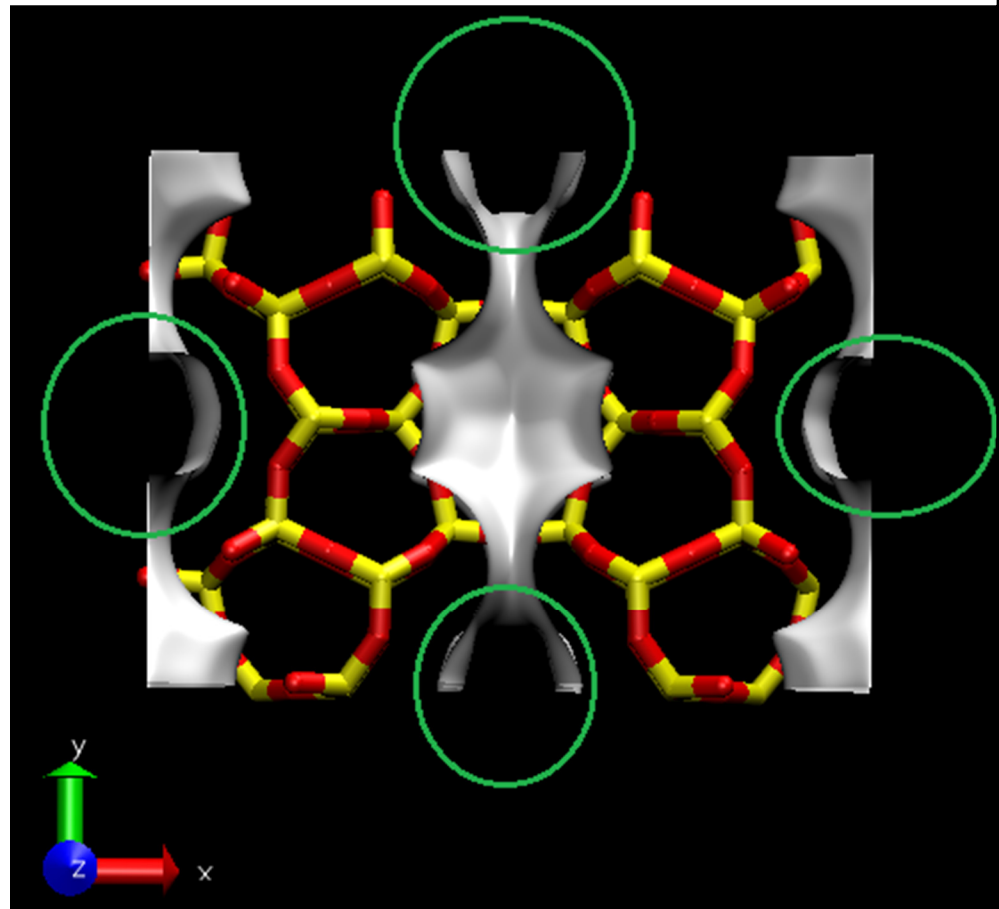
There are two 10-ring channels
There are two 8-ring channels



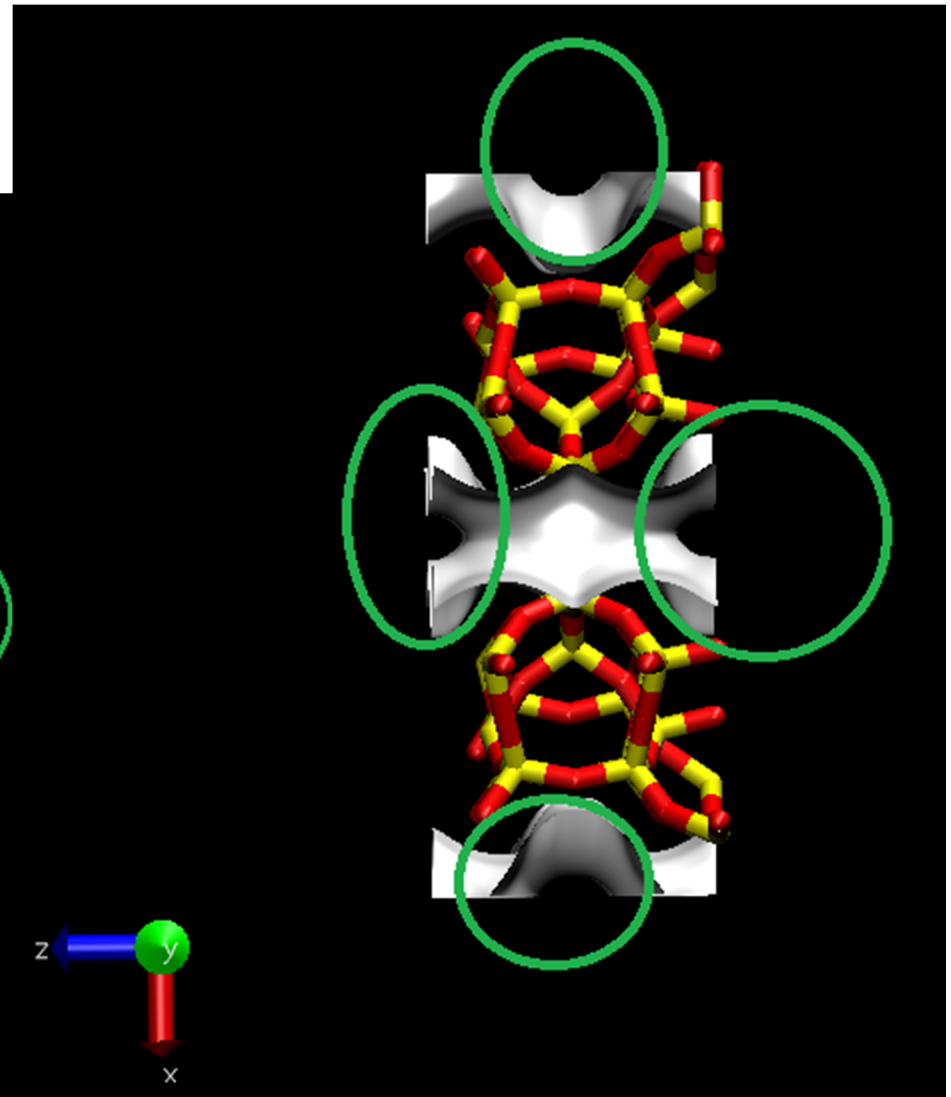
Structural information from: C. Baerlocher, L.B. McCusker, Database of Zeolite Structures, International Zeolite Association, <http://www.iza-structure.org/databases/>

FER pore landscape

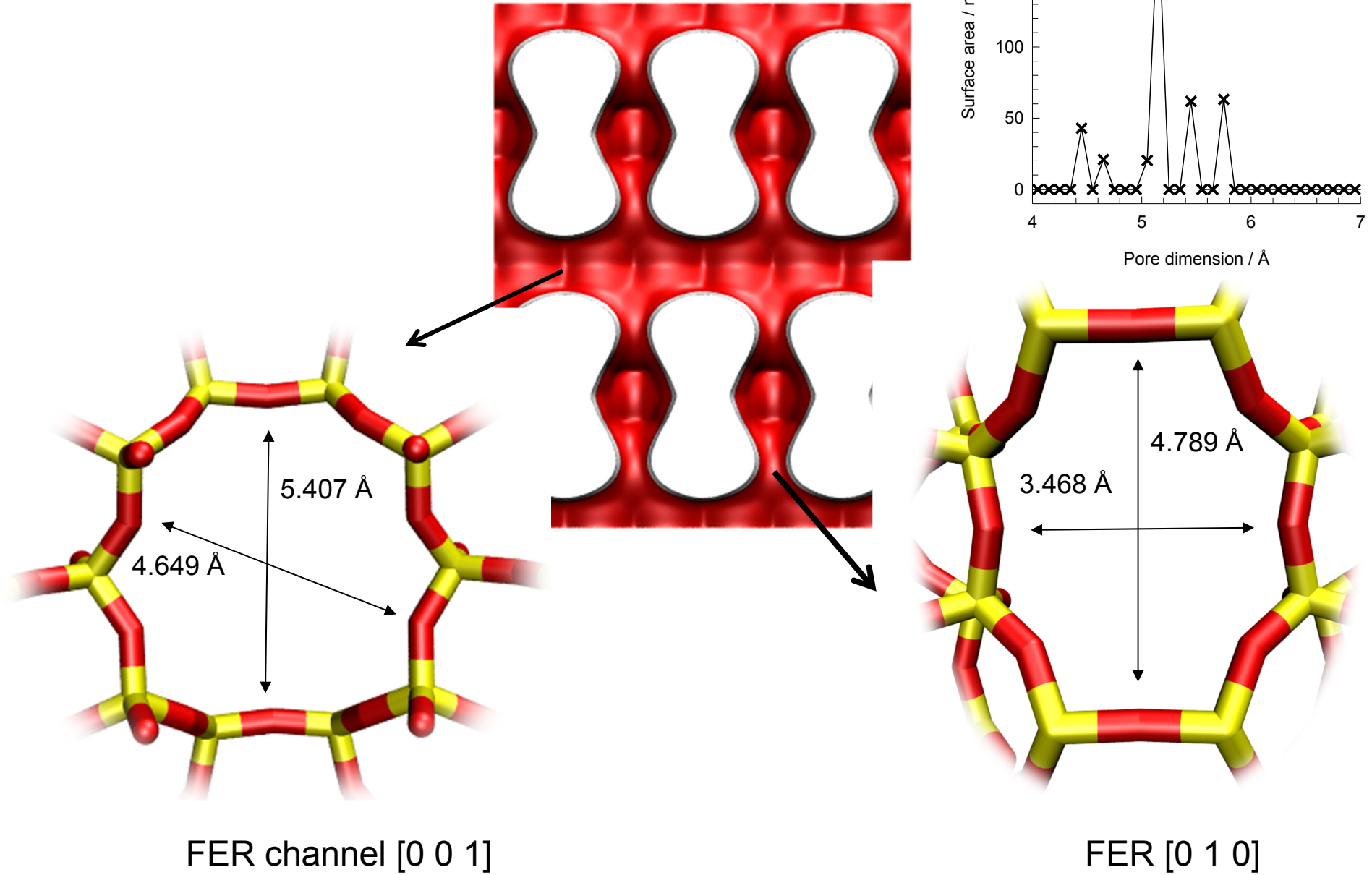
10-ring channels



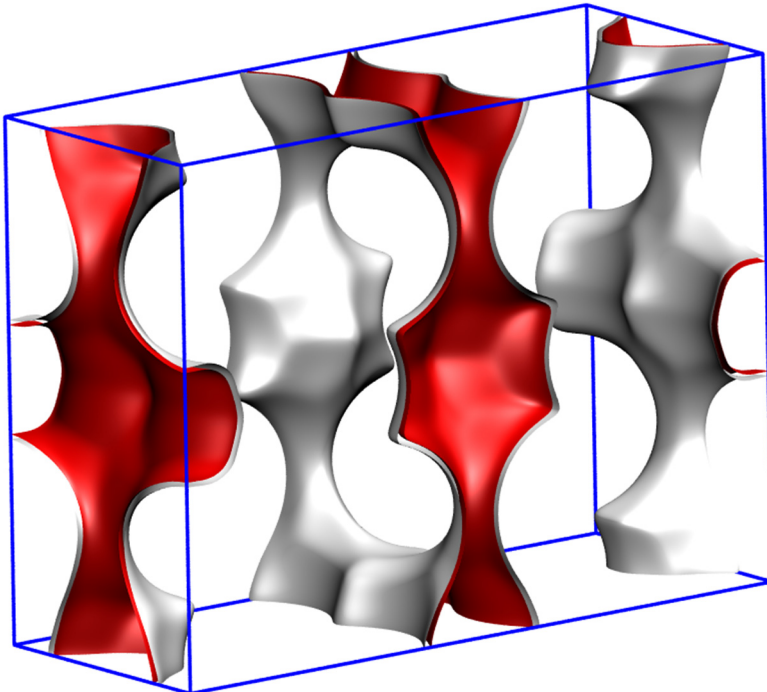
8-ring channels



FER pore dimensions

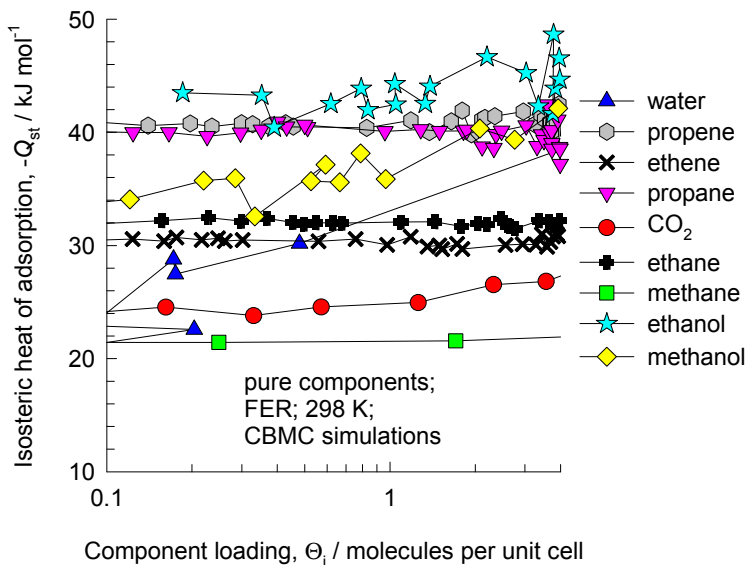
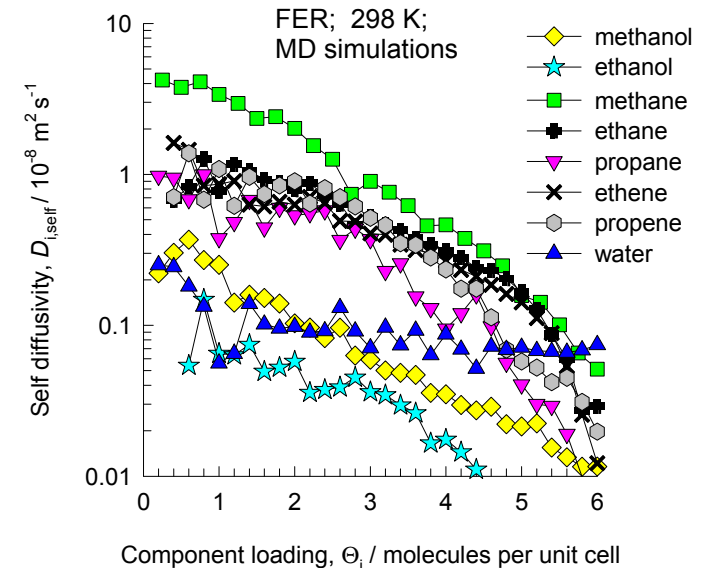
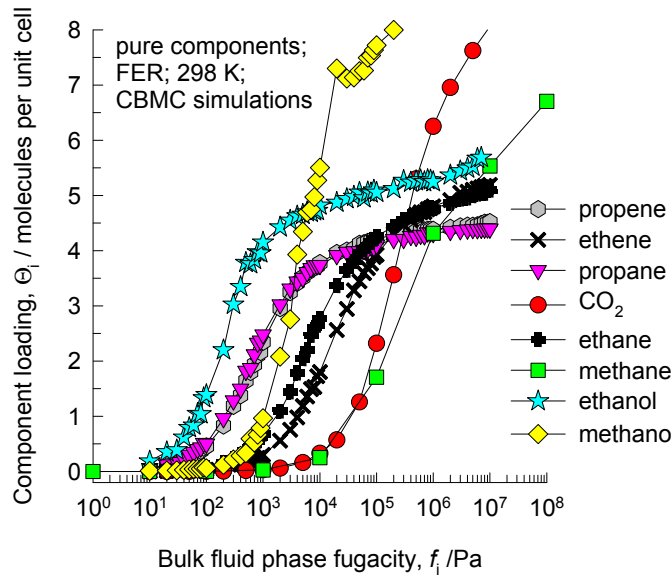


FER pore landscape



| | FER |
|--|----------|
| $a / \text{\AA}$ | 19.156 |
| $b / \text{\AA}$ | 14.127 |
| $c / \text{\AA}$ | 7.489 |
| Cell volume / \AA^3 | 2026.649 |
| conversion factor for [molec/uc] to [mol per kg Framework] | 0.4623 |
| conversion factor for [molec/uc] to [kmol/m ³] | 2.8968 |
| $\rho / \text{kg/m}^3$ | 1772.33 |
| MW unit cell [g/mol (framework)] | 2163.053 |
| ϕ , fractional pore volume | 0.283 |
| open space / $\text{\AA}^3/\text{uc}$ | 573.2 |
| Pore volume / cm^3/g | 0.160 |
| Surface area / m^2/g | 403.0 |
| DeLaunay diameter / \AA | 4.65 |

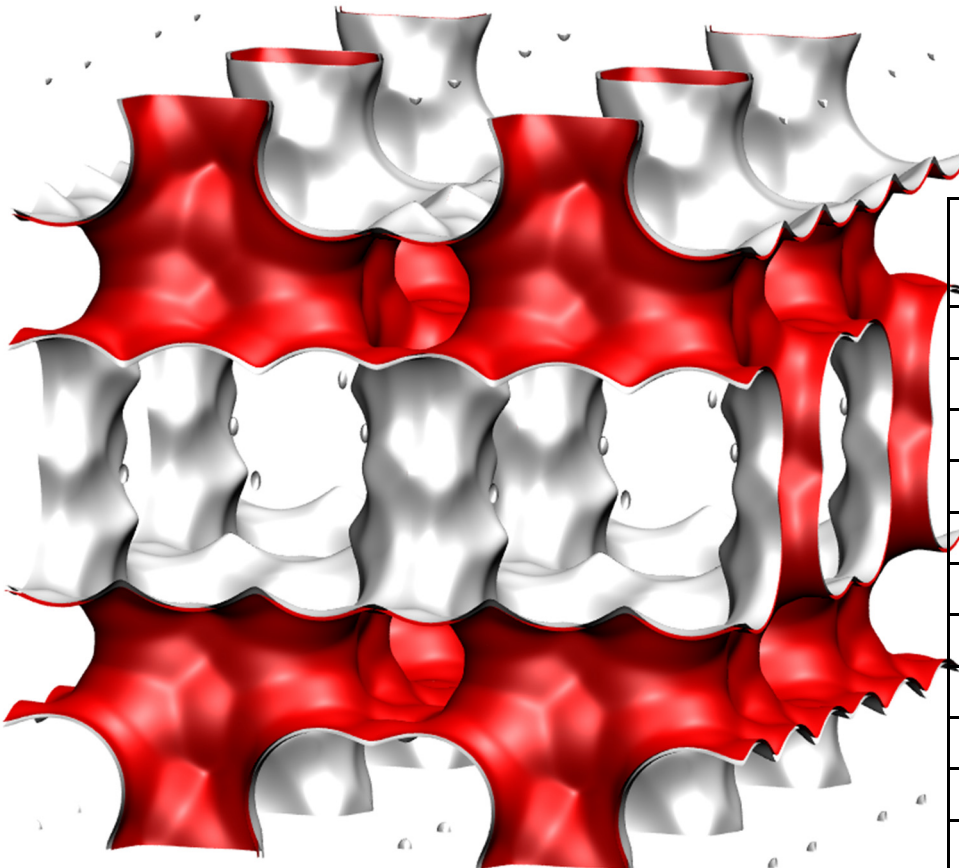
FER CBMC simulations of isotherms, and $-Q_{st}$; MD simulations of diffusivities



The diffusivities are along the 10-ring channels. The diffusivities in the other directions are too small to monitor accurately with MD.

ISV pore landscape

Intersecting 12-ring channels structure



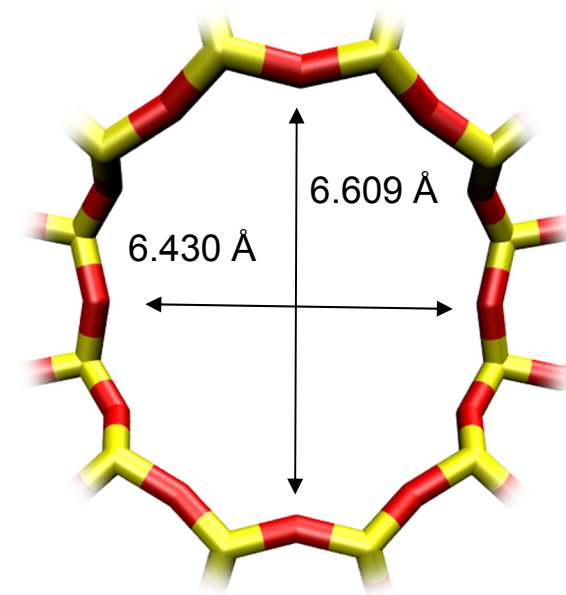
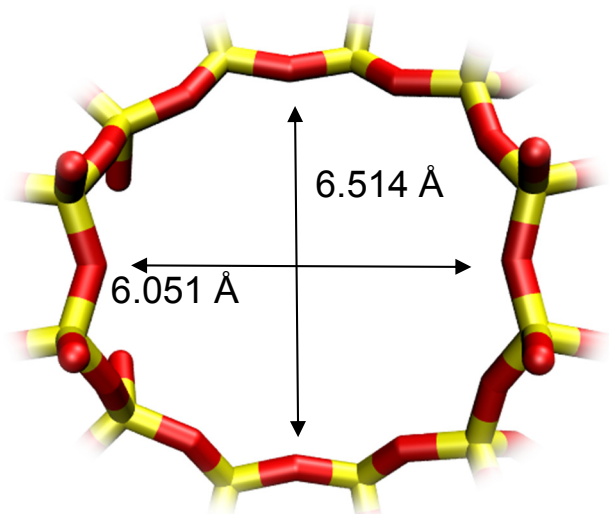
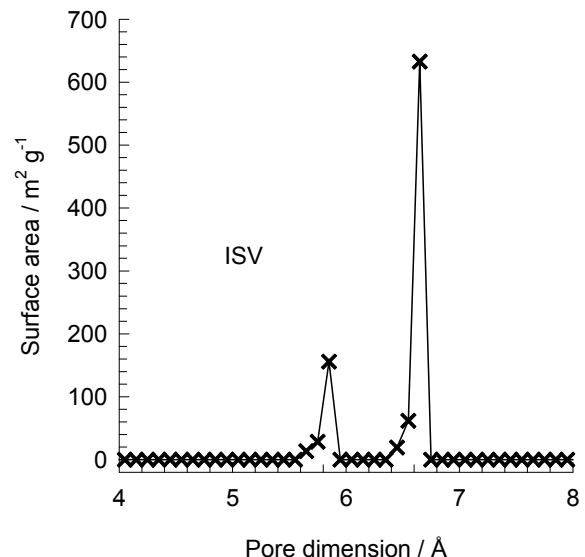
| | ISV |
|--|----------|
| $a / \text{\AA}$ | 12.853 |
| $b / \text{\AA}$ | 12.853 |
| $c / \text{\AA}$ | 25.214 |
| Cell volume / \AA^3 | 4165.343 |
| conversion factor for [molec/uc] to [mol per kg Framework] | 0.2600 |
| conversion factor for [molec/uc] to [kmol/m^3] | 0.9361 |
| $\rho [\text{kg}/\text{m}^3]$ | 1533.027 |
| MW unit cell [g/mol(framework)] | 3845.427 |
| ϕ , fractional pore volume | 0.426 |
| open space / $\text{\AA}^3/\text{uc}$ | 1773.9 |
| Pore volume / cm^3/g | 0.278 |
| Surface area / m^2/g | 911.0 |
| DeLaunay diameter / \AA | 5.96 |

Structural information from: C. Baerlocher, L.B. McCusker, Database of Zeolite Structures, International Zeolite Association,
<http://www.iza-structure.org/databases/>

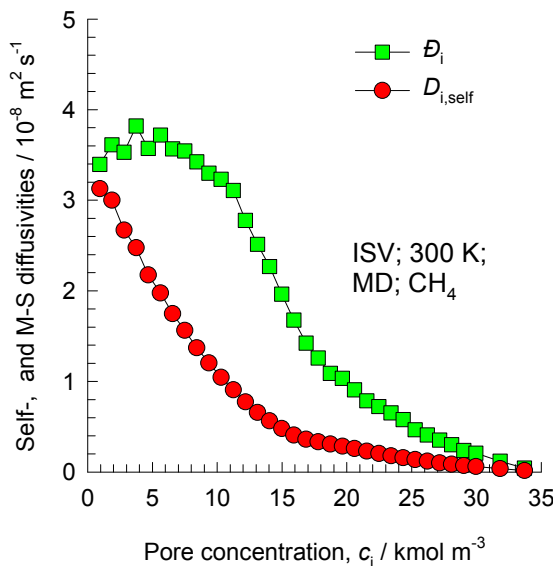
ISV pore dimensions

This plot of surface area versus pore dimension is determined using a combination of the DeLaunay triangulation method for pore dimension determination, and the procedure of Düren for determination of the surface area.

Intersecting 12-ring channels structure



Influence of Inverse Thermodynamic Factor on diffusivities



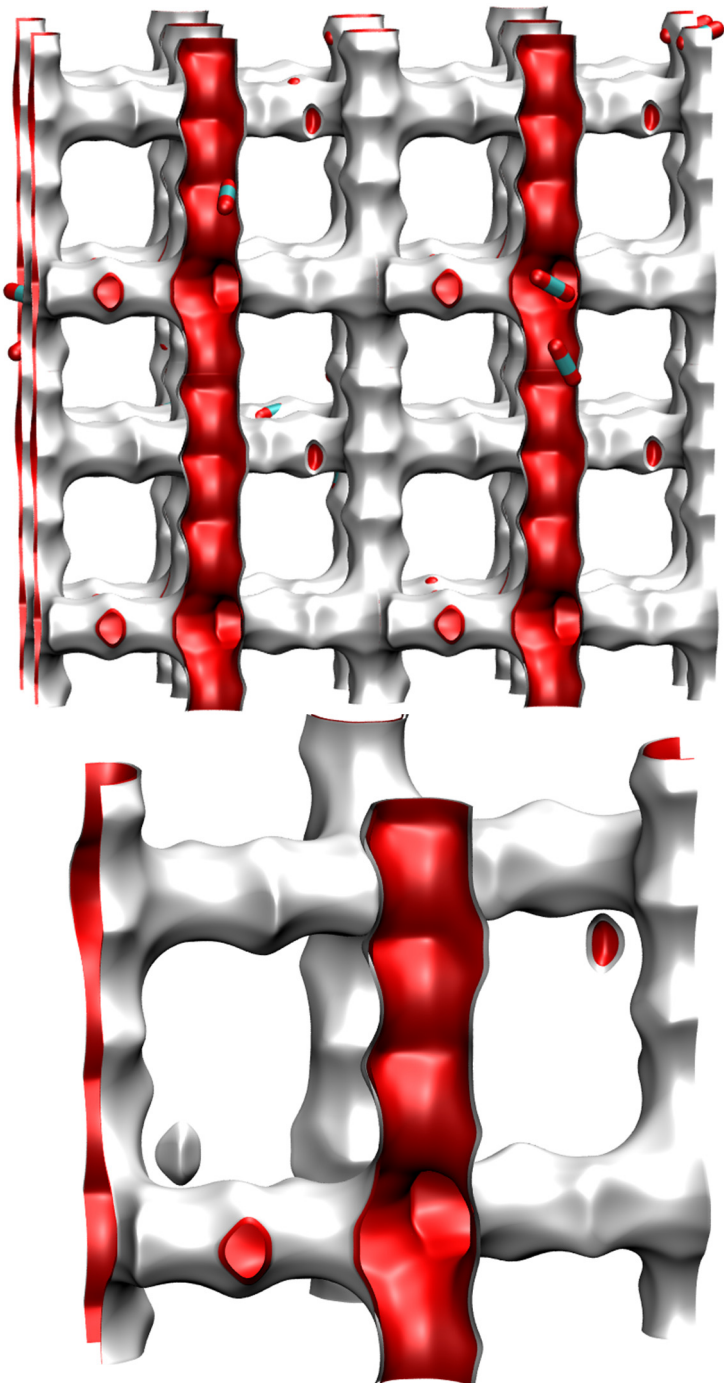
A detailed analysis of the loading dependence of CH₄ in ISV is contained in

E. Beerdsen, D. Dubbeldam and B. Smit, J Phys Chem B, 2006, 110, 22754-22772.

E. Beerdsen, D. Dubbeldam and B. Smit, Phys. Rev. Lett., 2006, 96, 044501.

MFI pore landscape

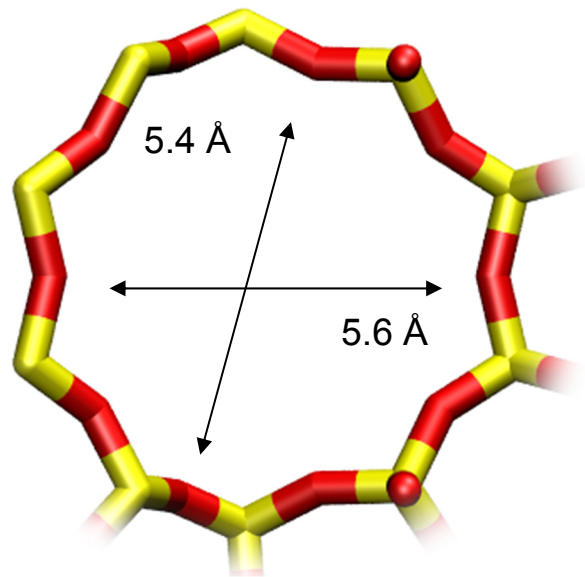
| | MFI |
|--|----------|
| $a / \text{\AA}$ | 20.022 |
| $b / \text{\AA}$ | 19.899 |
| $c / \text{\AA}$ | 13.383 |
| Cell volume / \AA^3 | 5332.025 |
| conversion factor for [molec/uc] to [mol per kg Framework] | 0.1734 |
| conversion factor for [molec/uc] to [kmol/m ³] | 1.0477 |
| $\rho / \text{kg/m}^3$ | 1796.386 |
| MW unit cell [g/mol(framework)] | 5768.141 |
| ϕ , fractional pore volume | 0.297 |
| open space / $\text{\AA}^3/\text{uc}$ | 1584.9 |
| Pore volume / cm^3/g | 0.165 |
| Surface area / m^2/g | 487.0 |
| DeLaunay diameter / \AA | 5.16 |



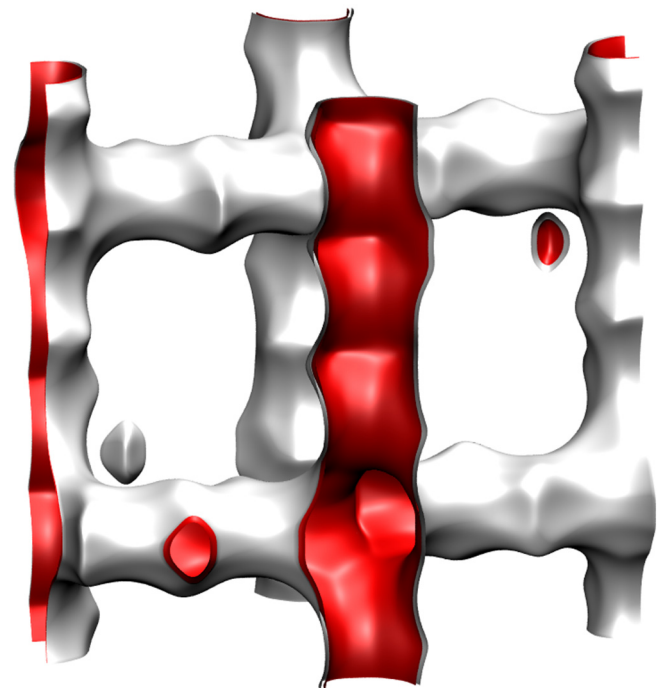
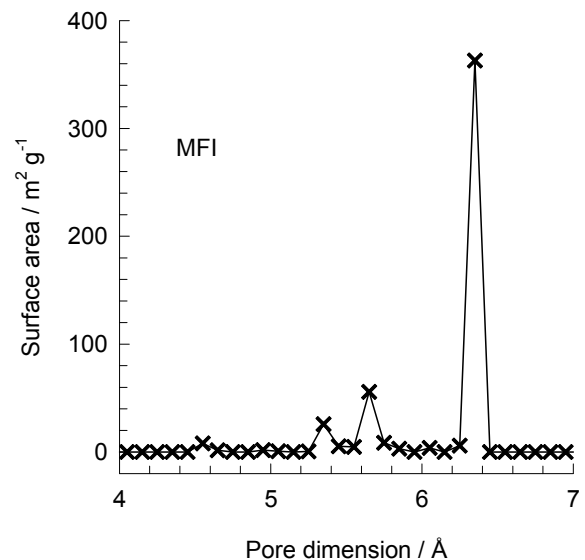
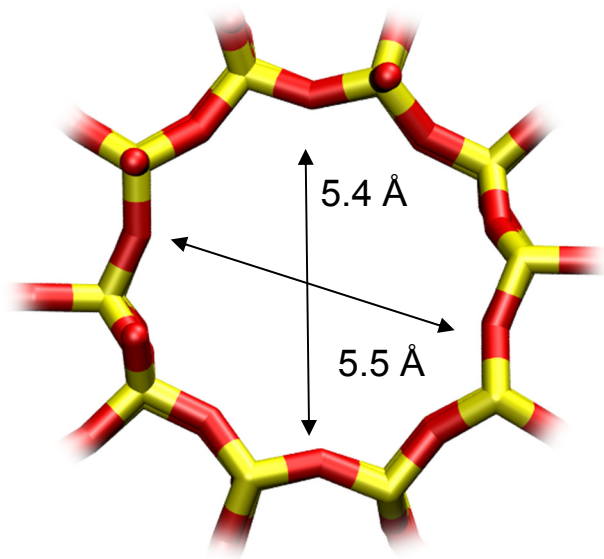
Structural information from: C. Baerlocher, L.B. McCusker,
Database of Zeolite Structures, International Zeolite Association,
<http://www.iza-structure.org/databases/>

MFI pore dimensions

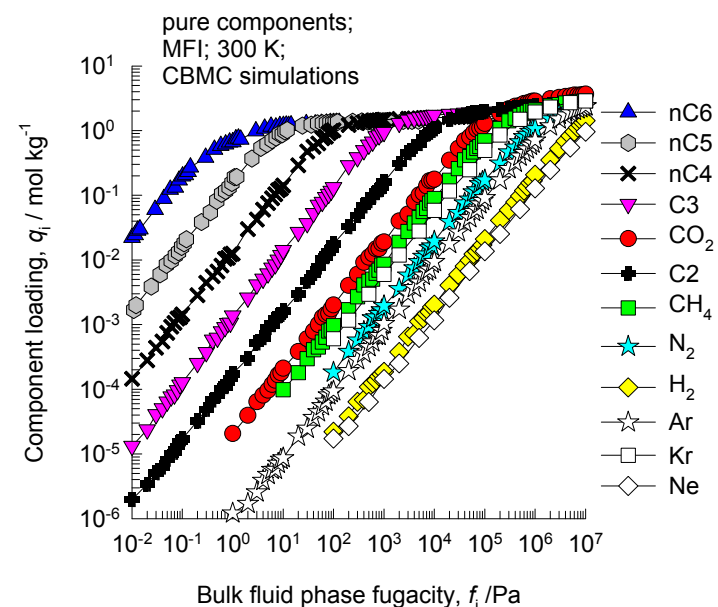
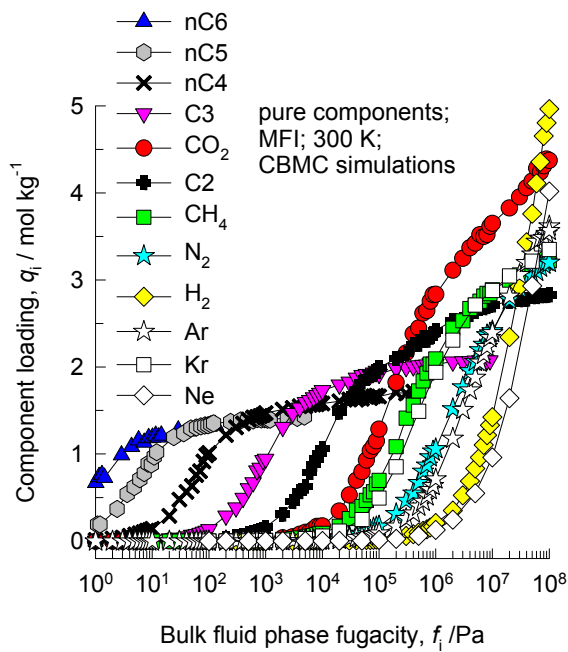
10 ring channel
of MFI viewed
along [100]



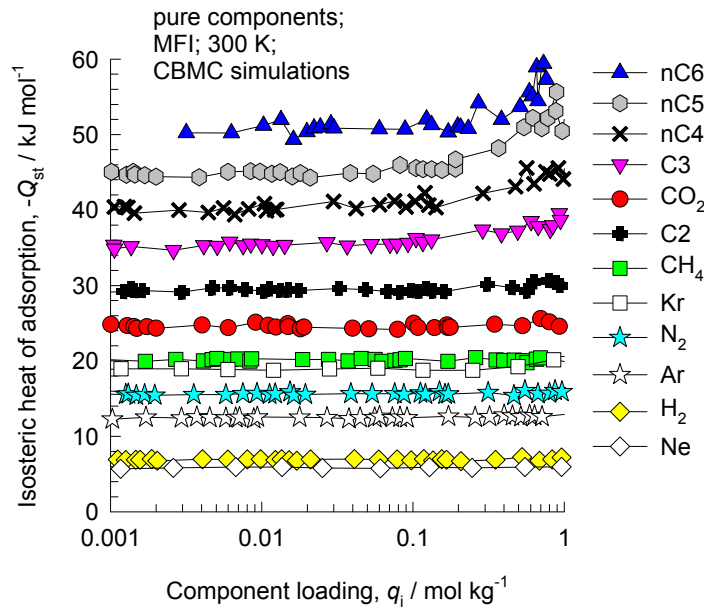
10 ring channel
of MFI viewed
along [010]



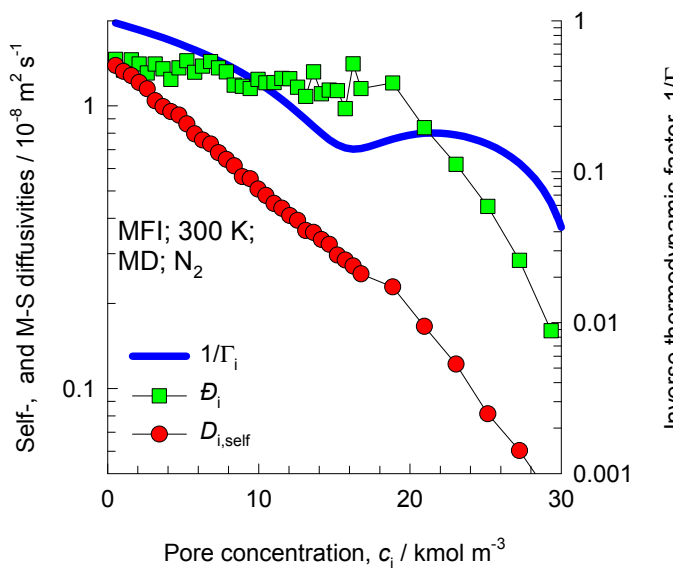
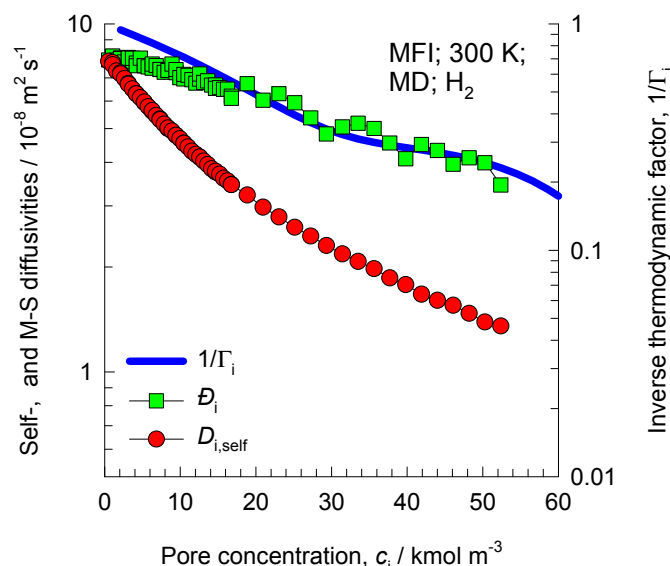
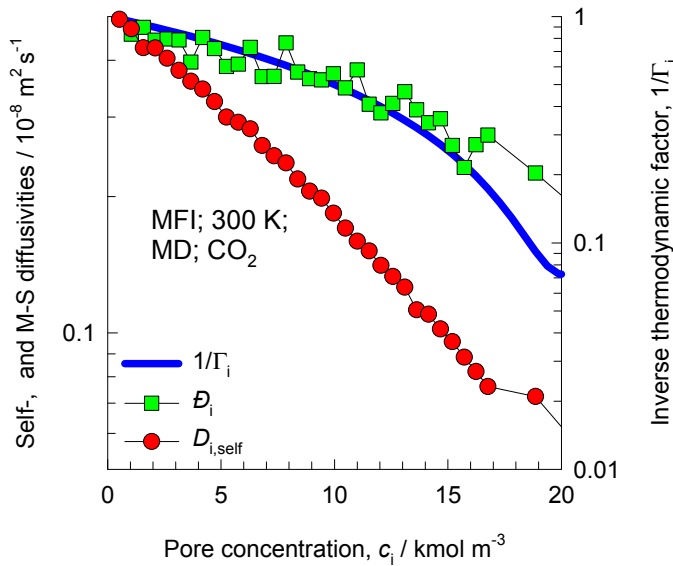
MFI CBMC simulations of isotherms, and isosteric heats of adsorption



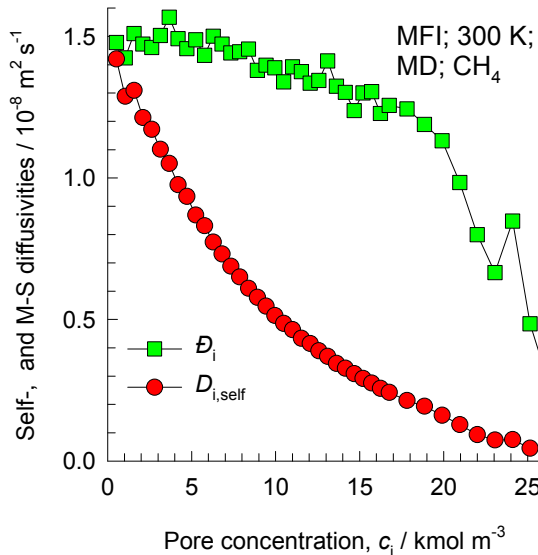
Note that C2 and C3 above refer to saturated alkanes



Influence of Inverse Thermodynamic Factor on diffusivities



Influence of Inverse Thermodynamic Factor on diffusivities

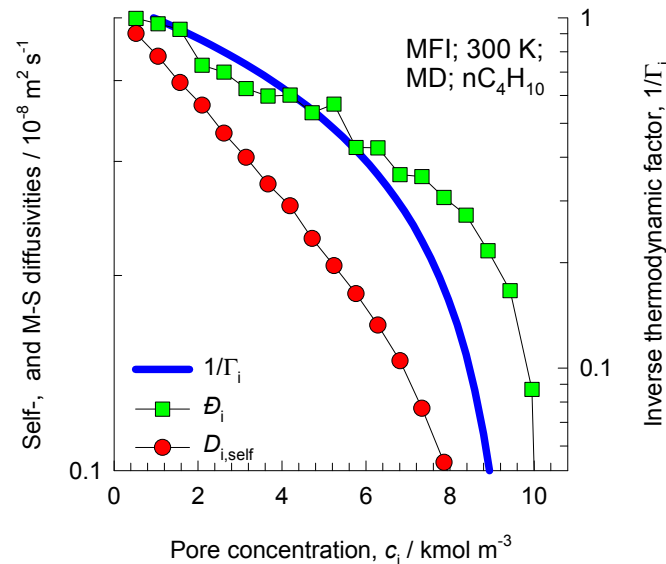
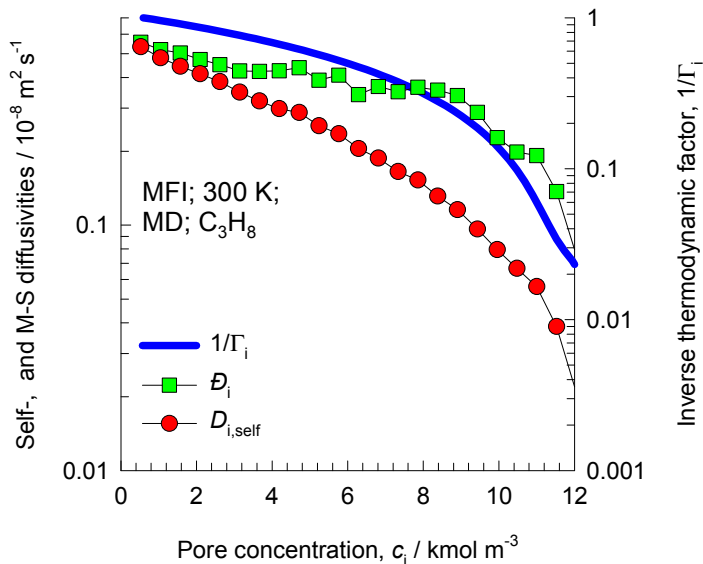
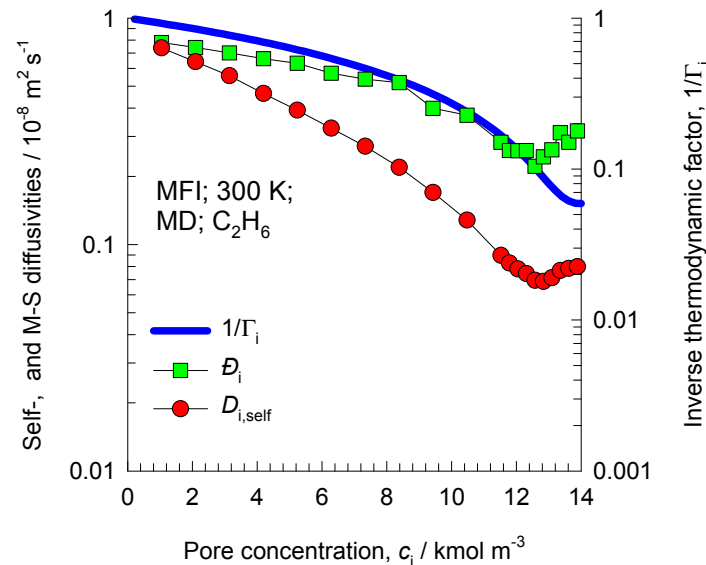


A detailed analysis of the loading dependence of CH_4 in MFI is contained in

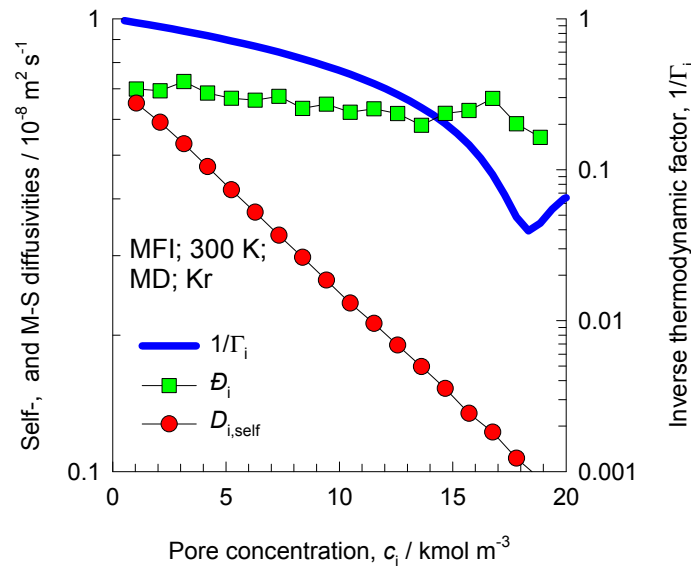
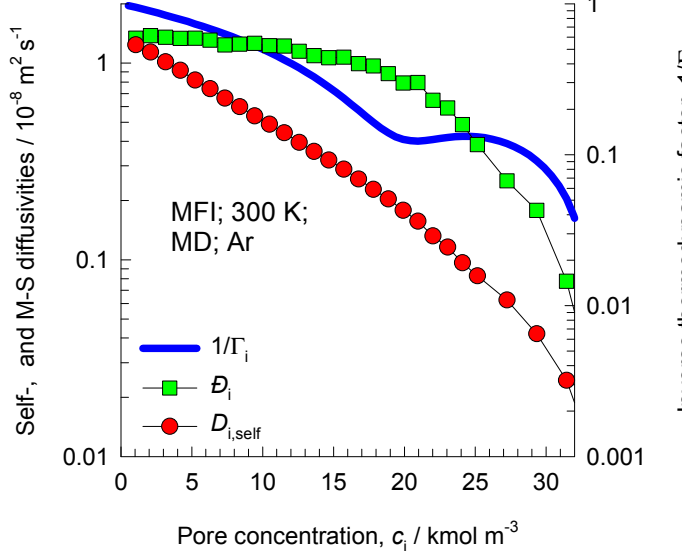
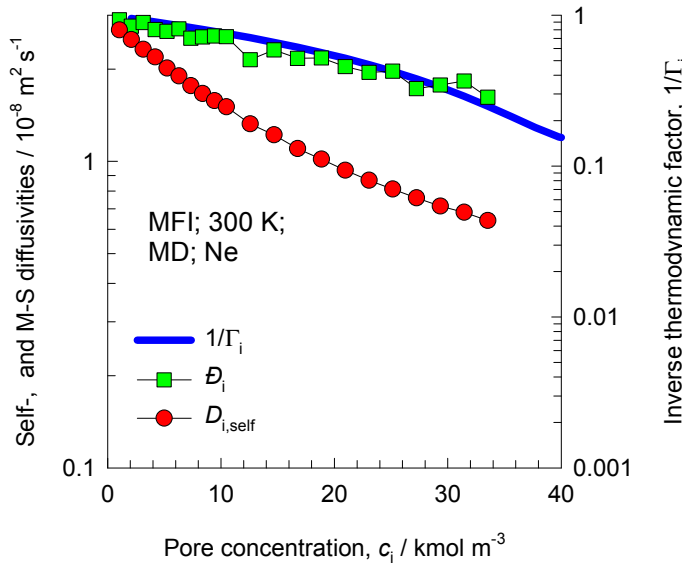
E. Beerdse, D. Dubbeldam and B. Smit, *Phys. Rev. Lett.*, 2005, **95**, 164505.

E. Beerdse, D. Dubbeldam and B. Smit, *J Phys Chem B*, 2006, **110**, 22754-22772.

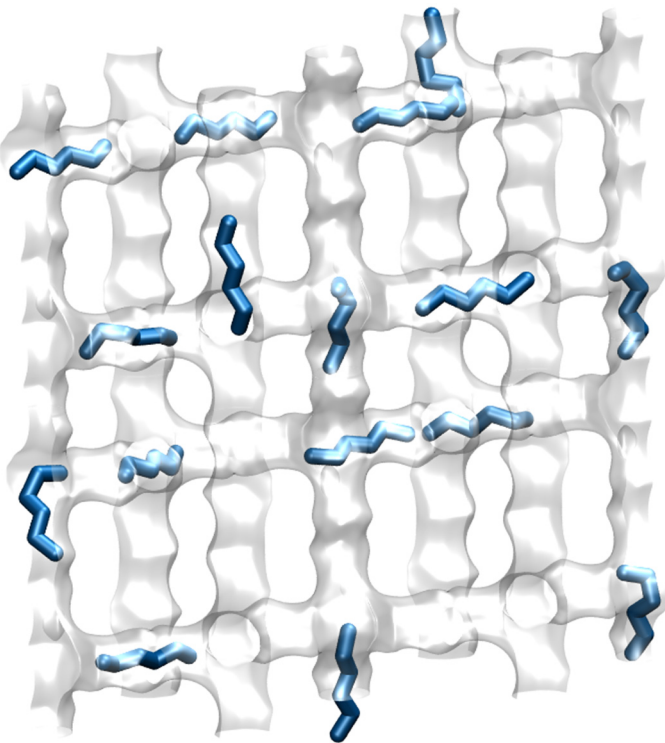
E. Beerdse, D. Dubbeldam and B. Smit, *Phys. Rev. Lett.*, 2006, **96**, 044501.



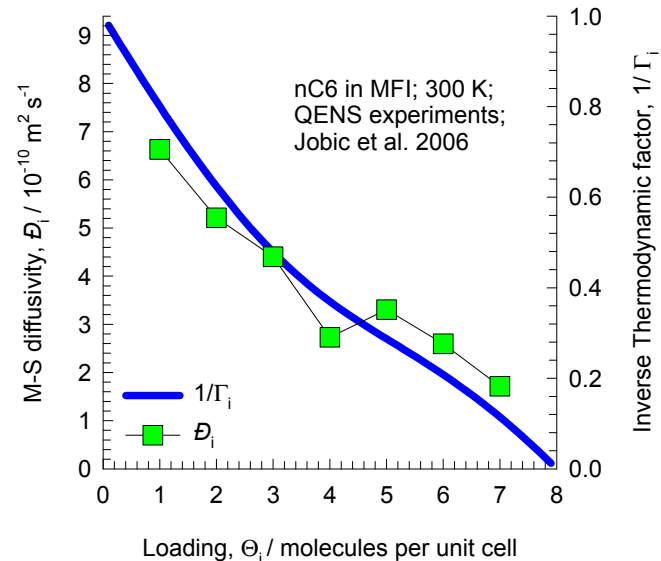
Influence of Inverse Thermodynamic Factor on diffusivities



nC6 diffusivity in MFI zeolite



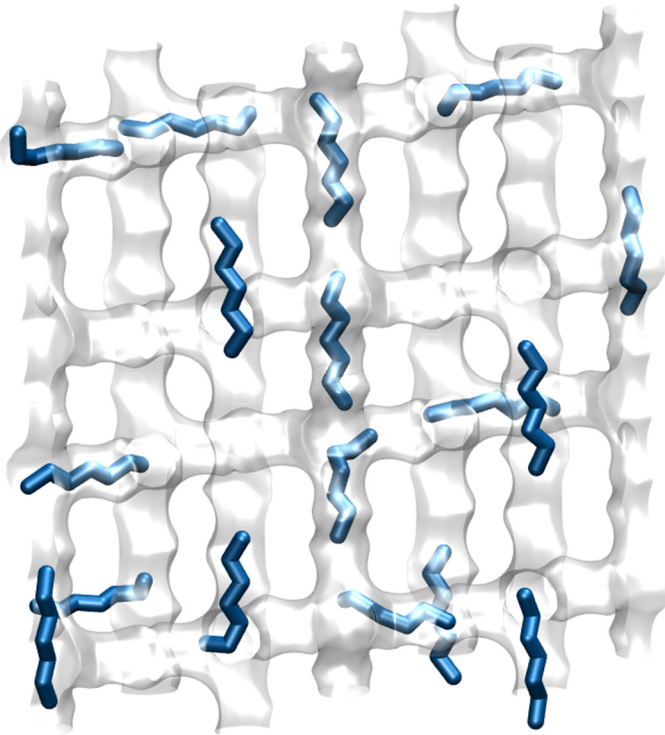
Linear, chain, alkanes can locate anywhere along the channels of MFI.
The length of nC6 is commensurate with the distance between two intersections



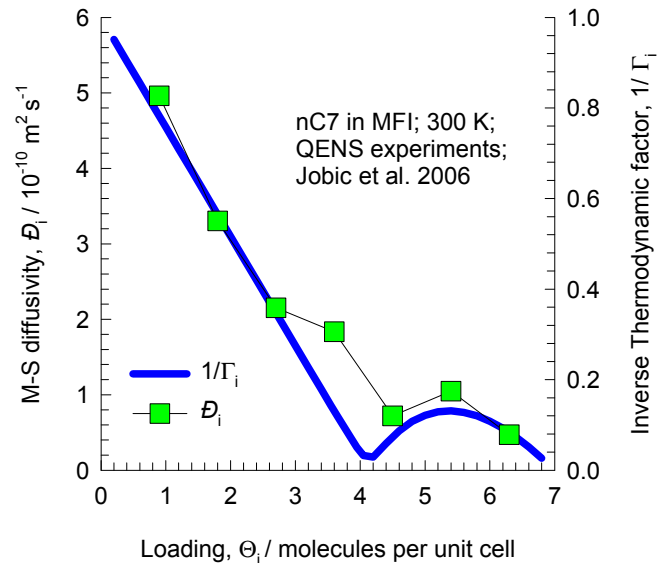
The QENS experimental data are re-plotted using the information in:

H. Jobic, C. Laloué, C. Laroche, J.M. van Baten, R. Krishna, Influence of isotherm inflection on the loading dependence of the diffusivities of n-hexane and n-heptane in MFI zeolite. Quasi-Elastic Neutron Scattering experiments supplemented by molecular simulations, J. Phys. Chem. B 110 (2006) 2195-2201.

nC7 diffusivity in MFI zeolite



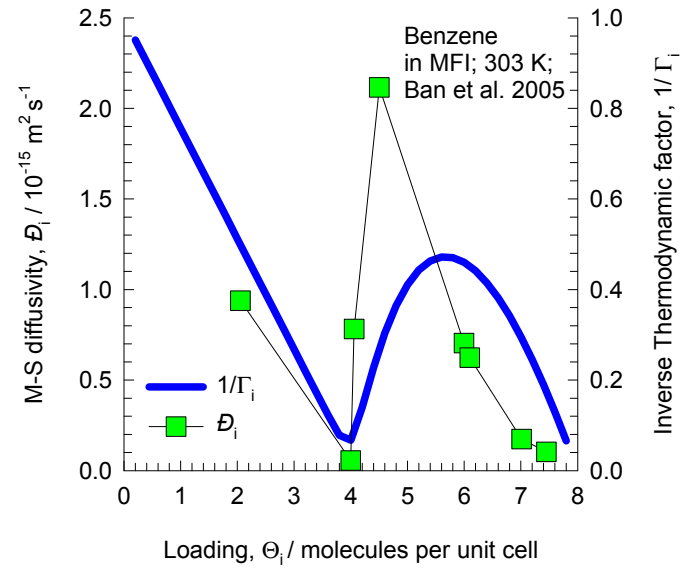
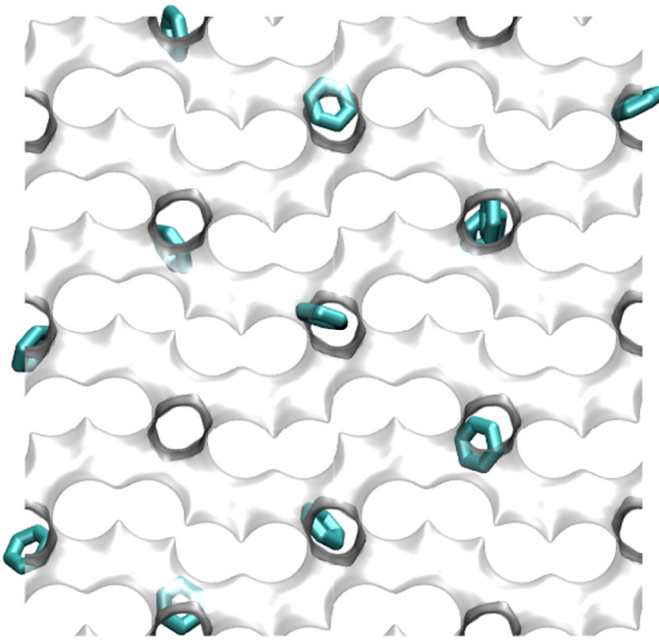
The length of nC7 is not commensurate with the distance between two intersections



The QENS experimental data are re-plotted using the information in:

H. Jobic, C. Laloué, C. Laroche, J.M. van Baten, R. Krishna, Influence of isotherm inflection on the loading dependence of the diffusivities of n-hexane and n-heptane in MFI zeolite. Quasi-Elastic Neutron Scattering experiments supplemented by molecular simulations, *J. Phys. Chem. B* 110 (2006) 2195-2201.

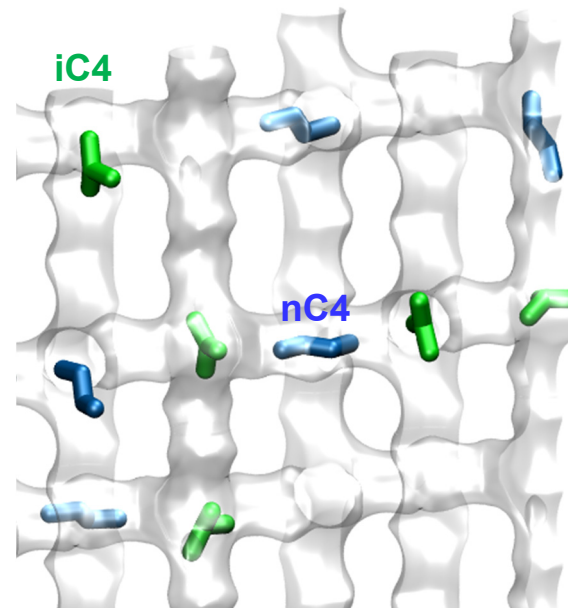
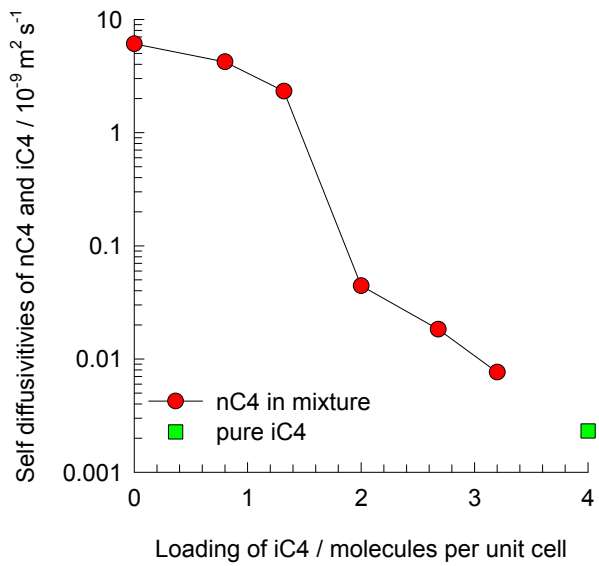
Benzene diffusivity in MFI zeolite



The experimental data are re-plotted after converting Fick diffusivities to Maxwell-Stefan diffusivities using:

Ban, H.; Gui, J.; Duan, L.; Zhang, X.; Song, L.; Sun, Z. Sorption of hydrocarbons in silicalite-1 studied by intelligent gravimetry. Fluid Phase Equilib. 2005, 232, 149-158.

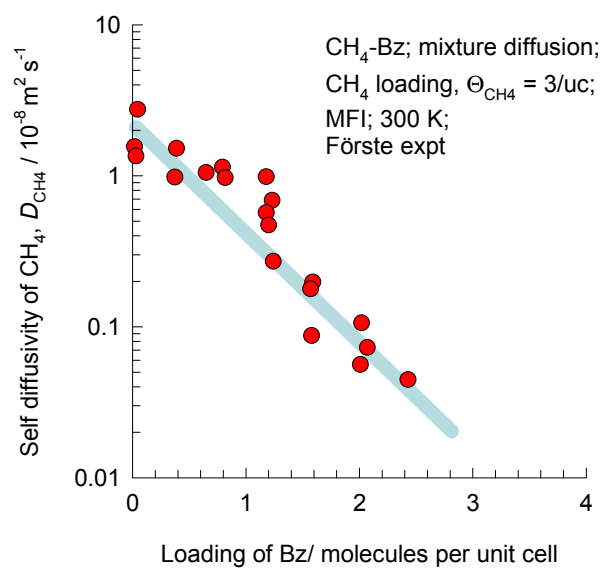
MFI: Traffic junction effects for nC4/iC4 mixture diffusion



The experimental data are re-plotted using the data of:

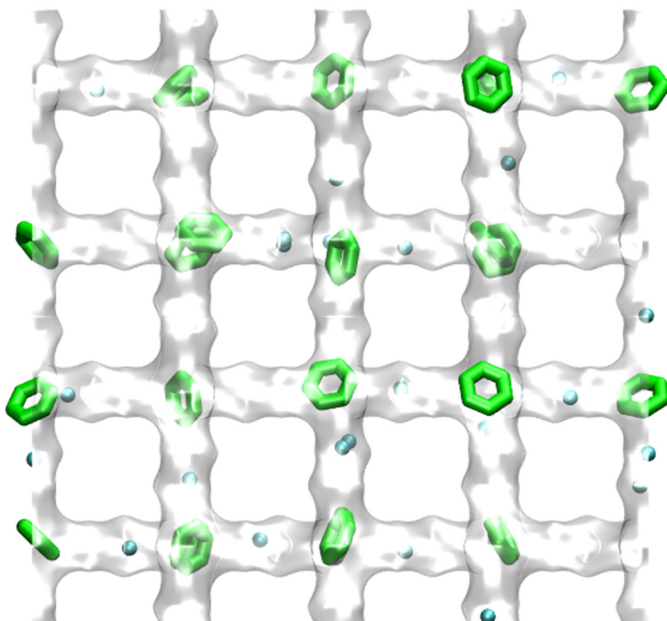
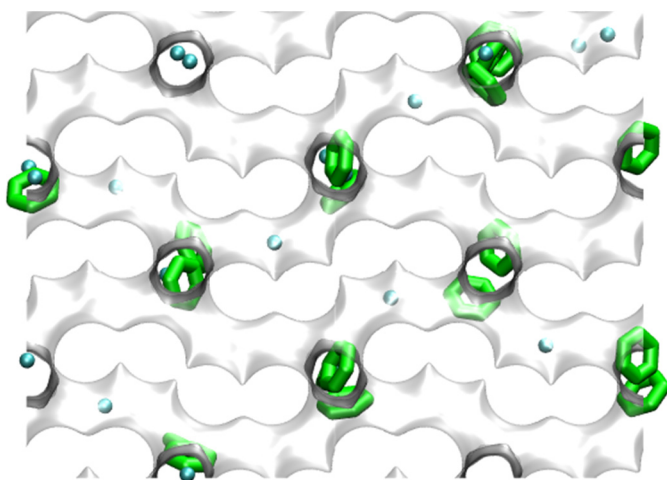
Fernandez, M.; Kärger, J.; Freude, D.; Pampel, A.; van Baten, J. M.; Krishna, R. Mixture diffusion in zeolites studied by MAS PFG NMR and molecular simulation, *Microporous Mesoporous Mater.* 2007, 105, 124-131.

MFI: Traffic junction effects for CH₄/Benzene mixture diffusion

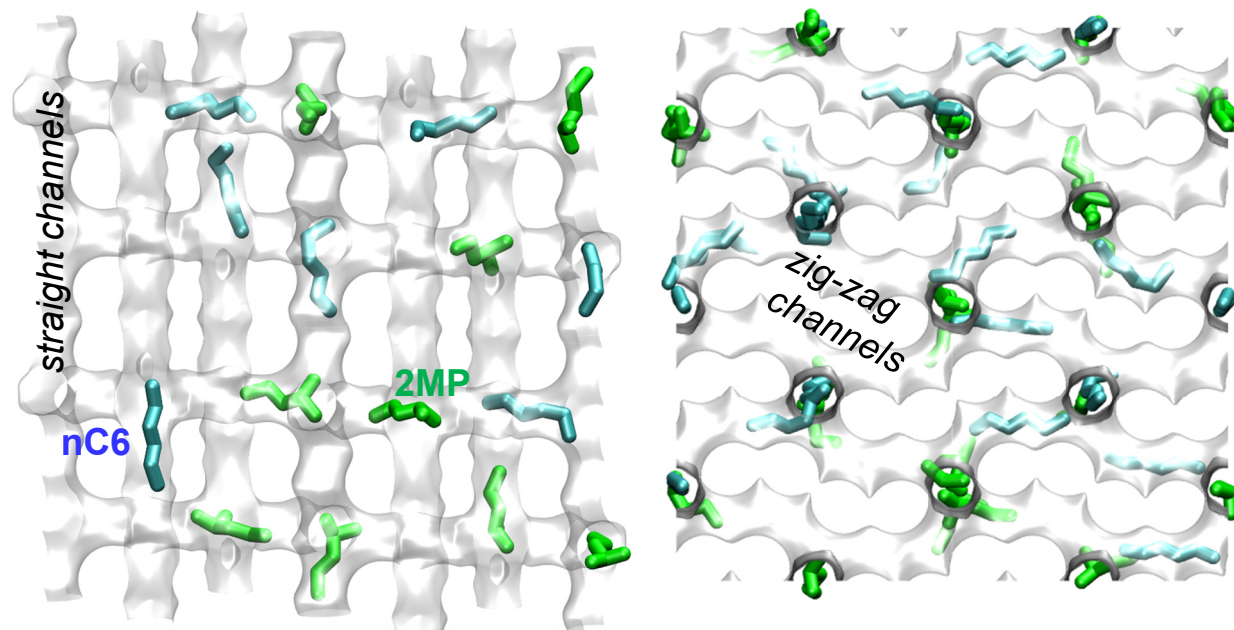
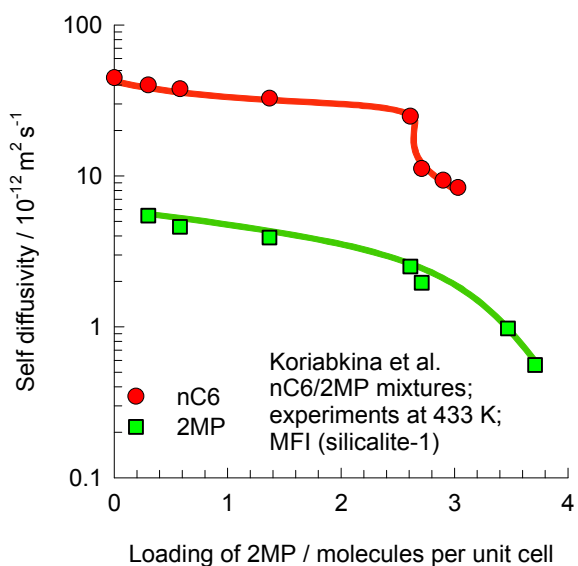


The experimental data are re-plotted using the data of:

Förste, C.; Germanus, A.; Kärger, J.; Pfeifer, H.; Caro, J.; Pilz, W.; Zikánová, A. Molecular mobility of methane adsorbed in ZSM-5 containing co-adsorbed benzene, and the location of benzene molecules, J. Chem. Soc., Faraday Trans. 1. 1987, 83, 2301-2309.



MFI: Traffic junction effects for nC₆/2MP mixture diffusion



The experimental data are re-plotted using the data of:

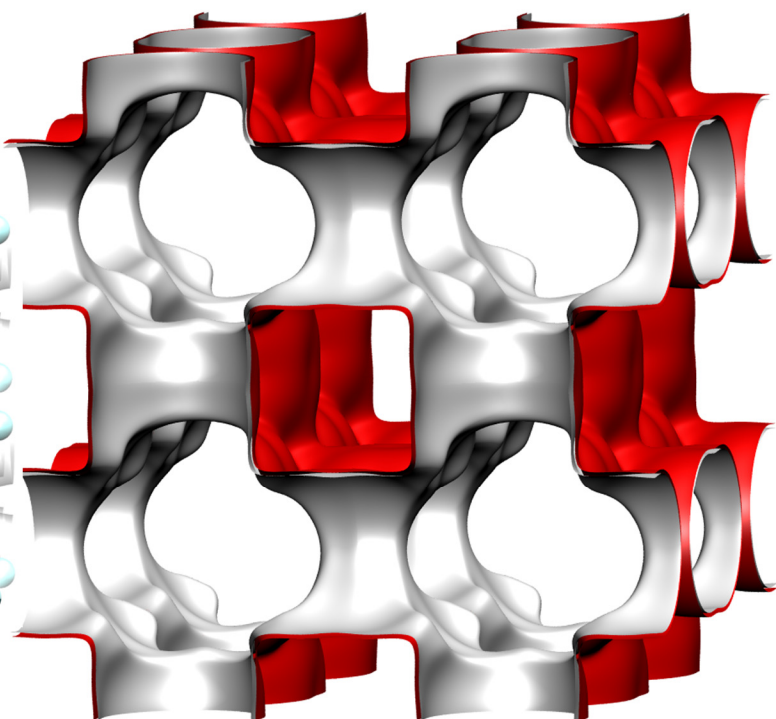
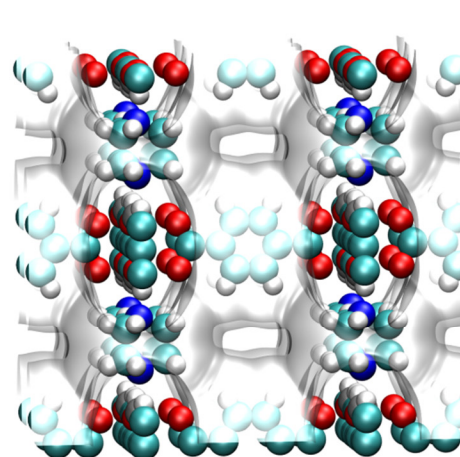
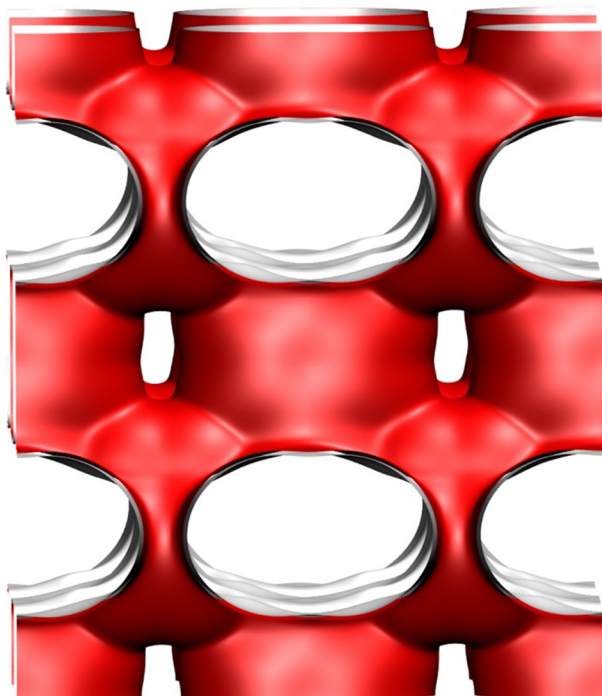
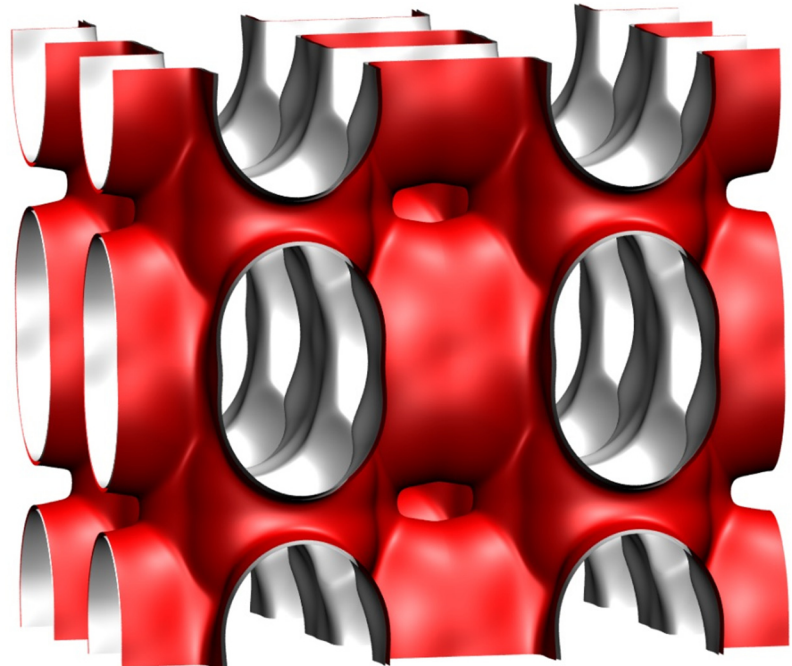
Koriabkina, A. O.; de Jong, A. M.; Schuring, D.; van Grondelle, J.; van Santen, R. A. Influence of the acid sites on the intracrystalline diffusion of hexanes and their mixtures within MFI-zeolites, *J. Phys. Chem. B* 2002, 106, 9559-9566.

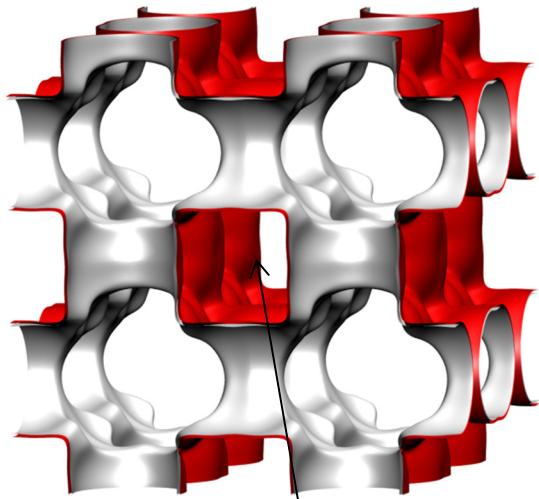
Zn(bdc)dabco landscapes

The structural information for Zn(bdc)(dabco)_{0.5}, commonly simply referred to as Zn(bdc)dabco, is from

P.S. Bárcea, F. Zapata, J.A.C. Silva, A.E. Rodrigues, B. Chen, Kinetic Separation of Hexane Isomers by Fixed-Bed Adsorption with a Microporous Metal-Organic Framework, *J. Phys. Chem. B* 111 (2008) 6101-6103.

J.Y. Lee, D.H. Olson, L. Pan, T.J. Emge, J. Li, Microporous Metal-Organic Frameworks with High Gas Sorption and Separation Capacity, *Adv. Funct. Mater.* 17 (2007) 1255-1262.





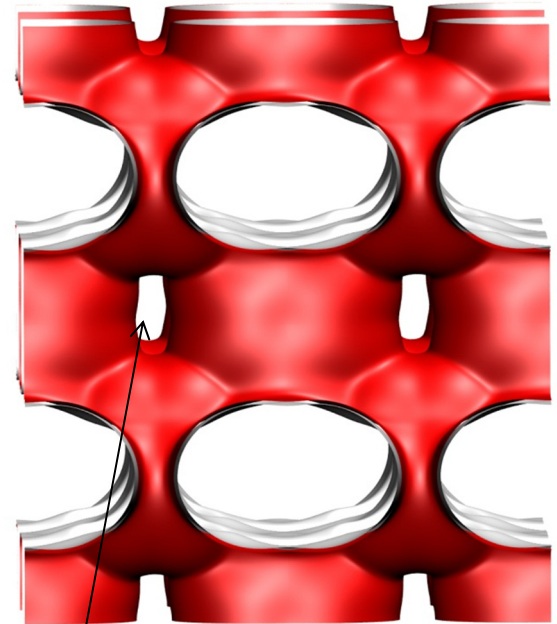
Wide
channels

$7.5 \text{ \AA} \times 7.5 \text{ \AA}$

Zn(bdc)dabco landscapes

3D intersecting channels

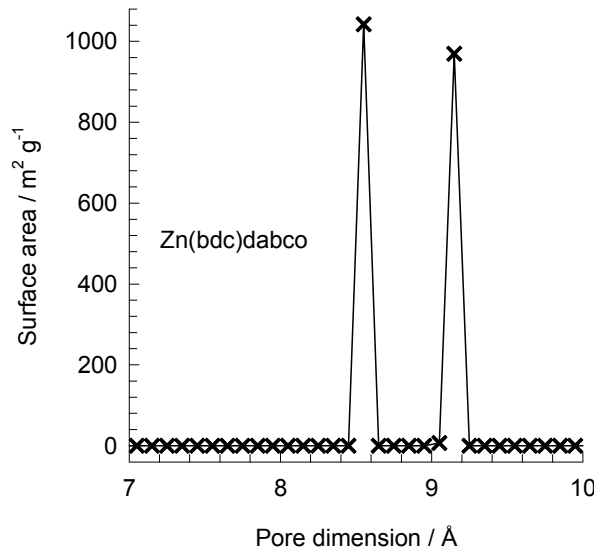
There exist two types of intersecting channels of about $7.5 \text{ \AA} \times 7.5 \text{ \AA}$ along the x-axis and channels of $3.8 \text{ \AA} \times 4.7 \text{ \AA}$ along y and z axes.



Narrow
channels

$4.7 \text{ \AA} \times 3.8 \text{ \AA}$

Zn(bdc)dabco pore dimensions



This plot of surface area versus pore dimension is determined using a combination of the DeLaunay triangulation method for pore dimension determination, and the procedure of Düren for determination of the surface area.

| Zn(bdc)dabco | |
|--|----------|
| a /Å | 10.9288 |
| b /Å | 10.9288 |
| c /Å | 9.6084 |
| Cell volume / Å³ | 1147.615 |
| conversion factor for [molec/uc] to [mol per kg Framework] | 1.7514 |
| conversion factor for [molec/uc] to [kmol/m³] | 2.1867 |
| ρ [kg/m³] | 826.1996 |
| MW unit cell [g/mol(framework)] | 570.9854 |
| ϕ , fractional pore volume | 0.662 |
| open space / Å³/uc | 759.4 |
| Pore volume / cm³/g | 0.801 |
| Surface area /m²/g | 2022.5 |
| DeLaunay diameter /Å | 8.32 |

Influence of Inverse Thermodynamic Factor on diffusivities

